

Optimization of Outflow Control Devices Design in Steam-Assisted Gravity Drainage Models
with Wellbore Trajectory Excursions

by

Anas Khalil Sidahmed

A thesis submitted in partial fulfillment of the requirements for the degree of

Master of Science

in

PETROLEUM ENGINEERING

Department of Civil and Environmental Engineering
University of Alberta

© Anas Khalil Sidahmed, 2018

ABSTRACT

Canada has giant oil reserves which ranks third worldwide with proven oil reserves of 171 billion barrels. Alberta alone contributes with 165.4 billion barrels found in oil sands. However, those oil sands are extremely viscous and only 10% are recoverable by means of open-pit mining. In-situ thermal recovery methods such as Steam-Assisted Gravity Drainage (SAGD) have been developed and adopted as an efficient mean to unlock the oil sands reserves.

Different reservoir geological settings and long horizontal wells impose limitations and operational challenges on the implementation of SAGD technology. Well pair trajectory excursions (unintentionally generated trajectory deviations due to suboptimal drilling operations) are some of the complications that lead to non-uniform steam chamber conformance, high cumulative Steam-Oil Ratio (cSOR) and low bitumen recovery.

Conventional dual-string completion scheme (a short tubing landed at the heel and a long tubing landed at the toe) has been widely adopted in most of the SAGD operations. Such configurations allow steam injection at two points: the toe and the heel sections of the horizontal well. However, these completions have demonstrated poor efficiency when reservoir/well complications exist. Tubing-deployed Flow Control Devices (FCD's) have been introduced to offer high flexibility in delivering specific amounts of steam to designated areas (such as low permeability zones) and ensure uniform development of steam chamber in the reservoir. The work in this thesis presents the results of a numerical effort for optimizing the design of Outflow Control Devices (OCD's) in SAGD wells for different scenarios of well pair trajectory excursions.

A coupled wellbore-reservoir SAGD simulation model was constructed to optimize the placement and number of ports in each single OCD. Three different cases were generated from the constructed

basic SAGD model with each case having a certain well pair trajectory which causes variable lateral distances between the well pair.

Results of the optimized OCD's cases demonstrate a higher SAGD efficiency compared to their corresponding conventional dual-string cases. Those enhancements were reflected in a higher steam chamber conformance, a higher cumulative oil production, and an improved Net Present Value (NPV).

ACKNOWLEDGEMENTS

First and foremost, I would like to express my sincere thanks and gratitude to my mother, sisters and brothers for their love, continuous support and encouragement.

My sincere thanks and gratitude are conveyed to my supervisor Dr. Alireza Nouri, for offering me such a great opportunity to pursue my graduate studies and for his patience, guidance and continuous support.

Also, I would like to thank Dr. Mohamed Kyanpour for his insightful comments on my thesis work proposal. Many thanks are also extended to all involved postdoctoral fellows for their help, support, suggestions, reviewing, and comments on my thesis.

Special thanks to my committee members Dr. Carlos Lange and Dr. Japan Trivedi for their valuable comments and recommendations.

I would like to acknowledge RGL Reservoir Management Inc. company and NSERC for funding this research through a Collaborative Research and Development (CRD) funding program. I would also like to thank CMG company and its technical team for securing necessary software packages and their support.

Many thanks to everyone who assisted or encouraged me during my research time.

TABLE OF CONTENTS

ABSTRACT.....	ii
ACKNOWLEDGEMENTS	iv
TABLE OF CONTENTS	v
LIST OF TABLES	xi
LIST OF FIGURES	xiii
LIST OF SYMBOLES AND ABBRIVATIONS	xx
CHAPTER ONE: INTRODUCTION.....	1
1.1 Background	1
1.2 Problem Statement	1
1.3 Research Hypothesis.....	2
1.4 Research Objectives	2
1.5 Methodology.....	3
1.6 Thesis Layout	4
CHAPTER TWO: LITERATURE REVIEW	6
2.1 Overview of SAGD Technology.....	6
2.1.1 History and Statistics of SAGD	6
2.1.2 Basic Concept of SAGD	7
2.1.3 SAGD Stages	8
2.2 Flow Control Devices.....	12
2.2.1 Types of Flow Control Devices	12
2.2.2 Tubing-Deployed versus Liner-Deployed FCD's.....	14
2.2.3 Modeling FCD's in CMG STARS.....	16
2.2.4 General Design Factors in Conventional Wells.....	18
2.2.5 ICD Design Steps for Conventional Wells	18

2.3	FCD's in SAGD.....	20
2.3.1	Implementation of OCD's/ICD's in SAGD	21
2.3.2	FCD's Utilization in SAGD Projects in Alberta	22
2.3.3	FCD's Simulation for SAGD	22
2.3.4	Impact of FCD's Specifications and Locations on SAGD Production	22
CHAPTER THREE: BASIC SAGD MODEL SETUP		25
3.1	SAGD Basic Model Construction Strategy	25
3.2	Overview of Suncor MacKay River SAGD Project	25
3.2.1	Project Overview	25
3.2.2	Production and Wells Status	27
3.2.3	Well Completion Schemes.....	29
3.3	Construction of Basic SAGD Reservoir Model.....	31
3.3.1	Symmetry Assumption.....	31
3.3.2	Model Dimensions	31
3.3.3	Modeling Geological Properties	32
3.3.4	Definition of System Components.....	33
3.3.5	Fluid Densities/Compressibilities	33
3.3.6	Modeling Rock-Fluid Data	34
3.3.7	Reservoir Bitumen Viscosity	37
3.3.8	Modeling Initial Conditions	40
3.4	Wellbore Hydraulics Modeling	40
3.4.1	Classical Sink/Source Model	41
3.4.2	FlexWell Model	41
3.4.3	Coupling of Reservoir/ FlexWell Models.....	44
3.5	Construction of Basic SAGD Wellbore Model.....	45

3.4.4	Well Pair Completion System.....	45
3.4.5	Definition of Sink/Source Wells.....	45
3.4.6	Modeling Circulation Stage.....	46
3.4.7	Modeling SAGD Stage.....	47
CHAPTER FOUR: BASE CASE MODEL ENHANCEMENT AND GRID SIZE SENSITIVITY ANALYSIS		49
4.1	Introduction	49
4.2	Overview of Conventional Grid Size Sensitivity Work.....	49
4.3	Grid Size Sensitivity Analysis with LGR.....	50
4.3.1	Grid Variations.....	51
4.3.2	Implementation of LGR.....	51
4.3.3	Ideal Trajectory with LGR.....	51
4.3.4	Trajectory-1 with LGR	55
4.3.5	Trajectory-2 with LGR	59
4.3.6	Trajectory-3 with LGR	63
4.4	Summary and Conclusions	67
4.4.1	Grid Size Sensitivity Analysis Summary.....	67
4.4.2	General Guideline for Models Enhancement with LGR.....	67
CHAPTER FIVE: DESIGN OF OPTIMIZATION PROCESS.....		69
5.1	Introduction	69
5.2	Design of Optimization Objective Function.....	69
5.2.1	Definition of Objective Function.....	69
5.2.2	Types of Objective Functions	69
5.2.3	NPV Objective Function.....	69
5.2.4	Simplification of NPV Objective Function.....	70

5.3	Fixed Optimization Parameters	71
5.3.1	Basic Assumptions for the Optimization Work.....	71
5.3.2	Placement of OCDs and Use of Packers.....	71
5.3.3	SAGD Well Life	74
5.3.4	OCD Type.....	74
5.3.5	Operation Constraints	75
5.4	Optimization Steps	75
5.4.1	Step 1	75
5.4.2	Step 2	76
5.5	CMOST Optimization Software.....	76
5.5.1	Optimization Algorithms in CMG CMOST	76
5.6	Optimization Workflow for OCD’s Number of Ports.....	77
5.6.1	Setting Optimization Parameters	77
5.6.2	Assigning NPV Objective Function to the Optimization Tool.....	78
5.6.3	Designing Experimental Sampling	78
5.6.4	CMG CMOST DECE Optimization Engine.....	79
5.6.5	Results Viewing and Analysis	80
CHAPTER SIX: OPTIMIZATION CASE STUDEIS		81
6.1	Introduction	81
6.2	Study # 1: Trajectory-1 OCD’s Optimization.....	81
6.2.1	Base Case Description	81
6.2.2	Optimization Analysis with OCD Deployment	83
6.2.3	Results Analysis.....	88
6.2.4	The Effect of Using Smaller Diameter Slotted Liner	89
6.3	Study # 2: Trajectory-2 OCD’s Optimization.....	98

6.3.1	Base Case Description	98
6.3.2	Optimization Analysis with OCD Deployment	99
6.3.3	Results Analysis.....	103
6.4	Study # 3: Trajectory-3 OCD's Optimization.....	112
6.4.1	Base Case Description	112
6.4.2	Optimization Analysis with OCD Deployment	113
6.4.3	Results Analysis.....	117
6.5	Comparison of the Trajectories Results	125
6.5.1	Comparison of NPVs	125
6.5.2	Comparison of Fine Models Results.....	126
CHAPTER SEVEN: CONCLUSIONS AND FUTURE WORK.....		128
7.1	Summary	128
7.2	Results of Grid Size Sensitivity Studies	128
7.3	Results of Optimization Work.....	129
7.3.1	Trajectory-1.....	129
7.3.2	Trajectory-2.....	130
7.3.3	Trajectory-3.....	130
7.4	Conclusions.....	131
7.5	Future Work	133
REFERENCES.....		134
APPENDIX A: GRID SIZE SENSITIVITY ANALYSIS WITH CONVENTIONAL GRIDS		
140		
A.1	Fine-Grid Model	140
A.2	Medium-Grid Model	140
A.3	Coarse-Grid model	141

A.4	Ideal Trajectory	142
A.5	Trajectory-1	143
A.6	Trajectory-2	145
A.7	Trajectory-3	147
A.8	Optimized Cases Side Elements/Fine Grids Analysis	150
A.9	Analysis of Variations in Production Data/Steam Chamber	154
APPENDIX B: CMG SOFTWARE INTERFACE.....		160
APPENDIX C: MISCELLANEOUS TOPICS.....		166
C.1	Long-Term Optimization Work SAGD Simulation Run Times	166
C.2	Design of Short-Term Optimization Work	168
C.3	Downhole Installation of OCD's	178

LIST OF TABLES

Table 2-1: Pros and Cons of Different Types of FCD's	13
Table 3-1: MacKay River SAGD Projects Reservoirs Properties	27
Table 3-2: MacKay River SAGD Project McMurray Formation Reservoir Properties	27
Table 3-3: MacKay River SAGD Project Active Well Pairs Statistics	28
Table 3-4: MacKay River SAGD Project Well Pairs Production Data	28
Table 3-5: MacKay River SAGD Project Well Operating Pressure Constraints.....	29
Table 3-6: SAGD 3D Model Gridding Dimensions	32
Table 3-7: SAGD 3D Model Reservoir Properties	33
Table 3-8: SAGD 3D Model Fluid Components Definition and Critical Properties.....	33
Table 3-9: SAGD Model Bitumen/CH ₄ Densities, Compressibilities and Thermal Properties...	34
Table 3-10: Thermal Properties Used in the SAGD Model.....	34
Table 3-11: Relative Permeability Data for the SAGD Model.....	35
Table 3-12: Comparison of Calculated versus Measured Values for Dead Bitumen Viscosities	38
Table 3-13: Liquid Methane Viscosity use in the SAGD Model.....	39
Table 3-14: Default Values for K-Values from CMG STARS.....	40
Table 3-15: Comparison of Sink/Source and Flexible Wellbore Models.....	42
Table 3-16: SAGD Wells Operating Constraints During Circulation Stage	47
Table 3-17: SAGD Wells Operating Constraints During SAGD Stage	48
Table 4-1: Dimensions of Models for Grid Size Sensitivity Analysis with 2-m LGR.....	51
Table 4-2: Execution Times Grid Size Sensitivity Analysis Cases	67
Table 4-3: Summary of Differences in Production Performance Data and Execution Times.....	68
Table 5-3: Fixed Parameters in the Optimization Process.....	75
Table 6-1: Optimum Number of Ports for Top 5 Designs, Trajectory-1	87
Table 6-2: Summary of SAGD Performance Data at the End of SAGD Simulation, Trajectory-1	97
Table 6-3: Summary of SAGD Performance Data at the End of Optimized OCD's Case Simulation, Trajectory-1.....	97
Table 6-4: Optimum Number of Ports for Top 5 Designs, Trajectory-2	103

Table 6-5: Summary of SAGD Performance Data at the End of SAGD Simulation, Trajectory-2	110
Table 6-6: Summary of SAGD Performance Data at the End of Optimized OCD's Case Simulation, Trajectory-2.....	111
Table 6-7: Optimum Number of Ports for Top 5 Designs, Trajectory-3	117
Table 6-8: Summary of SAGD Performance Data at the End of SAGD Simulation, Trajectory-3	124
Table 6-9: Summary of SAGD Performance Data at the End of Optimized OCD's Case Simulation, Trajectory-3.....	125
Table 6-10: Summary of Different Trajectories OCD's Distributions	126
Table 6-11: Summary of SAGD Performance of Optimized OCD's Case, Trajectory-1 Super Fine Model	126
Table 6-12: Summary of SAGD Performance of Optimized OCD's Case, Trajectory-2 Super Fine Model	127
Table 6-13: Summary of SAGD Performance of Optimized OCD's Case, Trajectory-3 Super Fine Model	127
Table A-1: Deviations of Ideal Trajectory Models SAGD Performance Data from Fine-Grid Model	142
Table A-2: Deviations of Trajectory-1 Models SAGD Performance Data from Fine-Grid Model	144
Table A-3: Deviations of Trajectory-2 Models SAGD Performance Data from Fine-Grid Model	146
Table A-4: Deviations of Trajectory-3 Models SAGD Performance Data from Fine-Grid Model	148
Table C-1: Ultimate Optimum Solution for Injection FCD's (6-Year Forecast).....	169
Table C-2: Ultimate Optimum Solution for Production FCD's (6-Year Forecast)	170
Table C-3: NPV's of Case A and Case B at Different Stages	172

LIST OF FIGURES

Figure 2-1: Oil Sands Deposits in Alberta	7
Figure 2-2: Basic SAGD Concept.....	8
Figure 2-3: SAGD Stages	8
Figure 2-4: Orifice Type FCD	13
Figure 2-5: Helical Type FCD	13
Figure 2-6: Autonomous Type FCD	14
Figure 2-7: Tubing-Deployed and Liner-Deployed FCD's	15
Figure 2-8: ICD's Design Steps for Conventional Wells	19
Figure 2-9: Optimum Equalization Pressure Drop	19
Figure 2-10: ICD Flow-Pressure Correlation	20
Figure 2-11: Fluid Flow Profiles Into Different Types of Reservoirs	21
Figure 3-1: Canadian Oil Sands Projects	26
Figure 3-2: Suncor Leases Oil Sands Project	26
Figure 3-3: MacKay River Project Phase-1 Completion Type.....	30
Figure 3-4: MacKay River Project Phase-5 Completion Type.....	30
Figure 3-5: H1 Well Production Performance after FCD Installation	31
Figure 3-6: SAGD 3D Model View.....	32
Figure 3-7: SAGD 3D Model Single Block View	32
Figure 3-8: Dover UTF Phase B SAGD Pilot Project and Modified Relative Permeability Curves	36
Figure 3-9: Dead Bitumen Viscosity Curve used in the SAGD Model.....	37
Figure 3-10: Liquid Methane Viscosity Curve used in the SAGD Model	39
Figure 3-11: Wellbore/Reservoir Models Coupling Process	44
Figure 3-12: SAGD Producer/Injector Dual-String Completion Scheme	45
Figure 3-13: Sink/Source Wells Timeline View in CMG	46
Figure 3-14: Temperature Map of the SAGD Model at the end of Circulation Stage.....	46
Figure 3-15: Producer/Injector Wells During SAGD Stage	48
Figure 4-1: Coarse Grid Models for Different Trajectories with/without 2-m LGR.....	50
Figure 4-2: Coarse Grid Model Blocks with/without 2-m LGR.....	50

Figure 4-3: Coarse and Medium Local Grids Refinement.....	51
Figure 4-4: Ideal Trajectory, 2-m Model	52
Figure 4-5: Ideal Trajectory, 10-m Model with 2-m LGR.....	52
Figure 4-6: Ideal Trajectory, 20-m Model with 2-m LGR.....	52
Figure 4-7: Ideal Trajectory, 30-m Model with 2-m LGR.....	53
Figure 4-8: Ideal Trajectory, 36-m Model with 2-m LGR.....	53
Figure 4-9: Ideal Trajectory, 50-m Model with 2-m LGR.....	53
Figure 4-10: SAGD Performance Data of Different Ideal Trajectory Models with 2-m LGR.....	54
Figure 4-11: Early-Stage SAGD Temperature Maps of Different Ideal Trajectory Models	55
Figure 4-12: Trajectory-1, 2-m Model.....	56
Figure 4-13: Trajectory-1, 10-m Model with 2-m LGR	56
Figure 4-14: Trajectory-1, 20-m-Model with 2-m LGR.....	56
Figure 4-15: Trajectory-1, 30 m Model with 2-m LGR.....	57
Figure 4-16: Trajectory-1, 36-m Model with 2-m LGR	57
Figure 4-17: Trajectory-1, 50-m Model with 2-m LGR	57
Figure 4-18: SAGD Performance Data of Different Trajectory-1 Models with 2-m LGR	58
Figure 4-19: Early-Stage SAGD Temperature Maps for Different Trajectory-1 Models	59
Figure 4-20: Trajectory-2, 2-m Model.....	59
Figure 4-21: Trajectory-2, 10-m Model with 2-m LGR	60
Figure 4-22: Trajectory-2, 20-m Model with 2-m LGR	60
Figure 4-23: Trajectory-2, 30-m Model with 2-m LGR	60
Figure 4-24: Trajectory-2, 36-m Model with 2-m LGR	61
Figure 4-25: Trajectory-2, 50-m Model with 2-m LGR	61
Figure 4-26: SAGD Performance Data of Different Trajectory-2 Models with 2-m LGR	62
Figure 4-27: Early-Stage SAGD Temperature Maps for Different Trajectory-2 Models	63
Figure 4-28: Trajectory-3, 2-m Model.....	63
Figure 4-29: Trajectory-3, 10 m-Model with 2-m LGR	64
Figure 4-30: Trajectory-3, 20-m-Model with 2-m LGR.....	64
Figure 4-31: Trajectory-3, 30-m Model with 2-m LGR	64
Figure 4-32: Trajectory-3, 36-m Model with 2-m LGR	65
Figure 4-33: Trajectory-3, 50-m Model with 2-m LGR	65

Figure 4-34: SAGD Performance Data of Different Trajectory-3 Models with 2-m LGR	66
Figure 4-35: Early-Stage SAGD Temperature Maps for Different Trajectory-3 Models	66
Figure 4-36: Model Enhancement with LGR	68
Figure 5-1: Initial Locations of OCD's.....	72
Figure 5-2: OCD's Optimization Steps.....	76
Figure 5-3: OCD's # of Ports Optimization Process Workflow	77
Figure 5-4: Formulation of NPV Objective Function in Microsoft Excel.....	78
Figure 6-1: Trajectory-1 SAGD Well Pair Trajectories	82
Figure 6-2: Trajectory-1 and Well Completion Scheme for the Base Case	82
Figure 6-3: Trajectory-1 Tubing-Deployed OCD's Completion Diagram	83
Figure 6-4: Trajectory-1 OCD Optimization Results (Short-Term)	85
Figure 6-5: Trajectory-1 OCD Optimization Results (Long-Term)	86
Figure 6-6: Optimum OCD Case for Trajectory-1	86
Figure 6-7: Optimum Number of Ports for Top 5 Designs, Trajectory-1	87
Figure 6-8: Trajectory-1 Temperature Maps of the SAGD Model at Different Stages.....	88
Figure 6-9: Distribution of Injected Steam Among Trajectory-1 OCD's at the End of SAGD Project Life.....	89
Figure 6-10: Comparison of Tubing Inside Small and Large Diameter Slotted Liner	90
Figure 6-11: Changes in OCD's Contribution to Injected Steam with the Use of Smaller Slotted Liner, Trajectory-1	90
Figure 6-12: Trajectory-1 Optimum Case Injector Tubing/Annulus Pressure Profiles	92
Figure 6-13: Pressure Profiles Inside Long Injector Tubing for Optimized OCD's and Dual-String Cases, Trajectory-1	93
Figure 6-14: Annular Pressure Profiles, Optimized OCD and Dual-String Cases, Trajectory-1 ..	93
Figure 6-15: Steam Chamber Growth of the Optimized OCD and Dual-String Cases, Trajectory-1	94
Figure 6-16: Distribution of Injected Steam at Different Points, Trajectory-1 at the End of Year 1	95
Figure 6-17: SAGD Performance Data of Optimized OCD and Dual-String Cases, Trajectory-1	96
Figure 6-18: Trajectory-2 SAGD Well Pair Trajectories	98

Figure 6-19: Trajectory-2 and Well Completion Scheme for the Base Case	99
Figure 6-20: Trajectory-2 Tubing-Deployed OCD's Completion Diagram	100
Figure 6-21: Trajectory-2 OCD's Optimization Results (Short-Term)	101
Figure 6-22: Trajectory-2 OCD's Optimization Results (Long-Term)	102
Figure 6-23: Optimum OCD Case for Trajectory-2	102
Figure 6-24: Optimum Number of Ports for Top 5 Designs, Trajectory-2.....	103
Figure 6-25 Trajectory-2 Temperature Maps of the Optimized OCD's Case SAGD Model at Different Stages	104
Figure 6-26: Distribution of Injected Steam Among Trajectory-2 OCD's at the End of SAGD Project Life.....	105
Figure 6-27: Trajectory-2 Optimum Case Injector Tubing/Annulus Pressure Profiles.....	106
Figure 6-28: Pressure Profiles Inside Long Injector Tubing for Optimized OCD's and Dual-String Cases, Trajectory-2	107
Figure 6-29: Annular Pressure Profiles, Optimized OCD and Dual-String Cases, Trajectory-2	107
Figure 6-30: Steam Chamber Growth of the Optimized OCD and Dual-String Cases, Trajectory-2	108
Figure 6-31: Distribution of Injected Steam at Different Points, Trajectory-2 at the End of Year 1	109
Figure 6-32: SAGD Performance Data of Optimized OCD's and Dual-String Cases, Trajectory-2	110
Figure 6-33: Trajectory-3 SAGD Well Pair Trajectories	112
Figure 6-34: Trajectory-3 and Well Completion Scheme for the Base Case	113
Figure 6-35: Trajectory-3 Tubing-Deployed OCD's Completion Diagram	114
Figure 6-36: Trajectory-3 OCD's Optimization Results (Short-Term)	115
Figure 6-37: Trajectory-3 OCD's Optimization Results (Long-Term)	116
Figure 6-38: Optimum OCD Case for Trajectory-3	116
Figure 6-39: Optimum Number of Ports for Top 5 Designs, Trajectory-3.....	117
Figure 6-40: Trajectory-3 Temperature Maps of the Optimized OCD's Case SAGD Model at Different Stages	118
Figure 6-41: Distribution of Injected Steam Among Trajectory-3 OCD's at the End of SAGD Project Life.....	119

Figure 6-42: Trajectory-3 Optimum Case Injector Tubing/Annulus Pressure Profiles	120
Figure 6-43: Pressure Profiles Inside Long Injector Tubing for Optimized OCD's and Dual-String Cases, Trajectory-3	121
Figure 6-44: Annular Pressure Profiles, Optimized OCD and Dual-String Cases, Trajectory-2	121
Figure 6-45: Steam Chamber Growth of the Optimized OCD and Dual-String Cases, Trajectory-3	122
Figure 6-46: Distribution of Injected Steam at Different Points, Trajectory-3 at the End of Year 1	123
Figure 6-47: SAGD Performance Data of Optimized OCD's and Dual-String Cases, Trajectory-3	124
Figure 6-48: Comparison of NPV for Different Trajectories	125
Figure A-1: Fine Grid System (12.5-m in Axial Direction)	140
Figure A-2: Medium Grid System (25-m in Axial Direction)	141
Figure A-3: Coarse Grid System (50-m in Axial Direction)	141
Figure A-4: SAGD Performance Data of Ideal Trajectory Models of Different Grid Systems .	142
Figure A-5: Temperature Maps of Ideal Trajectory Models of Different Grid Systems	143
Figure A-6: Trajectory-1 Model Well Pair Trajectory	143
Figure A-7: SAGD Performance Data of of Trajectory-1 Models of Different Grid Systems..	144
Figure A-8: Temperature Maps of Trajectory-1 Models of Different Grid Systems	145
Figure A-9: Trajectory-2 Model Well Pair Trajectory	145
Figure A-10: SAGD Performance Data of Trajectory-2 Models of Different Grid Systems	146
Figure A-11: Temperature Maps of Trajectory-2 Models of Different Grid Systems	147
Figure A-12: Trajectory-3 Model Well Pair Trajectory	147
Figure A-13: SAGD Performance Data of Trajectory-3 Models of Different Grid Systems	148
Figure A-14: Temperature Maps of Trajectory-3 Models of Different Grid Systems	149
Figure A-15: Temperature Maps with Different Side Elements Grid Sizes, Trajectory-1	151
Figure A-16: SAGD Performance Data of Trajectory-1 Model wth Different Side Elements Grid Sizes	151
Figure A-17: Temperature Maps with Different Side Elements Grid Sizes, Trajectory-2	152
Figure A-18: SAGD Performance Data of Trajectory-2 Model wth Different Side Elements Grid Sizes	152

Figure A-19: Temperature Maps with Different Side Elements Grid Sizes, Trajectory-3	153
Figure A-20: SAGD Performance Data of Trajectory-3 Model with Different Side Elements Grid Sizes	153
Figure A-21: Effect of Block Size on Modeling Trajectory Excursion Points	154
Figure A-22: Modeling of Heat Transfer by Conduction with Fine and Coarse Grid Blocks....	155
Figure A-23: Unswept Zones Due to FlexWell/STARS Coupling.....	156
Figure A-24: Wellbore Configuration Modeling in SAGD Using FlexWell	157
Figure A-25: Wellbore Configuration Modeling in SAGD Using Simple Sink/Source Models	157
Figure A-26: Temperature Maps of Ideal Trajectory SAGD Models with Sink/Source Well Models	158
Figure A-27: Production Data of Ideal Trajectory SAGD Model with Sink/Source Well Models	158
Figure A-28: Effect of Properties Averaging Among Coarse/ Fine Grid Systems in SAGD Models	159
Figure A-29: Effect of Properties Changes on Steam Trap	159
Figure B-1: CMG CMOST Engines	160
Figure B-2: Optimization Parameters Assignment in CMG CMOST	160
Figure B-3: Optimization Parameters Objective Function CMG CMOST	161
Figure B-4: Design of Experiments in CMG CMOST	161
Figure B-5: Experiment Design QC in CMG CMOST	162
Figure B-6: CMG CMOST DECE Optimizer Algorithm.....	162
Figure B-7: Optimization Cases Steam Injection Rates in CMG CMOST	163
Figure B-8: Optimization Cases Oil Production Rates in CMG CMOST	163
Figure B-9: NPV Objective Function in CMG CMOST	163
Figure B-10: Trajectory-1 OCD's Modeling in CMG.....	164
Figure B-11: Trajectory-1 OCD's Optimization Experiment Design Quality Check	164
Figure B-12: Trajectory-2 OCD's Modeling in CMG.....	164
Figure B-13 Trajectory-2 OCD's Optimization Experiment Design Quality Check	165
Figure B-14: Trajectory-3 OCD's Modeling in CMG.....	165
Figure B-15: Trajectory-3 OCD's Optimization Experiment Design Quality Check	165
Fig C-1: Trajectory-1 Optimization Top 50 Cases Simulation Run Times	166

Fig C-2: Trajectory-1 Optimization Top 50 Cases Recovery Factors	166
Fig C-3: Trajectory-2 Optimization Top 50 Cases Simulation Run Times	167
Fig C-4: Trajectory-2 Optimization Top 50 Cases Recovery Factors	167
Fig C-5: Trajectory-3 Optimization Top 50 Cases Simulation Run Times	168
Fig C-6: Trajectory-3 Optimization Top 50 Cases Recovery Factors	168
Figure C-7:Optimization of Number of Ports for Injection FCD's (16-Month Forecast)	169
Figure C-8:Optimization of Number of Ports for Production FCD's (2-Year Forecast)	170
Figure C-9:Camaprison of NPV's of Case A and Case B	171
Figure C-10:Temaprature Maps of Case A and Case B	172
Figure C-11: Short-Term Cases Ranking Based on NPV, Trajectory-1	173
Figure C-12: Short-Term Ranked Cases and Long-Term Run Candidates, Trajectory-1	174
Figure C-13: Long-Term Run Cases NPV's, Trajectory-1	174
Figure C-14: Short-Term Cases Ranking Based on NPV, Trajectory-2	175
Figure C-15: Short-Term Ranked Cases and Long-Term Run Candidates, Trajectory-2	175
Figure C-16: Long-Term Run Cases NPV's, Trajectory-2	176
Figure C-17: Short-Term Cases Ranking Based on NPV, Trajectory-3	176
Figure C-18: Short-Term Ranked Cases and Long-Term Run Candidates, Trajectory-3	177
Figure C-19: Long-Term Run Cases NPV's, Trajectory-3	177
Figure C-20: Variflux TM Steam Splitter	178
Figure C-21: OptiSteam TM Steam Splitter	178
Figure C-22: Single OCD Set Composed of Two Pieces of OCD Devices	179

LIST OF SYMBOLES AND ABBRIVATIONS

SYMBOLS

P_{up}	Upstream pressure, Pa
ρ_o	Upstream mass density of oil, kg/m^3
ρ_w	Upstream mass density of water, kg/m^3
ρ_g	Upstream mass density of gas, kg/m^3
f_o	Mass fractions of oil
f_w	Mass fractions of water
f_z	Mass fractions of gas
A_{up}	Upstream area, m^2
A_{dw}	Downstream area, m^2
F_p	Ratio of downstream and upstream pressure
C_{vo}	Heat capacity of oil at constant volume, J/(kg-C)
C_{vw}	Heat capacity of water at constant volume, J/(kg-C)
C_{vg}	Heat capacity of gas at constant volume, J/(kg-C)
M	Molecular mass
Z	Gas compressibility factor
R	Gas compressibility factor
Q^*	Critical flow rate, m^3/S
A	Orifice area, m^2
ρ	Mixture mass density, kg/m^3
C_d	Gas discharge coefficient, dimensionless
C_{di}	Gas discharge coefficient as read in data, dimensionless
Q	Subcritical flow rate, m^3/S
F_p^*	Critical pressure ratio
Δp	Friction pressure loss, Pa
K	Dimensionless factor
v	Velocity, m/s
ff	Fanning friction factor

L	Device Length, m
w_r	dimension parameter
D_h	Hydraulic diameter of the channel
R_t	Revenue, (\$)
E_t	Operation expenses, (\$)
C_{Capex}	Capital expenses, (\$)
D	Annual discount factor
T_p	Project life time, years
t_p	Project time step, years
Q_o	Oil production rate, (STB/D)
Q_w	Steam injection rate, (bbl of CWE/D)
r_o	Oil price, (\$/STB)
r_w	Steam cost, (\$/bbl of CWE)
t_k	Simulation time step
t_{ref}	Reference time, days
P	Pressure
T	Temperature
k_{v1}	Constant-1 for specific gases
k_{v2}	Constant-2 for specific gases
k_{v3}	Constant-3 for specific gases
k_{v4}	Constant-4 for specific gases
k_{v5}	Constant-5 for specific gases
P	Pressure (Pa)
L	Length (m)
ρ_m	Mixture density (g/m ³)
V_m	Mixture velocity (m/s)
F	Friction loss (m ² /s ²)
θ	Inclination angle
g	Gravity (m/s ²)
H_m	Mixture Enthalpy (J/g)
Q	Radial heat transfer rate (J/g)
ρ_p	Phase molar density (gmol/m ³)

V_p	Phase flow rate (m^3/s)
$m_{p,i}$	Phase mole fraction
B	Section volume (m^3)
ϕ_f	Fluid porosity fraction
S_p	Phase fraction (m^3/m^3)
H_p	Phase molar enthalpy (J/gmol)
B	Section Volume (m^3)
U_p	Phase internal energy (J/gmol)
U_w	Wall enthalpy (J/m^3)
ϕ_w	Wall porosity (fraction)
K	Gas-liquid equilibrium factor

ABBREVIATIONS

3D	Three-Dimensional
AERI	Alberta Energy Resources Inc.
AOSTRA	Alberta Oil Sands Research Technology Authority
BHP	Bottom Hole Pressure
CMG	Computer Modeling Group
cSOR	Cumulative Steam-Oil Ratio
CWE	Cold Water Equivalent
DE	Differential Evolution
DECE	Designed Exploration and Controlled Evolution
FCD's	Flow Control Devices
ICD's	Inflow Control Device
LGR	Local Grid Refinement
LHC	Latin Hypercube
MOP	Maximum Operating Pressure
OBIP	Original Bitumen in Place
OCD's	Outflow Control Devices
OF	Objective Function
PO	Proxy Optimization
PS	Particle Swarm Optimization
QC	Quality Check
RS	Random Search
SAGD	Steam-Assisted Gravity Drainage
TVD	True Vertical Depth
UTF	Underground Test Facility

CHAPTER ONE: INTRODUCTION

1.1 Background

Steam-Assisted Gravity Drainage (SAGD), first proposed by Dr. Roger Butler, is an advanced form of thermal recovery technology. SAGD is currently being widely adopted in developing the vast Canadian oil sands deposits distributed in three major areas in Alberta: Athabasca, Cold Lake and Peace River (Li et al. 2006).

SAGD technology involves drilling two horizontal wells, one above the other. The upper well is the steam injector, and the lower one is the producer well with a typical vertical spacing of 4-6m. Both wells are located close to the base of the reservoir formation. High-quality steam with high temperature is injected through the injector at certain points to transmit its latent heat to the reservoir bitumen. The heated bitumen flows towards the producer by the force of gravity.

The history of commercial-scale SAGD projects in Canada is relatively new. Examples of these SAGD projects in Western Canada are: Cenovus Foster Greek, Devon Jackfish, Suncor MacKay River, MEG Christina Lake, StatOil Leismer, Suncor Firebag and CNRL's Kirby South project (Ghesmat and Zhao 2015).

Any oil recovery technology has its own challenges and complications, and SAGD technology is not an exception. There are several challenges and concerns that have been reported on ongoing SAGD projects. Some of these problems include inefficient steam chamber growth, high cSOR, live steam production and low bitumen recovery (Ghesmat and Zhao 2015). The research work in this thesis is an attempt to alleviate some of these challenges.

1.2 Problem Statement

In SAGD operations, a dual-string tubing system is considered as the default completion scheme. For both injector and producer, a short tubing is landed at the heel section of the well, and a long tubing is extended all the way to the wellbore toe. This completion scheme offers two injection points along the well, and that leads to better steam chamber conformance than injecting steam at a single point only.

However, reservoir complications, such as reservoir heterogeneity, well pair trajectory excursions (i.e., undesired deviations in well pair trajectories that have been unintentionally generated during drilling operations), reservoir heterogeneities, bottom water, gas cap, mud barriers, and low reservoir ceiling, may lead to a non-uniform steam chamber growth, steam breakthrough, and heat

losses to the cap rock. Direct impact of these factors is reflected in low bitumen recovery, high cumulative Steam-Oil Ratio (cSOR) and waste of steam energy, leading to suboptimal operating conditions and inefficient project economics. Hence, the implementation and operation of SAGD becomes more challenging and overall project economics may be compromised. Most SAGD operators have reported less than 50% steam chamber conformance over the wellbore length during the first several years of wellbore operation, resulting in a significant impact on wellbore productivity and reservoir recovery ratio (Riel et al. 2014). To overcome these challenges, some SAGD operators have adopted Flow Control Devices (FCD's) to improve project economics by maximizing the ultimate bitumen recovery and minimizing the cSOR (Noroozi et al. 2015).

1.3 Research Hypothesis

Research hypothesis for this study is that trajectory excursions in the horizontal direction of SAGD injector and producer wells would impact the steam chamber growth, result in uneven subcool liquid level, cause poor sweep efficiency and, ultimately, lead to a suboptimal SAGD process. These unfavorable impacts are mainly due to the variable subcool level: intervals of thick subcool contribute less to the production and steam chamber growth in these intervals is slower. On the other hand, intervals with thin subcool are prone to the steam breakthrough phenomenon which reduces the energy efficiency of the operation and can compromise the integrity of the wellbore completion. Deployment of flow control devices at designated locations can help adjust the amounts of injected/produced fluids to achieve an even subcool level, a uniform steam chamber growth and ultimately an efficient SAGD process.

1.4 Research Objectives

Flow Control Devices (FCD) have been used with success in the conventional oil and gas industry for several years to control water and gas breakthrough (Riel et al. 2014). However, the implementation of these FCD's in SAGD wells is relatively recent. For instance, ConocoPhillips's first use of FCD's was in Surmont field SAGD project in 2009 (Stalder 2013). Suncor implemented its first FCD pilot in Suncor's MacKay River project in 2011 (Suncor Energy 2015). Further examples include Cenovus Pelican Lake in 2012, Husky Tucker in 2011 and 2012, Devon Jackfish in 2011, Nexen Long Lake in 2013, and Shell Orion in 2012 (Ghesmat and Zhao 2015).

In SAGD operations, FCD's offer a great flexibility in controlling the injection and production operations along the horizontal wells. FCD's in SAGD injectors are called Outflow Control

Devices (OCD's) or steam splitters, and they are meant to enhance steam conformance, control the amount of injected steam and steer injected steam towards designated areas via zonal steam injection. In SAGD producers, FCD's are known as Inflow Control Devices (ICD's), and they are used to create uniform inflow along the horizontal section of well and to maximize heated bitumen production while minimizing live steam production.

There are limited studies in the literature that have addressed the issue of wellbore completion design using FCD's' (Kaiser et al. 2000; Kumar et al. 2010; Livescu et al. 2010; Al Marzouqi et al. 2010; Noroozi et al. 2015). Hence, the FCD response in SAGD operations is not fully understood as the need for deeper understanding of their behavior has been brought up by several SAGD operators. Furthermore, none of these studies has addressed the implementation of FCD's in SAGD projects with well pair trajectory excursions.

The work in this research aims to enhance the SAGD performance by implementing the OCD's in the injection wells and optimizing the OCD parameters in terms of the number of OCD's, their locations, and number of ports. The optimization studies in this research focus on three different trajectory excursion scenarios (Trajectory-1, Trajectory-2 and Trajectory-3). For each scenario, the goal is to minimize/neutralize the negative impact of trajectory excursions by deploying OCD's at certain locations among the injector and then optimizing the number of ports for each OCD using a certain optimization workflow and tool.

1.5 Methodology

SAGD models with three different well pair trajectory excursion scenarios are built and investigated in this research. These scenarios were specified to reflect the actual cases that usually exist in real-world SAGD projects. OCD's were deployed and optimized to minimize the negative impact of trajectory excursions by promoting steam chamber conformance. Details of these three scenarios are described herein:

Trajectory-1 mimics one of the common practices in drilling SAGD well pairs, which is drilling the producer first, by following certain paths close to the base of the reservoir, aiming to maximize reserves recovery. This is then followed by drilling a horizontal injector which does not follow the producer trajectory. This scenario leads to variations in TVD vertical distances along the well pair path. Trajectory-2 is another customary practice. It is like Trajectory-1, but the injector is drilled following the same trajectory as the drilled producer with a constant separating distance of 5-m. In Trajectory-3, the producer and injector follow more complex trajectories with variable lateral

separating distances ranging from three meters at the narrowest point to seven meters at the widest point.

This research proposes an optimization workflow for determining the number of ports for each OCD for different wellbore trajectories with predetermined OCD locations. The basic SAGD model and wellbore completion scheme are the same for all cases. A coupled wellbore-reservoir simulation model is constructed using CMG's FlexWell for wellbore hydraulics modeling and STARS for thermal reservoir simulations. The default optimization tool that is utilized in the optimization work in this research is a tool developed by CMG, called CMOST. CMOST is an integrated optimization, history matching, sensitivity analysis tool that contains several optimization algorithms.

The completion scheme for all optimization case studies is the same. The injector is equipped with a 9 5/8" slotted liner and a 4 1/2" tubing that accommodates the OCD's. The producer is equipped with a dual-string completion scheme which is composed of 9 5/8" slotted liner accommodating short and long 4 1/2" tubings landed at the heel and toe sections, respectively. The performance of the completion equipped with the optimized OCD's is compared to its corresponding conventional default dual-string completion scheme where both injector and producer have slotted liner accommodating short and long tubings.

1.6 Thesis Layout

The work in this thesis is divided into seven chapters as follows:

Chapter 1: contains a brief introduction to SAGD technology, statement of the problem, research hypothesis, research objectives, methodology and general thesis layout.

Chapter 2: provides a general overview of SAGD concept, and a review of different types of Flow Control Devices along with features, implementation and modeling in SAGD wells. This chapter presents the basic equations that have been used to model FCD's in SAGD simulation based on published papers. Furthermore, this chapter summarizes some of the previous optimization case studies of SAGD operations using FCD's along with a critical review and identification of research gaps that emphasizes the importance of this research objectives.

Chapter 3: describes the construction of the base-case SAGD model that is used throughout this research. The chapter is continued with a summary of Suncor MacKay River SAGD project that was used to guide the input parameters of the base-case model.

Chapter 4: provides a detailed grid size sensitivity analysis using conventional simulation grids enhanced with Local Grid Refinement (LGR).

Chapter 5: covers the steps, details and construction of the optimization procedure using CMG CMOST optimization tool. Details include choice and design of the optimization objective function, basic assumptions, and input parameters.

Chapter 6: presents OCD's optimization case studies for different SAGD well pair trajectory excursions generated from the basic SAGD simulation model constructed in Chapter 3.

Chapter 7: discusses the results of the optimization case studies, summarizes findings, draws conclusions, and provides recommendations for further research beyond the scope of this research.

CHAPTER TWO: LITERATURE REVIEW

2.1 Overview of SAGD Technology

Steam-Assisted Gravity Drainage (SAGD) technology was originally proposed by Dr. Roger M. Butler (Butler et al. 1981; Butler and Stephens 1981). SAGD is a concept of in-situ thermal oil recovery from extra heavy oil and tar sands reservoirs where in-situ bitumen viscosity is so high that it cannot easily flow. A typical SAGD process involves drilling two horizontal wells one above the other with a typical true vertical depth (TVD) spacing of 4-6 m. Both wells are located near the bottom of the target reservoir. The upper well is the steam injection well, and the lower one is the producer well. High-temperature, high-quality steam is injected through the injector to form a steam chamber and give up its latent heat to the bitumen and reduce its viscosity. The heated bitumen drains towards the producer by the force of gravity (Butler 1991).

2.1.1 History and Statistics of SAGD

Alberta alone has the third largest oil reserves in the world (following Venezuela and Saudi Arabia) with total proven reserves of 165.4 billion barrels and crude bitumen production of 2.5 million barrels per day (mined and in-situ production) as of 2016 (Alberta's Energy Reserves and Supply/Demand Outlook Report 2017). However, more than 80% of proven reserves are too deep for conventional open-pit mining. Thus, in-situ technologies including SAGD draw attention as feasible means of production (Fermaniuk 2013).

History of commercial SAGD projects in Alberta is relatively new (less than five SAGD projects in 2000). However, this number of SAGD projects in Alberta increased steadily until it reached more than 16 projects by 2012. By 2022, in-situ production forecast is to reach 2.2 million barrels per day (AER SAGD Report 2013). **Figure 2-1** shows major areas of oil sands deposits concentration in Alberta.

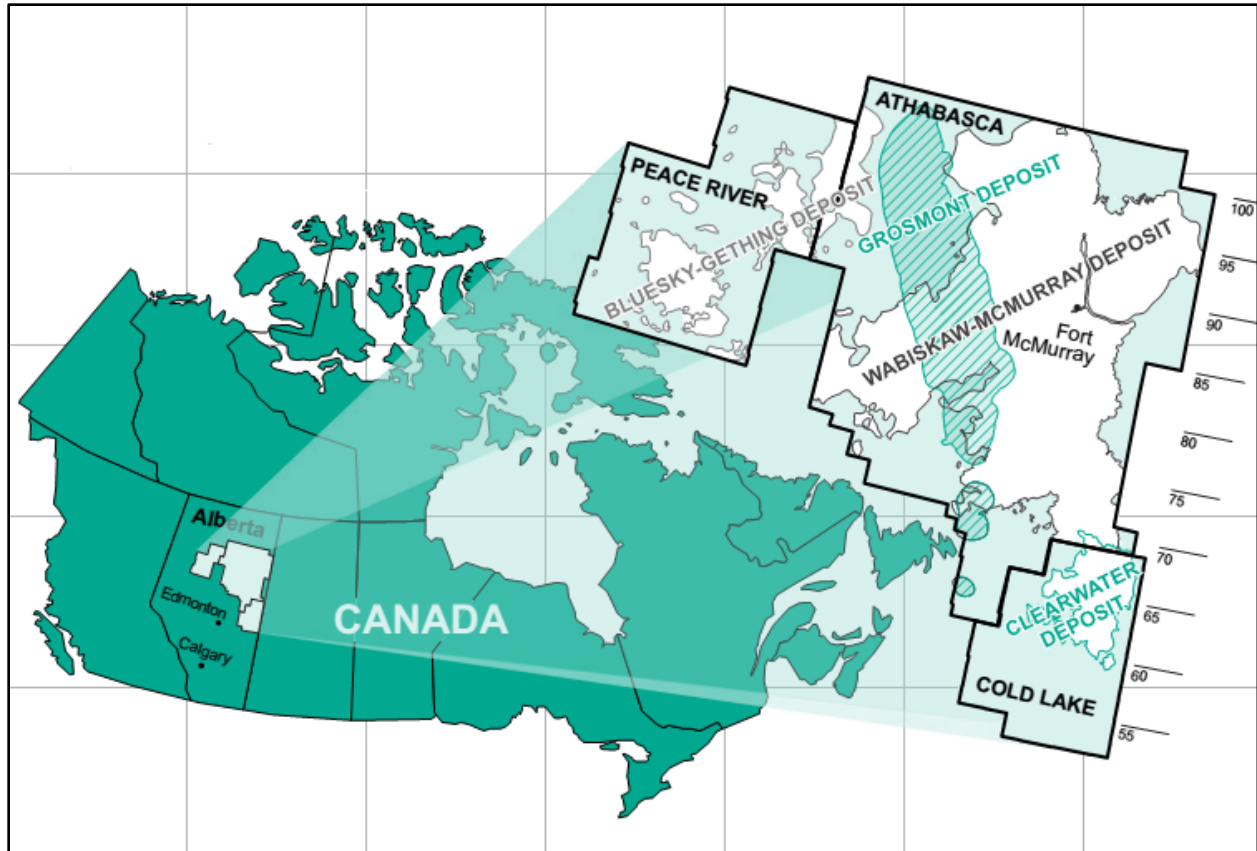


Figure 2-1: Oil Sands Deposits in Alberta, (Alberta's Energy Reserves and Supply/Demand Outlook Report 2017)

2.1.2 Basic Concept of SAGD

Before introducing the concept, Butler et al. (1981) pointed out that conventional thermal recovery means such as Cyclic Steam Stimulation (CSS) and Steam Flood (SF) have a major common problem: Poor sweep efficiency due to fingering phenomena caused by steam and hot water which have much less viscosity than that for the oil Butler et al. (1981).

Starting from the problem stated above, Butler et al. (1981) developed SAGD, where continuous steam could be provided while heated oil is being removed continuously. Butler et al. (1981) pointed out three main features of the process as shown in **Figure 2-2**. These are: (1) steam condensation at steam chamber interface, (2) drainage of heated oil and condensed steam to the bottom well by the force of gravity, and (3) upward and lateral growth of steam chamber.

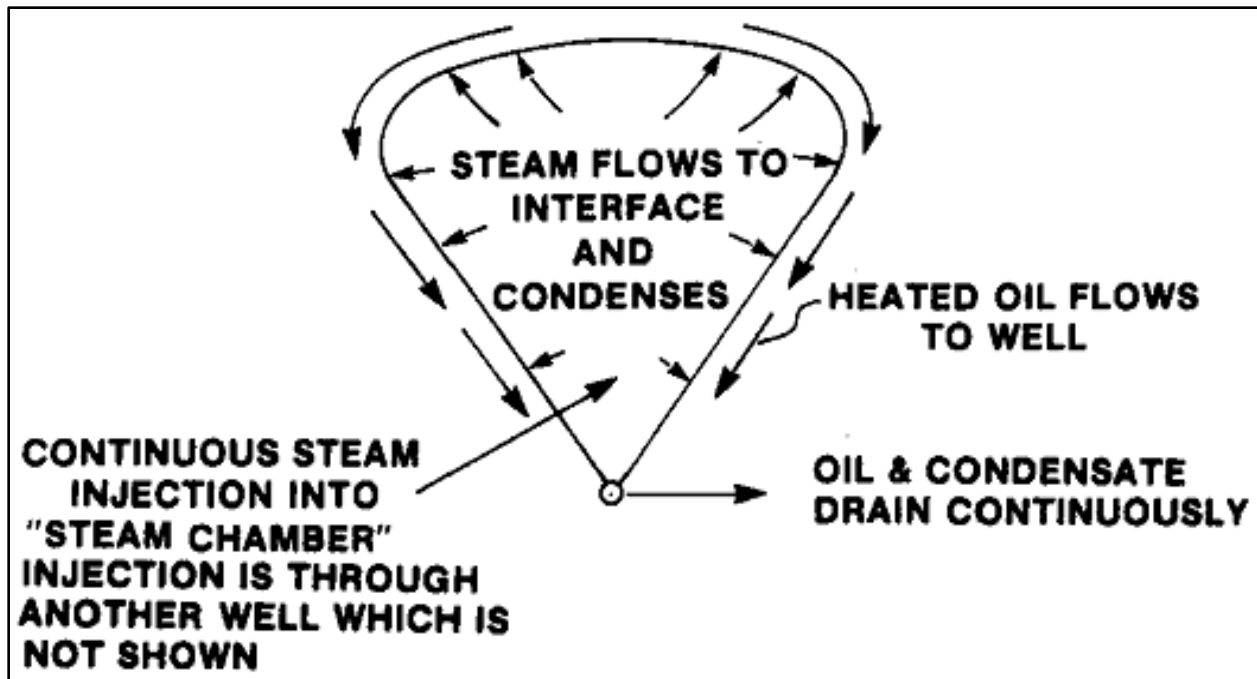


Figure 2-2: Basic SAGD Concept, (Butler et al. 1981)

2.1.3 SAGD Stages

A typical SAGD process involves four major stages: start-up stage, ramp-up stage, conventional SAGD stage, and blowdown stage. These stages are illustrated in Figure 2-3.

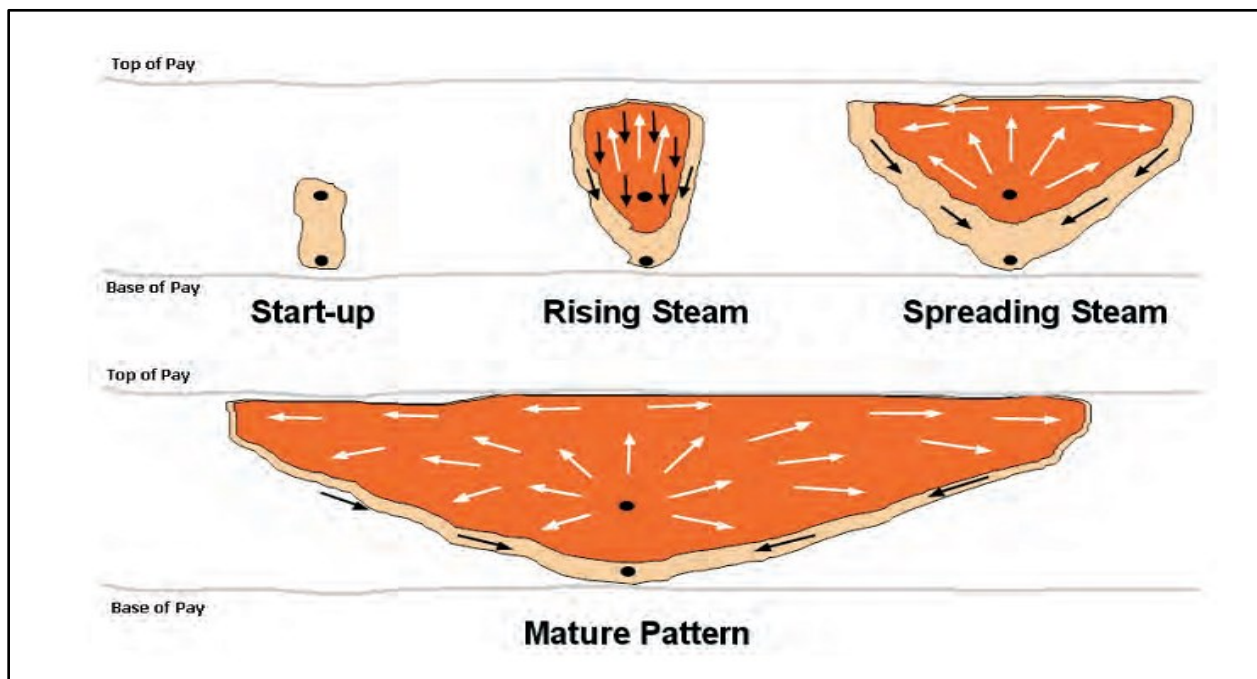


Figure 2-3: SAGD Stages, (Cenovus Telephone Lake Project Report 2011)

Start-up Stage

Start-up is the first stage in SAGD process. The main purpose of this stage is establishing enough thermal and hydraulic communication in the vertical spacing between the injector and producer. There are several types of SAGD start-up methods that will be discussed next.

Circulation Start-up

Circulation start-up is the most common start-up technique, where high-quality steam (typically 90% quality or higher) is conveyed through the long tubing all the way to the toe in both injector and producer wells and then circulated back to surface through the casing annulus. During this circulation process, the steam condenses as it loses its latent heat to the surrounding bitumen. In other words, bitumen is heated by thermal conduction. Also, it is important to keep the injection pressure below a certain level to avoid fracturing the formation (Cenovus Telephone Lake Project Report 2011).

The circulation operation continues until the bitumen viscosity falls to a point that allows the bitumen flow and the desired thermal and hydraulic communications between the wells are established. A typical circulation duration is 1-3 months depending on several factors such as reservoir quality in the vicinity of the SAGD well pair, vertical spacing between the injector and producer, injected steam quality, reservoir pressure and injection pressure (Cenovus Telephone Lake Project Report 2011).

Electrical Heater Start-up

This start-up technique involves utilizing downhole electrical heaters which are installed in the injector and producer. In these heaters, electrical energy is converted into a magnetic field that promotes heat transfer by radiation.

Electrical heater is a good and effective replacement for conventional circulation start-up technique, especially when the steam injection facilities and infrastructure are not ready yet. Typical duration of electrical heater start-up is the same as circulation start-up duration, which is 1-3 months (Cenovus Telephone Lake Project Report 2011). An example of electric heater start-up is the Wet Electric Heating process, where its applications have been tested and investigated at the lab and field scales for Athabasca and Cold Lake/Lloydminster heavy oil (Yuan et al. 2004).

Dilation Start-up

This start-up technique is useful when reservoir properties (particularly porosity and permeability) are poor and require enhancement. In this case, certain amounts of either cold water or steam are injected at pressure levels slightly higher than formation fracturing pressure to fracture the

formation and enhance the porosity and permeability. The most important issue in this technique is close monitoring of injection pressure in order to ensure that the above-fracturing pressure won't cause fracture propagation towards the reservoir cap rock or any direction other than in-between the injector and producer (Cenovus Telephone Lake Project Report 2011).

Maintaining an appropriate injection pressure will yield the required shear dilation of the formation between the SAGD well pair. This shall increase the wells productivity/injectivity indices by creating a negative skin, enhanced inter-well hydraulic communication, accelerated inter-well convection heating and increased fluid mobility (Collins 2005). Increased porosity and permeability dilation zones between SAGD well pairs have been created in Christina Lake SAGD project operated by Cenovus (Cenovus Christina Lake In-situ Oil Scheme 2012).

Bullheading Start-up

Bullheading start-up technique is preferred when reservoir fluids initially have enough mobility. Steam is injected through the long tubing but without circulating the steam back to the surface as in conventional circulation start-up, i.e., the entire injected steam is forced to leak-off into the formation. Hence, the heat is transferred to the medium by convection. Since there is no return steam to be circulated back to the surface, bullheading has a great advantage over conventional circulation in terms of thermal efficiency, operational simplicity, and steam requirement. However, one of this technique's drawbacks is the fact that steam injection rate may be too slow due to injection pressure limitations. Another drawback is the high possibility of losing more heat to bottom water in case of SAGD reservoirs with bottom water.

In 2011, simulation studies and field trials were carried out on Pad 107 of Suncor Firebag in-situ project. Pad 107 has 14 well pairs with each well having horizontal length of 1,000 m and well pairs having spacing of 90 m and TVD lateral separation of 5-6 m between the producer and injector. Six out of the 14 wells were scheduled for bullheading start-up, and the remaining eight wells underwent circulation. Both bullheaded and circulated wells were distributed in a sequential manner in order to evaluate the effectiveness of each start-up technique.

Bullheaded wells were found to be much easier to operate compared to those circulated ones. Also, bullheaded wells reached an effective steady steaming rate under the designated Maximum Operating Pressure (MOP), while the circulated wells required constant scrutiny and adjustment of steam injection rates and pressures to maintain fluid returns (Anderson and Kennedy 2012).

FCD's are sometimes used in bullheading for a more uniform and effective distribution of steam and steam energy along the horizontal section of the well.

Solvent Assisted Start-up

According to a project description report about Cenovus Telephone Lake Project (2011), conventional circulation start-up technique can be enhanced, especially in terms of duration by utilizing solvents. Certain solvents (typically xylene or combinations of light hydrocarbon fluids such as diesel, toluene, butane, pentane, and hexane) are injected into the formation and allowed to soak for a period of time. This helps in reducing the high bitumen viscosity to a certain level and subsequently less steam and less circulation duration will be required for the whole start-up stage (Cenovus Telephone Lake Project Report 2011).

Ramp-up Stage

After the start-up stage and establishment of thermal and hydraulic communications, steam is no longer circulated back to the surface, and is injected through the injector only. Heated bitumen and steam condensate are drained and collected at the producer.

During the ramp-up stage, two phenomena take place: One is that the established thermal and hydraulic communications propagate axially along the well pair. The other is the vertical expansion of steam chamber until it hits the top of the reservoir. Ramp-up stage requires steam chamber pressure to be maintained within the MOP. When the inter-well region over the entire length of the well pair has been heated and the developed steam chamber has reached the reservoir top, the oil production rate peaks and begins to decline while the steam injection rate reaches a maximum and levels off (Cenovus Telephone Lake Project Report 2011).

SAGD Stage

Once ramp-up stage is complete and full vertical growth of steam chamber has been achieved, conventional SAGD stage begins where steam chamber starts to expand laterally. During this period, a considerable amount of heat loss occurs to the cap rock, and that leads to lower bitumen production at fixed steam injection rates.

Also, during this SAGD stage, it is extremely important to maintain a certain reservoir subcool level, i.e., the differential temperature between the steam chamber and the production well should be maintained at a fixed value as much as possible. Appropriate reservoir subcool prevents steam breakthrough and live steam production at the producer by keeping the producer submerged in the liquid (heated bitumen and condensed steam). Excessive live steam production is an unfavorable condition as it causes further problems and complications such as waste of energy and damage to

the downhole completion system. SAGD stage continues until at least 50% of the original bitumen in place (OBIP) is produced and steam injection rate will usually be ramped-down to zero by the end of this stage (Cenovus Telephone Lake Project Report 2011).

Blowdown Stage

Blow-Down stage begins by the end of SAGD stage where steam injection is replaced by a non-condensable gas such as air, mainly to maintain the steam chamber pressure. During this stage, bitumen production rate continues to decline due to slow rate of lateral steam chamber growth. This bitumen production rate decline is allowed until the economic level is reached. Usually, at least 65% of original bitumen production will have been produced by the end of this stage (Cenovus Telephone Lake Project Report 2011).

2.2 Flow Control Devices

The term FCD refers to Flow Control Device. In practice, injection well FCD is known as Outflow Control Device (OCD) and production well FCD is known as Inflow Control Device (ICD). All FCD's follow the same design concept which is, creating flow restriction by imposing an additional pressure drop. First implementation of FCD's was in Nork Hydro's Troll field in 1998 (Al Marzouqi et al. 2010).

FCD is a small device installed along a horizontal section of the well to optimize the outflow/inflow profile inside the horizontal well. This optimized outflow/inflow profile has several advantages such as production optimization, and controlling and delaying water breakthrough (Bybee 2008; Al Marzouqi et al. 2010).

2.2.1 Types of Flow Control Devices

There are three major types of FCD's, and they share the same principle which is creating flow restriction by imposing an additional pressure drop. These device types vary in how this additional pressure drop is created (Bybee 2008; Banerjee et al. 2013). **Table 2-1** summarizes the types and pros and cons of the three FCD types.

Table 2-1: Pros and Cons of Different Types of FCD's, (Banerjee and Hascakir 2017)

Type	Mechanism of Action	Strengths for SAGD Applications	Weakness for SAGD Applications
Channel-Style FCD	Friction drag	Low risk of plugging/erosion	Sensitive to flowing fluid viscosity
		May control steam flushing	
		No moving parts	
Restriction-Style FCD	Bernoulli principle	Inexpensive	Significant risk of plugging /Erosion
		No moving parts	May cause steam flashing
Autonomous FCD	Varied	Additional steam trap control	Varied

Orifice Type Flow Control Devices

The orifice type FCD is also known as tube/nozzle type or restriction-style. An example of orifice type flow control device is shown in **Figure 2-4**. This type uses a fluid constriction to create the required pressure drop across the FCD. Flow resistance is created by forcing the fluid to cross into the tubing from a large area through a small-diameter orifice.

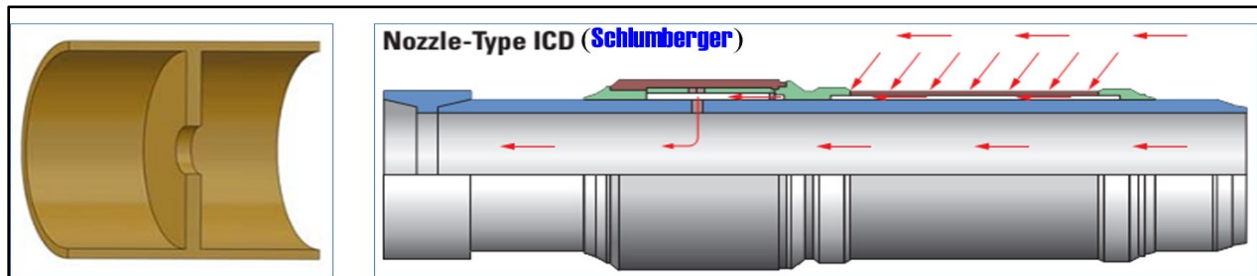


Figure 2-4: Orifice Type FCD, (Banerjee et al. 2013)

Helical Type Flow Control Devices

This type is also known as channel type, baffled pathway type or friction-style. It utilizes surface roughness that causes friction to create a pressure drop. Hence, device channel specifications and flowing fluid rheological properties influence the pressure drop level. **Figure 2-5** shows a helical type ICD.



Figure 2-5: Helical Type FCD, (Banerjee et al. 2013)

Autonomous Type Flow Control Devices

This FCD type, also known as Hybrid-Geometry Autonomous FCD, is composed of a baffled pathway that contains a series of constrictions. **Figure 2-6** shows internal structure of a typical autonomous ICD type. The function of this FCD depends on the instantaneous composition of the flowing fluids. Thus, it can adapt to changing flow conditions and control the production of undesired fluids while imposing the required pressure drop.

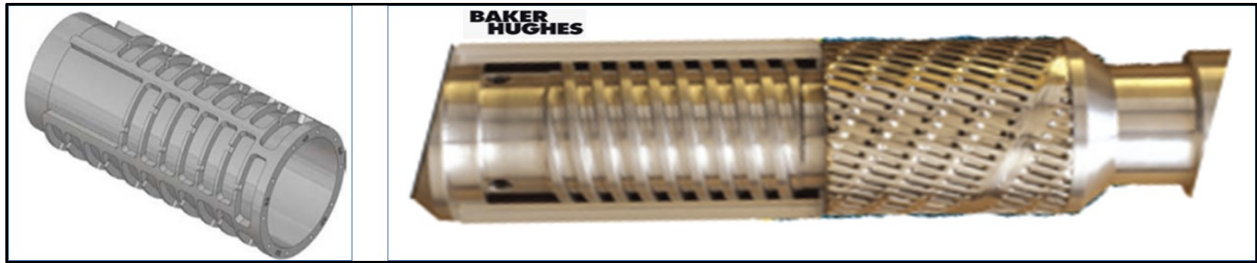


Figure 2-6: Autonomous Type FCD, (Banerjee et al. 2013)

2.2.2 Tubing-Deployed versus Liner-Deployed FCD's

Figure 2-7 illustrates a schematic of tubing-deployed and liner-deployed FCDs. Tubing-deployed FCD's have the same size of conveying tubing (e.g. 4 1/2"). For injector FCDs, the injected fluid departs the injector tubing through the FCD orifices into the liner-tubing annulus, then to the formation. In case of production FCD's, the produced fluids enter the annulus first, and then enters the production tubing through FCD orifices.

Liner-deployed FCD's have larger diameter (e.g. 6 5/8"), and they are installed on blank liners. Unlike tubing-deployed FCD's, the injected fluid departs the blank liner into the sand screen through the FCDs orifices. For production FCDs, produced fluids enter the annulus through the sand control and exit through FCD orifices. The choice of using liner-deployed or tubing-deployed FCD's is an important technical and economical design factor.

Letourneau (2015) suggests liner-deployed FCD completions have hydraulic advantage as the large diameter pipes (7" or more) induce lower pressure drops as compared to smaller-diameter pipes (say 4 1/2") used in tubing-deployed FCD completions. Further, liner-deployed FCD's are argued to be more cost-effective, where tubing cost is eliminated, and sand control systems can be coupled with the FCD's. Furthermore, no thermal packers are required to isolate production zones when liner-deployed FCD's are used.

The pressure drop along the horizontal section from heel to toe are exaggerated with reduced pipe sizes (e.g. 4 1/2") in tubing-deployed FCD's completions. This pressure drop can be problematic even in homogeneous formations and can cause preferential flow at the heel section of SAGD well pair (preferential steam flow out of the injector heel and preferential fluid flow into the producer heel) (Letourneau 2015).

Tubing-deployed FCD's completions have some benefits. For instance, they can reduce completion risk and have more operation flexibility, where devices can be installed, removed, recompleted and shifted to adjust flow. These benefits justify larger number of tubing-deployed FCD's completions applications, especially in infill applications. However, if risks of liner-deployed FCD's completions are reduced, they can be considered as the principal FCD's completion (Letourneau 2015).

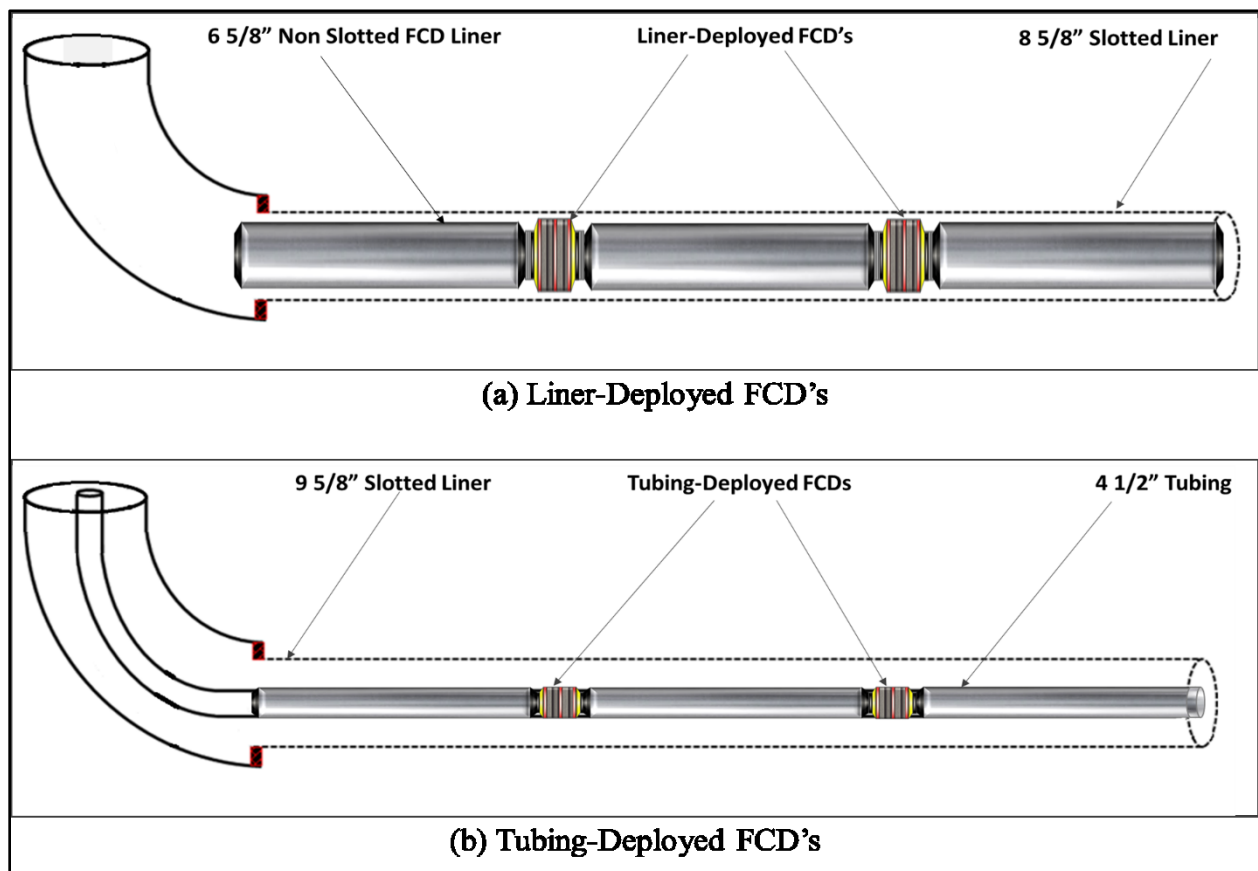


Figure 2-7: Tubing-Deployed and Liner-Deployed FCD's

2.2.3 Modeling FCD's in CMG STARS

Modeling FCD's performance in CMG STARS for both orifice and friction types is based on published papers. The modeling process focuses on the desired critical (choked) flow rate and friction pressure loss calculations and does not take into account the distribution pattern or the direction of the ports along the FCD joint. For instance, CMG STARS does not take into account whether the FCD ports are at the bottom or top of the pipe. A similar issue exists when it comes to the location of the port, whether it is at the far end or middle of the FCD joint. It only assumes the FCD port is located at the middle of the FCD joint.

Orifice-Type FCD

Pressure drops across the orifice-type FCD's in CMG STARS can be evaluated based on equations in the published papers (Chien 1990; Perkins 1993; Boone et al. 1998; Boone et al. 2001). The desired critical (choked) flow takes place when the fluid flows through the orifice, and downstream/upstream pressure ratio is less than the critical pressure ratio (F_p^*). The equations used to model this type of FCD's in CMG are described in CMG in FlexWell keywords guide (CMG FlexWell User's Guide 2015).

The magnitude of critical pressure ratio (F_p^*) is determined for the maximum possible mass flow rate Q_m , i.e., when the derivate $\frac{dQ_m}{dF_p^*} = 0$. Mass flow rate Q_m is given by Eq. (2.3) as follows:

$$Q_m = \frac{2P_{up}\rho \left(\lambda (1 - F_p^{k-1/k}) + \alpha (1 - F_p) \right)}{\sqrt{\left(f_g F_p^{-1/k} + \alpha \right)^2 - A_{dw}^2 / A_{up}^2 (f_g + \alpha)^2}} \quad (2.3)$$

where P_{up} is upstream pressure, ρ is mixture mass density, F_p is the ratio of downstream and upstream pressures, f_g is mass fraction of gas, A_{dw} is downstream area, A_{up} is upstream area, and λ and α are factors given by Eq. (2.4) and Eq. (2.5) respectively:

$$\lambda = f_g + \frac{M(f_g C_{vg} + f_o C_{vo} + f_w C_{vw})}{ZR} \quad (2.4)$$

$$\alpha_p = (f_o / \rho_o + f_w / \rho_w) \quad (2.5)$$

where M is molecular mass, C_{vg} is heat capacity of gas at constant volume, C_{vo} is heat capacity of oil at constant volume, f_o is mass fraction of oil, C_{vw} is heat capacity of water at constant volume, f_w is mass fraction of water, R is Universal gas constant, Z is gas compressibility factor, ρ_o is upstream mass density of oil, and ρ_w is upstream mass density of water.

The critical volumetric flow rate Q^* is estimated using **Eq. (2.6)**:

$$Q^* = AC_d Q_m / \rho \quad (2.6)$$

where Q^* is subcritical flow rate and A is orifice area

If gas content is significant, then the dimensionless discharge coefficient C_d should be corrected to account for gas content using **Eq. (2.7)** as follows:

$$C_d = \max(C_{di} f_g^{0.031}, 0.61 C_{di}) \quad (2.7)$$

where C_d is gas discharge coefficient, C_{di} is gas discharge coefficient as read in CMG input data file.

When pressure ratio turns into a value that is less than the critical pressure ratio, then the volumetric flow rate is calculated in **Eq. (2.8)** as follows:

$$Q = Q^* \sqrt{1 - [(F_p - F_p^*) / (1 - F_p^*)]^2} \quad (2.8)$$

where Q is subcritical flow rate and F_p^* is the critical ratio of downstream and upstream pressures.

Friction Type FCD

Friction type FCD's in CMG STARS are modeled based on published papers (Coronado et al. 2009; Garcia et al. 2009). They are modeled based on friction calculations of the fluid flowing through the FCD between tubing and annulus and/or annulus and reservoir. Details of the equations used for modeling in CMG are described in CMG FlexWell user's guide (CMG FlexWell User's Guide 2015).

Pressure drop is calculated using **Eq. (2.9)**:

$$\Delta P = K \rho \frac{v^2}{2} \quad (2.9)$$

where Δp is friction pressure loss, K is a dimensionless factor and v is velocity.

Dimensionless friction factor is calculated using two different expressions. The first expression is given by **Eq. (2.10)**.

$$K = f_2 + \frac{f_1 + f_2}{\left(1 + \left(\frac{Re}{t}\right)^c\right)^d} \quad (2.10)$$

where Re is Reynolds number, t is time, c and d are calibration constants and f_1 and f_2 are factors given by Eq. (2.11) and Eq. (2.12).

$$f1 = a_1 * Re^{b1} \quad (2.11)$$

$$f2 = a_2 * Re^{b2} \quad (2.12)$$

where a_1 , a_2 and b_2 are calibration constants

2.2.4 General Design Factors in Conventional Wells

There are several factors that need to be considered when it comes to the design and installation of the FCD's in conventional reservoirs. These factors depend on both reservoir and well conditions. Some of these factors are summarized in the next sections.

Reservoir Heterogeneity

High-permeability zones in heterogeneous reservoirs will have the highest contribution to production, where fluids flow more easily from those zones and via non-isolated annulus to the tubing leaving lower permeability zones unproduced. Annulus isolation via packers and implementation of FCD's can significantly balance and control flow contribution from each zone regardless of variation in permeability (Al Marzouqi et al. 2010).

Multi-stacked Reservoirs

Multi-stacked reservoirs that share completion may have different pressure systems and that increases the risk of cross-flow between layers. FCD's along with a single string can be utilized in this case to avoid cross-flow (Al Marzouqi et al. 2010).

Long Horizontal Wells

A primary goal of using FCD's in a long horizontal well is imposing additional pressure losses to promote equalized flow by imposing additional pressure restriction to zones with a higher production (Al Marzouqi et al. 2010).

Thin Oil Layers

Thin oil layers are highly sensitive to the production rate and can easily develop gas/water coning. Installing FCD's can reduce risk of coning (Al Marzouqi et al. 2010).

2.2.5 ICD Design Steps for Conventional Wells

As described in Figure 2-8, four basic steps are involved for the design and selection of ICD's in conventional wells (Al Marzouqi et al. 2010). Further details are discussed next.



Figure 2-8: ICD's Design Steps for Conventional Wells

Determination of Minimum Production Target Rate

Better equalization can be achieved by using ICD's for high production rates at higher pressure drawdowns. Low production rates (lower than target rate) at low pressure drawdowns may not benefit from equalization effect from ICD's (Al Marzouqi et al. 2010).

Determination of Pressure Drop Magnitude across ICD

As a rule of thumb, to achieve the optimum equalization effect, the required pressure drop across ICD should always be greater than or equal to pressure drop across the reservoir as shown in **Figure 2-9**. In other words, the ratio between pressure drop across ICD and pressure drop across the reservoir should be greater than 1:

$$\frac{\Delta P_{ICD}}{\Delta P_{Sand}} \geq 1 \quad (2.1)$$

where ΔP_{ICD} is pressure drop across the ICD, and ΔP_{Sand} is pressure drop across the formation sand.

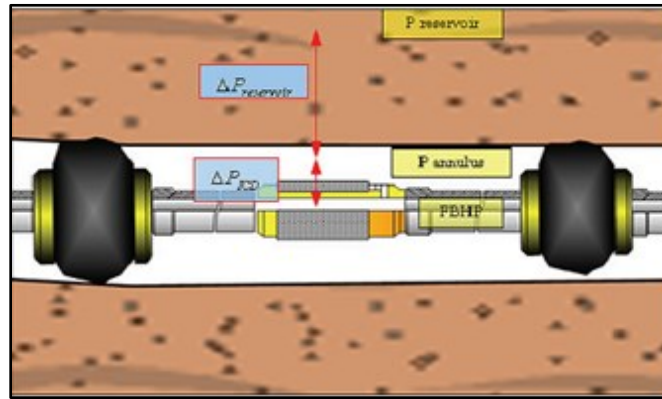


Figure 2-9: Optimum Equalization Pressure Drop, (Al Marzouqi et al. 2010)

Determination of Total Number of ICD's

Each ICD device has its own characteristic ICD flow-pressure correlation chart, (i.e., fluid flow rate and pressure differential across ICD) such as the one shown in **Figure 2-10**, which is provided by the manufacturer of the ICD. This correlation chart is used to determine the rate per single ICD.

Initial estimation of total number of required ICD's can be achieved by dividing the minimum target rate by the rate per single ICD (Al Marzouqi et al. 2010).

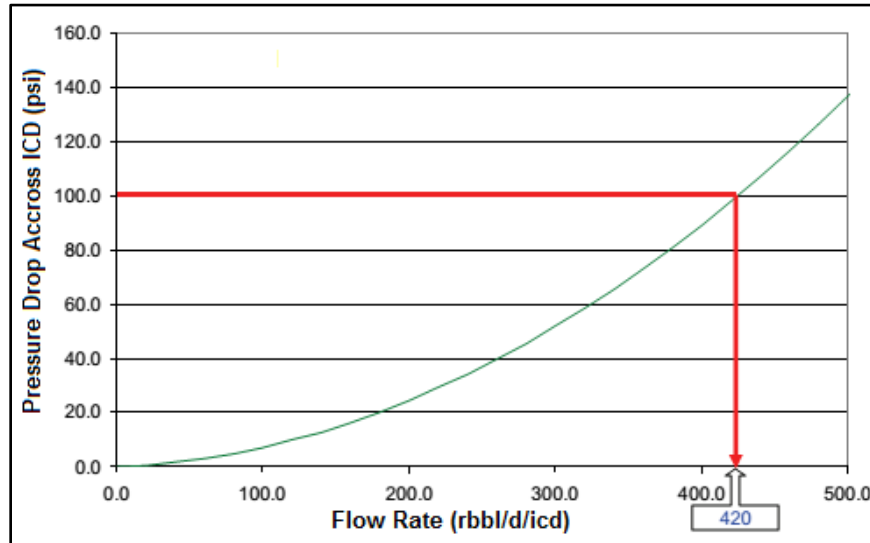


Figure 2-10: ICD Flow-Pressure Correlation, (Al Marzouqi et al. 2010)

Optimization of Total Number of ICD's via Simulation Runs

Various simulation cases with different compartmentalization and ICD combinations have to be designed and run to pick the optimum design. The total number of ICD's in the optimum design may slightly differ from the number estimated in the previous step depending on reservoir heterogeneity and number of required compartments (Al Marzouqi et al. 2010).

2.3 FCD's in SAGD

Fluid flux from the injector wellbore into the reservoir or from the reservoir into producer wellbore is significantly affected by the reservoir geology and frictional pressure losses along the horizontal sections. Deploying FCD's along horizontal section of the wellbore chokes fluid flux into/out of high-permeable zones and induces flow at zones that have less flow rate.

In homogenous reservoirs, the dominant factor is the frictional pressure losses along the horizontal section of the wellbore, where fluid flux gradually declines as the distance increases from the heel to the toe (**Figure 2-11a**). In such case, using tubing-deployed FCD's to restrict flow to the heel section and allow more fluid flow at the toe section would help in achieving equalized fluid flux.

In reservoirs with high permeability at the heel, most of the fluid flow occurs at the heel section due to high permeability and less resistance to flow, and the toe section experiences the least fluid flow (**Figure 2-11b**). Installing FCD's at the toe section in this case helps to equalize fluid flow.

In the opposite case, where the toe section has high permeability, deploying FCD's at heel section restores equalized flow along the entire horizontal section (**Figure 2-11c**). In reservoirs with variable permeability strata, such as reservoirs with sand/shale-streaks and heterogeneous reservoirs, using FCD'S can control flow at high permeability zones and allow more flow into low permeability zones (**Figure 2-11d**).

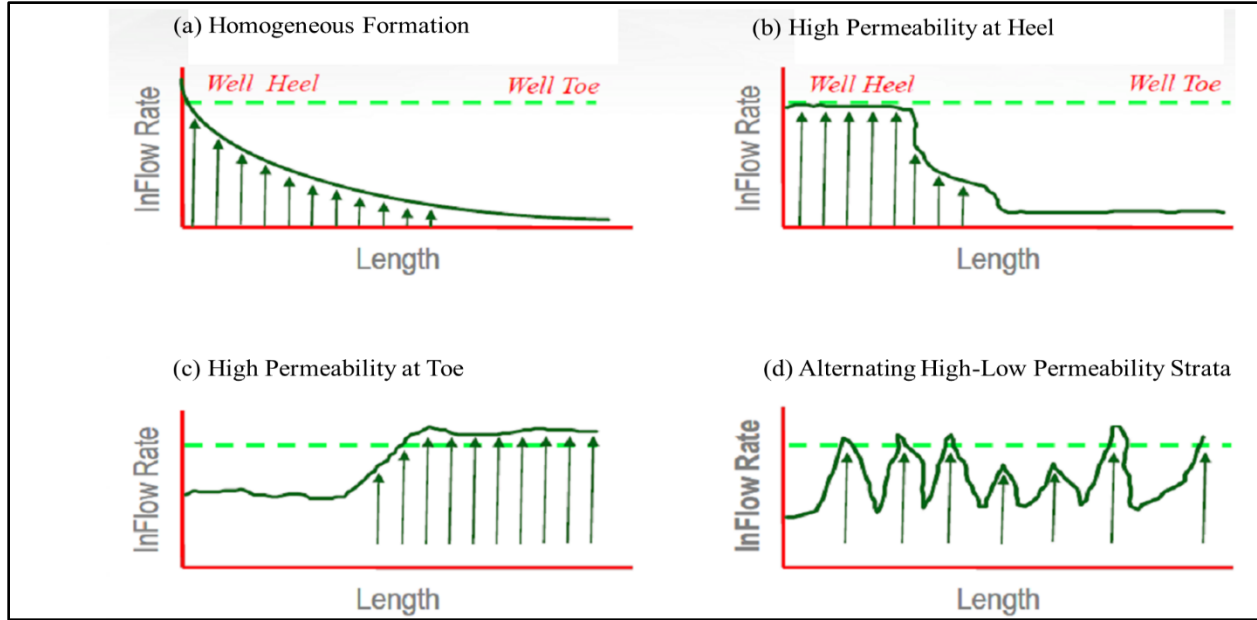


Figure 2-11: Fluid Flow Profiles Into Different Types of Reservoirs, (Baker Hughes Equalizers 2011)

2.3.1 Implementation of OCD's/ICD's in SAGD

Outflow control devices in SAGD are also sometimes referred to as steam splitters (Noroozi et al. 2014). They are installed at predetermined locations of SAGD injectors along the tubing inside the slotted liner of the SAGD injector to convey certain amounts of steam to those designated locations. OCD's in SAGD projects are meant to improve the production capacity by creating a uniform steam chamber growth. They also help in reducing the overall operation expenditure by enhancing the thermal efficiency and reducing surface injection pressure requirements (Banerjee et al. 2013).

Inflow Control Devices (ICD's) are used to achieve equalized inflow along the horizontal section of SAGD producer and to control steam breakthrough. ICD's have also been reported to reducing operation expenses by impeding steam breakthrough and maximizing conformance by creating a uniform pressure profile inside the SAGD producer (Banerjee et al. 2013).

Overall benefit of OCD's/ICD's used in SAGD is reflected in increased bitumen production rate, improved recovery factors, reduced cSOR, and reduced long-term drilling costs.

2.3.2 FCD's Utilization in SAGD Projects in Alberta

Several SAGD projects have been implemented in Alberta with daily bitumen production of more than 700,000 STB/D by 2014 (Ghesmat and Zhao 2015). For instance, Conoco Phillips utilized liner-deployed FCD's in Surmont field SAGD project in 2009 (Stalder 2013), and Suncor implemented its first FCD pilot in Suncor's MacKay River project in 2011 (Suncor Energy 2015). Also, Southern Pacific has equipped six wells with ICD's, where scab liner with swell packers and ICD's have been used as a default completion scheme. Statoil Leismer SAGD Pad-5 has five injectors completed with wire wrapped screen and two OCD's, and three producers completed with wire wrapped screen and four ICD's. Two wells utilized ICD's in Devon Jackfish field with the aim of better understanding of FCD's technology in SAGD.

Further examples of SAGD projects include Husky Tucker in 2011 and 2012, Cenovus Pelican Lake in 2012, Shell Orion in 2012, Nexen Long Lake in 2013, MEG Christina Lake, Cenovus foster Greek, Suncor Firebag, CNRL's Kirby South project (Ghesmat and Zhao 2015).

2.3.3 FCD's Simulation for SAGD

In a study conducted by Riel et al. (2014), a model was built to validate the hypothesis of improved performance of SAGD when FCD's are used. The authors built a synthetic 3D homogeneous SAGD model. Then, two different cases were generated with outflow control devices installed at every open perforation of the injector. Both cases were alike, except that outflow control devices in Case 1 induce four times more pressure drop than those ones in Case 2. Results revealed that cumulative bitumen production was increased by 30% compared to the base case. Also, reduced cSOR of FCD's cases compared to base case indicated improved thermal efficiency (Riel et al. 2014). They concluded several limitations with respect to implementation of FCD's in SAGD. These limitations are related to computation convergence, numerical stability, and long running time. These limitations are mainly triggered by model complexity, model grid size, fluid description, frequency of changes in operating constraints and choice of simulation time step.

2.3.4 Impact of FCD's Specifications and Locations on SAGD Production

A case study by Noroozi et al. (2014) investigated the impact of different properties of FCD's, such as number of FCD's, port size, number of ports and impact of locations of these devices on SAGD process, using a coupled wellbore-reservoir simulation approach. Furthermore, the authors proposed a workflow for the optimization process.

First part of the study consisted of a quick sensitivity analysis to investigate the impact of number, locations and properties of FCD's. The sensitivity analysis for the number of FCD's concluded that cumulative oil production at the end of six years simulation period increased by 36% for the single-OCD case and by 63% for the two-OCD case. They also found that the effect of production ICD's was less significant compared to the effect of injection OCD's, especially during the early life of the production. Results of sensitivity analysis for properties of production ICD's indicated that number of ports had the most significant impact on the production.

The second part of the study involved FCD's optimization, and it included location, properties and total number of injection OCD's and production ICD's. The objective function of the optimization study was Net Present Value (NPV), and proposed an optimization workflow that had four steps (Noroozi et al. 2014). Results showed that optimizing injection OCD's increased the NPV by 30%. Further optimization by adding production ICD's increased NPV by 150% compared to the base case. These results appear to be inconsistent with their initial conclusions that the effect of OCD's on NPV was greater than that of ICD's.

The proposed optimization workflow by Noroozi et al. (2014) might have not yielded optimum results because it neglected the interaction between injector and producer where OCD's were optimized first, then ICD's were optimized assuming fixed optimum OCD's configuration for the injector. Also, 150% increment in NPV compared to base case seems too large, and this could be because of the adopted default completion scheme in the base case with long tubing only at the toe for steam injection.

A study by Kyanpour and Chen (2014) proposed a method to optimize size and position of injection OCD's and production ICD's in SAGD operations. The method has been validated on a case study using field data (well pair H1 of Senlac SAGD project).

Kyanpour and Chen (2014) stated that the proposed method could be used for both simple and complex reservoirs such as reservoirs with heterogeneities or various flow barriers such as mud channels. The authors performed the optimization process in three integrated steps: Impact of FCD's locations versus size, and optimization of number of ports for injection OCD's and producer ICD's.

The studies conducted by Noroozi et al. (2014) and Kyanpour and Chen (2014) did not investigate the effect of well pair trajectory excursions on SAGD performance. Also, they did not investigate the effect of zonal steam injection. As an attempt to bridge some of the gaps identified in the

literature review, the work in this research examines the effect of well pair trajectory excursions on SAGD performance. It also investigates the potential performance enhancement using OCD's and compares the results to those of dual-string completion scheme in the injector.

CHAPTER THREE: BASIC SAGD MODEL SETUP

3.1 SAGD Basic Model Construction Strategy

To build models with different well pair trajectory configurations for each optimization case study in this research, it is essential to build a base case SAGD model. The base case SAGD model in this research consists of a homogenous reservoir with one SAGD well pair completed by dual-string scheme depicted in **Figure 3-13**.

The reservoir geological properties, thermal rock properties, rock-fluid data, bitumen data, and well completion scheme of the SAGD model are based on publicly available data of Suncor MacKay River SAGD project.

3.2 Overview of Suncor MacKay River SAGD Project

3.2.1 Project Overview

MacKay River SAGD project is owned by Suncor Energy and located 60 km North West of McMurray adjacent to Dover UTF/AOSTRA Project. **Figure 3-1** shows oil sands projects in Alberta including open-pit mining and in-situ production. **Figure 3-2** shows Suncor leases of oil sands projects including MacKay River SAGD project.

MacKay River is the first Suncor Energy's SAGD operated facility, which began producing oil in 2001. The Original Bitumen In Place (OBIP) of the lease is 43,784,000m³ with an approved daily production rate of 11,600 m³ of bitumen per day (Suncor Energy 2015).

As of Sept. 2015, the project contained 11 patterns targeting Athabasca McMurray formation. A SAGD pattern is the reserve area targeted and drained by a SAGD well pair or certain group of wells. **Table 3-1** and **Table 3-2** summarize each pad's reservoir properties and average properties of the Athabasca McMurray formation, respectively.

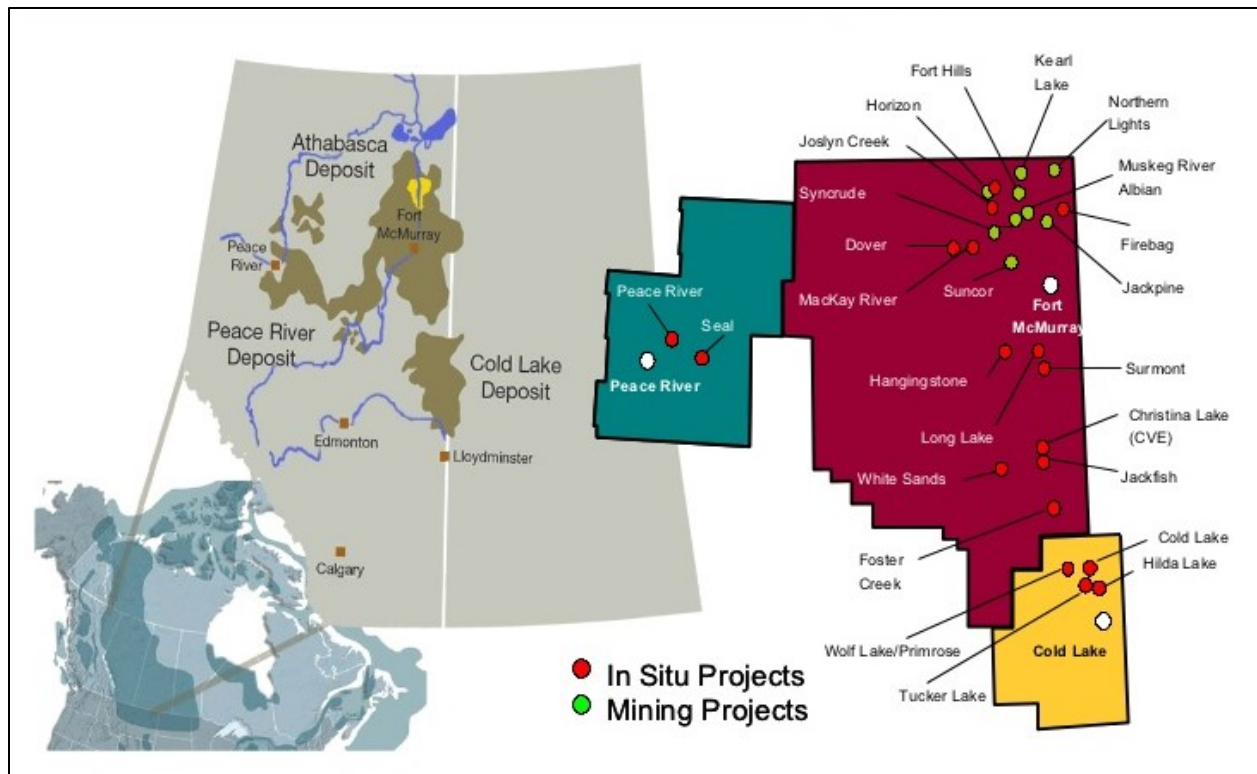


Figure 3-1: Canadian Oil Sands Projects, (Collyer 2011)

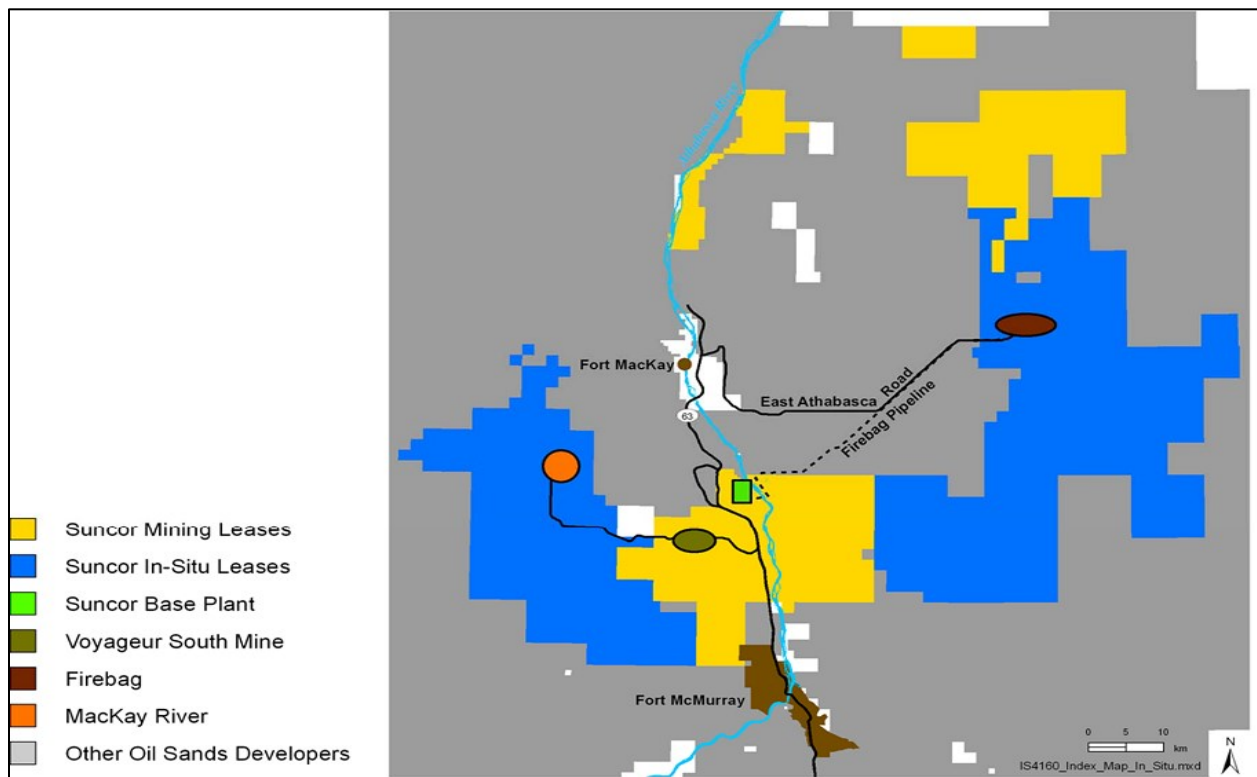


Figure 3-2: Suncor Leases Oil Sands Project, (Suncor Energy 2015)

Table 3-1: MacKay River SAGD Projects Reservoirs Properties, (Suncor Energy 2015)

Pattern	Sand NTG (%)	So (%)	Ø (%)	OBIP (x10³ m³)
A	91	82	31	2,389
B	95	86	32	3,319
C	95	89	32	4,238
D	96	91	31	2,741
E	92	84	31	3,728
F	95	89	32	3,616
G	93	86	32	4,155
H	94	84	31	1,756
NN	95	85	32	7,010
OO	93	84	31	5,251
QQ	87	84	31	5,581
Total				43,784

Table 3-2: MacKay River SAGD Project McMurray Formation Reservoir Properties, (Suncor Energy 2015)

Property	Unit	Value
Depth	m	98-145
Initial Reservoir Pressure	kPa	480
Initial Reservoir Temperature	°C	6-7
Horizontal Permeability	md	1,700-8,500
Vertical Permeability	md	1,100-6,500
Average Porosity	%	31
Average Net Sand Ratio	%	91
Average Oil Saturation	%	86

3.2.2 Production and Wells Status

Project development was initiated with 25 well pairs. First steam was introduced in September 2001; then first production started in November 2001 (2-months circulation period). As of August 2015, total number of well pairs were increased gradually to 137 with 95 active well pairs, 40 non-producing well pairs, and two abandoned well pairs. **Table 3-3** provides additional information about active well pairs for this project.

Table 3-4 summarizes production data of different well patterns. **Table 3-5** shows pressure operating conditions of well patterns. The approved maximum operating bottom hole pressure, or MOP, was considered to be 80% below the formation fracture closure pressure at the base of the cap rock. All wells were operated under approved MOP.

Table 3-3: MacKay River SAGD Project Active Well Pairs Statistics, (Suncor Energy 2015)

Pad	Pattern	Phase	# Well Pairs	Spacing	First Steam
20	A	1	7	100	Sept. 2002
	C		6	100	
21	B		7	100	
	D		5	100	
22	E	2	7	100	Jan 2006
	G		7	100	
23	F	3	7	100	Sept. 2007
24	OO	4	3	75	Oct 2008 to Apr 2009
		5B-1	6	75	Feb 2012
		5DF	6	75	May 2014
	H	4	4	100	Feb 2009 to Jun 2010
25	QQ	4	2	75	Nov 2008
		5A	2	75	Jul 2011
		5B-2	5	75	Jan 2013 to May 2013
		5DF	6	75	Jun 2014
	NN	4	1	75	Dec 2008
		5A	4	75	Jun 2011 to Jul 2011
		5B-2	5	75	Jan 2013 to Feb 2013
		5DF	6	75	Jun 2014

Table 3-4: MacKay River SAGD Project Well Pairs Production Data, (Suncor Energy 2015)

Pattern	OBIP (x10 ³ m ³)	Cum. Oil (x10 ³ m ³)	Recovery (As of Aug 2015, %)	cSOR (m3/m3)	Ultimate Recovery (%)
A	2,389	1,000	43.0	4.4	47
B	3,319	2,627	72.4	2.2	82
C	4,238	3,370	75.5	2.2	89
D	2,741	1,870	76.6	2.4	85
E	3,728	2,189	55.2	2.0	70
F	3,616	2,204	57.8	2.3	81
G	4,155	1,796	47.3	2.4	54
H	1,756	369	9.7	3.3	47
NN	7,010	955	24.6	2.8	58
OO	5,251	547	14.1	3.4	52
QQ	5,581	950	25.0	1.9	55
Average			45.6	2.7	65
Total	43,784	17,877			

Table 3-5: MacKay River SAGD Project Well Operating Pressure Constraints, (Suncor Energy 2015)

Pattern	Wells	Maximum Operating Pressure		Average Pressure Sept. 14 - Aug 15
		Surface (kPa)	Bottomhole (kPa)	Bottomhole (kPa)
A	A1-7	2,010	1,790	1,351
B	B1-7	1,910	1,700	1,318
C	C1-6	1,670	1,490	1,383
D	D1-5	1,500	1,340	1,060
E (S)	E1-4	1,575	1,410	1,176
E (N)	E5-7	1,530	1,370	1,290
F	F1-7	1,610	1,440	1,342
G	G1-7	1,830	1,630	1,184
H	H1-4	2,110	1,880	1,733
NN	NN1-5	1,990	1,780	1,561
NN	NN6-10	2,070	1,850	1,709
NN	NN11-16	2,020	1,800	1,708
OO	OO1-3	1,780	1,590	1,429
OO	OO4-9	1,810	1,620	1,602
OO	OO10-15	1,790	1,600	1,490
QQ	QQ2-5	1,470	1,310	1,193
QQ	QQ6-10	1,450	1,300	1,261
QQ	QQ11-16	1,450	1,300	1,027

3.2.3 Well Completion Schemes

There are two types of completion schemes that have been adopted in MacKay River project. The injector in the first type has 7" slotted liner accommodating 2 7/8" single tubing string. The producer has 7" slotted liner with dual-string (3 1/5" short tubing landed at the heel and 3 1/5" long tubing landed at the toe). **Figure 3-3** shows a typical completion scheme of Phase-1.

A typical example of second type completion was adopted in Phase-5 where the injector has 9 5/8" slotted liner with 4 1/2" short tubing landed at the heel and 4 1/2" long tubing landed at the toe. The producer also has 9 5/8" slotted liner with 4 1/2" short tubing landed at the heel and 4 1/2" long tubing landed at the toe. **Figure 3-4** shows Phase-5 type completion scheme.

Also, FCD's have been installed in 16 well pairs in MacKay River project (one well pair in E pattern, one in F pattern, one in G pattern, one in H pattern, five in NN pattern and seven in OO pattern). **Figure 3-5** shows improvement in production performance of pattern H2 after the FCD installation.

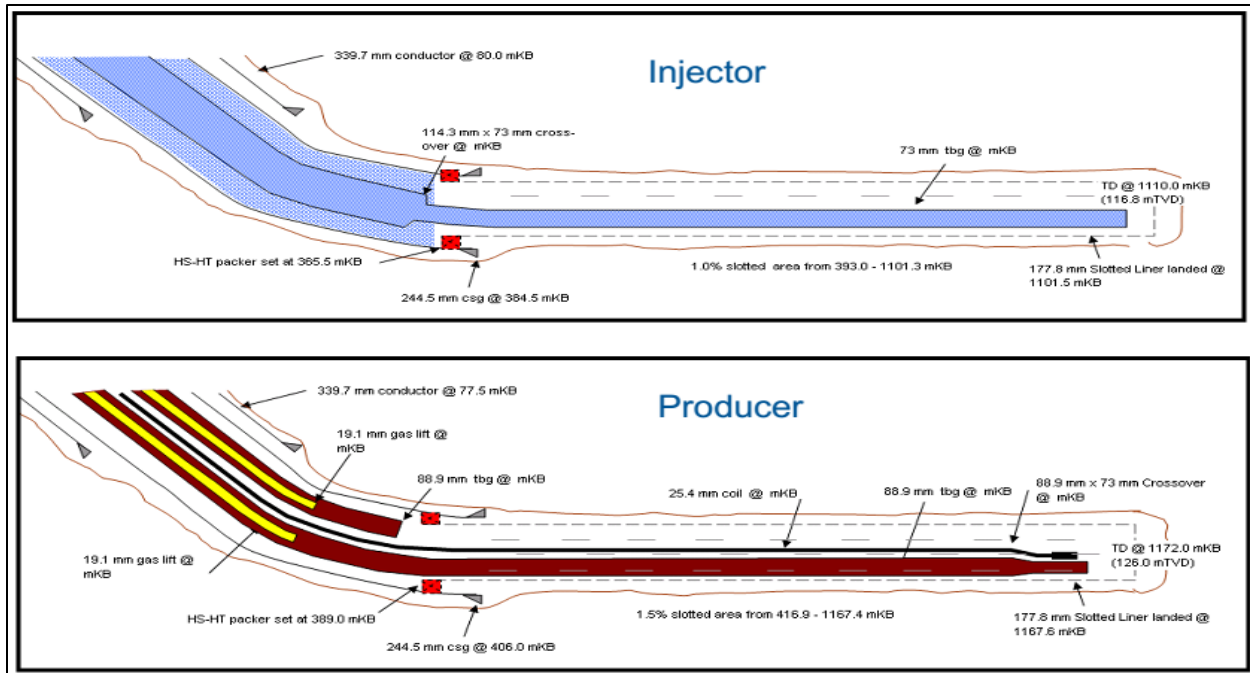


Figure 3-3: MacKay River Project Phase-1 Completion Type, (Suncor Energy 2015)

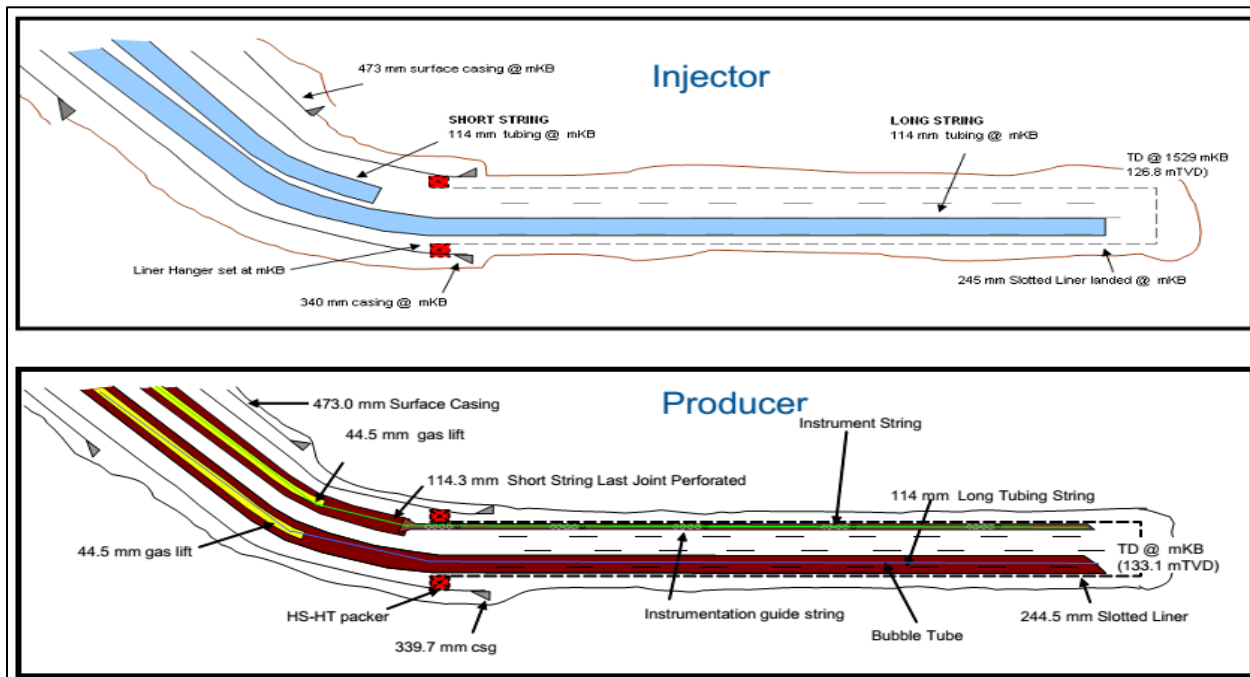


Figure 3-4: MacKay River Project Phase-5 Completion Type, (Suncor Energy 2015)

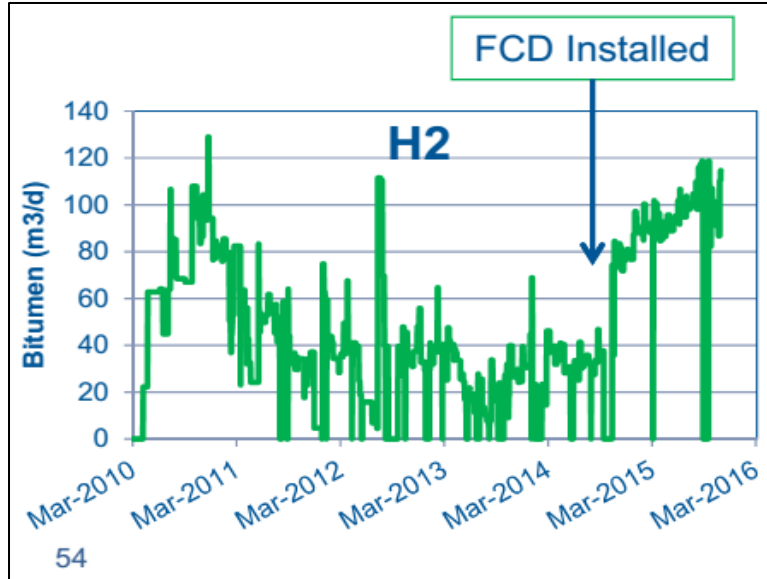


Figure 3-5: H1 Well Production Performance after FCD Installation, (Suncor Energy 2015)

3.3 Construction of Basic SAGD Reservoir Model

A three-dimensional (3D) synthetic SAGD model was constructed using CMG Builder. The model was based on publicly available data of SUNCOR MacKay River project which has been discussed previously.

3.3.1 Symmetry Assumption

To minimize simulation run time, the 3D model is assumed to be symmetric along the well pair trajectory axis, (along J-direction as shown in **Figure 3-6**). Hence, flow rates, and the grid block volumes and flowable areas which contain the set of horizontal well pairs will have to be modified to account for the symmetry as follows:

- 1) The 3D model is sliced vertically along the axial plane (J-K plane as in **Figure 3-6**). Thus, all block volumes on this plane are multiplied by 0.5.
- 2) Production and injection rates of the wells must be reduced to half. In STARS, this is done by using a fraction of 0.5 in well definitions section.
- 3) Flowable areas perpendicular to well pair direction in the grid blocks containing these wells (I-K planes) are also multiplied by 0.5.

3.3.2 Model Dimensions

The established 3D model gross dimensions were set based on average dimensions of a typical SAGD well pair length and operating volume dimensions in MacKay River project. The model

has a length of 1,000 m along the horizontal well pair directions (J-direction), width of 34 m (I-direction) and height of 30 m (K-direction). The established model dimensions were gridded into 10,200 grid blocks ($I \times J \times K = 17 \times 20 \times 30$) as shown in **Figure 3-6**. The 1,000-m horizontal length in J-direction was divided into 20 blocks with each grid block having 50 m in J-direction. The 34-m in I-direction was divided into 17 grid blocks with each grid block having 2-m length. The 30 m in K-direction was divided into 30 grid blocks with each grid block having 1-m length. **Table 3-6** shows the details of model dimensions. **Figure 3-7** shows the dimensions of a single grid block in the model.

Table 3-6: SAGD 3D Model Gridding Dimensions

Direction	# of Grid Blocks	Grid Block Length (m)	Total Length (m)
I	17	2	34
J	20	50	1,000
K	30	1	30
Bulk Volume (m ³)			1,020,000

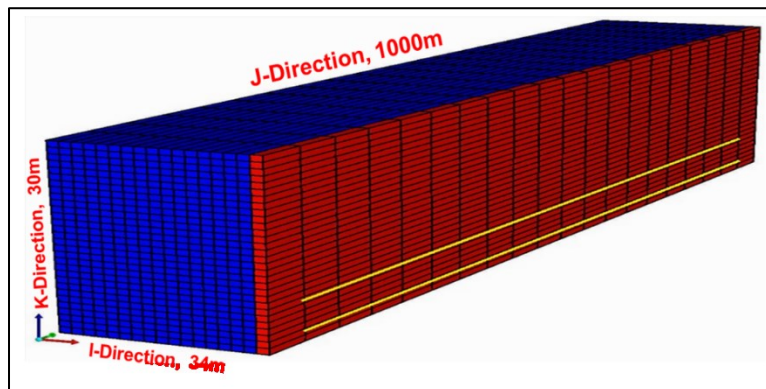


Figure 3-6: SAGD 3D Model View

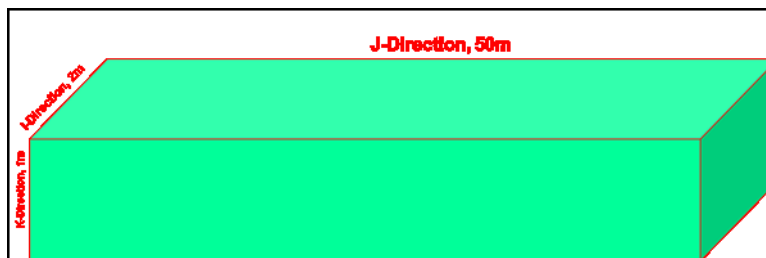


Figure 3-7: SAGD 3D Model Single Block View

3.3.3 Modeling Geological Properties

Initial pressure, temperature, bitumen saturation distribution, and reservoir geological properties in the model were guided (but not necessarily the same) based on the properties of Athabasca

McMurray formation in MacKay River project as summarized in **Table 3-2**. **Table 3-7** shows the properties that have been used in the model:

Table 3-7: SAGD 3D Model Reservoir Properties

Property	Unit	Value
Depth	m	110
Initial Reservoir Pressure	kPa	400
Initial Reservoir Temperature	°C	7
Horizontal Permeability	md	1,500
Vertical Permeability	md	825
Average Porosity	%	32
Average Net Sand Ratio	%	95
Average Oil Saturation	%	85

3.3.4 Definition of System Components

A joint industry report prepared by several operating companies (Paramount Resources Ltd., EnCana Corp., Petro-Canada, ConocoPhillips Canada Corp., and Nexen Inc.) for Alberta Energy Resources Inc. (AERI) provided detailed information about fluid properties of MacKay River reservoirs (Coates et al. 2005). The SAGD simulation model in the research work of this thesis consists of a 3-phase fluid system composed of bitumen, dissolved methane and water. Critical properties of these fluids were borrowed from CMG standard demonstrative FlexWell Tubing/Annulus SAGD cases. MacKay River bitumen molecular weight was taken from the joint industry report (Coates et al. 2005). Summary of critical properties of the three components are shown in **Table 3-8**.

Table 3-8: SAGD 3D Model Fluid Components Definition and Critical Properties

Component	P_{crit}	T_{crit}	MW
WATER	22,048	374	0.018
C1	4,600	-83	0.016
Bitumen	1,360	625	0.611

3.3.5 Fluid Densities/Compressibilities

MacKay River bitumen density was obtained from the joint industry report (Coates et al. 2005). Liquid methane density, bitumen/methane compressibilities, and 1st thermal expansion coefficient (as shown in **Eq. (3.1)**) were borrowed from CMG standard demonstrative FlexWell Tubing/Annulus SAGD cases. The first thermal expansion coefficient is used in a correlation

involved in the calculations of partial molar volumes of components in different phases, and they are entered in densities tab in CMG interface (CMG STARS User's Guide 2015).

$$\text{Thermal Expansion Coefficient} = C_{t1}(k) + T * C_{t2}(k) \quad (3.1)$$

where $C_{t1}(k)$ and $C_{t2}(k)$ are 1st and 2nd temperature dependent thermal expansion coefficients and T is temperature expressed in the corresponding absolute temperature scale (K).

Table 3-9 summarizes the properties that have been used in the reservoir simulation model.

Table 3-9: SAGD Model Bitumen/CH4 Densities, Compressibilities and Thermal Properties

Item	Bitumen	CH ₄	Unit
Density	1,011	602	kg/m ³
Liquid Compressibility	5.500E-07	5.500E-07	1/kPa
1 st Thermal Expansion Coefficient	8.000E-04	8.000E-04	1/°C

Table 3-10 shows a summary of the thermal properties of the reservoir sand, reservoir fluids, cap rock and base rock. These properties were selected based on data available from published papers on the MacKay River project (Chang et al. 2012 and Parmar et al. 2009), UTF/AOSTRA project (Good et al. 1997) and CMG standard demonstrative FlexWell Tubing/Annulus SAGD cases.

Table 3-10: Thermal Properties Used in the SAGD Model

Group	Item	Value	Unit
Rock Compressibility	Porosity Reference Pressure	100	kPa
	Formation Compressibility	0.000007	1/kPa
	Reservoir Rock Volumetric Heat Capacity	2,350,000	J/m ³ .°C
Rock & Fluid Thermal Properties	Reservoir Rock Thermal Conductivity	660,000	J/(m.day.°C)
	Oil Phase Thermal Conductivity	11,500	J/(m.day.°C)
	Water Phase Thermal Conductivity	53,400	J/(m.day.°C)
	Gas Phase Thermal Conductivity	140	J/(m.day.°C)
Cap & Base Rock Thermal Properties	Overburden Heat Capacity	2,350,000	J/m ³ .°C
	Overburden Thermal Conductivity	172,800	J/(m.day.°C)
	Underburden Heat Capacity	2,350,000	J/m ³ .°C
	Underburden Thermal Conductivity	172,800	J/(m.day.°C)

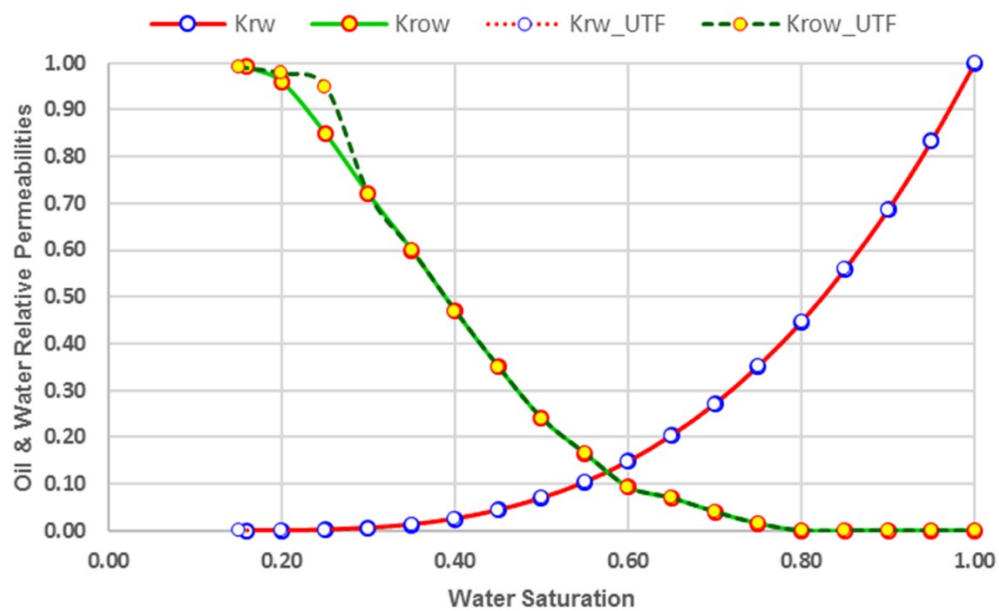
3.3.6 Modeling Rock-Fluid Data

MacKay River project is adjacent to UTF/AOSTRA. Hence, it was assumed they have similar oil-water and liquid-gas relative permeability curves, for use in the synthetic 3D SAGD model. The relative permeability curves for the UTF/AOSTRA project, as reported by Good et al. (1997), were

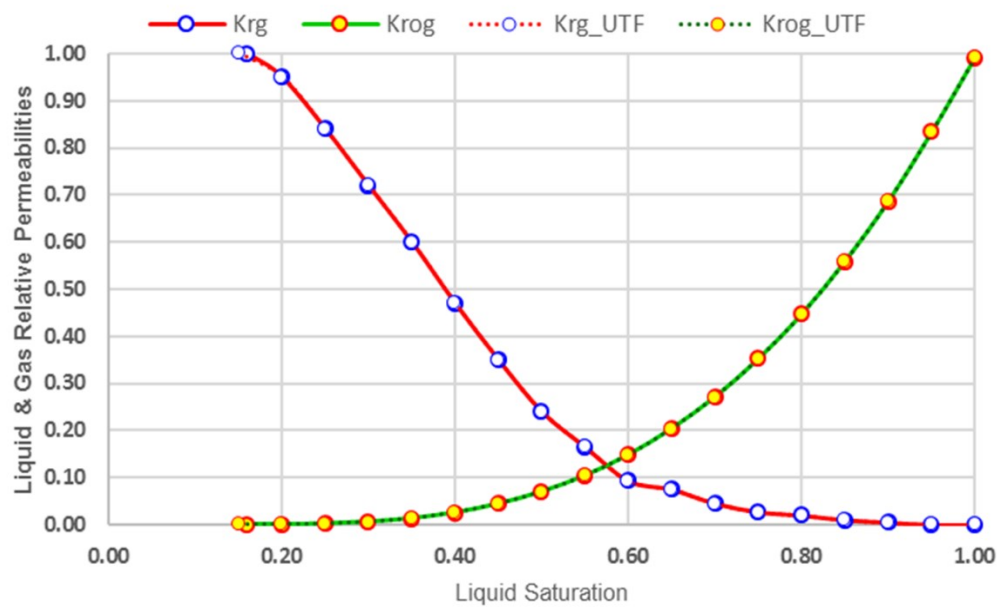
used after minor modifications to match the MacKay River initial bitumen saturations. The modifications involved slight changes in the value of initial water saturation and its corresponding relative permeability values (e.g. S_w changed from 0.16 to 0.15 and the water relative permeability was smoothed to avoid numerical problems. **Table 3-11** presents the modified sets of relative permeability curves for the oil-water and liquid-gas systems. **Figure 3-8** shows the set of relative permeability curves from the original history matched Phase-B SAGD pilot project of Dover UTF and the modified set that have been used in this research.

Table 3-11: Relative Permeability Data for the SAGD Model

Oil-Water Relative Permeability			Gas-Liquid Relative Permeability		
S_w	K_{rw}	K_{row}	S_l	K_{rg}	K_{rog}
0.160	0.0000	0.9920	0.160	1.0000	0.0000
0.200	0.0002	0.9600	0.200	0.9500	0.0002
0.250	0.0016	0.8500	0.250	0.8400	0.0016
0.300	0.0055	0.7200	0.300	0.7200	0.0055
0.350	0.0130	0.6000	0.350	0.6000	0.0130
0.400	0.0254	0.4700	0.400	0.4700	0.0254
0.450	0.0440	0.3500	0.450	0.3500	0.0440
0.500	0.0698	0.2400	0.500	0.2400	0.0698
0.550	0.1040	0.1650	0.550	0.1650	0.1040
0.600	0.1480	0.0930	0.600	0.0930	0.1480
0.650	0.2040	0.0700	0.650	0.0750	0.2040
0.700	0.2710	0.0400	0.700	0.0450	0.2710
0.750	0.3520	0.0150	0.750	0.0270	0.3520
0.800	0.4470	0.0000	0.800	0.0200	0.4470
0.850	0.5590	0.0000	0.850	0.0100	0.5590
0.900	0.6870	0.0000	0.900	0.0050	0.6870
0.950	0.8340	0.0000	0.950	0.0000	0.8340
1.000	1.0000	0.0000	1.000	0.0000	0.9920



(a) Oil-Water Relative Permeability Curves



(b) Gas-Water Relative Permeability Curves

Figure 3-8: Dover UTF Phase B SAGD Pilot Project and Modified Relative Permeability Curves

3.3.7 Reservoir Bitumen Viscosity

Dead Bitumen Viscosity

Walther's Viscosity-Temperature relationship shown in **Eq. (3.2)** has been used to predict MacKay River project's dead bitumen viscosity shown in **Eq. (2.3)** (Coates et al. 2005). The constants m and n for MacKay River bitumen were also determined in the joint industry AERI report to be -3.583 and 22.889, respectively. The term 0.8 is usually neglected for heavy oils and bitumen. Values predicted using Walther's equation were cross checked with measured values reported in AERI report and a reasonable match was found as shown in **Figure 3-9** and **Table 3-12**.

$$\log \log(\mu + 0.8) = m \times \log(T) + n \quad (3.2)$$

$$\log \log(\mu) = -3.583 \log(T) + 22.889 \quad (3.3)$$

where μ is bitumen viscosity, T is temperature, m & n are constants depending on the crude type.

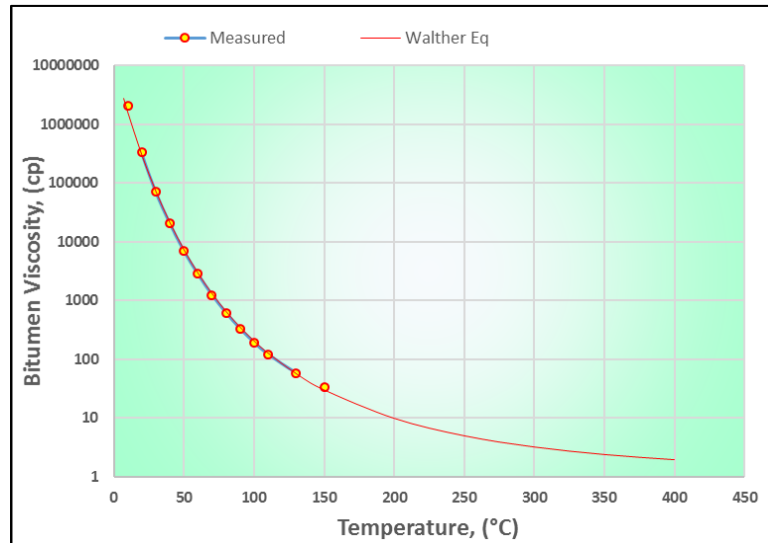


Figure 3-9: Dead Bitumen Viscosity Curve used in the SAGD Model

Table 3-12: Comparison of Calculated versus Measured Values for Dead Bitumen Viscosities

Temperature, T (°C)	Walther Eq., μ (cp)	Measured, μ (cp)
7	2,798,256	--
10	1,605,017	2,048,454
20	301,882	330,472
30	72,323	71,437
40	21,175	20,595
50	7329	6,988
60	2919	2,811
70	1309	1,240
80	649	614
90	350	329
100	203	191
110	126	120
130	56.20	58
150	29.58	33
200	9.68	--
250	4.87	--
300	3.13	--
350	2.33	--
400	1.90	--

Liquid Methane Viscosity

Walther's model in **Eq. (3.2)** was utilized to predict pure liquid methane viscosity after determining the unique values of the constants m and n ($m=-3.34$ and $n=20.72$) as shown in **Eq. (3.4)**. Predicted values once again have been cross checked with measured values of the joint industry report (Coates et al. 2005) with a good match. Results are summarized in **Figure 3-10** and **Table 3-13**.

$$\log \log(\mu + 0.8) = -3.34 \log(T) + 20.72 \quad (3.4)$$

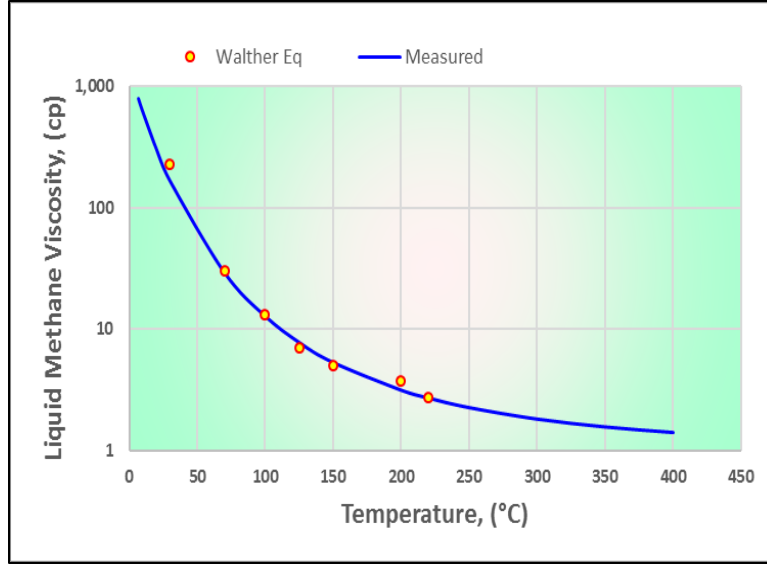


Figure 3-10: Liquid Methane Viscosity Curve used in the SAGD Model

Table 3-13: Liquid Methane Viscosity use in the SAGD Model

Temperature, T (°C)	Walther Eq., μ (cp)	Measured, μ (cp)
7	790	--
10	626	--
20	309	--
30	168	231
70	30	31
100	13	13
125	8	7
150	5	5
200	3	4
220	3	3
250	2	--
300	2	--
350	2	--
400	1	--

Live Bitumen Viscosity

Bitumen contains some gas in solution. The initial methane mole fraction in MacKay River bitumen is around 0.03 (Chang et al. 2012.). CMG STARS numerical simulator uses **Eq. (3.5)** proposed by Shu (1984) to obtain the viscosity of MacKay River live bitumen (Coates et al. 2005).

$$\ln \mu_m = \sum_{i=1} [X_i * \ln(\mu_i)] \quad (3.5)$$

where μ_m is mixture viscosity, X_i is mole fraction of component i in oil phase (inverse of gas-liquid equilibrium factor) and μ_i is viscosity of pure component i .

Methane K-values have been measured and reported in the joint industry report to AERI (Coates et al. 2005), but they turned to be different from CMG STARS default values of Methane K-values as shown in **Table 3-14**. A cross check of initial methane mole fraction in MacKay River oil phase was carried out using **Eq. (3.6)** (Coates et al. 2005). A good match was found between the predicted value using **Eq. (3.3)** (methane mole fraction = 0.0297) and the one in Chang et al. (2012) (methane mole fraction = 0.03).

$$K = \left[\frac{kv1}{p} + kv2 \times p + kv3 \right] \times e^{\left(\frac{kv4}{T - kv5} \right)} \quad (3.6)$$

where K is gas-liquid equilibrium factor, P is Pressure, T is temperature, $kv1$, $kv2$, $kv3$, $kv4$ and $kv5$ are constants for specific gases.

Table 3-14: Default Values for K-Values from CMG STARS

Symbol	CH ₄ K-Values	Units
kv1	40,689	kPa
kv2	4.8680E-04	kPa
kv3	1.1616E+00	--
kv4	-118.3600	°C
kv5	-99.4700	°C

3.3.8 Modeling Initial Conditions

SAGD model initialization process in this research involves the initial pressure distribution in the model. The initial pressure is a function of depth. The reference pressure of 400 kPa was used at the reference depth of 100 m (Good et al. 1997; CMG STARS User's Guide, 2015). Capillary pressure was ignored, as was also neglected in the SAGD model constructed for the UTF/AOSTRA by Good et al. (1997) and the optimization work published by Noroozi et al. (2014), in addition to the CMG SAGD standard cases.

3.4 Wellbore Hydraulics Modeling

In conventional sink/source horizontal wells in SAGD, the only primary variable is set as the bottom hole pressure (BHP) or rates. SAGD operators later realized that flow behavior inside wellbore also affects project economics, requiring the inclusion of wellbore flow simulation (Oballa & Buchanan 2009). Several enhancements were introduced in the literature into the

classical sink/source model. The enhancements include incorporation of heat loss, frictional pressure-drop calculations, and treating fluid mixtures as a homogeneous fluid. However, these enhancements were not enough or valid for modeling complex situations such as multilateral wells and nested tubes. Incorporation of wellbore models such as CMG's FlexWell was in response to such shortcomings (Oballa & Buchanan 2009).

3.4.1 Classical Sink/Source Model

As discussed in the paper published by Oballa and Buchanan (1997), the flow from (producer) or into (injector) a reservoir is represented by a single term in classical sink/source well models as shown in **Eq. (3.7)**:

$$q_{ij} = WI_i \lambda_{ij} (p_w - p_{ij}) \quad (3.7)$$

where q is injection/production rate, j is phase (oil, water or gas), i is block number, WI is the well index, λ is fluid mobility and p_w is flowing bottomhole pressure and p_i is reservoir block pressure.

The model assumes steady-state flow and that there are no fluid composition changes, no temperature changes and no heat losses between the wellbore and reservoir and the only primary variable in the equation is the flowing bottomhole pressure. Such simplifications and assumptions are not valid when there is more than one tubing in the wellbore, especially at high temperatures and when there are some tubings for injection while some others are for production in SAGD models, especially during the circulation stage, where the same wellbore can act as an injector and producer at the same time using nested tubings (Oballa and Buchanan 2009).

3.4.2 FlexWell Model

The term FlexWell is a contraction of Flexible Wellbore. FlexWell model is a mechanistic discretized wellbore model that is able to model horizontal wells, vertical wells, slanted wells and deviated wells. The wellbore is discretized in the same manner as the corresponding reservoir gridding system, i.e., the wellbore is divided into segments and each segment is considered as a grid block (Oballa et al. 1997). **Table 3-15** shows a brief comparison between the characteristics of the classical sink/source model and FlexWell model.

Table 3-15: Comparison of Sink/Source and Flexible Wellbore Models, (Oballa and Buchanan 2009)

Feature	Sink/Source	FlexWell
Gravity	Explicit Head	Implicit
Frictional Heat Loss	Optional	Automatic
Cross-Flow W-R	Optional (Very Simple)	Automatic
Multilaterals	Optional	Optional
Trajectory	Optional	Optional
Transients	No	Automatic
Fluid Segregation	No	Automatic
Tubing	No	3 (Max.)
Wellbore Heat Loss and Friction, Wellhead to Pay Top	Optional	Optional
Orifice Flow A-R	Optional	Optional
Orifice Flow T-A	No	Optional
Well Plugging by Solids	No	Optional

Components of FlexWell Model

FlexWell can simulate up to three tubing strings accommodated into a casing or a slotted liner annulus. Tubing strings can have various lengths, and variable diameters over length and can be fully or partially insulated. Tubing strings can communicate with each other and with the annulus. Communication of tubing with annulus can be at the toe only or at different sections using flow control devices.

Each annulus and accommodated tubing string is considered as a single FlexWell model and is discretized, and the equations corresponding to these sections are solved concurrently. Each FlexWell model is solved separately from other FlexWell models and independently from the reservoir model. All FlexWell models are coupled with the reservoir through the annulus-reservoir flow term (Oballa & Buchanan 2009).

FlexWell Formulation

The governing equations for each stream (single tubing or annulus) consist of Fluid Phase Momentum and Energy Balance Equations, Mass Conservation Equation and Energy Conservation Equation (Oballa & Buchanan 2009). Details of these equations are discussed next.

Fluid Phase Momentum and Energy Balance Equations

A mechanistic approach is used to solve fluid-phase momentum equations. The solution shown in **Eq. (3.8)** consists of calculating the frictional pressure drop in relation to the flow regime (laminar, turbulent, transition) and flow pattern (e.g., segregated, bubble).

$$\frac{dP}{dL} = \rho_m V_m \frac{dV_m}{dL} + \rho_m \frac{dF}{dL} + g \rho_m \sin \theta \quad (3.8)$$

where P is pressure, L is length, ρ_m is mixture density, V_m is mixture velocity F is friction loss θ is inclination angle and g is gravity acceleration.

Conductive radial heat transfer rate is calculated based on Eq. (3.9):

$$-\frac{dH_m}{dL} = V_m \frac{dV_m}{dL} + g \sin \theta - \frac{dQ}{dL} \quad (3.9)$$

where H_m is mixture enthalpy and Q is radial heat transfer rate.

The inverse heat resistance (also called heat transfer coefficient) is composed of: (1) conductive resistance through the tubing/annulus wall (depends on the wall thickness and metal conductivity); (2) conductive resistance of fluids and reservoir block (depends on the fluid composition).

The calculated heat transfer coefficient multiplied by temperature difference between adjoining wellbore parts (fluid inside tubing + tubing wall + fluid inside annulus + annulus wall + adjacent reservoir grid block) yields conductive radial heat transfer rate (Q_H)

Mass Conservation Equation

Implementation of mass conservation for fluid components is essential to modeling fluid transient and segregation behaviors in the wellbore:

$$\sum \rho_p V_p m_{p,i} = B \frac{\partial}{\partial t} [\phi_f \sum \rho_p S_p m_{p,i}] \quad (3.10)$$

where ρ_p is phase molar density, V_p is phase flow rate, $m_{p,i}$ is phase mole fraction, B is section volume ϕ_f is fluid porosity fraction, S_p is phase fraction.

Energy Conservation Equation

Energy conservation for fluid components is also required to model temperature transient and heat flow in the wellbore:

$$\sum \rho_p V_p H_p + \text{Conductive heat } 1, r = B \frac{\partial}{\partial t} [\phi_f \sum \rho_p S_p U_p + \phi_w U_w] \quad (3.11)$$

where H_p is phase molar enthalpy, B is section volume, U_p is phase internal energy, U_w is wall enthalpy and ϕ_w is wall porosity.

3.4.3 Coupling of Reservoir/ FlexWell Models

Time coupling of FlexWell and reservoir models together is not fully implicit. Thus, FlexWell equations are not solved simultaneously with the reservoir equations, i.e., reservoir solution always lags by one iteration. The following procedure is followed during each iteration of the coupled non-linear reservoir equations (Buchanan et al. 1997; Oballa and Buchanan 2009): FlexWell equations are solved assuming constant conditions in the surrounding reservoir region. Only perforated cells are involved in the annulus reservoir flow terms. Each FlexWell equation set is solved simultaneously and iteratively to a tight convergence tolerance using Newton's method (CMG STARS User's Guide 2015). The FlexWell solution consists of pressure, temperature, phase saturations and compositions in each section of each stream, including the annulus.

Each iteration of the reservoir equations is done assuming constant conditions in the annulus of each FlexWell when calculating the annulus reservoir flow terms (Buchanan et al. 1997; Oballa and Buchanan 2009). **Figure 3-11** illustrates the coupling process of wellbore/reservoir models using CMG STARS and FlexWell.

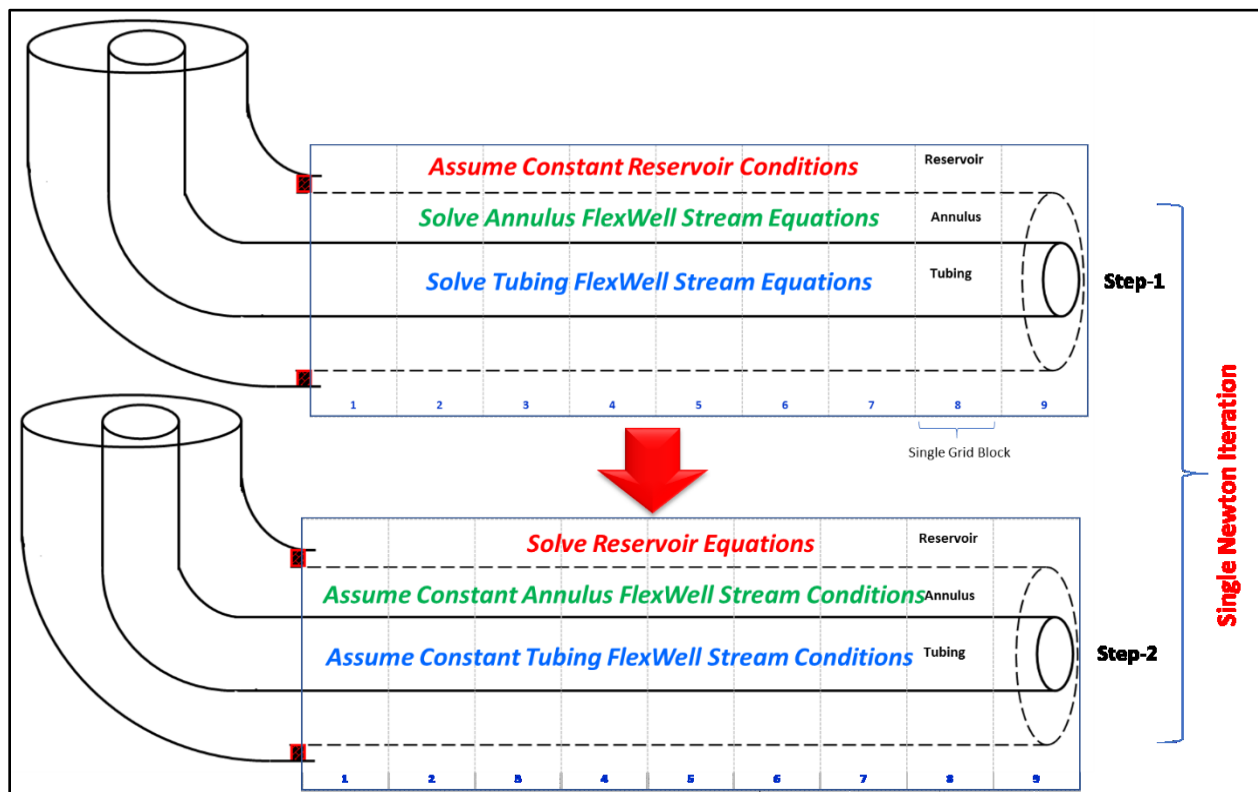


Figure 3-11: Wellbore/Reservoir Models Coupling Process

3.5 Construction of Basic SAGD Wellbore Model

3.4.4 Well Pair Completion System

The default completion scheme of the SAGD model base case well pair in this research is dual-string completion. The injector is 900-m long and is completed with a 9 5/8" slotted liner, a 4 1/2" short tubing string landed at the heel, and a 4 1/2" 900-m-long tubing string landed and open at the toe only.

The producer well is 900-m long and it is completed with a 9 5/8" slotted liner, 4 1/2" short tubing string landed at the heel and 4 1/2" 900-m-long tubing string landed and open at the toe only. **Figure 3-12** depicts the dual-string completion scheme for both the injector and producer.

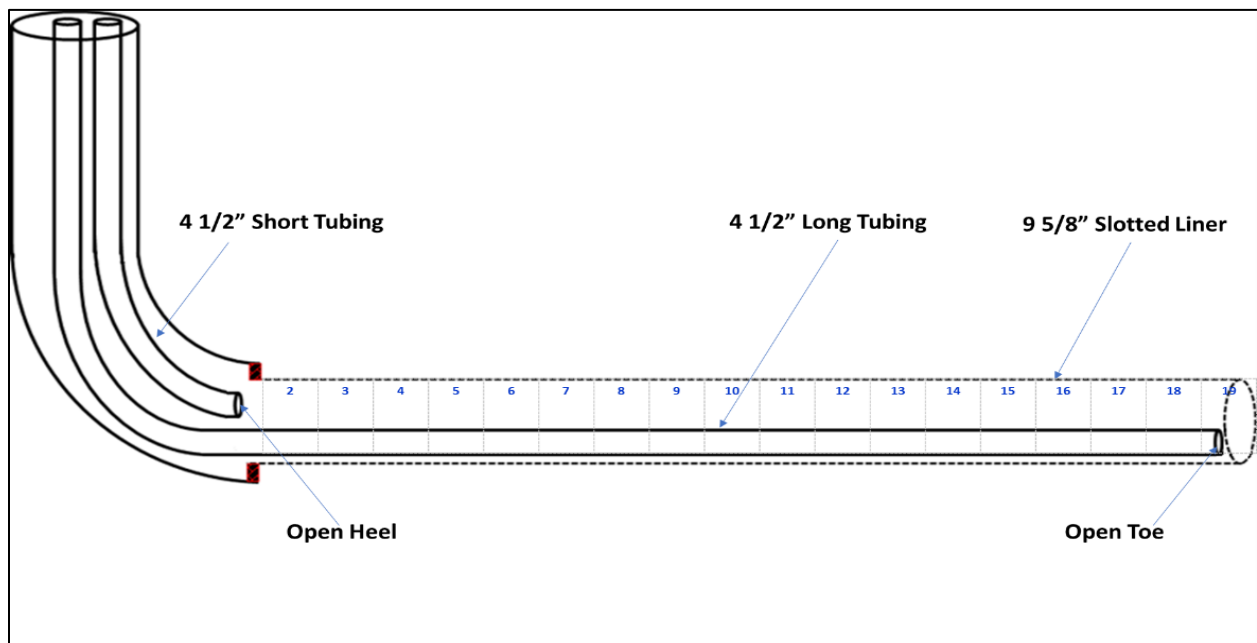


Figure 3-12: SAGD Producer/Injector Dual-String Completion Scheme

3.4.5 Definition of Sink/Source Wells

To be able to use FlexWell in a model, it is essential to define sink/source wells. The total number and type of wells (injectors/producers) to be defined depend on how the circulation/SAGD stages are modelled and how the injection/production processes are carried out. In this research, both circulation and SAGD stages are modeled using FlexWell; thus, six wells need to be defined in total (three injectors and three producers). **Figure 3-13** illustrates a timeline view of the created sink/source wells in the CMG Builder for the whole periods of circulation and SAGD stages. The injection annulus was initially defined as producer during circulation stage (for three months), then converted into an injector at the end of circulation stage. The long tubing inside the injection

annulus was defined as injector for the whole periods of circulation and SAGD stages. The production annulus was defined as producer during the entire periods of circulation and SAGD stages. The long tubing inside the production annulus was defined as injector during circulation stage, then converted to producer during SAGD stage.

Wells	Type	2013	2014	2015	2016	2017	2018	2019	2020	2021	2022	2023
Injector Annulus	Injector (SAGD Only)											
Injector Annulus	Producer (Circulation Only)											
Injector Long	Injector (Circulation+SAGD)											
Production Annulus	Producer (Circulation+SAGD)											
Production Tubing	Producer (SAGD Only)											
Production Tubing	Injector (Circulation Only)											

Figure 3-13: Sink/Source Wells Timeline View in CMG

3.4.6 Modeling Circulation Stage

Circulation start-up technique described in Section 2.1.3 has been adopted here. In the injector, high-quality steam is injected through the long tubing injector (Injector Long Tubing) and allowed to be circulated and produced back to the surface through the annulus (Injector Annulus Producer). In the producer, high-quality steam is injected through the long tubing producer (Producer Long Tubing Injector) and allowed to be circulated and produced back to surface through the production annulus (Producer Annulus). Circulation stage is allowed to continue for three months (90 days) until the bitumen in well pair vicinity is heated and becomes mobile with an average well pair temperature of 125°C as shown in **Figure 3-14**. **Table 3-16** summarizes the constraints for production/injection wells during the circulation stage.

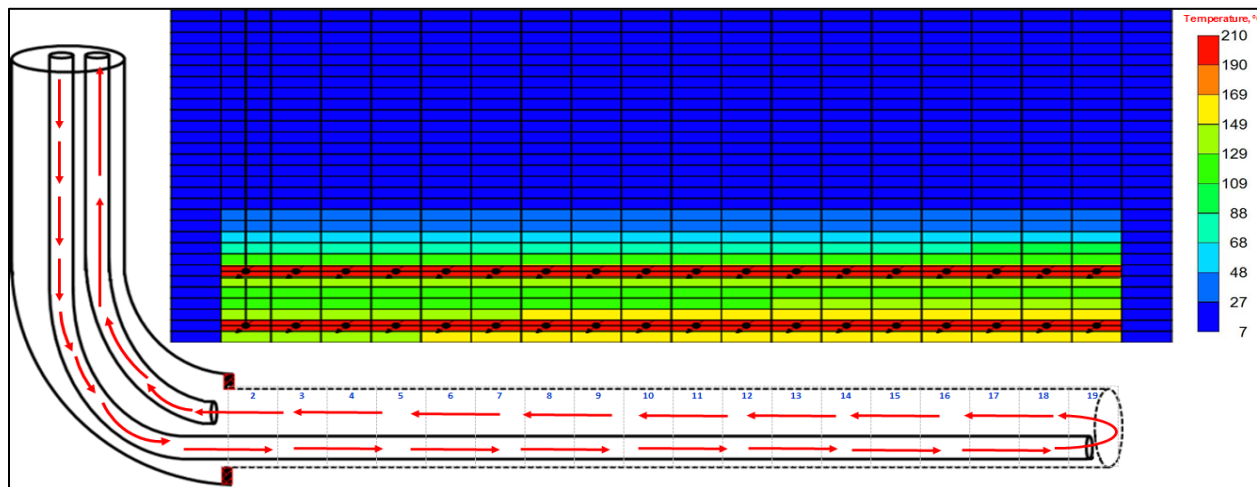


Figure 3-14: Temperature Map of the SAGD Model at the end of Circulation Stage

Table 3-16: SAGD Wells Operating Constraints During Circulation Stage

Well Name	Type	Injection Data				Production Data		Period	
		Max. Steam Inj. Rate (m ³ /d CWE)	Steam Quality (%)	Steam Inj. Temp. (°C)	Max. Inj. BHP (kPa)	Max. Liquid Prod. Rate (m ³ /d)	Min. Prod. BHP (kPa)	Start-up Date	Shut-in Date
Injector Annulus	Producer	--	--	--	--	1,000**	900*	1-Jan-13	1-Apr-13
Injector Long Tubing	Injector	700**	90	224	1,780*	--	--	1-Jan-13	--
Producer Annulus	Producer	--	--	--	--	1,000**	900*	1-Jan-13	--
Producer Long Tubing	Injector	700**	90	224	1,780*	--	--	1-Jan-13	1-Apr-13
* Primary Constraint ** Secondary Constraint									

3.4.7 Modeling SAGD Stage

At the end of circulation stage, the system is converted into SAGD operation. This is done by converting both injector annulus and long injector wells into injectors to secure two injection points (at the heel and toe) aiming to achieve uniform steam injection and steam chamber growth. Also, both production annulus and long production tubing strings are converted to producers, i.e., there are two production points, one at the heel (annulus) and one at the toe (long tubing). **Table 3-17** shows a summary of operating conditions during the SAGD stage. Because the amount steam required varies over the SAGD project lifespan, constant injection bottom hole pressure constraint was chosen rather than constant injection rate. This choice allows also to mimic MacKay River SAGD project in terms of keeping the injection pressure within the maximum operating pressure. **Figure 3-15** is a schematic diagram of fluid path through the well pair.

In CMG simulation models, the maximum steam injection pressure is defined at the first block that contains the trajectory of the injector (i.e., the landing point of the of the horizontal section of the SAGD injector), and its value has been selected based on maximum operating pressure values of MacKay River SAGD well pair reported in **Table 3-5**.

Other operation constraints and steam quality were selected based on several published papers related to MacKay River SAGD project (Vincent et al. 2004; Li et al. 2006; Parmar et al. 2009;

Chang et al. 2012, Wang and Morris 2013), UTF/AOSTRA project (Good et al. 1997) and CMG standard demonstrative FlexWell Tubing/Annulus SAGD cases.

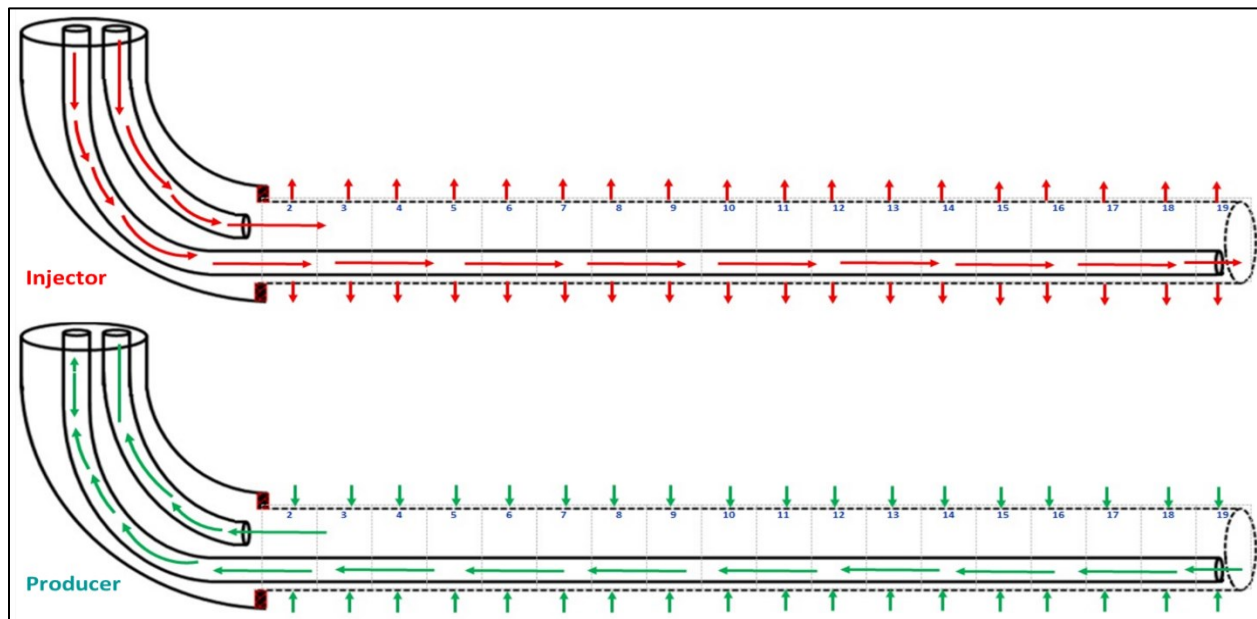


Figure 3-15: Producer/Injector Wells During SAGD Stage

Table 3-17: SAGD Wells Operating Constraints During SAGD Stage

Well Name	Type	Injection Data				Production Data			Period	
		Max. Steam Inj. Rate (m³/d CWE)	Steam Quality (%)	Steam Inj. Temp. (°C)	Max. Inj. BHP (kPa)	Max. Liquid Prod. Rate (m³/d)	Min. Prod. BHP (kPa)	Max. Steam Prod. Rate (m³/d CWE)	Start-up Date	Shut-in Date
Injector Annulus	Injector	700**	90	224	1,615*	--	--	--	1-Apr-13	End of SAGD Project Life
Injector Long Tubing	Injector	700**	90	224	1,780*	--	--	--	1-Apr-13	
Producer Annulus	Producer	--	--	--	--	1,000***	1550*	4**	1-Apr-13	
Producer Long Tubing	Producer	--	--	--	--	1,000***	1550*	4**	1-Apr-13	
* Primary Constraint ** Secondary Constraint *** Tertiary Constraint										

CHAPTER FOUR: BASE CASE MODEL ENHANCEMENT AND GRID SIZE SENSITIVITY ANALYSIS

4.1 Introduction

Considering the vast number of simulation runs that would be carried out for each single study during the optimization work in Chapter 6, it is important to adopt the coarsest yet accurate model that consumes the least amount of computation time. However, before proceeding with optimization studies, it is crucial to conduct a grid size sensitivity analysis to verify and determine the validity of the constructed coarse-grid models compared with the finer models. The validity of the coarse-grid models would be verified by examining the modeling output in terms of bitumen and water production, cSOR, and the size of steam chamber.

4.2 Overview of Conventional Grid Size Sensitivity Work

Initially, a grid size sensitivity analysis was carried out using a conventional grid system, where three different grid designs were generated and analyzed for each trajectory case. The grid design consists of uniform $1 \times 1 \text{ m}^2$ grid blocks in the section perpendicular to the well pair. This grid design has been found to be necessary for an accurate SAGD simulation (Perez et al. 2017). The conventional grid size sensitivity consisted of three grid length variations of 50, 20, and 10 meters in the direction parallel to the wells.

Results show high variations in the production data and discrepancies in steam chamber growth due to several reasons. Details of the initial grid size sensitivity work, which show discrepancies in the results and the root causes are demonstrated in **Appendix A**. The level of discrepancies increases with the increase of well pair trajectory complexity.

The conclusions from this initial attempt was that either the mesh had to be further refined in the axial direction, or the mesh had to be locally refined in the zones with high pressure and temperature gradients. Given the considerable number of simulation cases in an optimization work, the use of a uniform fine mesh in the axial CMG STARS' Local Grid Refinement (LGR) module was used for targeted local refinement of grid blocks around the well pair to obtain more accurate results without a significant increase in the computation time.

4.3 Grid Size Sensitivity Analysis with LGR

The base case model in this section consists of a $1 \times 1\text{-m}^2$ grid design in the section perpendicular to the wells and a uniform $2 \times 1\text{-m}^2$ grid for the section parallel to the wells. The LGR technique was implemented to increase the grid size parallel to the well, while still maintaining the 2-m grid size adjacent the wells. The smaller grid length (2-m) was used along the well pair trajectories aiming to achieve the following targets:

- Accurate modeling of heat transfer by conduction in the axial direction (J-Direction).
- Maintaining the original well pair trajectory of fine-grid models as shown in **Figure 4-1**. **Figure 4-2** shows how the grid design can impact an accurate implementation of the wellbore trajectory in the model.
- Accurate modeling of rapid changes in temperature and pressures near the well pair.

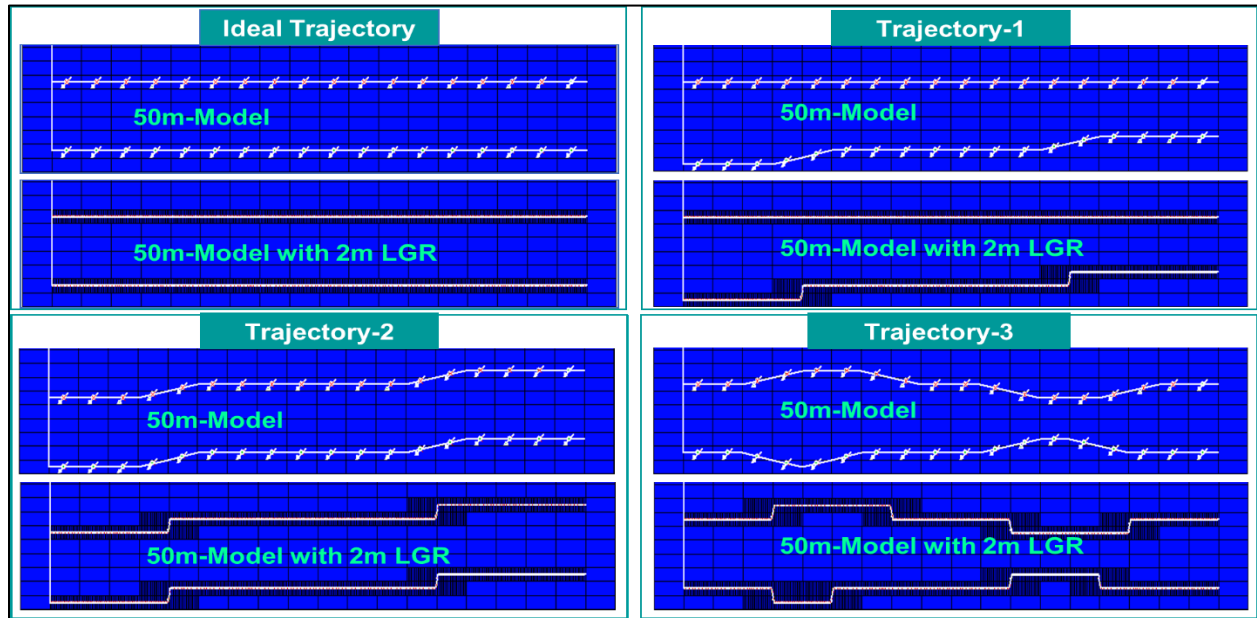


Figure 4-1: Coarse Grid Models for Different Trajectories with/without 2-m LGR

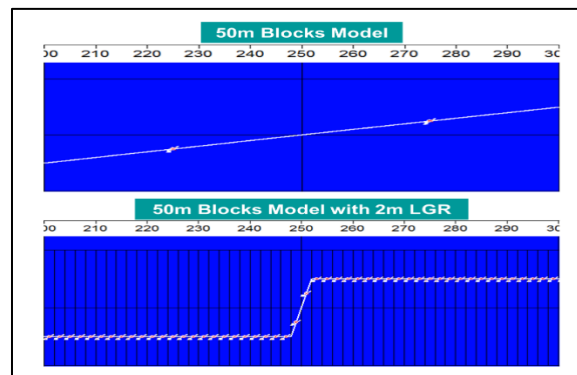


Figure 4-2: Coarse Grid Model Blocks with/without 2-m LGR

4.3.1 Grid Variations

For each trajectory case, six different models were constructed for grid size sensitivity analysis. The base case in the set of models for each trajectory is the model with the finest grid (2 m in the axial direction). The rest of models, as summarized in **Table 4-1**, are five models with 10-m, 20-m, 30-m, 36-m, and 50-m block lengths in J-Direction. All of these models are enhanced with the 2-m LGR in the blocks containing well pair trajectories.

Table 4-1: Dimensions of Models for Grid Size Sensitivity Analysis with 2-m LGR

No.	Model	# of Blocks				Blocks Lengths (m)		
		I	J	K	Total	I	J	K
1	2-m Model	17	452	30	230,520	2	2	1
2	10-m Model	17	92	30	47,640	2	10	1
3	20-m Model	17	47	30	24,780	2	20	1
4	30-m Model	17	32	30	17,160	2	30	1
5	36-m Model	17	27	30	14,620	2	36	1
6	50-m Model	17	20	30	11,064	2	50	1

4.3.2 Implementation of LGR

In LGR process, each parent grid block along well pair trajectory is refined into smaller child grid blocks. For instance, a 50-m-long parent grid block is divided into 25 2-m child grid blocks as depicted in the illustrative diagram shown in **Figure 4-3**.

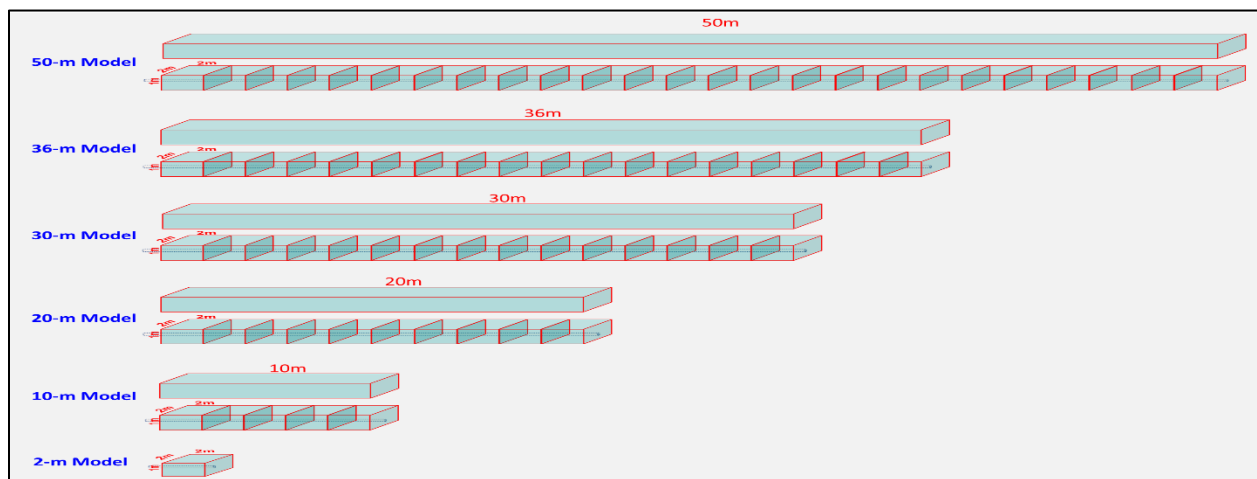


Figure 4-3: Coarse and Medium Local Grids Refinement

4.3.3 Ideal Trajectory with LGR

Figures 4-4 through 4-9 show six models with the ideal trajectory wells with 2-m LGR around the straight well pair trajectories.

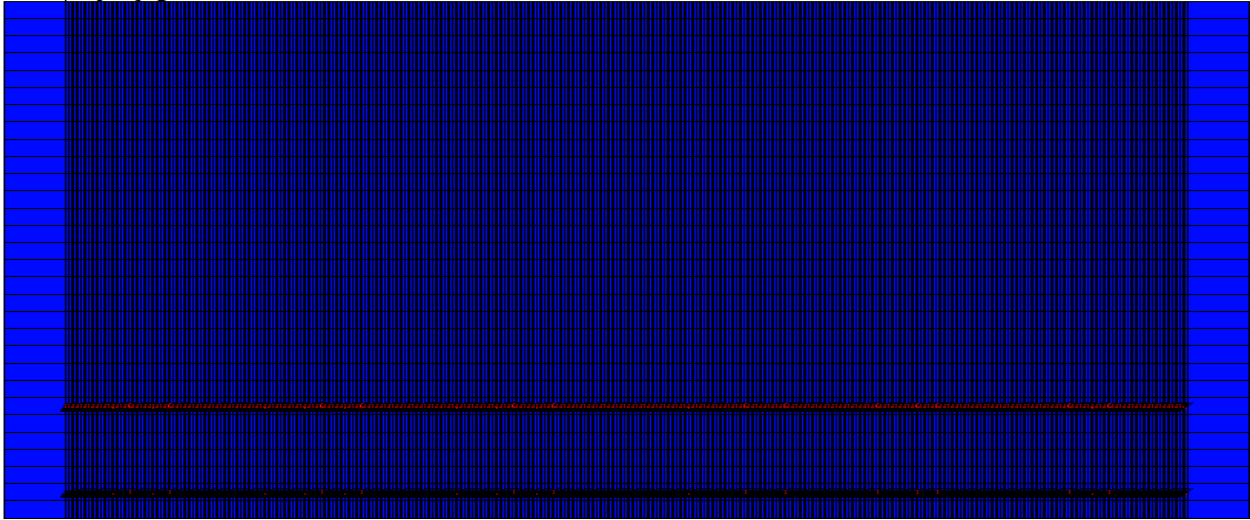


Figure 4-4: Ideal Trajectory, 2-m Model

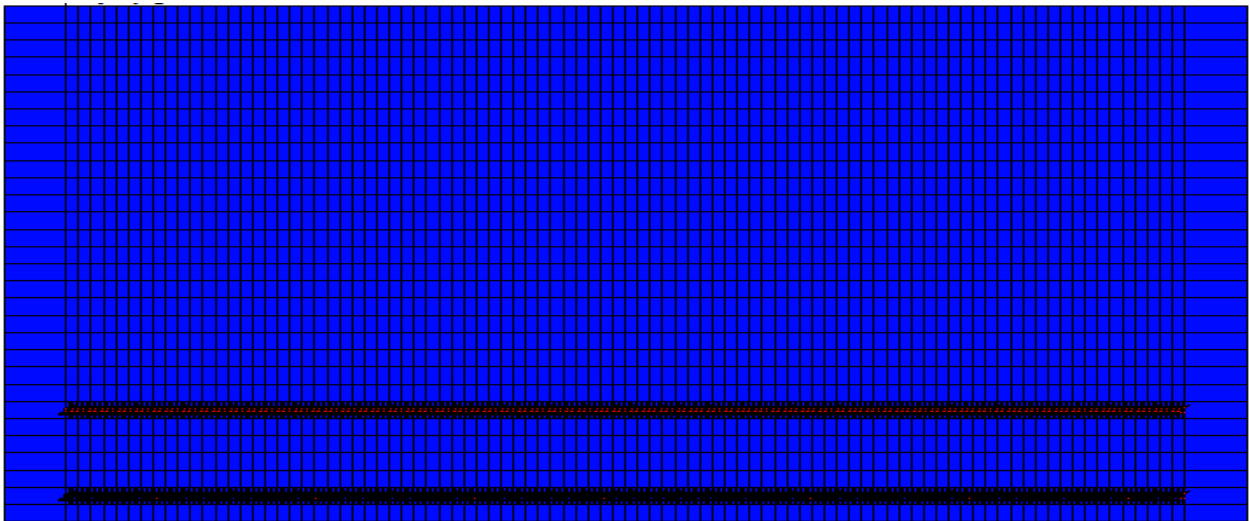


Figure 4-5: Ideal Trajectory, 10-m Model with 2-m LGR

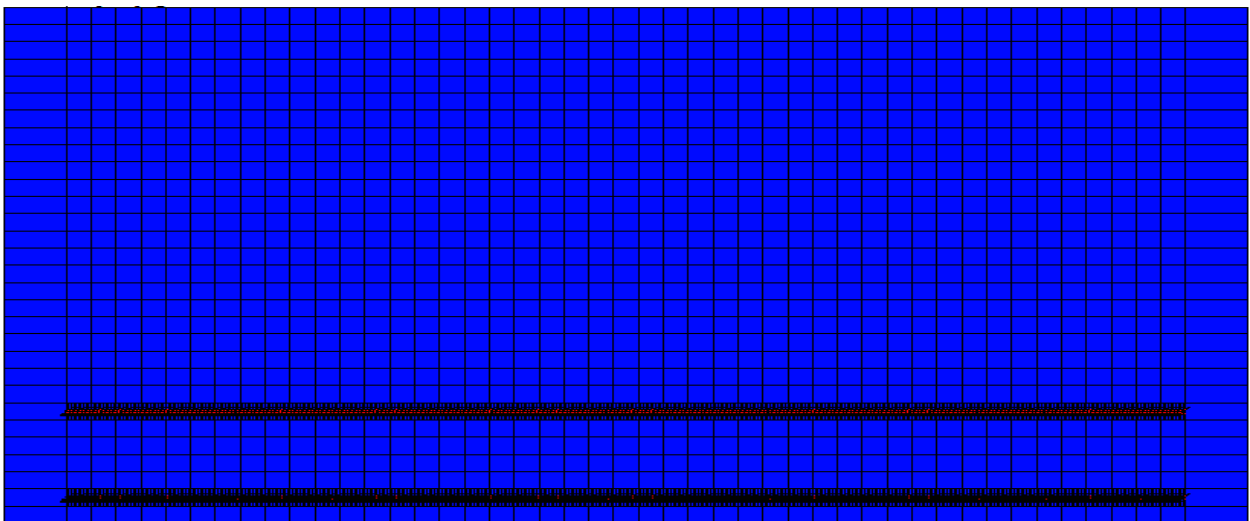


Figure 4-6: Ideal Trajectory, 20-m Model with 2-m LGR

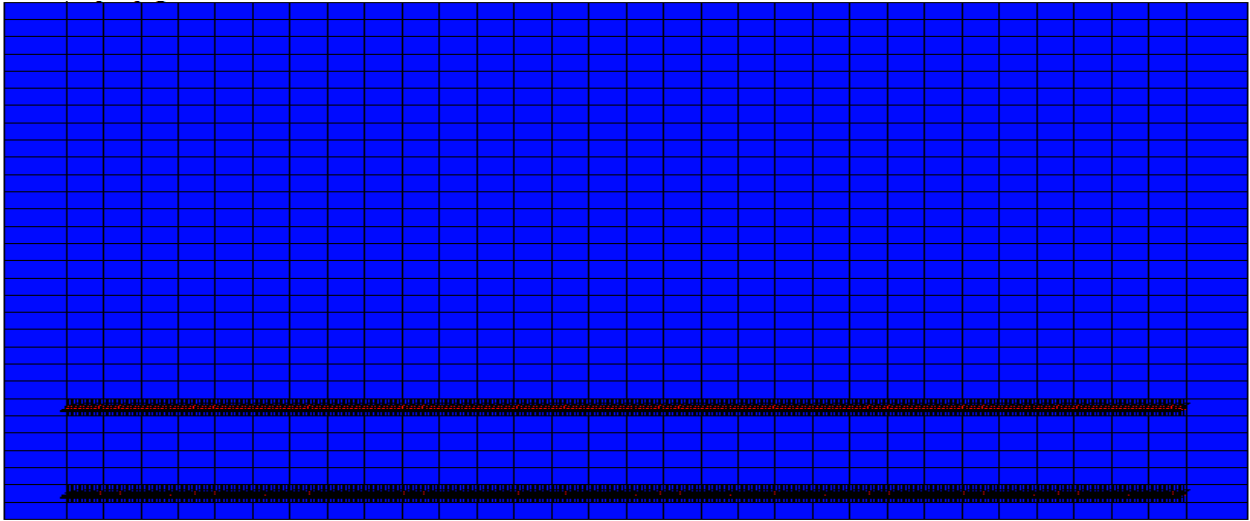


Figure 4-7: Ideal Trajectory, 30-m Model with 2-m LGR

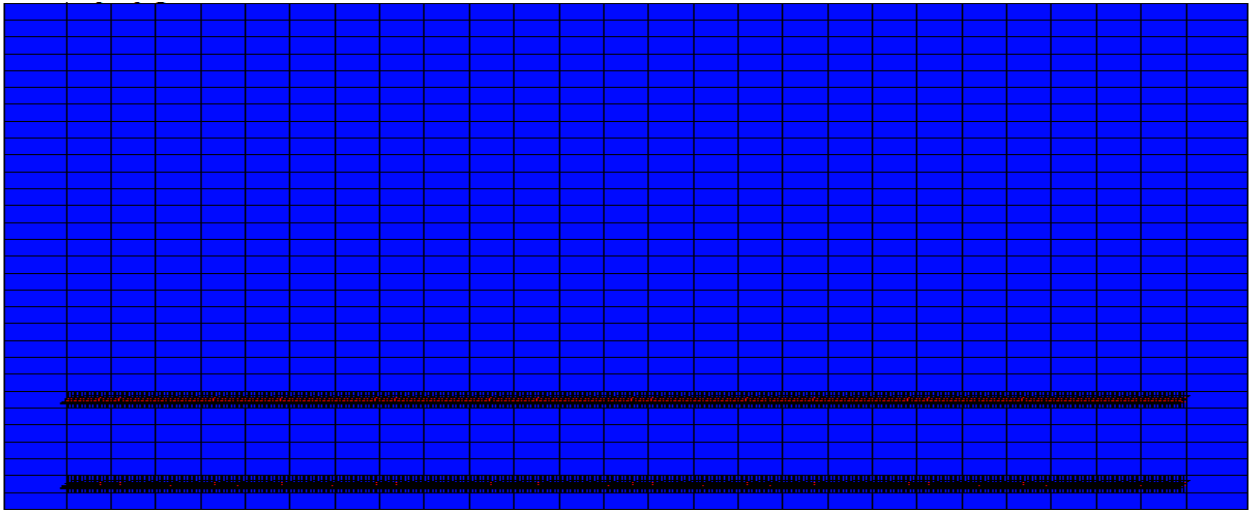


Figure 4-8: Ideal Trajectory, 36-m Model with 2-m LGR

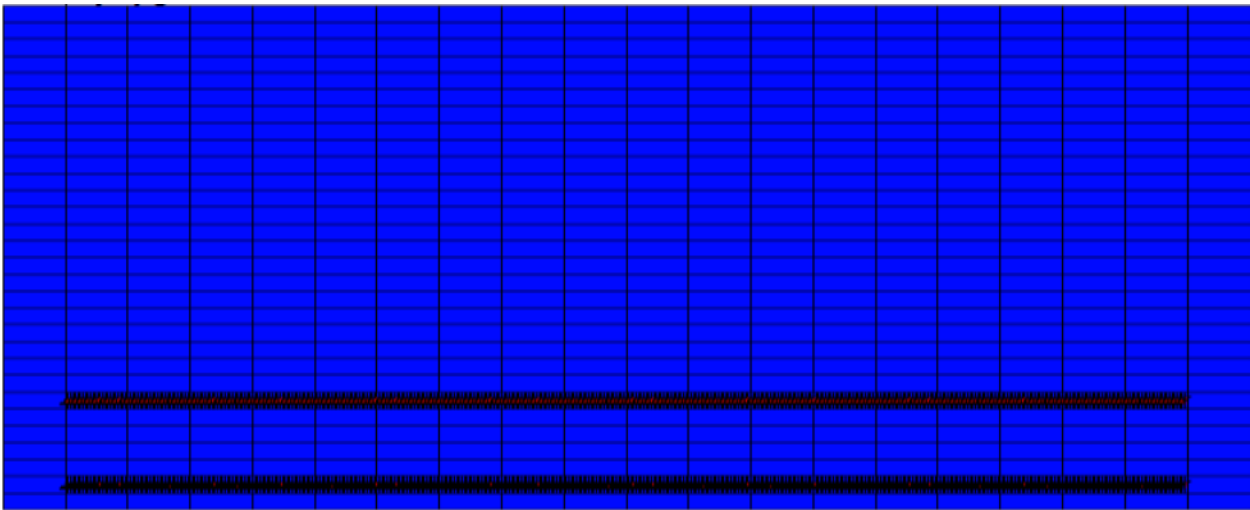


Figure 4-9: Ideal Trajectory, 50-m Model with 2-m LGR

Production Data

Figure 4-10 shows cumulative bitumen production (in m^3), cumulative steam injection (in m^3 CWE), cSOR (in m^3/m^3) and NPV (in \$M USD), which will be discussed in detail in Chapter 5. Results indicate a good agreement for these results among the six models with differences in SAGD performance data within 4%.

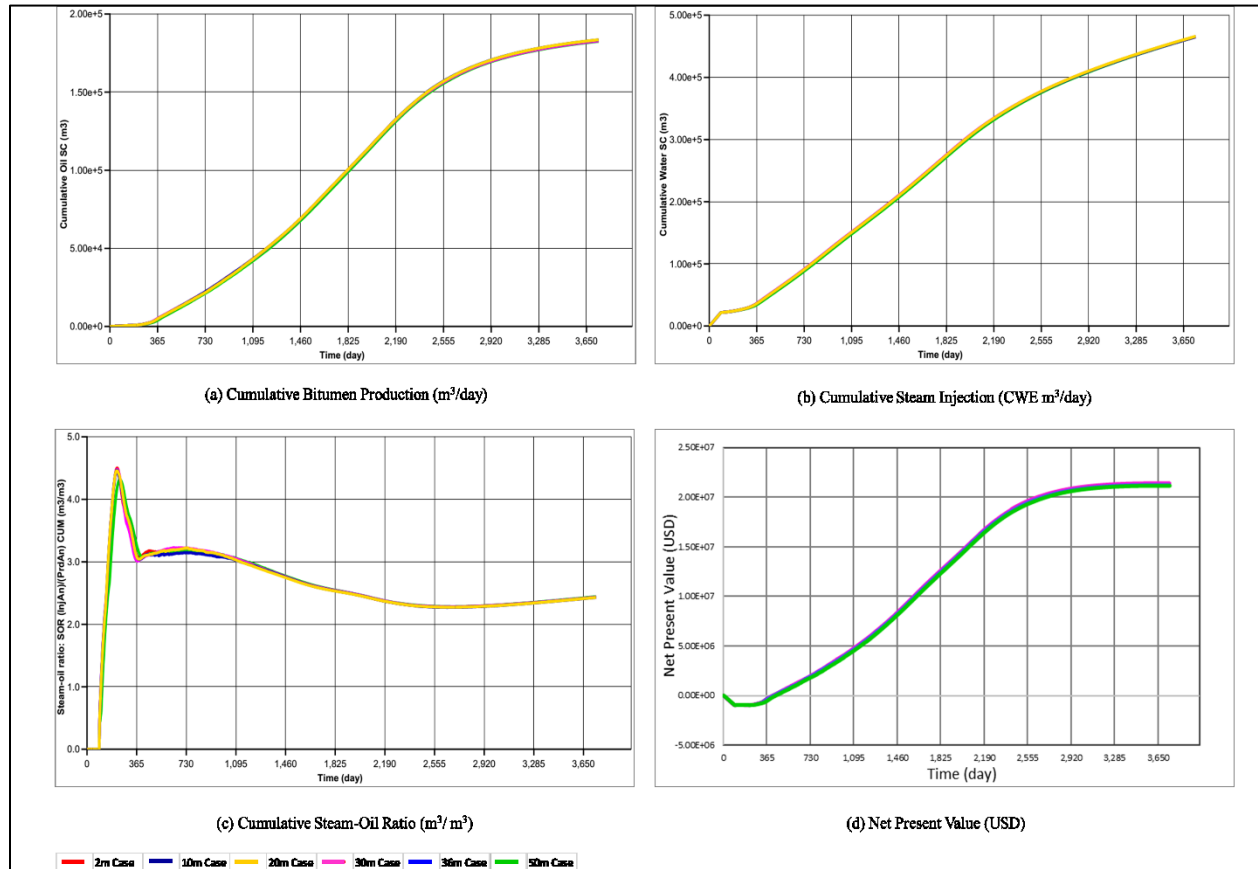


Figure 4-10: SAGD Performance Data of Different Ideal Trajectory Models with 2-m LGR

Steam Chamber

Consistent and smooth steam chamber growth during first, second and third years of SAGD can be observed in **Figure 4-11**.

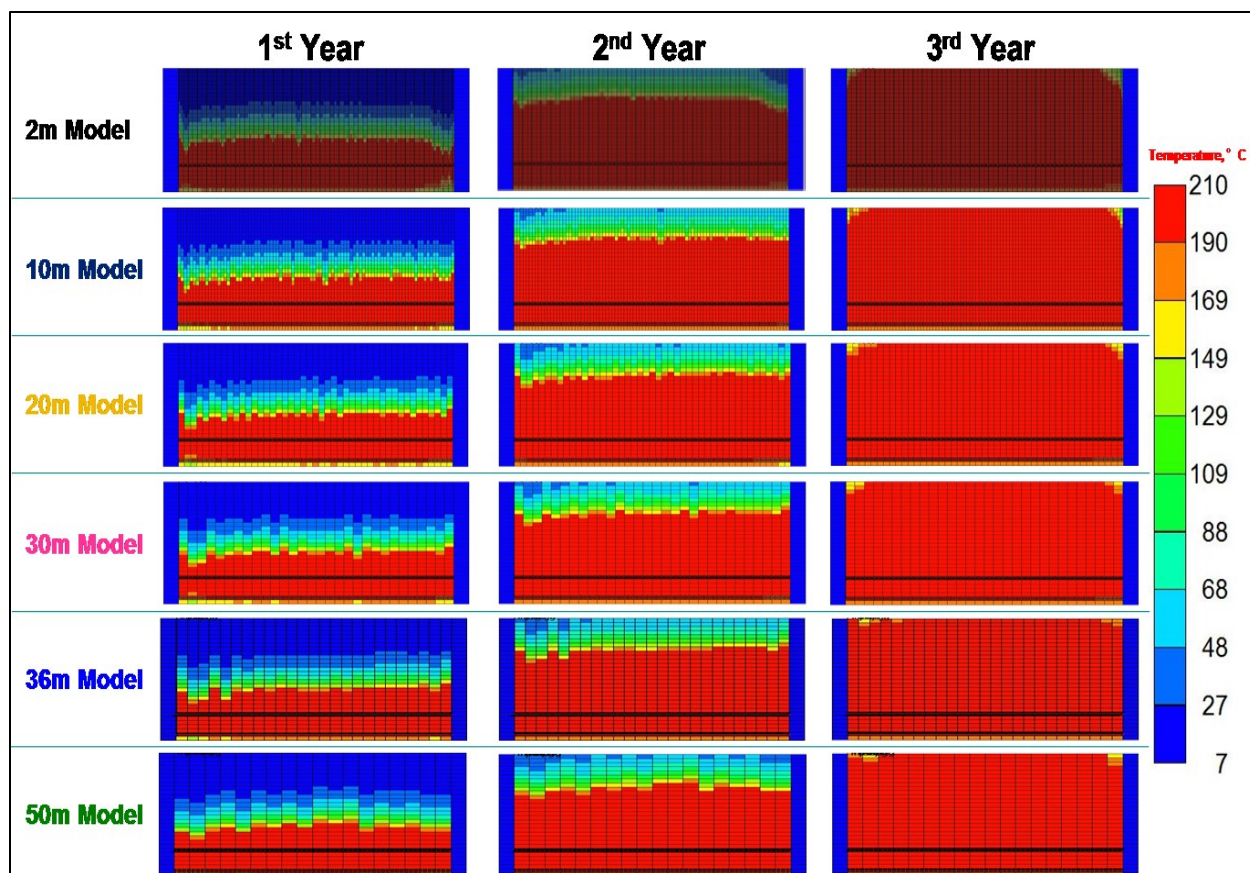


Figure 4-11: Early-Stage SAGD Temperature Maps of Different Ideal Trajectory Models

4.3.4 Trajectory-1 with LGR

Figures 4-12 through 4-17 show the 2-m, 10-m, 20-m, 30-m, 36-m, and 50-m models of Trajectory-1 after applying the 2-m LGR along the injector and producer trajectories. The 2-m LGR was also applied within 50-m distances left and right of each trajectory excursion point for more accurate results when compared to the original 2-m model.

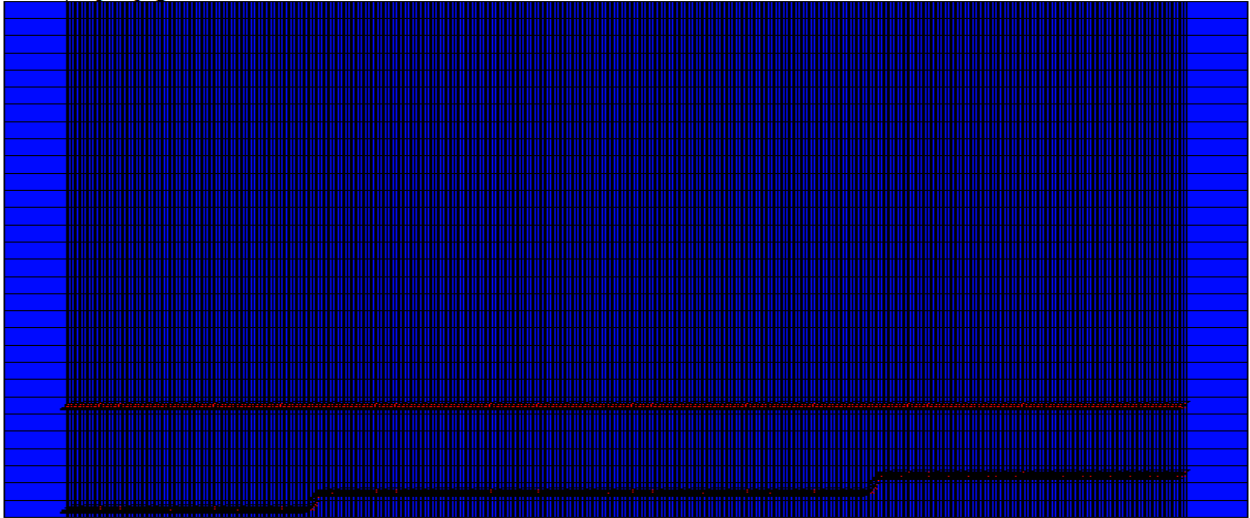


Figure 4-12: Trajectory-1, 2-m Model

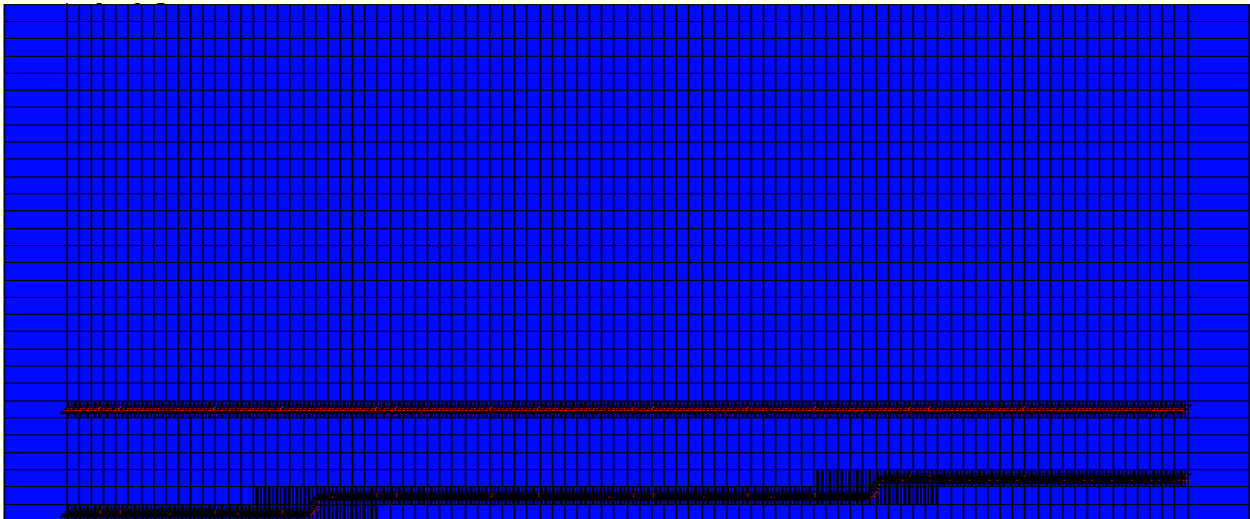


Figure 4-13: Trajectory-1, 10-m Model with 2-m LGR

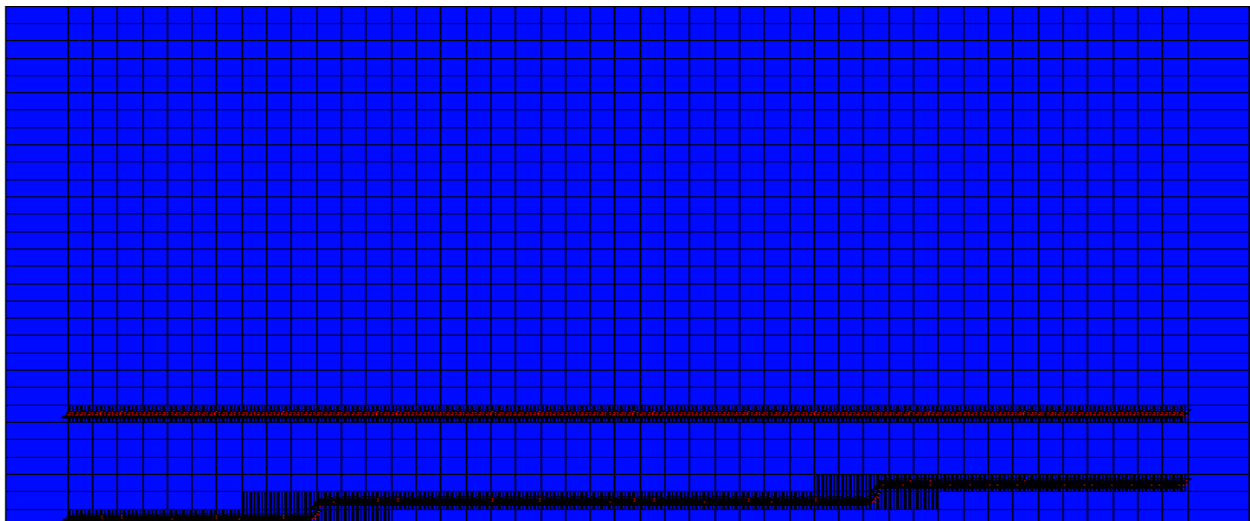


Figure 4-14: Trajectory-1, 20-m-Model with 2-m LGR

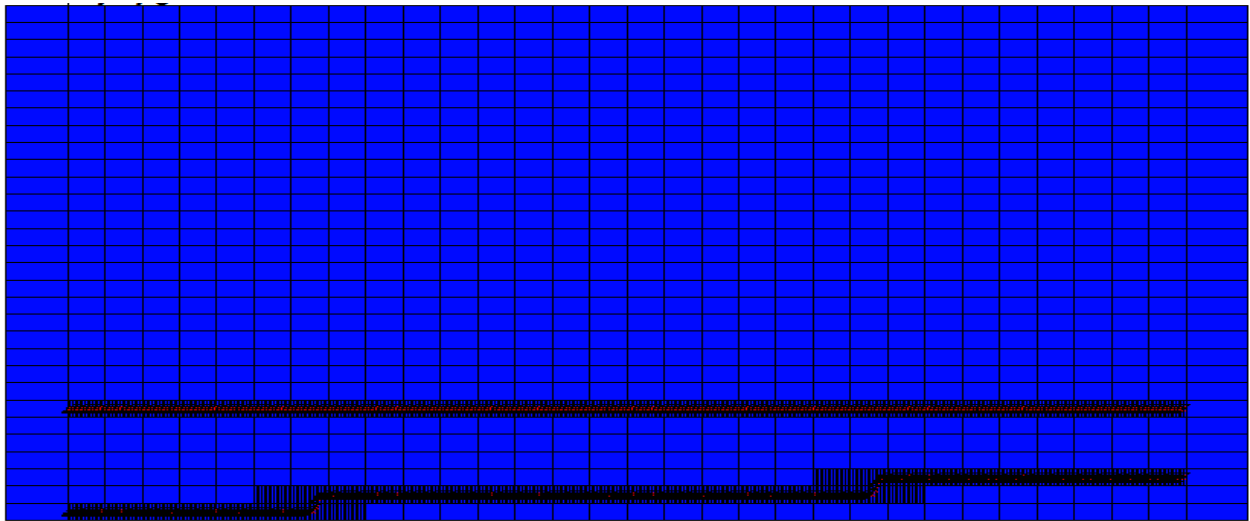


Figure 4-15: Trajectory-1, 30 m Model with 2-m LGR

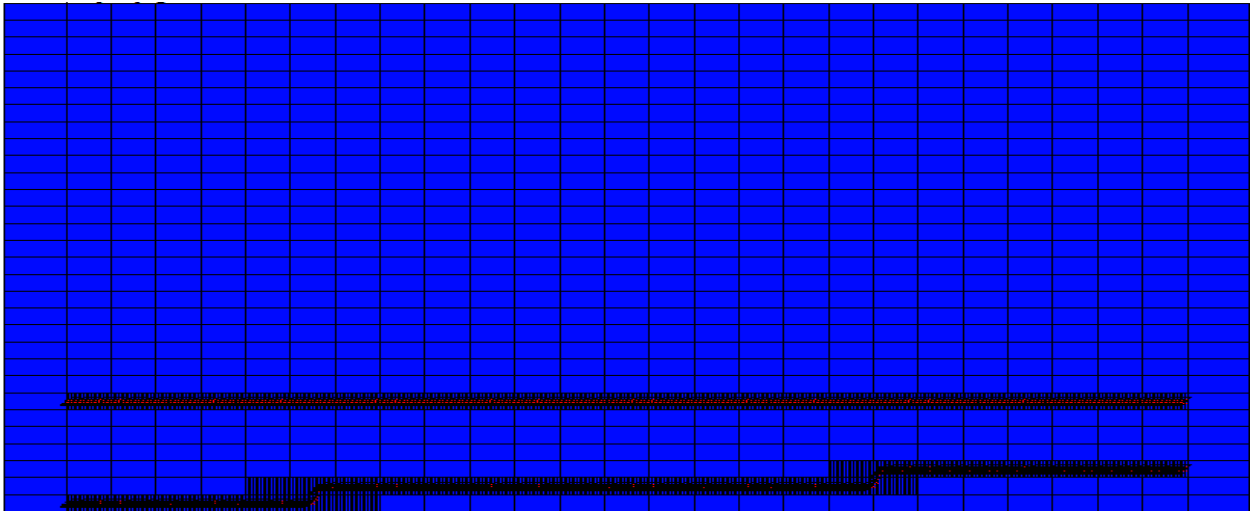


Figure 4-16: Trajectory-1, 36-m Model with 2-m LGR

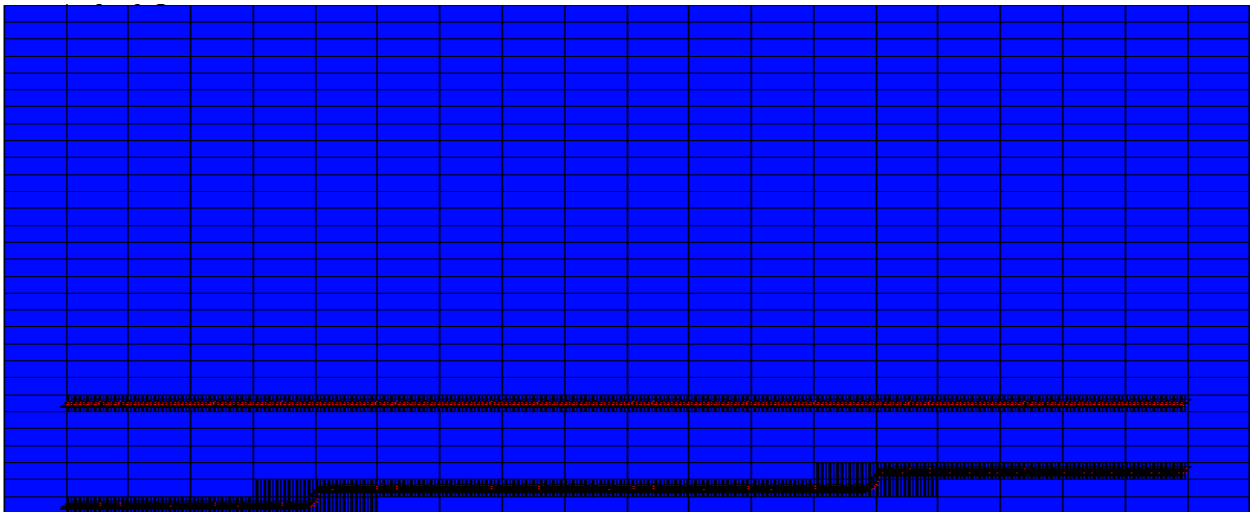


Figure 4-17: Trajectory-1, 50-m Model with 2-m LGR

Production Data

An appropriate matching of SAGD performance data of Trajectory-1 six models can be observed in **Figure 4-18**, where the differences in SAGD performance data are within 6%.

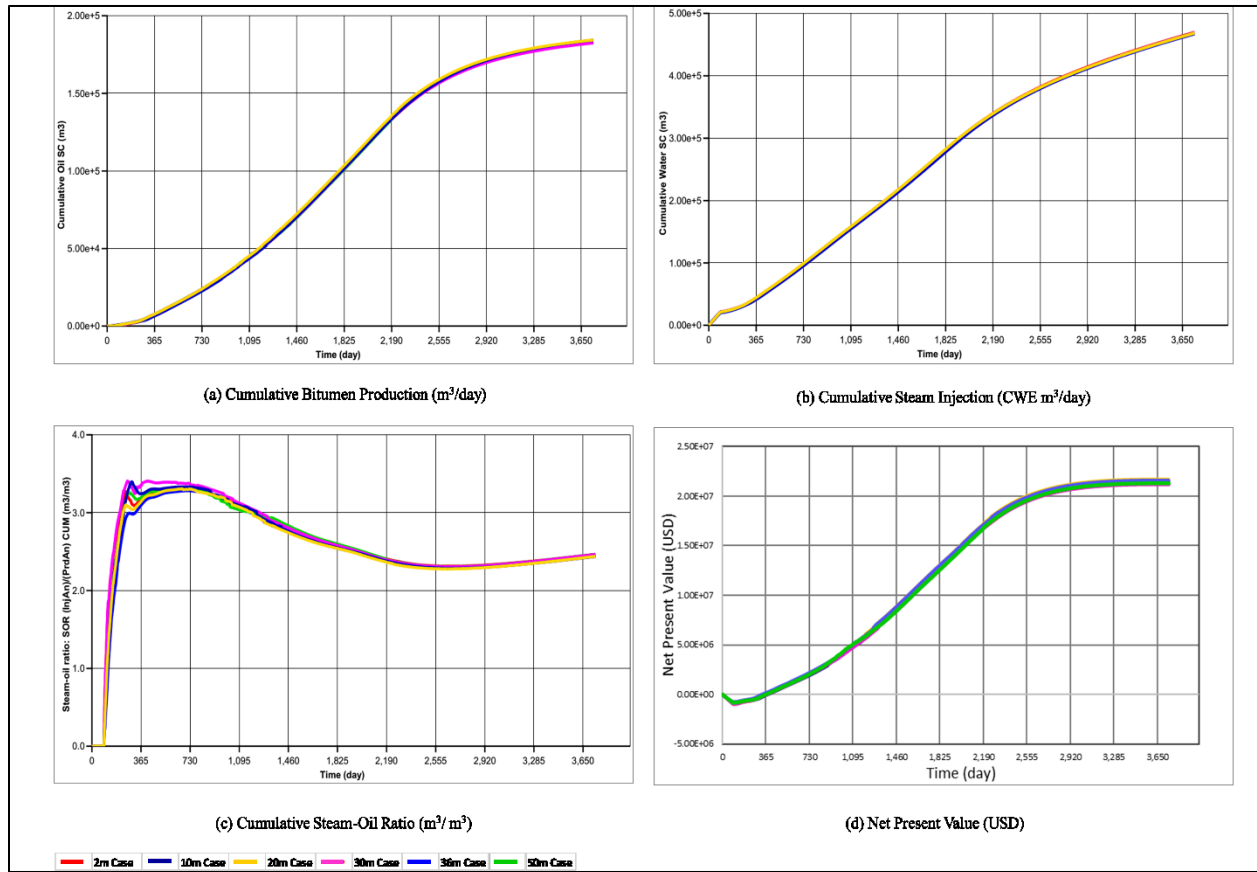


Figure 4-18: SAGD Performance Data of Different Trajectory-1 Models with 2-m LGR

Steam Chamber

Temperature maps of different models are in good match as illustrated in **Figure 4-19**. Three intervals with distinct temperature signatures are identified along the well pair trajectory. Temperature maps show that steam chamber height (or distance from the reservoir ceiling) depends on the excursions of the injector wellbore trajectory, where less steam chamber height can be noticed when the distance between the injector and reservoir ceiling is higher.

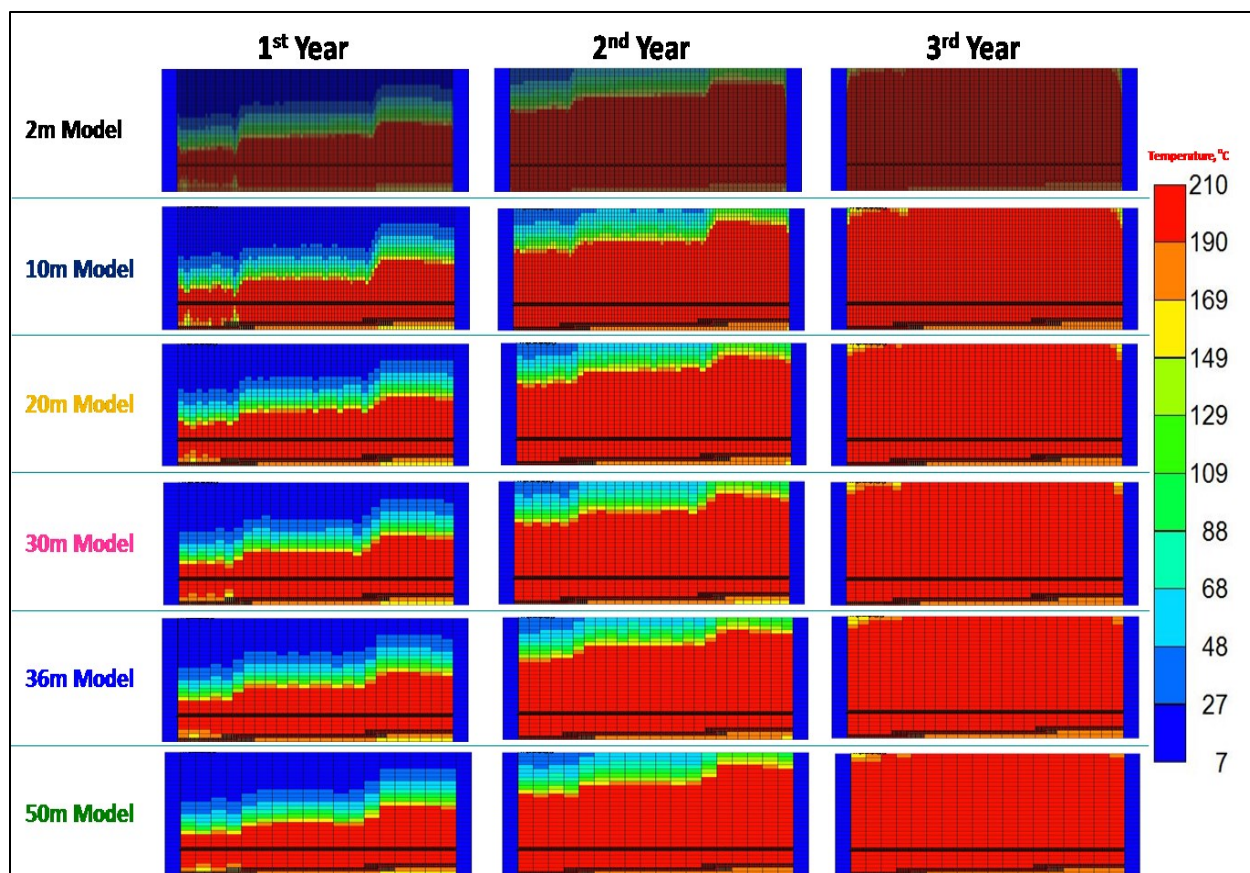


Figure 4-19: Early-Stage SAGD Temperature Maps for Different Trajectory-1 Models

4.3.5 Trajectory-2 with LGR

Figures 4-20 to 4-25 are the six Trajectory-2 models. As in previous cases, the 2-m LGR has been implemented along the injector and producer trajectories.

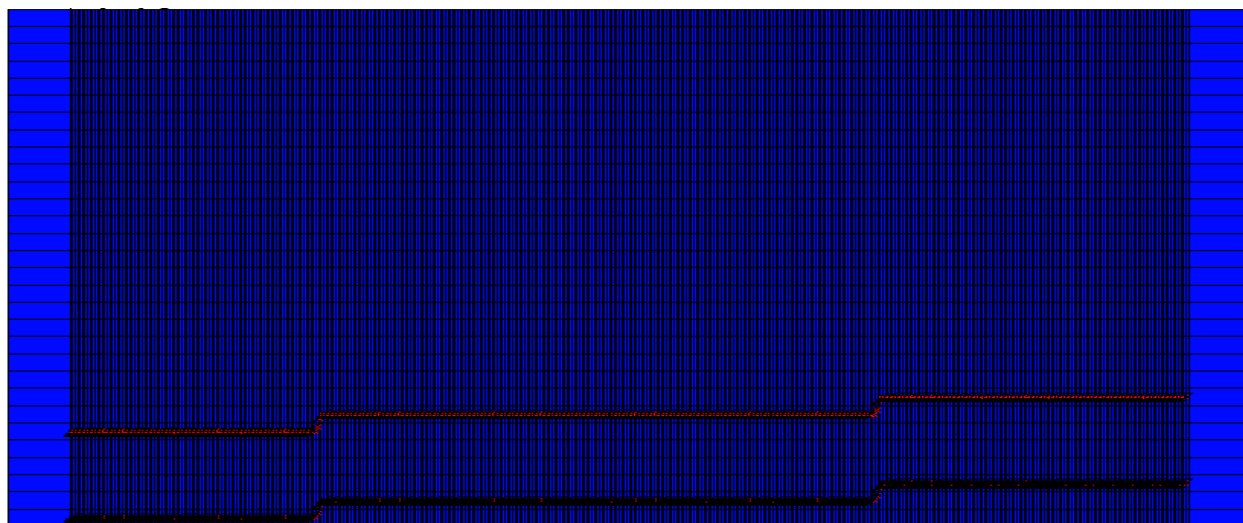


Figure 4-20: Trajectory-2, 2-m Model

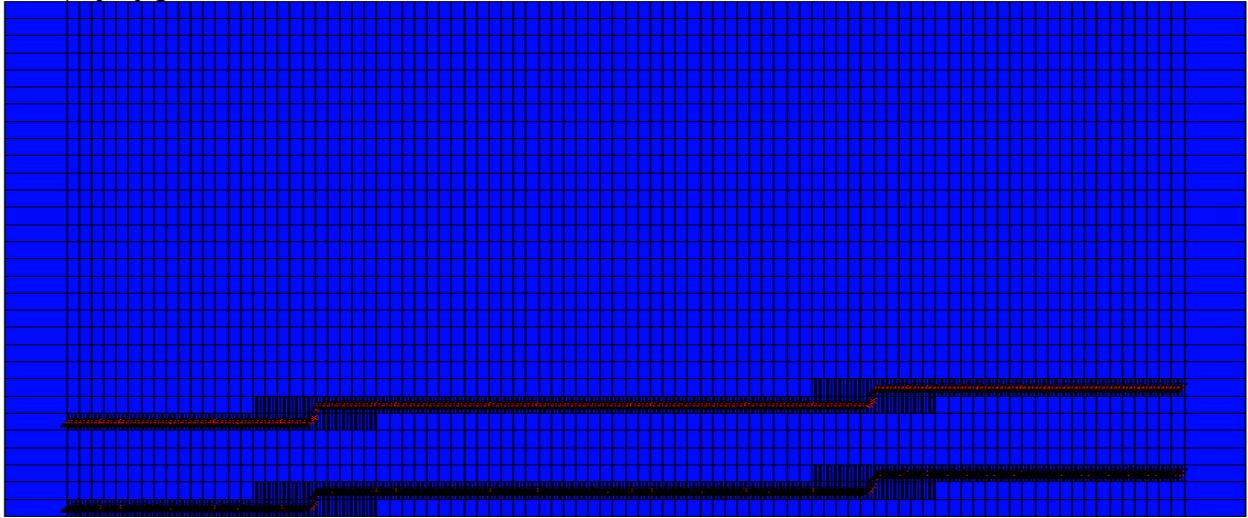


Figure 4-21: Trajectory-2, 10-m Model with 2-m LGR

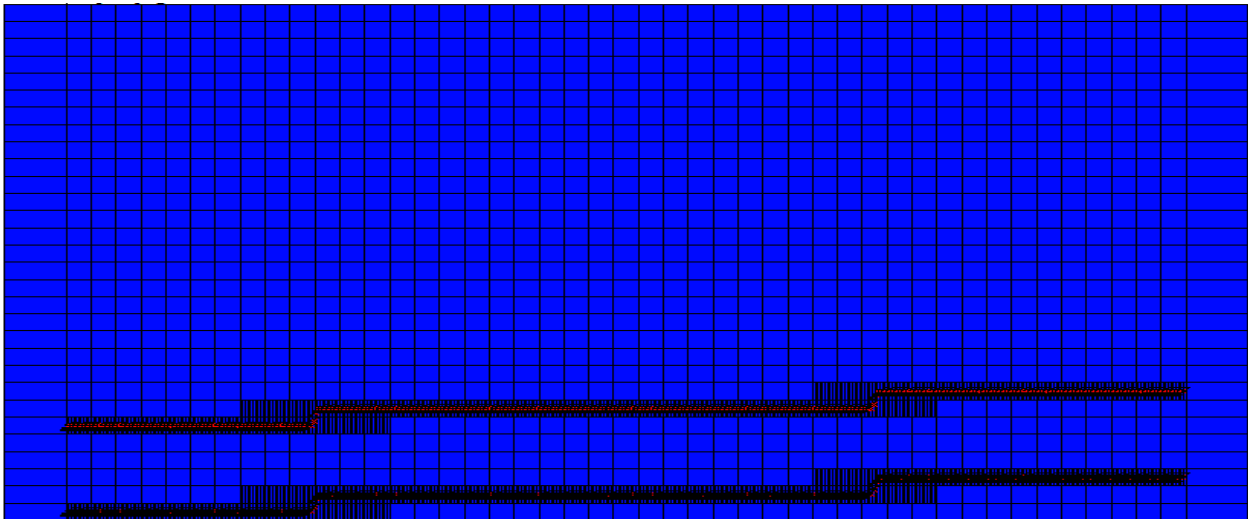


Figure 4-22: Trajectory-2, 20-m Model with 2-m LGR

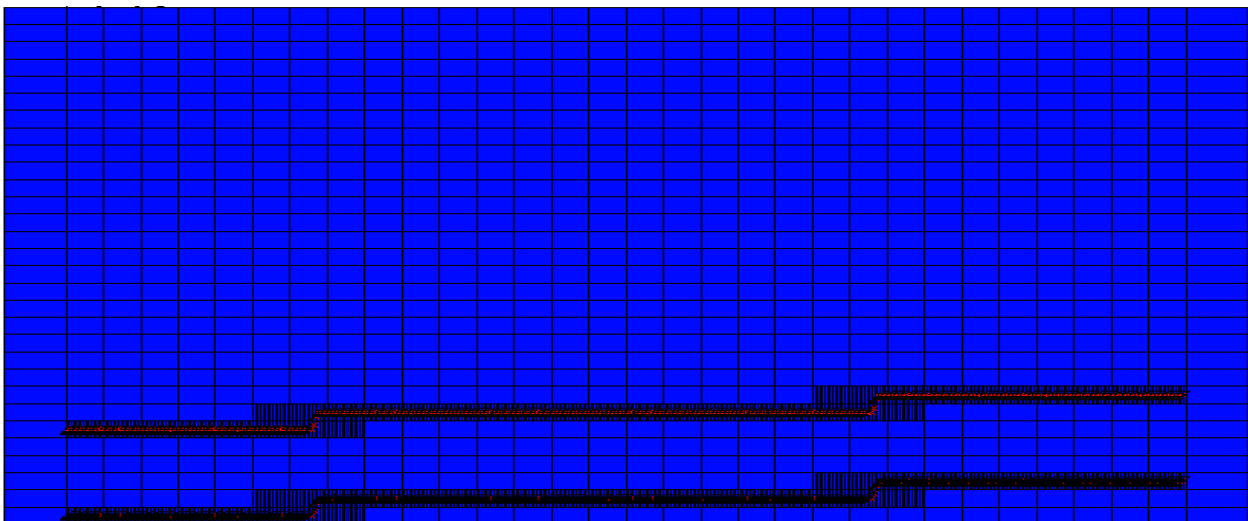


Figure 4-23: Trajectory-2, 30-m Model with 2-m LGR

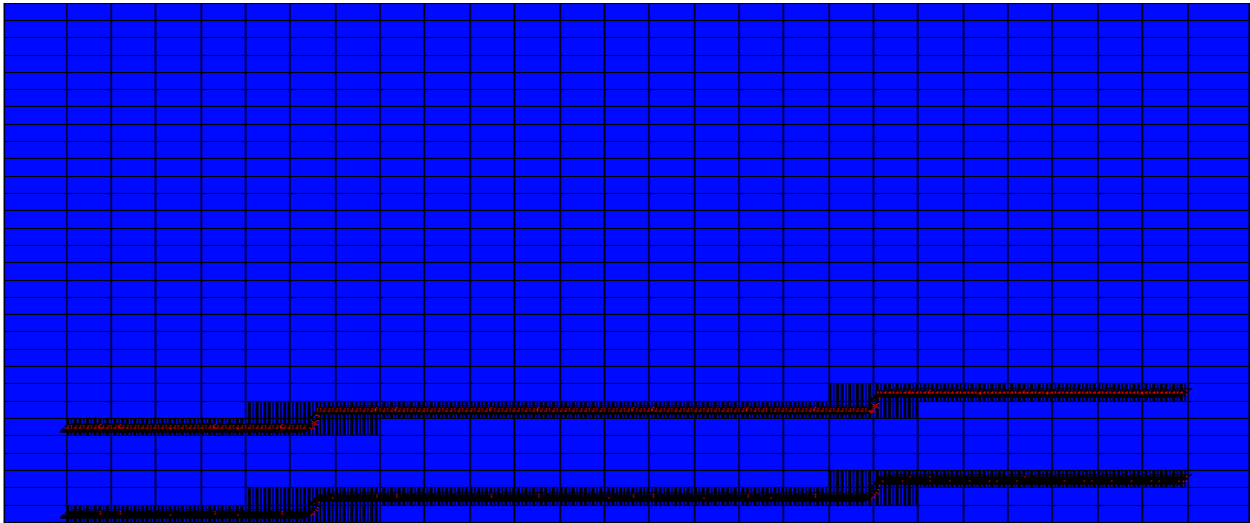


Figure 4-24: Trajectory-2, 36-m Model with 2-m LGR

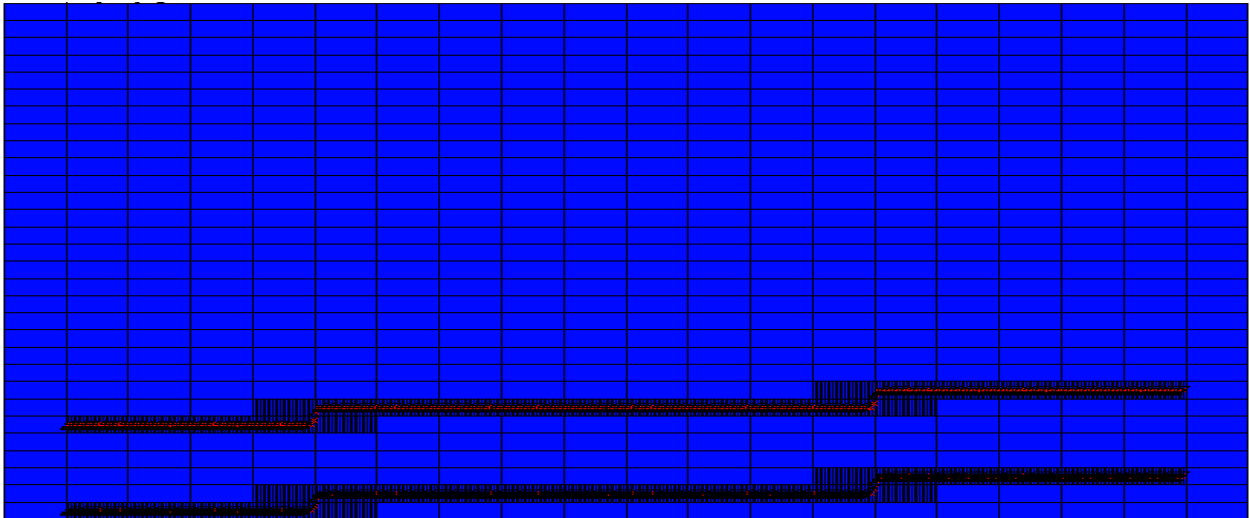


Figure 4-25: Trajectory-2, 50-m Model with 2-m LGR

Production Data

Production data of Trajectory-2 models are in good match as shown in **Figure 4-26**, and the differences in production data are within 6%.

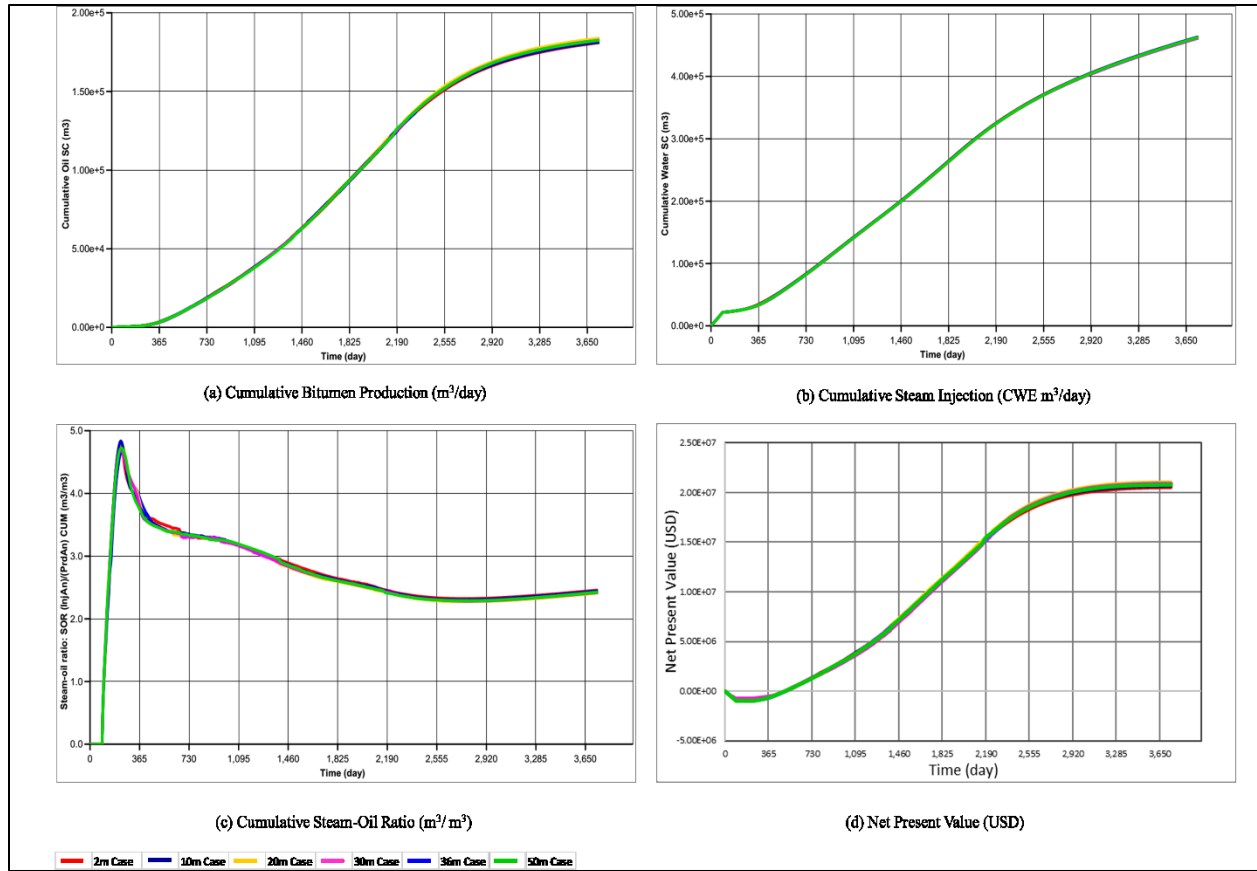


Figure 4-26: SAGD Performance Data of Different Trajectory-2 Models with 2-m LGR

Steam Chamber

Figure 4-27 shows temperature maps for different Trajectory-2 models. Results indicate a general agreement among the models.

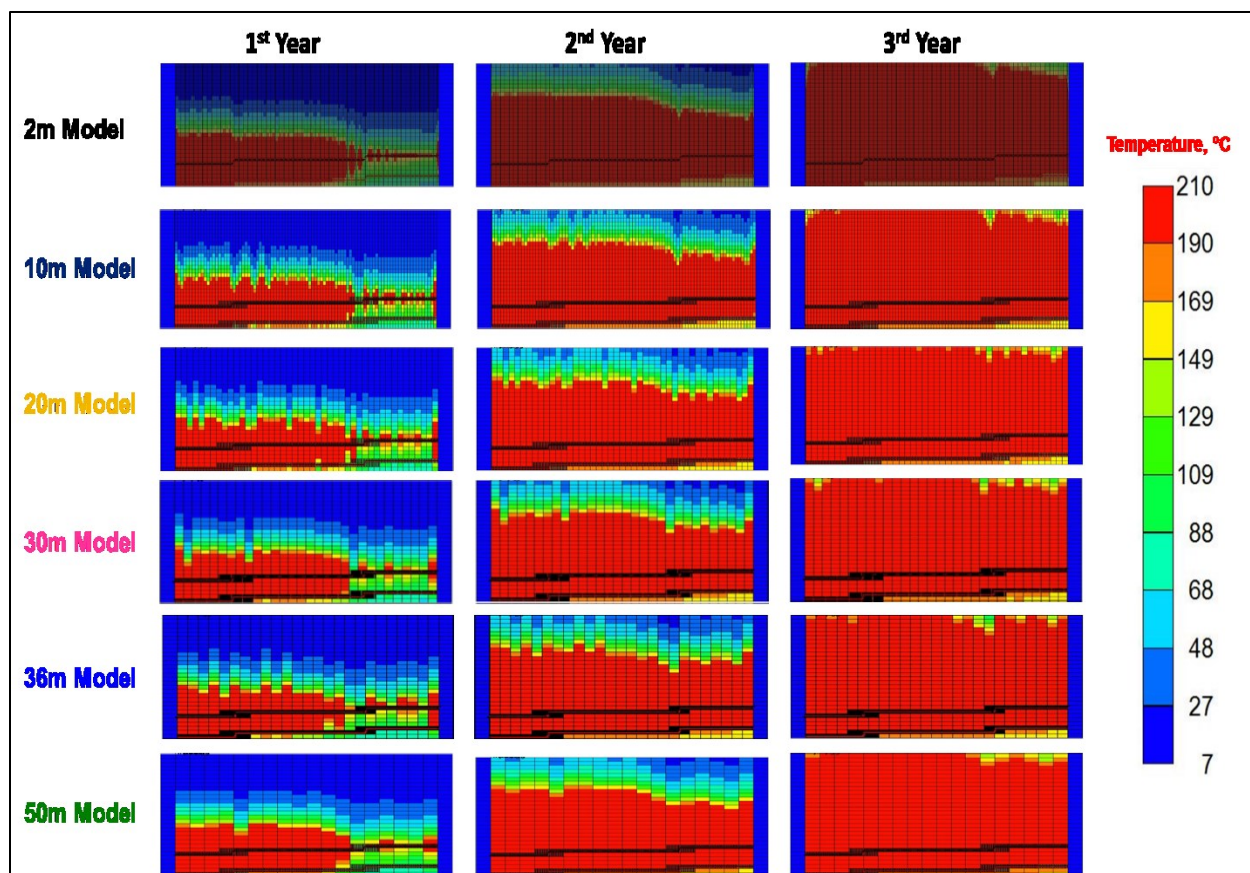


Figure 4-27: Early-Stage SAGD Temperature Maps for Different Trajectory-2 Models

4.3.6 Trajectory-3 with LGR

Trajectory-3 model with 2-m LGR are shown in **Figures 4-28 through 4-33**. **Figure 4-34** shows the production data agree within 4%. Also, a reasonable match of temperature maps is indicated in **Figure 4-35**.

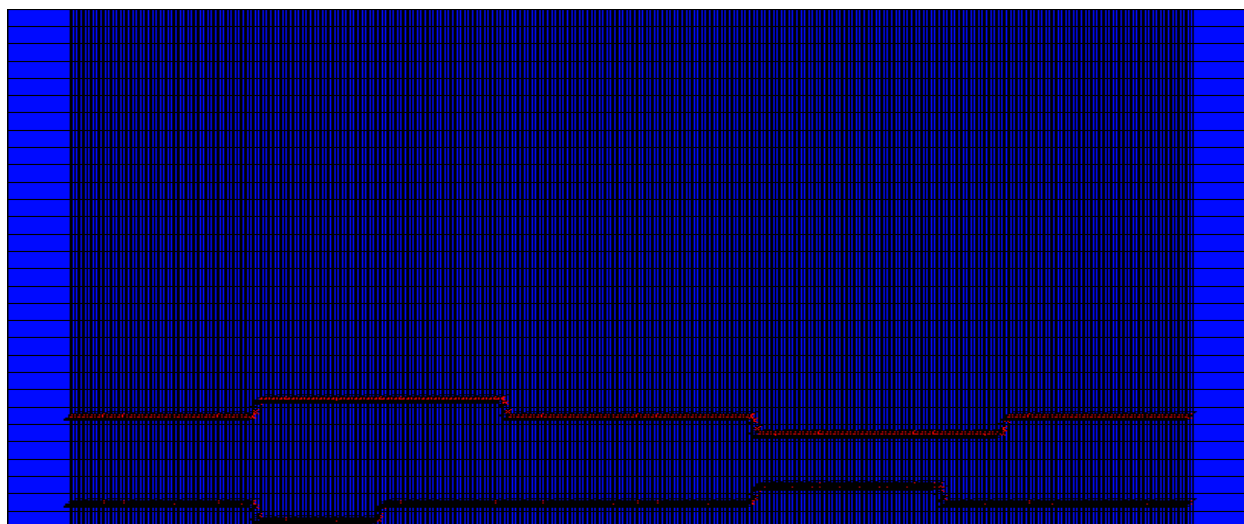
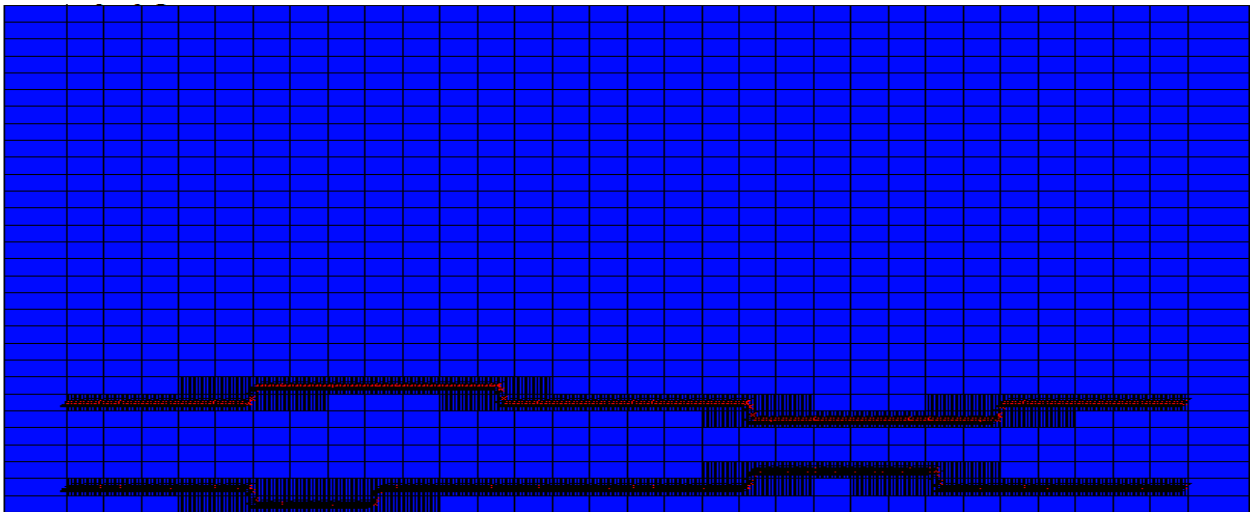
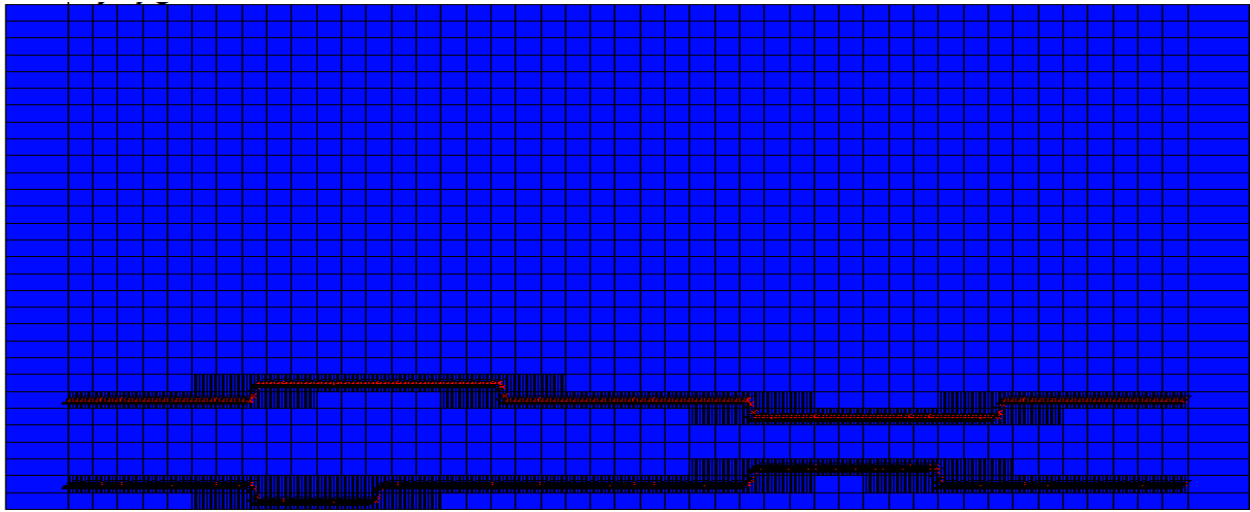
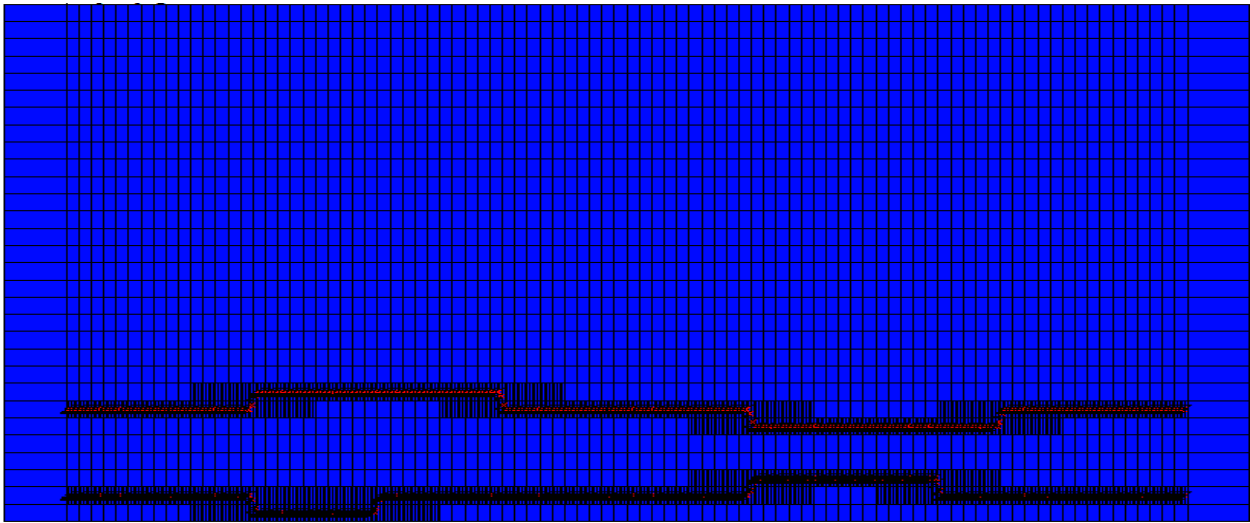


Figure 4-28: Trajectory-3, 2-m Model



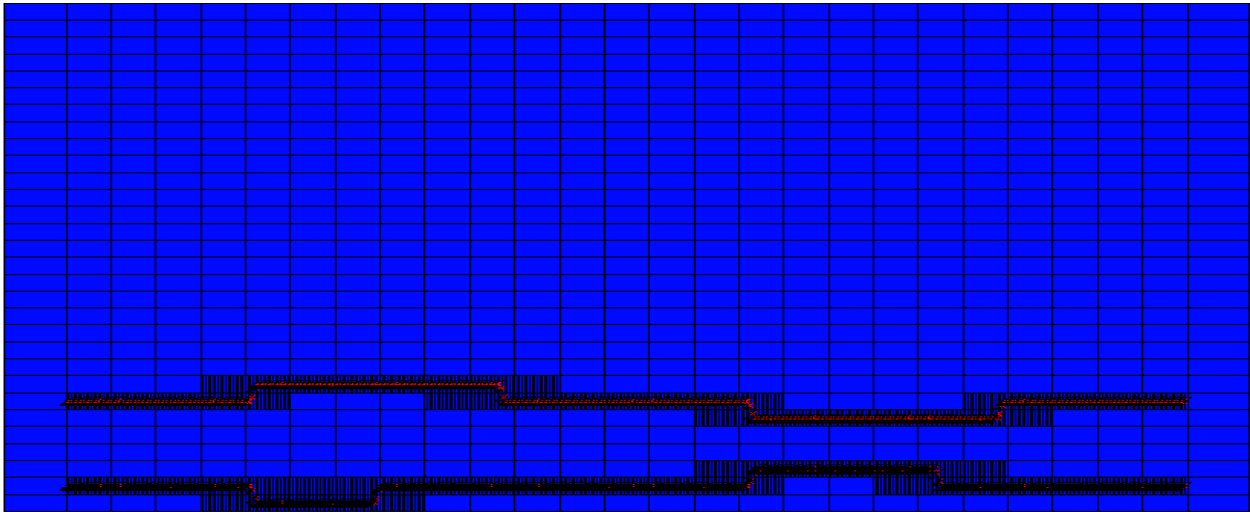


Figure 4-32: Trajectory-3, 36-m Model with 2-m LGR

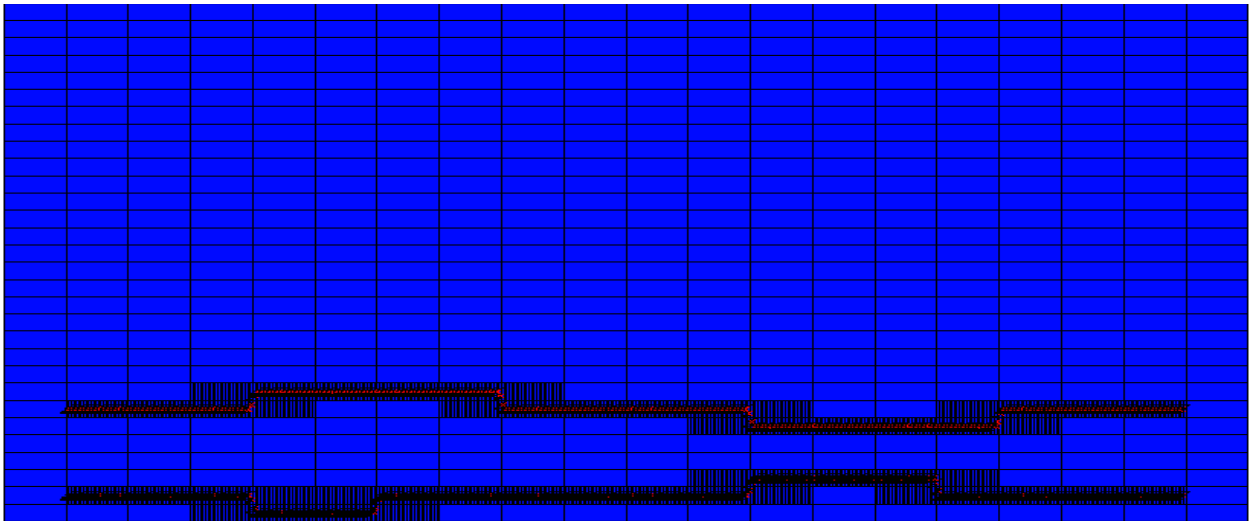


Figure 4-33: Trajectory-3, 50-m Model with 2-m LGR

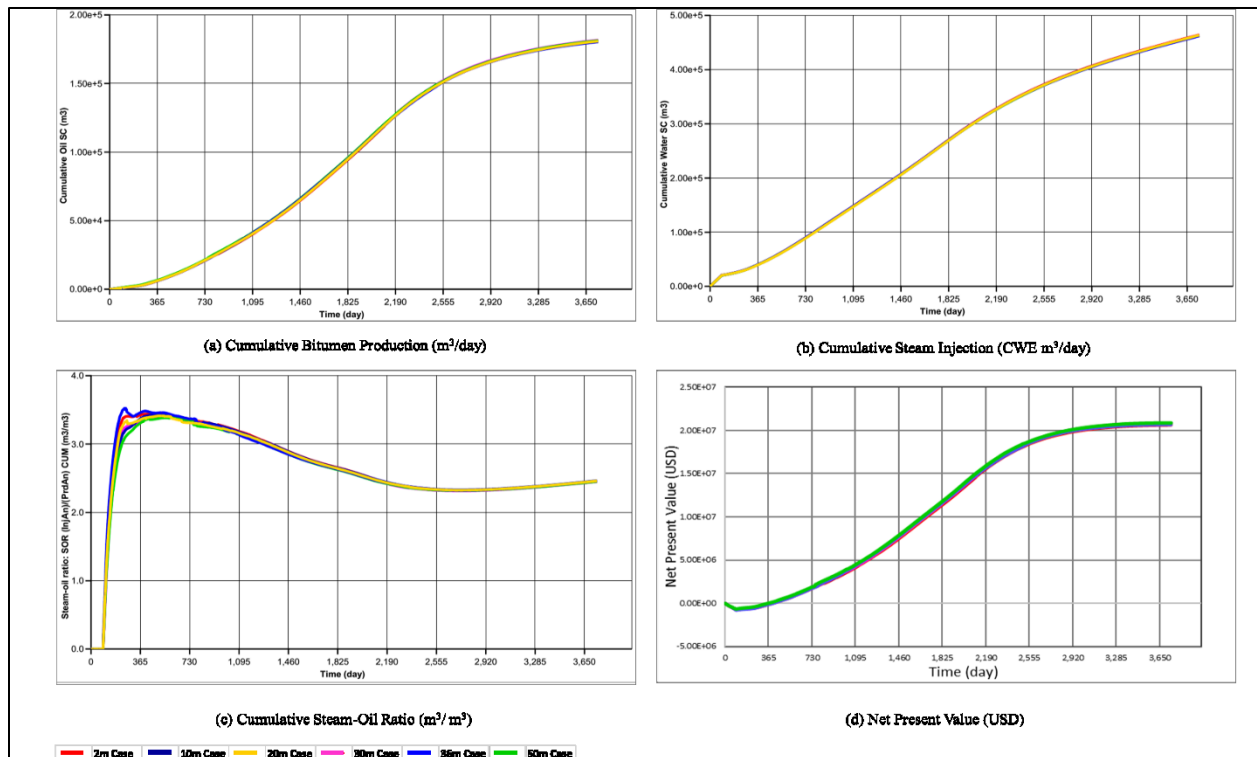


Figure 4-34: SAGD Performance Data of Different Trajectory-3 Models with 2-m LGR

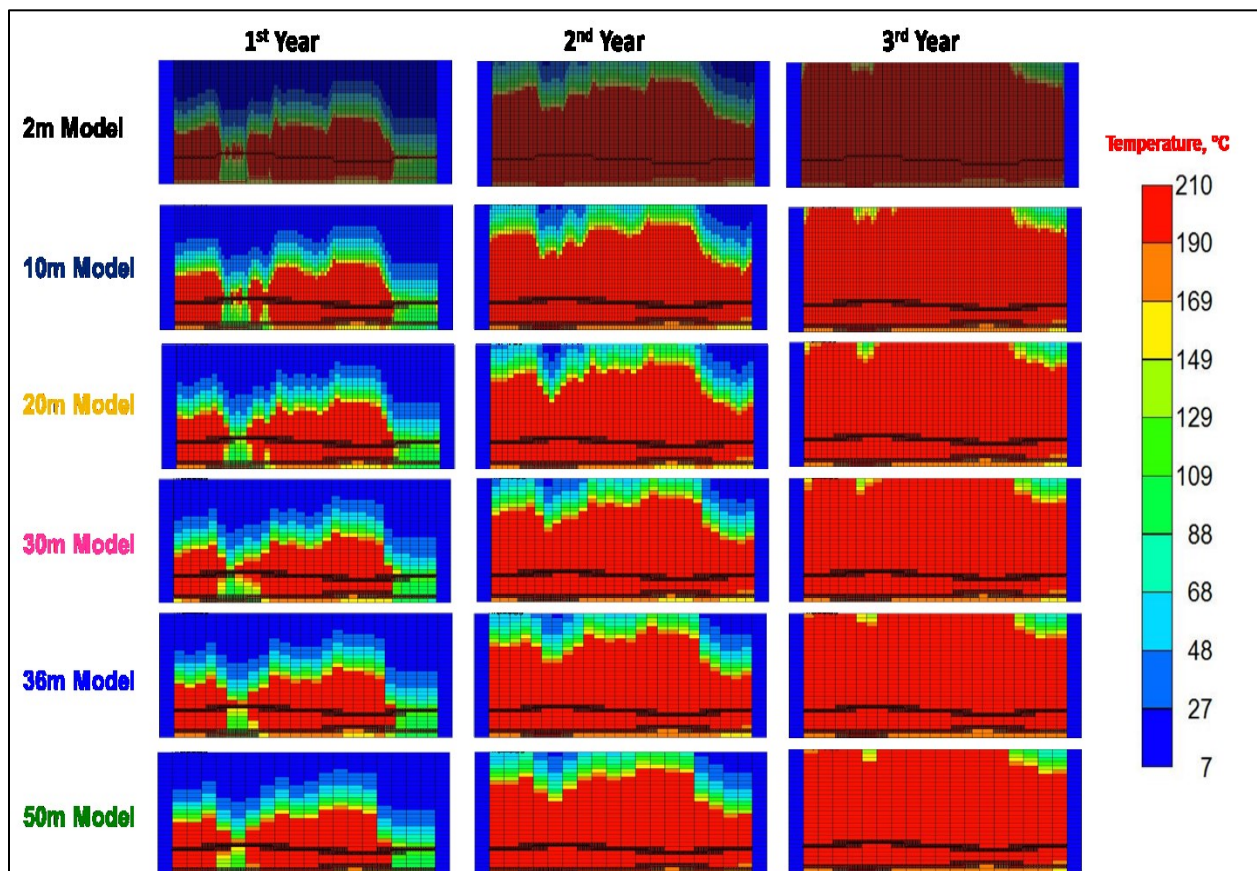


Figure 4-35: Early-Stage SAGD Temperature Maps for Different Trajectory-3 Models

4.4 Summary and Conclusions

4.4.1 Grid Size Sensitivity Analysis Summary

A detailed grid size sensitivity analysis was conducted for four trajectory scenarios: Ideal, Trajectory-1, Trajectory-2 and Trajectory-3. All the models share the same grid design in the plane perpendicular to the well but vary in the grid size parallel to the wells. The mesh sensitivity analysis indicated a fine mesh was required parallel to the wells. However, the use of a fine mesh in the axial direction renders a costly and time-consuming optimization work. Hence, the LGR technique was used to refine the grid blocks around the wells and the results of locally refined models were compared with those of the same model but with a uniform fine mesh across the entire model. Six grid systems were generated with 2-m, 10-m, 20-m, 30-m, 36-m, and 50-m block sizes in the axial direction combined with the LGR.

Implementing the LGR technique yielded an excellent match in the production data and consistent temperature maps among the set of six models for each individual trajectory case. Hence, the 50-m grid block size combined with the 2-m LGR is selected for all trajectory cases for further simulations in the optimization work. The use of LGR slightly increases the execution times (simulation run times) compared to the coarse model without LGR (50-m Model), as shown in **Table 4-2**.

Table 4-2: Execution Times Grid Size Sensitivity Analysis Cases

Trajectories	Simulation Execution Times (Hours)						
	2-m Model	10-m Model (with 2-m LGR)	20-m Model (with 2-m LGR)	30-m Model (with 2-m LGR)	36-m Model (with 2-m LGR)	50-m Model (with 2-m LGR)	50-m Model (without LGR)
Ideal Trajectory	102.6	10.8	5.4	2.4	2.1	1.8	0.9
Trajectory-1	110.3	17.1	11.2	9.3	8.8	7.3	1.7
Trajectory-2	109.7	19.7	11.9	9.1	8.6	3.0	1.3
Trajectory-3	116.8	10.1	8.3	6.2	4.9	4.7	1.3
Average Times	109.8	14.4	9.2	6.8	6.1	4.2	1.3

4.4.2 General Guideline for Models Enhancement with LGR

Figure 4-36 depicts a general guideline that can be followed to carry out grid size sensitivity analysis using LGR for any purpose such as optimization work. The first step would be constructing the fine grid model and then checking the simulation execution (run) time. If the fine

model has an acceptable run time, then it can be used for the optimization work; otherwise, the second step will be considered, where the fine model will be upscaled into a coarse model. If the coarse model has an acceptable simulation time and reasonable simulation results quality compared to the fine model, it can be used for the optimization work. However, the coarse model simulation results are not consistent with fine model results, then LGR option can be considered to enhance coarse model simulation results while keeping an acceptable simulation execution time that would be suitable for the optimization work.

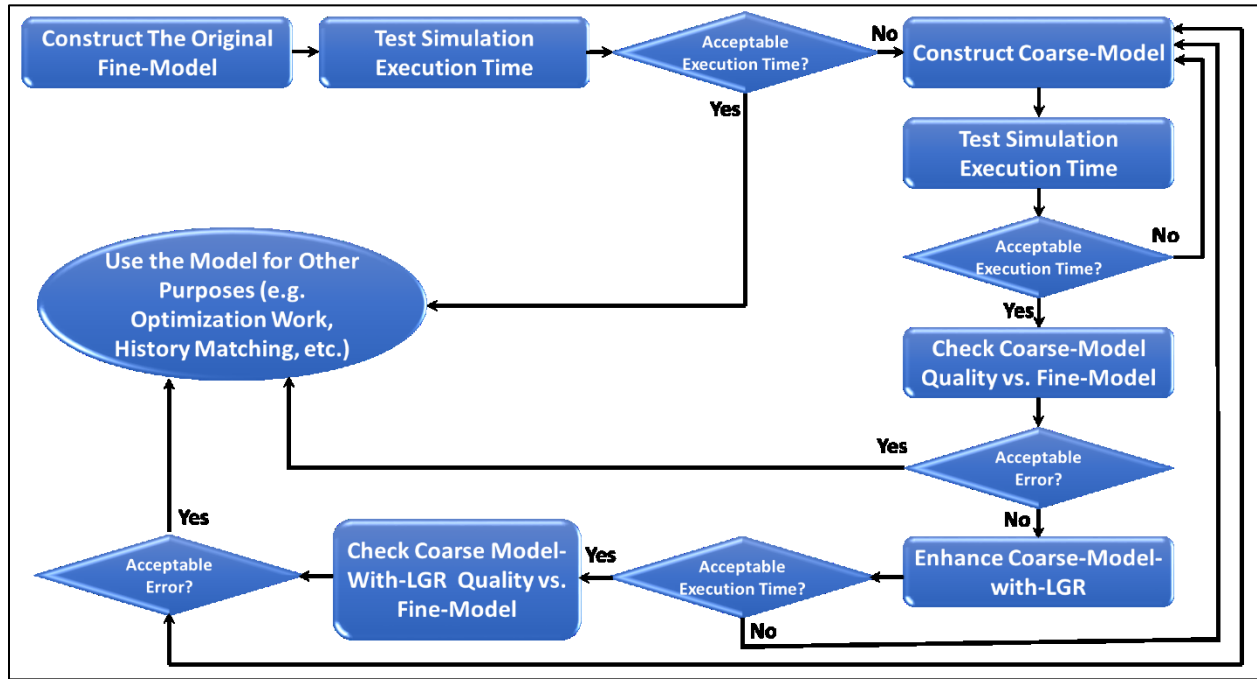


Figure 4-36: Model Enhancement with LGR

Table 4-3 summarizes differences in SAGD production performance of 50-m and 50-m with LGR models (expressed as percentage and referenced to 2-m model) among the four trajectories. Differences for 50-m models are (6-18%) and have been reduced to (1-4%) after enhancing the models using LGR. Also, it can be observed that simulation times have been reduced from (103-117 hours) in fine models down to (3-7 hours) in 50-m models with LGR.

Table 4-3: Summary of Differences in Production Performance Data and Execution Times

Data	Ideal Trajectory			Trajectory-1			Trajectory-2			Trajectory-3		
	2-m	50-m	50-m with 2m LGR	2-m	50-m	50-m with 2m LGR	2-m	50-m	50-m with 2m LGR	2-m	50-m	50-m with 2m LGR
Difference in Cumulative Oil Production (%)	--	8	1	--	11	3	--	13	2	--	13	3
Difference in Cumulative Water Production (%)	--	6	2	--	11	2	--	9	3	--	11	3
Difference in NPV (%)	--	7	1	--	15	4	--	14	3	--	18	4
Execution Time (hrs)	102.6	0.9	1.8	110.3	1.7	7.3	109.7	1.3	3.0	116.8	1.3	4.7

CHAPTER FIVE: DESIGN OF OPTIMIZATION PROCESS

5.1 Introduction

This chapter provides a detailed discussion about different types of optimization studies that were conducted in this research, the optimization objective function, and fixed parameters (such as wellbore life) during the optimization process. This chapter also discusses the optimization software used for the optimization work and the proposed optimization workflow for the placement and design of OCD's.

5.2 Design of Optimization Objective Function

5.2.1 Definition of Objective Function

An Objective Function (OF) is a performance index that indicates the quality of different alternatives. In other words, it is an expression or single quantity that has been designed to achieve a certain goal (usually maximizing or minimizing) (Khan and Awotunde 2016).

5.2.2 Types of Objective Functions

There are several types of objective functions depending on the nature of the problem under study. The following are three common types of objective functions:

- a) Fitness function, i.e., solution quality assessment.
- b) Cost formula that involves several parameters such as in projects economics.
- c) Error function such as in reservoir simulation history matching problems where the major goal always remains minimizing the error between actual field data and simulation results data.

5.2.3 NPV Objective Function

In SAGD reservoir simulation optimization problems, objective functions are used to guide the optimization towards finding the global optimal solution. These objective functions can be physically measurable quantities (such as recovery factor, bitumen production rate, steam injection rate, cumulative bitumen production, cumulative steam injection, cSOR, etc.) or a formulated economic index such as the NPV (Chen 2013). The latter one (NPV) is ranked up as the best option when it comes to screening feasibility of different EOR scenarios including thermal operations (Khan and Awotunde 2016). In SAGD production optimization problems, NPV objective function takes into account the following parameters:

- 1) Revenue from bitumen production (bitumen production rate).
- 2) Expenses of operations, steam generation, produced water treatment and recycling, waste water management and scheduled maintenance operations.
- 3) Capital expenses of drilling, exploration, produced bitumen processing facilities, and steam generation facilities.
- 4) Time value of the entire project money (annual money discount rate).

Equation (21) represents the NPV function formula and it is similar to the one used by Fedutenko et al. (2012) which links the above-mentioned parameters all together:

$$NPV = \sum_{t=1}^{T_p} \frac{R_t - E_t}{(1 + D)^{t_p - t_{ref}}} - C_{Capex} \quad (5.1)$$

where R_t is revenue, E_t is operational expenses, C_{Capex} is capital expenses, D is annual discount factor, T_p is project life time, t_p is cumulative project time and t_{ref} is project reference time.

5.2.4 Simplification of NPV Objective Function

For the work in this research, a simplified version of **Eq. (5.1)** was used based on the following assumptions:

- 1) **Zero Capital Cost:** Since various optimization studies in this research use the same model that consists of only one well pair and does not involve other wells which may not be drilled concurrent, the capital cost will be fixed for all cases and it will be eliminated when those cases are compared to each other. Also, capital cost of FCD's is assumed to be negligible.
- 2) **Revenue** is represented by daily bitumen production rate (STB/d) multiplied by an estimated average oil price of \$50/STB after deduction of processing expenses.
- 3) **Operational Expenses** are governed by daily steam injection rate (bbl/d) which is multiplied by the cost of steam (\$8/bbl of CWE) including steam generation and produced water treatment cost.
- 4) **Fixed Annual Discount Factor:** Annual discount factor of 10% has been chosen based on typical discount factors used in several papers (Dehdari and Deutsch 2012; Fedutenko et al. 2012; Noroozi et al. 2014; Stone et al. 2014).

With the above-mentioned assumptions, **Eq. (5.1)** is simplified into the form in **Eq. (5.2)**:

$$NPV = \sum_{t=1}^{T_p} \frac{Q_o r_o - Q_w r_w}{(1 + D)^{t_p - t_{ref}}} \quad (5.2)$$

where Q_o is oil production rate, Q_w is steam injection rate, r_o is oil price, r_w is steam cost and t_{ref} is reference time.

5.3 Fixed Optimization Parameters

5.3.1 Basic Assumptions for the Optimization Work

Due to limited computational resources and time, and because of parameters involved in the optimization work are highly non-linear, it is essential to set reasonable ranges for optimization parameters. For instance, maximum number of OCD's per well in this research was limited to four OCD's. Also, number of ports was limited within a range of (0-70) with a constant increment of 5. With these assumptions, any optimization work done in Chapter 6 involves 50,625 possible optimum solutions, and the optimization algorithm has to determine the optimum solution by running 500/50,625 cases, i.e., only less than 1% of all possible combinations.

Each of the optimization case studies done in Chapter 6 has two stages, short-term (500 cases for 3 years) and long-term (top 50 optimum cases from short-term for the whole life of SAGD project as discussed in Section 5.3.2). Short-term duration of 3 years represents the early-stage SAGD performance, and it is crucial to determine the general trend of SAGD performance for the rest of project life. A uniform growth of steam chamber during the early-stage of SAGD ensures continued uniform growth and propagation of steam chamber during later stages. More details about the short-term optimization approach are discussed in Section C.2 of **Appendix C**.

5.3.2 Placement of OCDs and Use of Packers

To determine locations of OCD's among the injector, a quick sensitivity analysis was performed using up to five OCD's in addition to the fully open-to-flow toe. As shown in **Figure 5-1**, the first OCD (OCD#A) was fixed at the heel to mimic short tubing of dual-string injection case and locations of the remaining OCD's have been determined depending on the TVD lateral separating distance, vertical distance between the injector and the SAGD model reservoir ceiling at different segments of the wellbore trajectories and relative distance between the OCD's. Using 10mm port size and 5 ports for each OCD, simulation cases of different combinations of those 5 OCD's were run and ranked according to NPV as summarized in **Table 5-1**. Although the first two cases (Cases # 1 and 2) have the highest NPV, their corresponding locations have not been considered for the

optimization work because they involve only 2-3 OCDs and may not be enough when higher number of ports are required in the actual optimization work. Also, the third scenario (case#3) has not be considered for the optimization work because it has five OCDs while its NPV (\$16,382,132) is close to NPV of Case #4 (\$16,355,233) which utilizes only 4 OCD's, thus, the latter case (Case #4) has been considered as the default scenario during optimization work of all trajectories keeping in mind slight changes in the locations may be noticed in each trajectory case depending on wellbore trajectory excursion and relative locations of those OCD's.

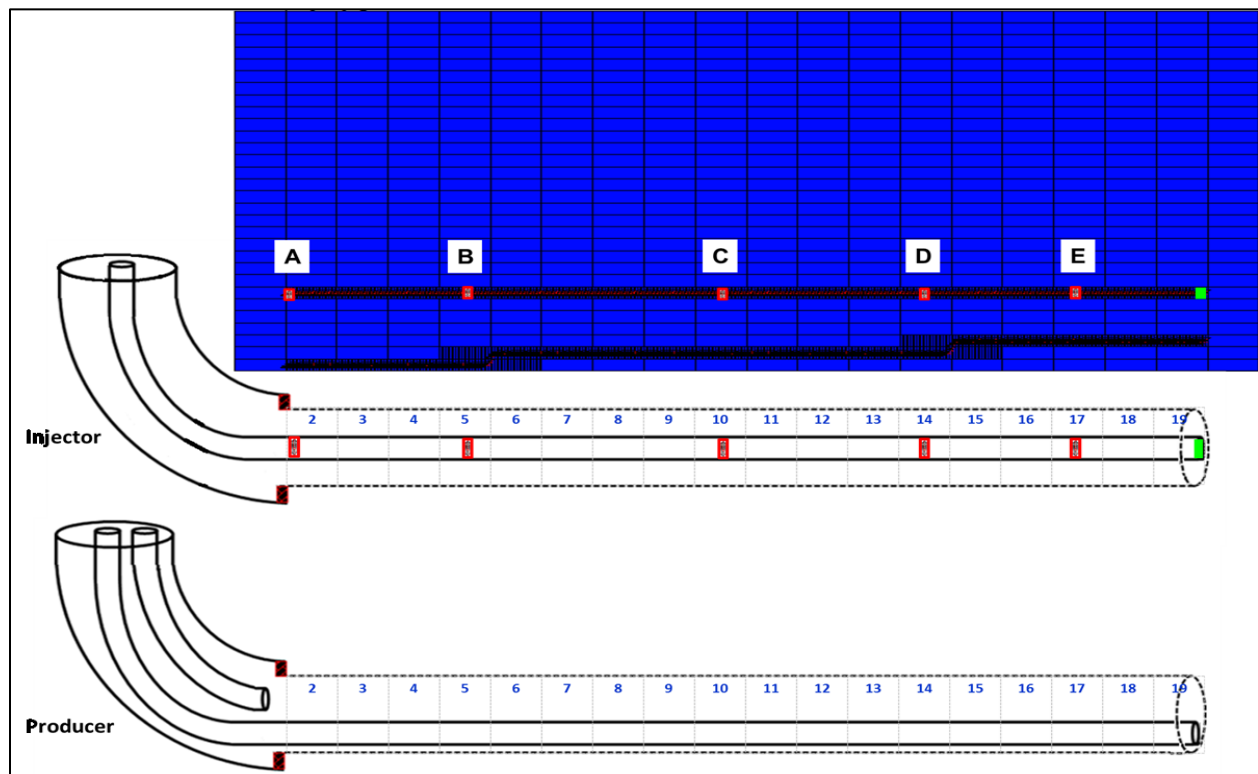


Figure 5-1: Initial Locations of OCD's

Table 5-1: Sensitivity Results of OCD's Locations

Case No.	OCD's Locations	NPV (USD)	Remarks
1	A+B+E	16,534,400	
2	A+B	16,446,717	
3	A+B+C+D+E	16,382,132	
4	A+B+C+D	16,355,233	Selected Case
5	A+B+D+E	16,304,999	
6	A+B+C	16,270,418	
7	A+E	16,126,369	
8	A+C	16,122,360	
9	A+C+D	16,111,219	
10	A+B+D	16,082,114	
11	A+D+E	15,969,550	
12	A+B+C+D	15,775,657	
13	A+D	15,765,281	
14	A+C+D+E	15,705,328	
15	B+C+E	15,591,474	
16	A+C+E	15,584,214	
17	B+C	15,393,417	
18	B+D	14,888,352	
19	B+C+D+E	14,865,995	
20	B+E	14,446,091	
21	B+C+D	14,426,684	
22	B+D+E	14,342,284	
23	C+D+E	13,483,987	
24	C+D	13,442,615	
25	C+E	13,078,341	
26	D+E	11,667,596	

Another sensitivity study was carried out to examine the effect of using isolation packers along with OCD's for zonal steam injection at different locations of previous **Figure 5-1**. Results summarized in **Table 5-2** indicate that cases without packers are still superior to cases with packers. However, results obtained from sensitivity analysis using packers may not be conclusive or enough to determine the effectiveness of isolation packers, especially in highly heterogenous reservoirs where some segments have low permeability values and need more steam compared to other segments.

Table 5-2: Sensitivity Results of OCD's Locations with Packers

Case No.	OCD's Locations	No. of Packers & Locations Block Indices	NPV(USD)
1	A+B+C+E	2 Packers: 4&5, 15&16	14,903,361
2	A+B	2 Packers: 4&5, 13&14	14,192,066
3	A+B+C	3 Packers: 4&5, 8&9, 13&14	13,778,022
4	A+B+C+E	4 Packers: 4&5, 8&9, 13&14, 15&16	13,301,442
5	A+B+D+E	4 Packers: 4&5, 12&13, 15&16, 17&18	12,539,989
6	A+B+D	3 Packers: 4&5, 8&9, 15&16	12,081,711
7	A+C+D	3 Packers: 4&5, 12&13, 15&16	11,878,437
8	A+C+D+E	4 Packers: 4&5, 12&13, 15&16, 17&18	10,937,116
9	A+C	2 Packers: 4&5, 15&16	10,738,290
10	B+D	2 Packers: 7&8, 14&15	10,573,627
11	A+D	2 Packers: 4&5, 15&16	10,003,455
12	C+D	2 Packers: 11&12, 15&16	9,453,562
13	B+C+D+E	5 Packers: 4&5, 8&9, 12&13, 15&16, 17&18	8,882,855
14	B+D+E	4 Packers: 4&5, 12&13, 15&16, 17&18	8,611,624
15	A+B+C+E	4 Packers: 4&5, 8&9, 13&14, 17&18	8,233,773
16	A+C+E	3 Packers: 4&5, 12&13, 17&18	7,884,544
17	C+D+E	3 Packers: 12&13, 15&16, 17&18	7,249,889
18	A+D+E	3 Packers: 4&5, 15&16, 17&18	7,193,831
19	D+E	2 Packers: 15&16, 17&18	3,223,271

5.3.3 SAGD Well Life

In all dual-string and optimization models of different trajectories, the SAGD process was allowed to continue until the daily increment of the NPV becomes zero, i.e., ($\frac{\Delta NPV}{\Delta t} = 0$). The NPV function formula is designed to perform automatic termination of the SAGD process when daily incremental NPV of the project becomes nil. Each single simulation case in the optimization work in Chapter 6 has its own SAGD simulation duration. Details of simulation run times for each case study are shown in Section C.1 of **Appendix C**.

5.3.4 OCD Type

Restriction-style OCD's (e.g. orifice type) were adopted throughout this research. The maximum number of OCD's per well in the optimization work in this research is set at four. However, this number can be reduced depending on optimization results of placement and number of those OCD's.

Generally, number and size of OCD ports (orifice diameter) vary from one manufacturer to another and standard port sizes of ICD's are usually less than those ones for OCD's. In this research, a typical OCD port size of 10 mm is used (Jones et al. 2009; Becerra et al. 2014; Noroozi et al.

2015). Also, maximum number of ports per single FCD is assumed to be 70 ports with fixed increments of 5, i.e., (5, 10, 15, ..., 70). Also, this study assumes that the toes of long-tubing strings are fully open to flow, and no OCD's installed at the toes. More Details are given in Section C.3 of Appendix C.

5.3.5 Operation Constraints

All operating constraints set in **Table 3-17** were kept constant during the optimization work, except that the short tubing in producer and injector was removed and the long tubing in the injector was equipped with the OCD's. **Table 5-3** summarizes all fixed parameters that have been discussed above.

Table 5-3: Fixed Parameters in the Optimization Process

Item	Value
SAGD Process Termination Criteria	$\frac{\Delta NPV}{\Delta t} = 0$
OCD's Port Size (mm)	10
Number of OCD's per Well (Max.)	4
Number of Ports per OCD (Min.)	0
Number of Ports per OCD (Max.)	70
Number of Ports Increment	5

5.4 Optimization Steps

The optimization workflow consists of two steps as depicted in **Figure 5-2**: Step 1 (short-term optimization) and Step 2 (long-term optimization). Details of both steps are illustrated next.

5.4.1 Step 1

First, the number of ports in each of the installed OCD's is optimized using CMG CMOST optimization tool. The range for number of ports for each OCD is (0-70). Setting the lower bound for the number of ports to zero allows to optimize the locations and number of required OCD's within the maximum considered number. If there is unneeded OCD at a certain location, its number of ports will converge to zero or a small number.

All simulation cases during this step are run for three years. Then, results are ranked based on the NPV. Cases that have the highest NPV are included for the full SAGD project life analysis in the next step.

5.4.2 Step 2

After ranking the simulation results in Step 1, the simulation durations of the top 50 cases are extended and allowed to run until the end of SAGD project life. The case that has the highest NPV is considered to be the optimum case among steps one and two, i.e., the case that has the optimum number, locations and number of ports for OCD's.

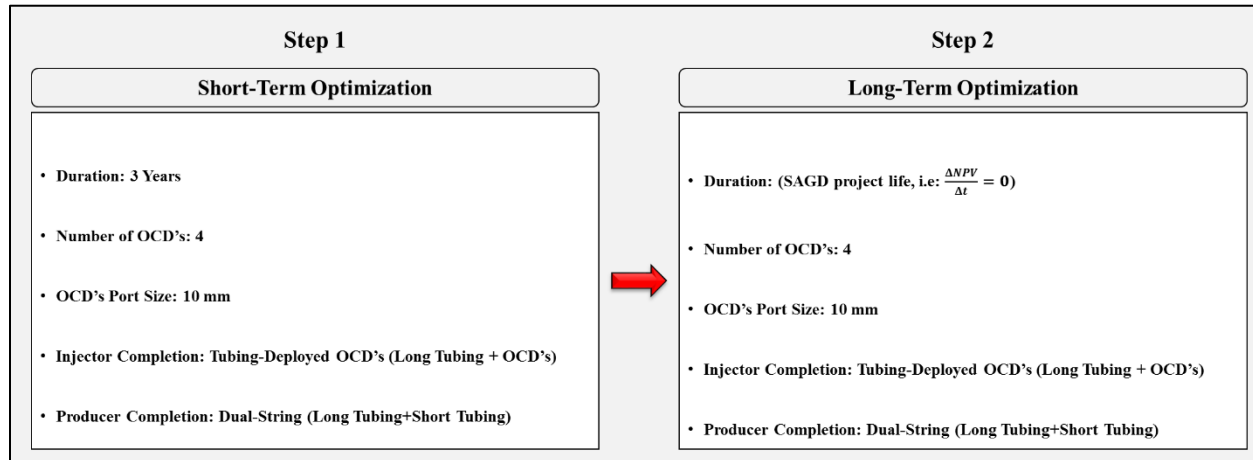


Figure 5-2: OCD's Optimization Steps

5.5 CMOST Optimization Software

Each single optimization study in this research involves the use of four OCD's with number of ports ranging of (0-70) with constant increment of five, and that means more than 50,000 possible combinations ($15 \times 15 \times 15 \times 15 = 50,625$ cases). However, this enormous number of possible combinations imposes the need for an automatic optimization tool. CMOST optimization tool was utilized to run optimization problems.

CMOST is an optimization tool, developed by Computer Modeling Group, MG, that works in conjunction with CMG reservoir simulators. CMOST has the capability to perform several tasks including sensitivity analysis, history matching, uncertainty analysis and optimization. Each of these tasks has its own appropriate set of algorithms as will be discussed in the next section.

5.5.1 Optimization Algorithms in CMG CMOST

CMG CMOST library contains several optimization algorithms. Each optimization algorithm is designed to handle particular types of problems. CMG Designed Exploration and Controlled Evolution (DECE) optimization algorithm has been successfully applied in many real-world reservoir simulation studies including SAGD NPV optimization models. Results have demonstrated that DECE optimization method is reliable and efficient (CMG CMOST User's

Guide 2015). Yang et al. (2009) applied the DECE optimization algorithm to optimize the NPV of a real field reservoir with two SAGD well pairs with bottom water (Fedutenko et al. 2012).

For the work in this research, DECE was used to optimize the number of ports in OCD's of SAGD well pairs as described in Section 5.6.4. Other optimization algorithms embedded in CMOST library are Particle Swarm Optimization algorithm (PSO), Latin Hypercube plus Proxy (LHC + Proxy), Proxy Optimization (PO), Differential Evolution algorithm (DE) and Random Search (RS) that is suitable only when parameters search space is narrow, e.g. optimization of SAGD bottom hole pressure constraints (CMG CMOST User's Guide 2015). **Figure B-1 in Appendix B** shows a list of available engines and corresponding suitable study type.

5.6 Optimization Workflow for OCD's Number of Ports

The optimization steps discussed in Sections 5.4.1 and 5.4.2 follow a fixed optimization workflow as shown in **Figure 5-3**. Details of this optimization workflow are addressed in this section.

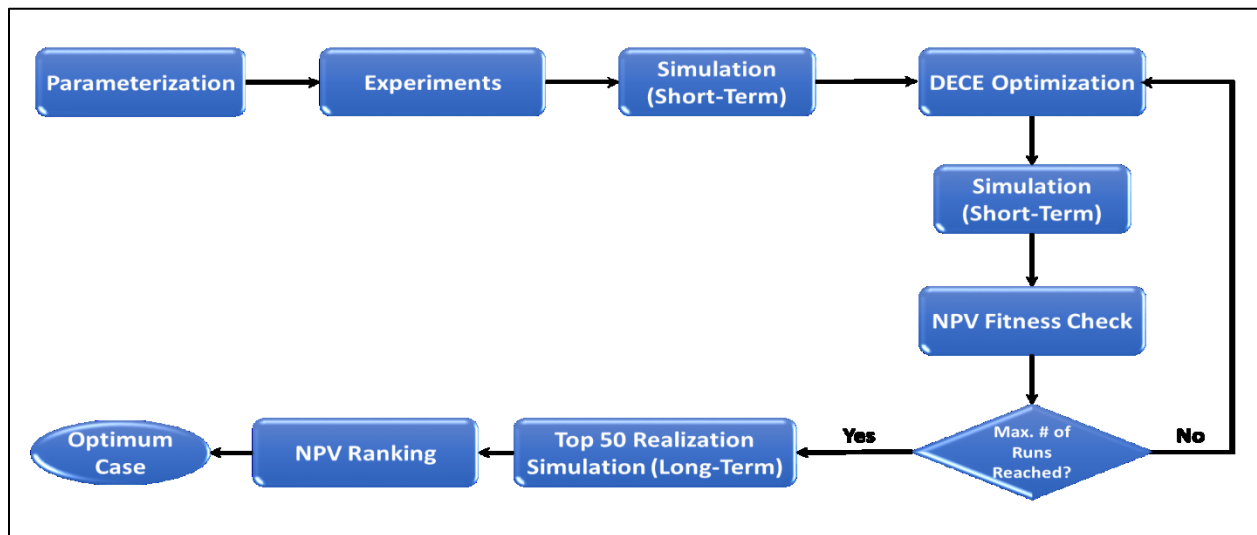


Figure 5-3: OCD's # of Ports Optimization Process Workflow

5.6.1 Setting Optimization Parameters

Optimization parameters and their corresponding values are entered into CMOST parameterization section. For the work in this research, the aim is to optimize OCD's number of ports for each OCD in the range of (0- 70) with a fixed increment of five. Hence, total number of optimization variables is 60. **Figure B-2 in Appendix B** is an example of OCD's properties assignment interface in CMOST software.

5.6.2 Assigning NPV Objective Function to the Optimization Tool

The NPV objective function described by Eq. (5.2) is packed into a Microsoft Excel spreadsheet and then the spreadsheet is linked to CMOST, so it can automatically calculate the NPV for different solutions as fitness assessment indices during the optimization process. **Figure 5-4** is NPV function formulation in Microsoft Excel spreadsheet and **Figure B-3** in **Appendix B** is CMOST software objective function assignment interface.

1 m ³ =6.29 bbl		Time		Simulation Case#1		
		Date	Days	Q _{oProd} (m ³ /d)	Q _{wInj} (m ³ /d)	ΔNPV (\$)
Oil Price (\$/bbl)	50	09-Mar-18	1893	84.5	167.3	10,810
Steam Cost (\$/bbl)	8	10-Mar-18	1894	84.5	167.3	10,807
Annula Discount Factor (1/year)	0.1	11-Mar-18	1895	84.5	167.3	10,802
Reference Time (Days)	0	12-Mar-18	1896	84.5	167.3	10,800
Simulation Case#1 NPV (\$)	21,315,928	13-Mar-18	1897	84.5	167.3	10,798
		14-Mar-18	1898	88.7	166.9	11,599
		15-Mar-18	1899	89.1	166.9	11,657
		16-Mar-18	1900	89.1	166.9	11,655
		17-Mar-18	1901	89.1	166.9	11,651
		18-Mar-18	1902	87.6	165.4	11,410
		19-Mar-18	1903	86.9	164.7	11,297
		20-Mar-18	1904	86.9	164.7	11,294
		21-Mar-18	1905	86.9	164.7	11,291
		22-Mar-18	1906	86.9	164.7	11,288

$$NPV = \sum_1^{T_p} \frac{Q_o r_o - Q_w r_w}{(1 + D)^{t_p - t_{ref}}}$$

Figure 5-4: Formulation of NPV Objective Function in Microsoft Excel

5.6.3 Designing Experimental Sampling

As mentioned, dealing with more than 50,000 possible optimum cases during each study makes it difficult to pick the optimum case by running only 500 cases out of those 50,000 cases (less than 1% of total possible cases). Although the CMOST DECE optimization tool is reliable in picking the optimum case out of those 50,000 possible optimum cases, running some preselected cases prior to automatic generation of possible optimum cases using the optimization tool helps in exploring the possible optimum cases and improving chances of determining the search direction to be followed by the optimization tool. The process of selecting those exploratory cases is called “Design Experimental Sampling”. The term “Experimental” refers to a single simulation case that has been created based on selected sample values for each parameter, and the selected set of experiments is called “Design”, and “Sampling” simply means selection, and it is done with a

known design space that depends on parameters (number of OCD's) and sample values (number of ports).

Experimental Sampling can be done using several techniques such as Latin Hypercube Sampling (LHC), Full Factorial Sampling and Manual Sampling (CMG CMOST User's Guide 2015). The first two techniques are used in the optimization work of this research.

A typical design (set of experiments) that efficiently explores design space should maintain orthogonality and good sample space filling, i.e., selected experiments should be evenly distributed among the sampling space. In this research 25-79 experiments are generated depending on the selected technique for each study (CMG CMOST User's Guide 2015). These 25-79 experiments represent 5-15% of the total available cases to run (500), and they are enough to cover and explore sampling space as shown in sampling quality check results in **Figures B-11, B-13 and B-15** of **Appendix B**.

In Latin Hypercube Sampling technique, each pair of columns is considered orthogonal if the pair have zero correlation, and the entire design becomes orthogonal when all columns within the design are orthogonal, thus, an orthogonal Latin hypercube is defined as a Latin Hypercube for which every pair of columns has zero correlation (CMG CMOST User's Guide 2015). CMOST has an internal iterative optimizer that improves the initial design of Latin Hypercube by maintaining approximate orthogonality and ensuring that selected experiments are evenly distributed in the parameter space. **Figure B-4** in **Appendix B** shows experiment design procedure in CMOST.

To carry out a quick quality check (QC) on the selected set of experiments, CMOST checks for orthogonality using maximum pair-wise correlation (maximum absolute value of correlation coefficients for all pair of columns). Pair-wise correlation range is (0-1), zero pair-wise correlation means perfect orthogonality, and one means worst case indicating that at least one column in the design is a linear combination of the remaining columns. **Figure B-5** in **Appendix B** shows an example of design experiments QC.

5.6.4 CMG CMOST DECE Optimization Engine

The default optimization engine that will be adopted in the optimization work of this research is CMG CMOST DECE engine. The term DECE stands for Designed Exploration and Controlled Evolution. This tool has been developed by CMG and successfully applied in several real-world

simulation problems including several SAGD NPV optimization studies. The results demonstrated reliability, thus it is a recommended optimization tool (CMG CMOST User's Guide 2015).

DECE is a two-stage iterative optimizer. In the first stage (Designed Exploration), the optimizer explores the search space in a designed random manner and gathers maximum amount of information about the solution space. Experimental designs discussed in the previous section are used in this stage. In the second stage (Controlled Evolution), certain statistical analysis techniques are applied to simulation results obtained during first stage. Candidate values of each parameter (number of ports in each FCD in our case) are examined for a better chance to improve the possible solution quality. During examination, the algorithm rejects and prevents poor performance candidates from being used in the next Designed Exploration stage (the performance quality is measured by NPV objective function).

It should be noted that to minimize risk of getting trapped in local optima, the DECE algorithm keeps an eye on banned candidate values and examines them on regular basis to check whether the banned decision is still valid or not. If the banned decision is valid, banned candidate values will stay banned. If not, those banned candidate values will be recalled and utilized in exploration stage again. **Figure B-6** in **Appendix B** shows details of CMG CMOST DECE algorithm.

5.6.5 Results Viewing and Analysis

Time-dependent simulation output results such as daily bitumen production rate (m^3/day), daily steam injection rate (in m^3/d CWE) and other desired output results can be viewed at any time during optimization study run. Also, NPV objective function versus simulation case number can be viewed during the run. **Figures B-7 through B-9** in **Appendix B** show daily steam injection rate, daily bitumen production rate and NPV objective plots respectively as produced by CMG CMOST.

CHAPTER SIX: OPTIMIZATION CASE STUDIES

6.1 Introduction

This chapter contains an optimization effort for the FCD placement and design for different wellbore excursion scenarios. Although well excursions from the ideal trajectory during the drilling may occur in the vertical as well as the horizontal direction, the effort in this chapter only considers the cases where the true vertical distance between the injector and producer fluctuates along the wellbore axis. In other words, lateral excursions are not considered. It is believed that lateral excursions may not have a significant effect on the SAGD process which is primarily based on gravity drainage. Vertical wellbore excursions, on the other hand, can cause difficulties in maintaining an appropriate subcool level, inducing a non-uniform steam chamber growth, and facilitating potential steam breakthrough events.

In Trajectory-1, the injector is straight (ideal) and the producer has excursions at two segments resulting in varying TVD lateral separating distance of 4-6 m at three different sections. In Trajectory-2, both injector and producer have excursions at two segments but with fixed 5-m TVD lateral separation along the entire well pair path. In Trajectory-3, both producer and injector have more severe excursions in an arbitrary manner with ± 2 m deviations from the 5-m ideal TVD lateral separating distance.

6.2 Study # 1: Trajectory-1 OCD's Optimization

6.2.1 Base Case Description

The base model for this trajectory is considered to be the one completed with dual string tubing (no FCD's) with 50-meter-long blocks in the axial direction combined with the 2-m LGR described in **Figure 4-17**. As depicted in **Figure 6-1**, the injector has a straight (ideal) trajectory, but the producer has excursions at two segments leading to a lateral separating distance of 4-6 m.

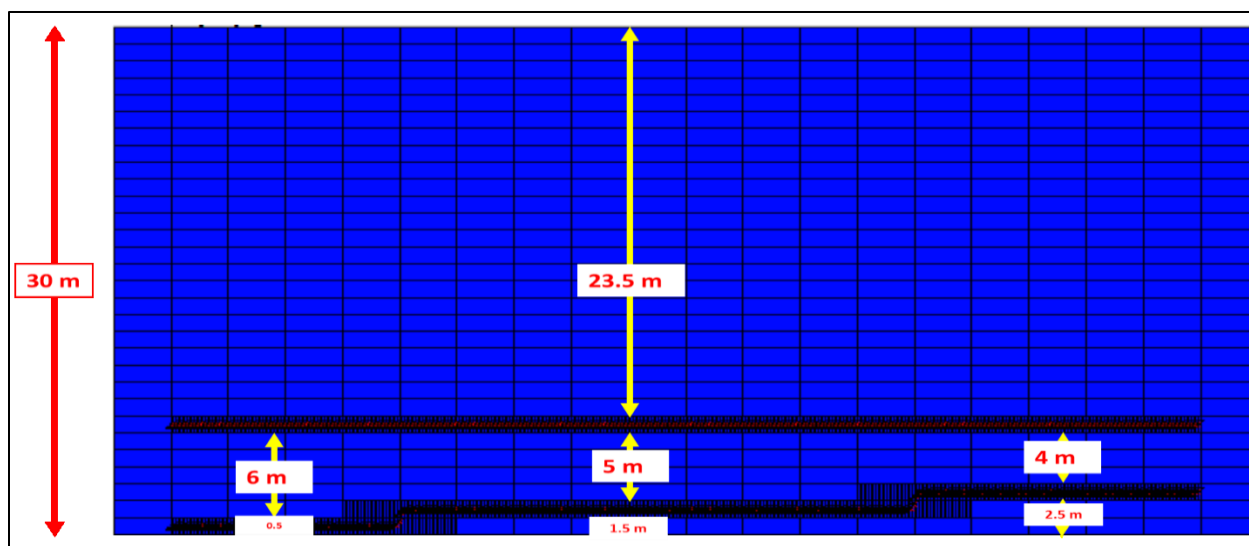


Figure 6-1: Trajectory-1 SAGD Well Pair Trajectories

Both injector and producer have dual-string completion scheme as shown in **Figure 6-2**. The well pair are completed by a 9 5/8" slotted liner and 4 1/2" short and long tubing strings.

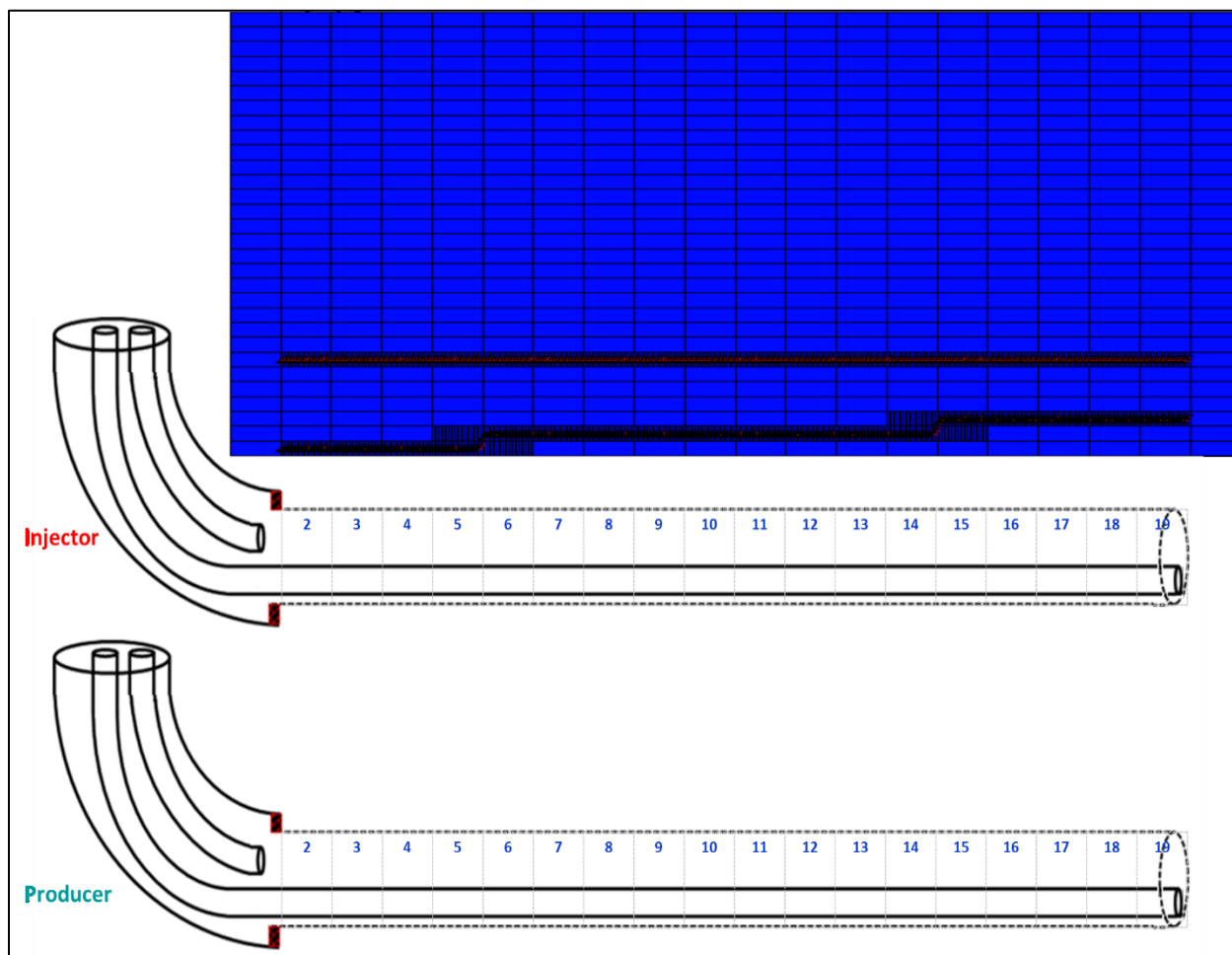


Figure 6-2: Trajectory-1 and Well Completion Scheme for the Base Case

6.2.2 Optimization Analysis with OCD Deployment

Figure 6-3 shows the configuration of tubing-deployed OCD completion system, where the short tubing string of the injector has been removed and the long string has been retained but equipped with four OCD's at 2 m, 176 m, 426 m, and 626 m from the landing point in addition to the toe section which was kept fully open-to-flow. The original dual-string completion of the producer was kept without alteration.

As described in **Figure B-10** of **Appendix B**, four sets of orifice-type OCD's were specified in the simulation input data file at block cells #2, 6, 10, and 14 containing the injector long tubing. Columns (1-7) indicate cell numbers and corresponding child blocks. Columns 8, 9, 10, and 11 indicate FCD type (orifice type OCD in this case), port size (10 mm), discharge coefficient (0.65) and number of ports per FCD (maximum 70 ports per OCD), respectively. The latter one (number of ports) is the main varying optimization parameter in the optimization study.

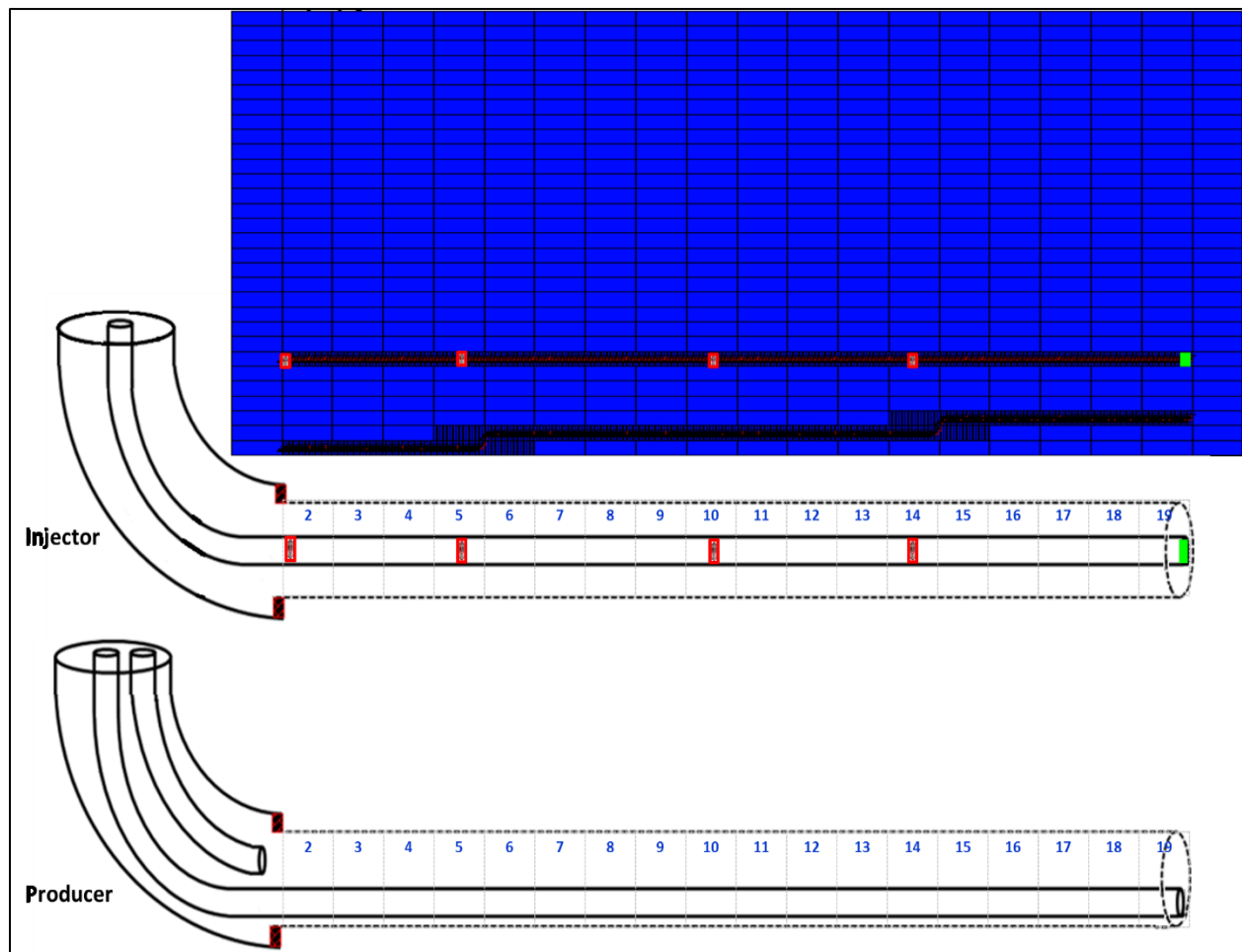


Figure 6-3: Trajectory-1 Tubing-Deployed OCD's Completion Diagram

OCD's # of Ports Parameterization

In CMG CMOST optimization tool, the four OCD's were entered as main optimization parameters in the parametrization section of the tool. Each parameter (OCD) has number of ports with a range of (0-70) as sampling values.

Experiments and Samples

Latin Hypercube sampling technique described in Section 5.6.3 was used as the sampling technique. To have an effective set of sampled parameters, and to make sure that the generated experiments will cover wider range of sampling space, sampling was done by treating all sample values (port numbers) equally probable. Initially, 79 experiments were generated and sampling design quality was improved using CMOST iterative optimizer with 1,000,000 iterations. Results of design quality check are shown in **Figure B-11** of **Appendix B** where orthogonality value was 0.0065 (nearly orthogonal range) indicating a good design quality (green zone).

Short-Term Optimization of Number of Ports

In short-term optimization stage, all 500 cases were run for three years of SAGD operation. Initially, 79 experimental samples were run to explore the sampling space to feed the DECE optimizer with appropriate hints. Next, the remaining 421 new cases were generated and run using the DECE tool. Short-term optimization results are shown in **Figure 6-4**, where it can be noticed that the solution cases show a trend which means the optimizer general solutions are heading towards the optimum solution.

It can be observed that there are scattered cases laying between the dual-string case and the main trend of solution cases. This is because the DECE tool focuses on the solutions that give the optimum results based on the set objective function. During optimization runs, it is quite normal that some cases give results below the average optimum results, but the DECE optimizer quickly adjusts the solution direction towards the optimum solution range. Dashed linear trend line shows that the overall trend of the solution is positive.

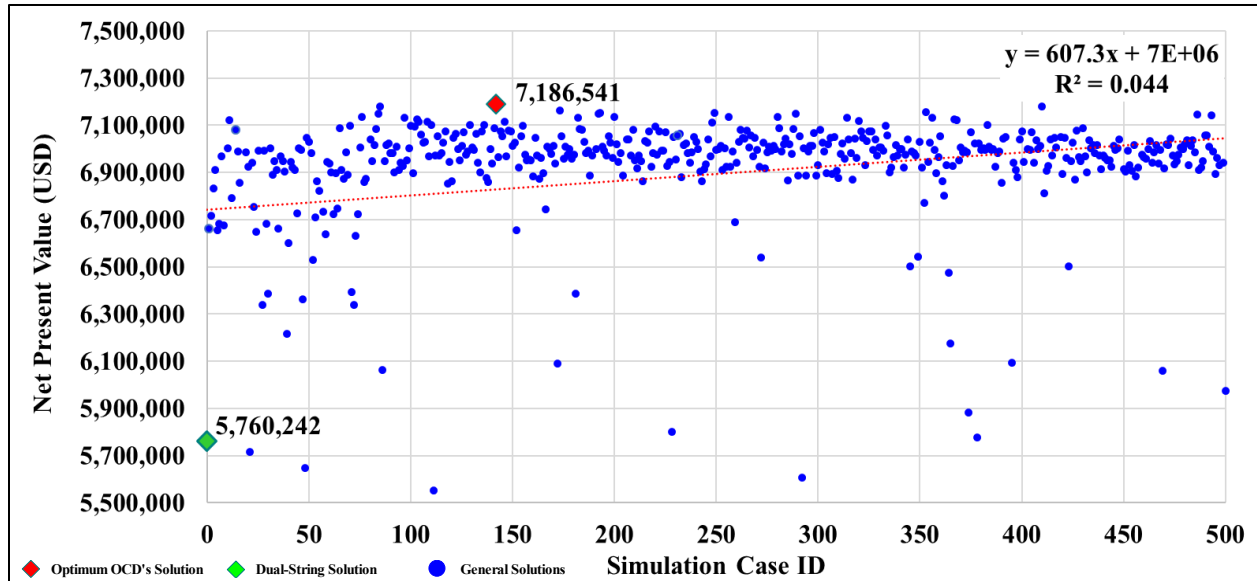


Figure 6-4: Trajectory-1 OCD Optimization Results (Short-Term)

Long-Term Optimization of Number of Ports

In this stage, results of short-term optimization runs are ranked based on the NPV. The top 50 simulation cases (with highest NPV) are then allowed to run for an extended period (full SAGD project life) and ranked according to the NPV again. Simulation results of those top 50 cases are plotted in **Figure 6-5**, the identified optimum case has the NPV of \$21,736,170. Also, the NPV of conventional dual-string case (\$21,128,653) has been projected on the same chart for comparison purposes. As depicted in **Figure 6-6**, the optimum case that has been identified has four OCD's (OCD#1, OCD#2, OCD#3 and OCD#4) with 70, 20, 35 and 70 ports respectively. SAGD project life for each case in the top 50 is plotted in **Figure C-1** of **Appendix C**. Also, ultimate recovery factors of these top 50 cases are depicted in **Figure C-2** of **Appendix C**, which shows a range of 70.0-70.6% for the top 50 cases and 70.6% for the optimized OCD case.

Upon running the top 50 cases from the short-term (3 years) runs for the full SAGD project life, it is found that the long-term optimum case lies within the first 10 cases (Case # 5 for Trajectory 1). The dotted trend line demonstrates a decreasing trend for the data points, i.e., the NPV's of the cases decrease as the case ranking decreases among the top 50 cases. In addition to the top 50 cases, some extra cases were analyzed for the whole SAGD project life for confirmation of this decreasing trend. Details are shown in Section **C.2.3** of **Appendix C**.

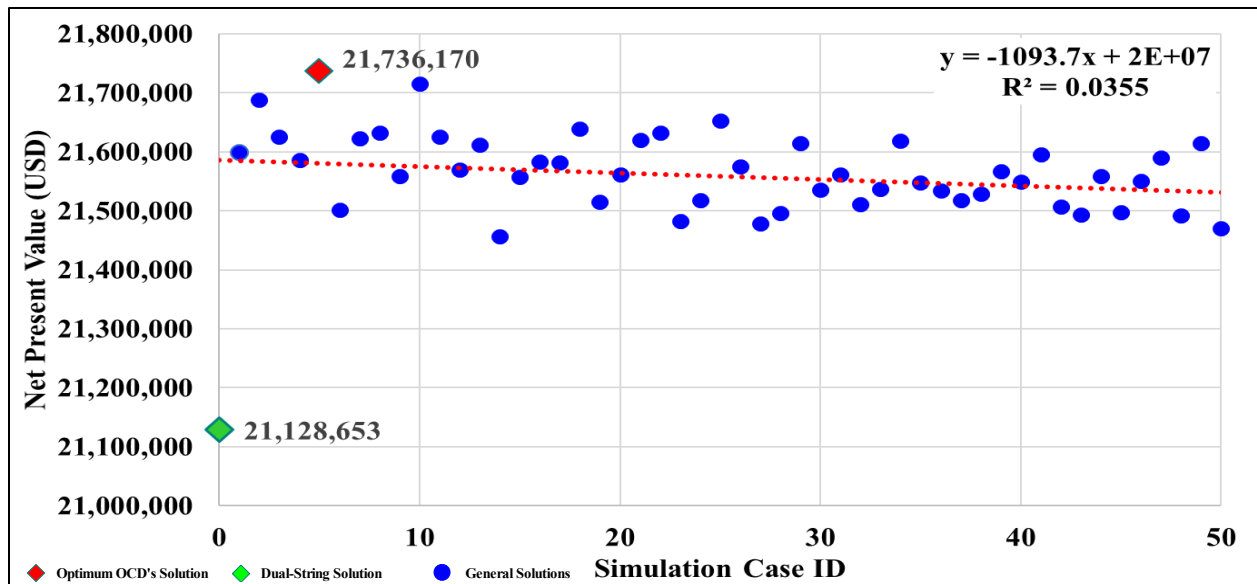


Figure 6-5: Trajectory-1 OCD Optimization Results (Long-Term)

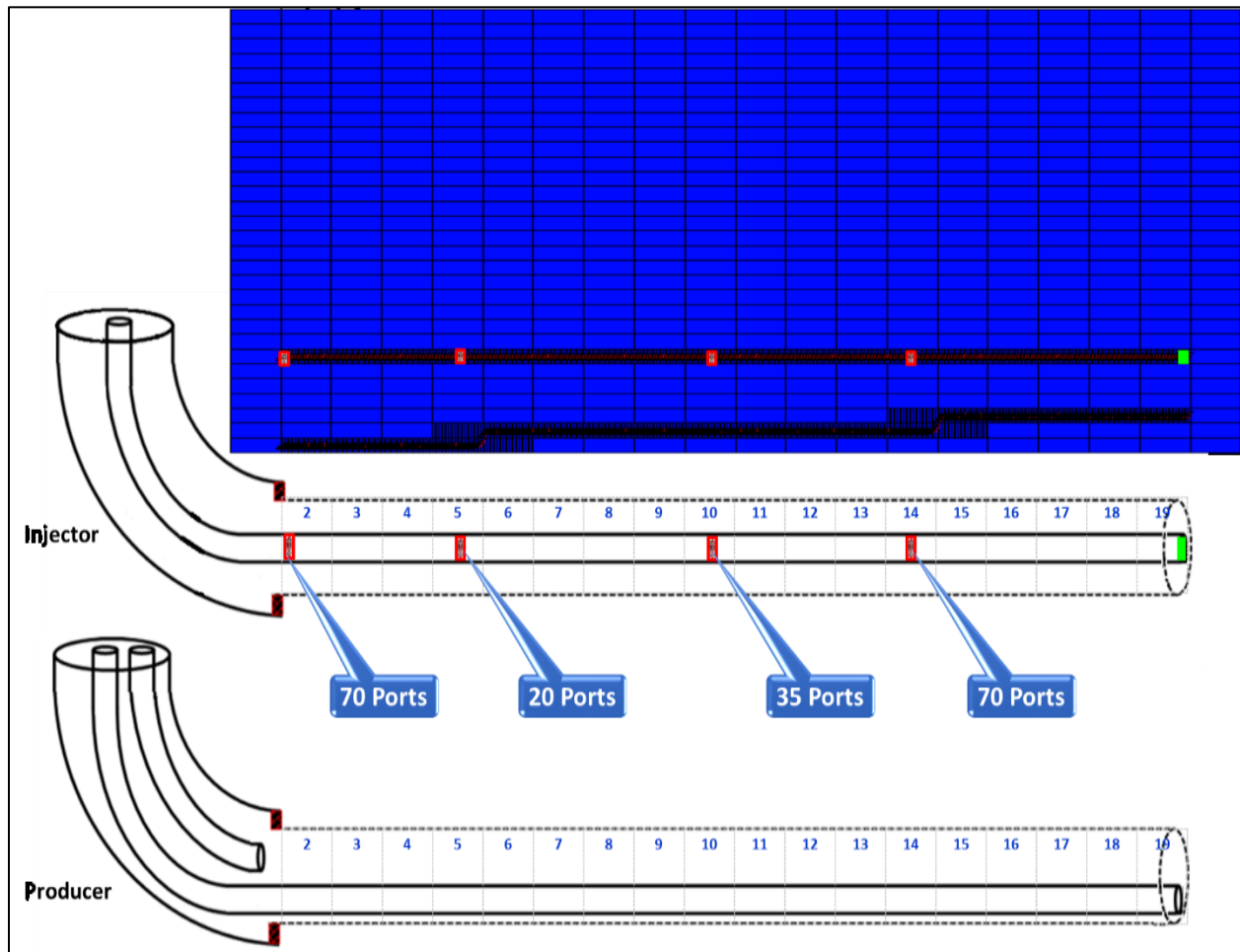


Figure 6-6: Optimum OCD Case for Trajectory-1

Optimum Range of Number of Ports

Checking the range for the number of ports for the top five optimum cases indicates that the optimum number of ports for each individual OCD converges towards a certain range as follows: OCD#1:70-70, OCD#2: 15-20, OCD#3: 15-35 and OCD#4: 50-70. It can be noticed the edge OCD's (OCD#1 and OCD#4) have reached or are close to the maximum number of ports limit that has been set in this study (70 ports). This finding suggests that increasing the limit for the number of ports for this study beyond the current limit may yield more optimized scenarios. **Figure 6-7** and **Table 6-1** show the range for the number of ports for each OCD for the top five optimum cases.

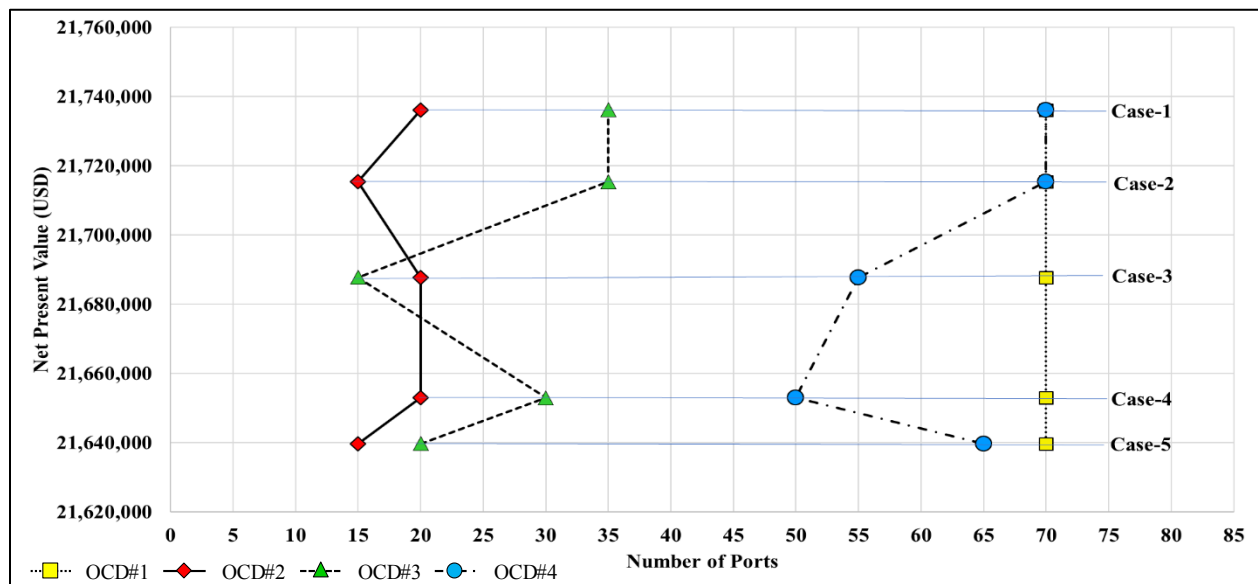


Figure 6-7: Optimum Number of Ports for Top 5 Designs, Trajectory-1

Table 6-1: Optimum Number of Ports for Top 5 Designs, Trajectory-1

ID	OCD's Distribution				NPV (USD)
	OCD#1	OCD#2	OCD#3	OCD#4	
1	70	20	35	70	21,736,170
2	70	15	35	70	21,715,385
3	70	20	15	55	21,687,763
4	70	20	30	50	21,652,951
5	70	15	20	65	21,639,717

6.2.3 Results Analysis

Steam Chamber for Optimized OCD's Case

Figure 6-8 illustrates temperature maps of the optimized model until the end of the SAGD project starting from the circulation stage. In each year, axial (along SAGD well pair trajectory) and cross-sectional (at 10th layer) views of temperature maps are plotted. Yellow points are the locations of the deployed OCD's, while the green points are the fully open-to-flow toe. It can be observed that steam chamber reaches reservoir ceiling (top) before the end of the 3rd year, then starts to expand laterally until it hits reservoir boundaries by the 6th year.

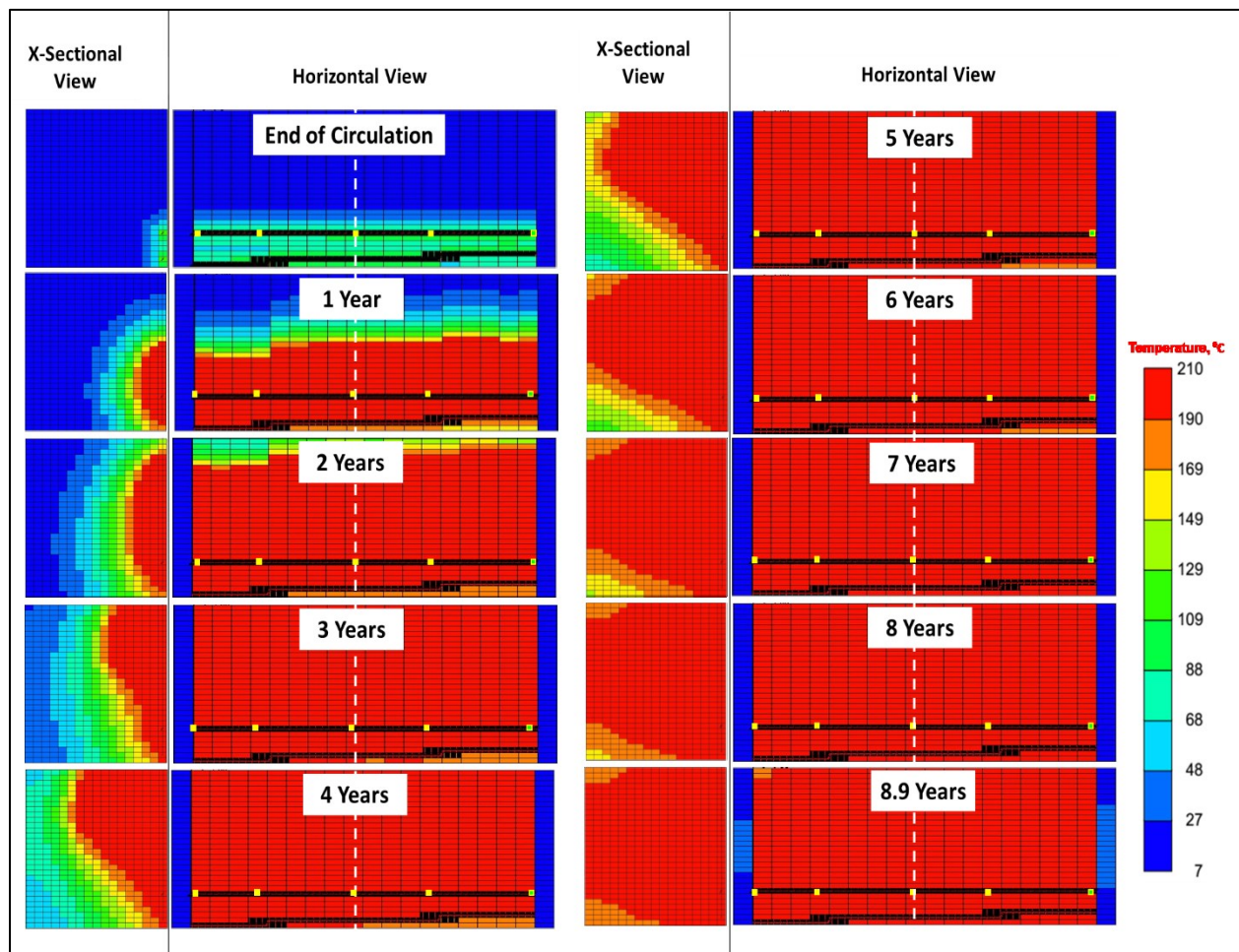


Figure 6-8: Trajectory-1 Temperature Maps of the SAGD Model at Different Stages

Steam Distribution via OCD's

Figure 6-9 shows contribution of each single OCD and open toe to the total amount of steam injected at the end of SAGD project life as a percentage. About 69% of the total injected steam has been injected via OCD#1, 11% through OCD#2, 9% through OCD#3, 7% through OCD#4 and

4% through the open toe. It can be observed that the amount of the injected steam decreases for the injection points at farther distances from the landing point.

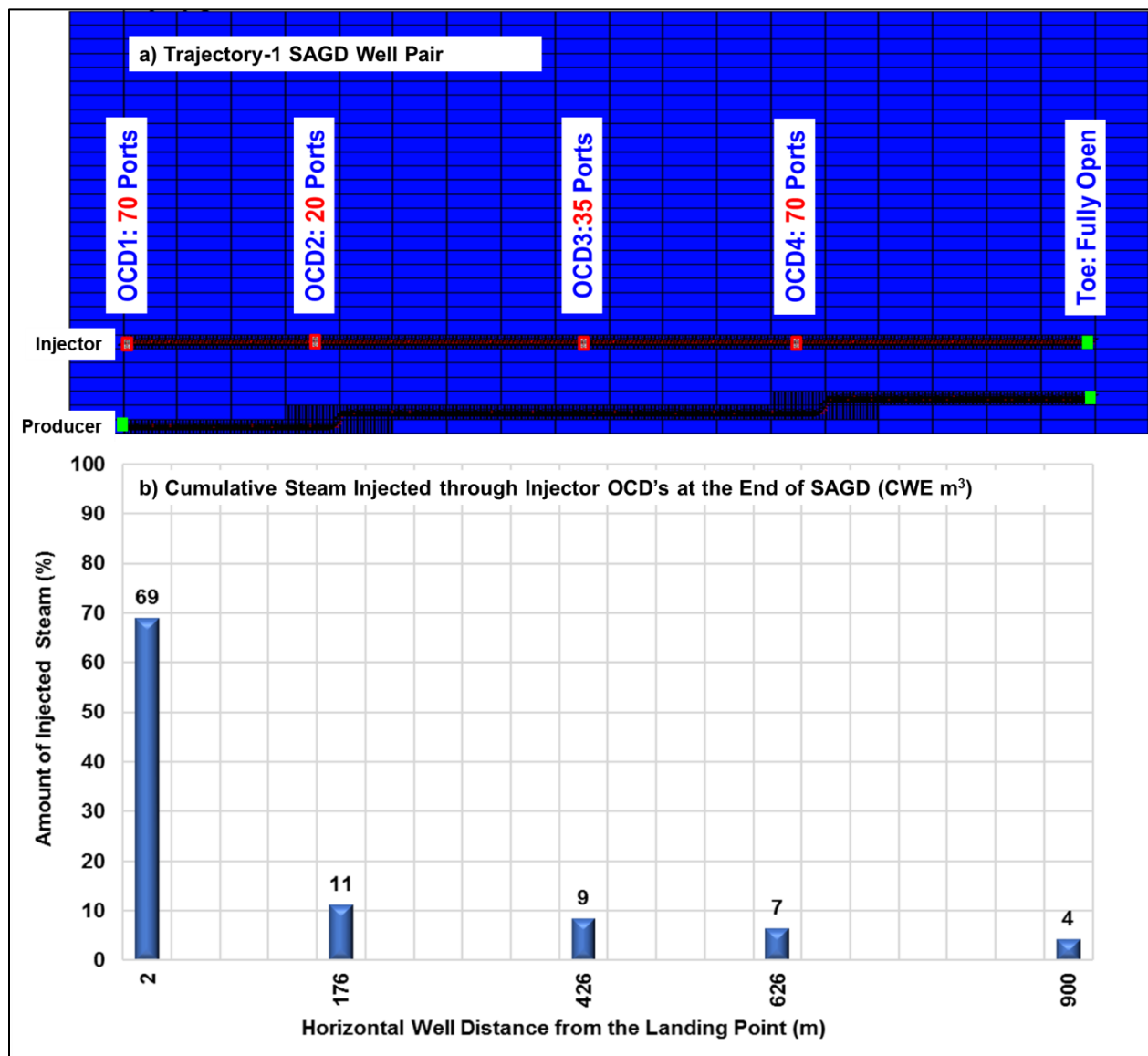


Figure 6-9: Distribution of Injected Steam Among Trajectory-1 OCD's at the End of SAGD Project Life

6.2.4 The Effect of Using Smaller Diameter Slotted Liner

The major factor that causes the OCD#1 to be the major contributor to the total amount of steam injected is the large annular cross-sectional area between the slotted liner and the tubing compared to the tubing diameter. The slotted liner has 9 5/8" diameter (72.6 in² cross-sectional area), and the tubing has 4 1/2" diameter (15.9 in² cross-sectional area), and that means the annular space between the slotted liner and the tubing has more than 3.5 times larger cross-sectional area (56.9 in²) compared to the tubing cross section area. The injected steam tends to take the path that has the

least resistance to flow. **Figure 6-10** shows a comparison of 4 ½” inside 9 5/8” and 7” slotted liners. The optimized OCD’s case obtained using 9 5/8” slotted liner has been run again using 7” slotted liner, and results in **Figure 6-11** show that contribution of OCD’s further away from heel section increased when 7” slotted liner has been used compared with original optimized OCD’s case using 9 5/8” slotted liner.

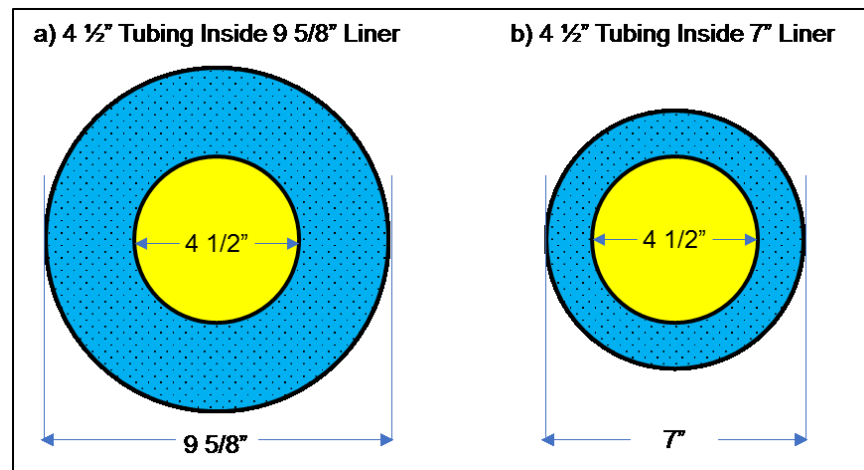


Figure 6-10: Comparison of Tubing Inside Small and Large Diameter Slotted Liner

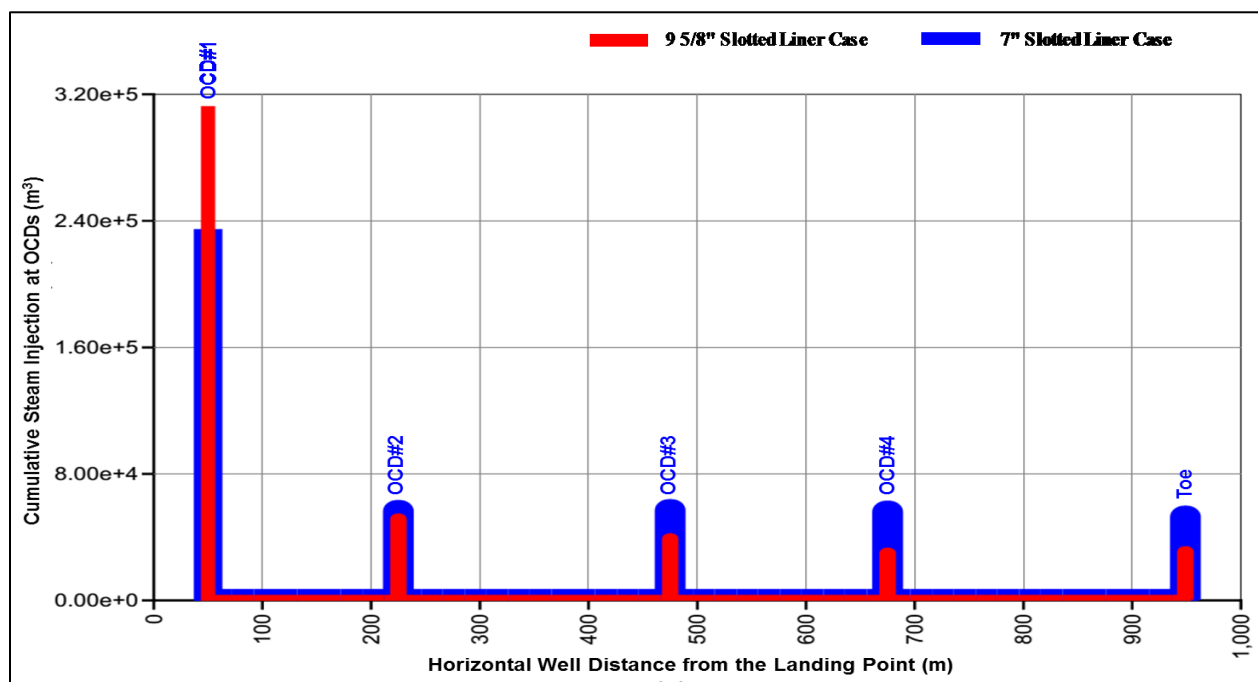


Figure 6-11: Changes in OCD's Contribution to Injected Steam with the Use of Smaller Slotted Liner, Trajectory-1

Injector Tubing/Annulus Pressure Profiles

Another parameter that controls the instantaneous and total amount of steam injected through each OCD and open toe is the pressure differential across the OCD ports. This pressure drop also controls the number of ports in each OCD. **Figure 6-12** depicts the pressure profiles inside the injector tubing and annulus for the first eight years of SAGD process. The highest pressure drop occurs at the heel section of the well, then it continues to drop at farther points from the heel. This high pressure drop at the heel section combined with high number of ports explains the great contribution of OCD#1 to the total amount of steam injected.

Another observation is that overall pressure profile levels increase each year with the progress of SAGD; hence, a reduction in pressure drops between the injector tubing and annulus. This increase in pressure profiles is due to SAGD reservoir pressurization over the time by continuous steam injection, the reduced pressure drops between the injector tubing and annulus means less contribution of OCD's at late stages of SAGD.

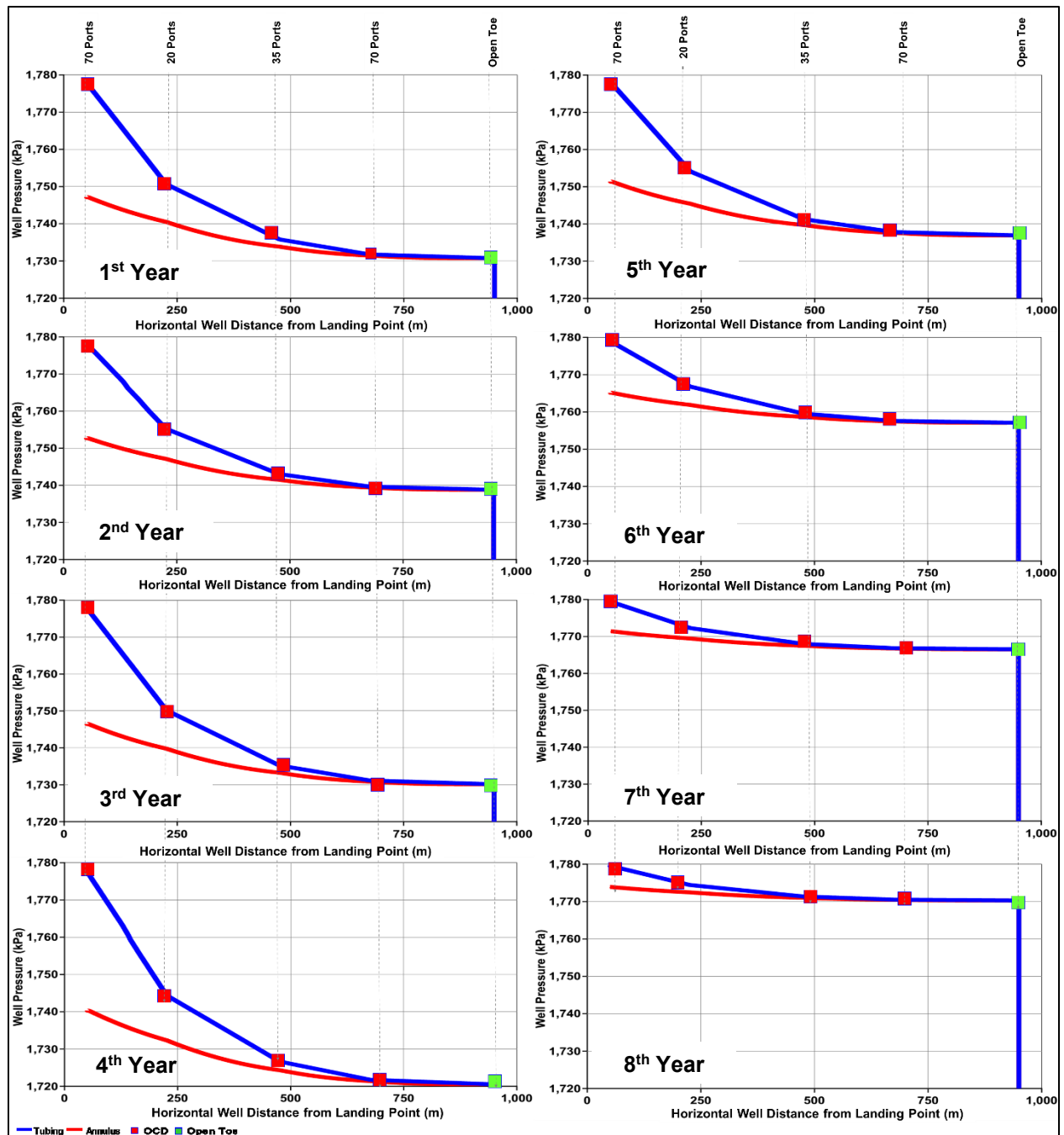


Figure 6-12: Trajectory-1 Optimum Case Injector Tubing/Annulus Pressure Profiles

Comparison with Dual-String Case

Pressure Profiles

Figure 6-13 compares pressure profiles inside the long injector tubing string for the optimized OCD case and base case. In the optimized OCD case, the pressure profile is less steep and pressure gradients steadily decrease at OCD points from the heel to the toe. The frictional pressure losses

in the tubing for the optimized OCD case (50 kPa) are lower by more than 70% compared to the same for the dual-string case (175 kPa). The lower frictional pressure losses for optimized OCD case has several advantages including a more uniform steam penetration into the reservoir. **Figure 6-14** compares the annular injector (Figure 6-14 a) and producer (Figure 6-14 b) pressure profiles for the dual-string and optimized OCD cases. It is observed that the average operating pressure for the OCD case is 1,715 kPa compared to 1,590 kPa for the dual string case.

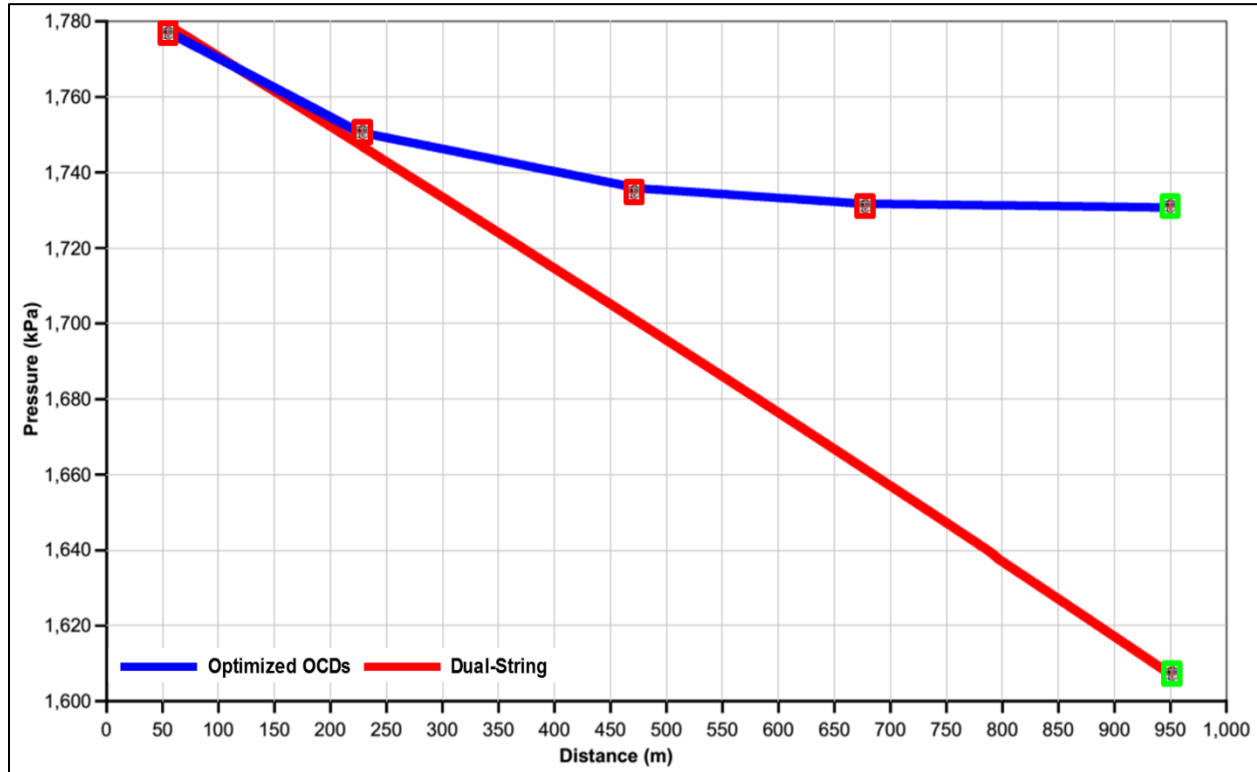


Figure 6-13: Pressure Profiles Inside Long Injector Tubing for Optimized OCD's and Dual-String Cases, Trajectory-1

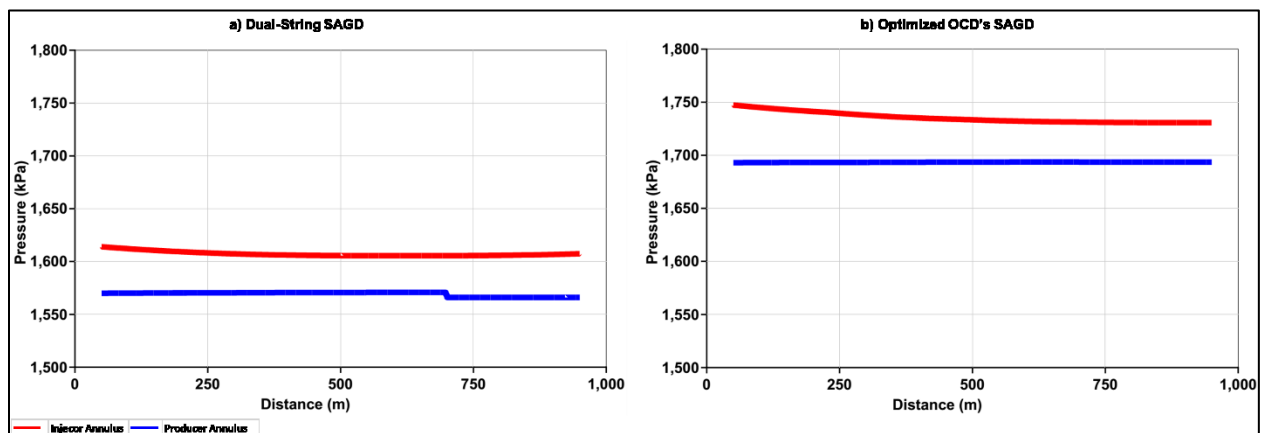


Figure 6-14: Annular Pressure Profiles, Optimized OCD and Dual-String Cases, Trajectory-1

Comparison of Steam Chamber Growth

Figure 6-15 depicts steam chamber growth of dual-string and optimized OCD injection cases. Propagation of steam chamber at the heel section of the models starts late in dual-string case compared to the OCD injection case. This is caused by the higher TVD lateral distance between the injector and the producer at the heel section due to the dipping trajectory of the producer and this leads to a higher subcool level in the heel section.

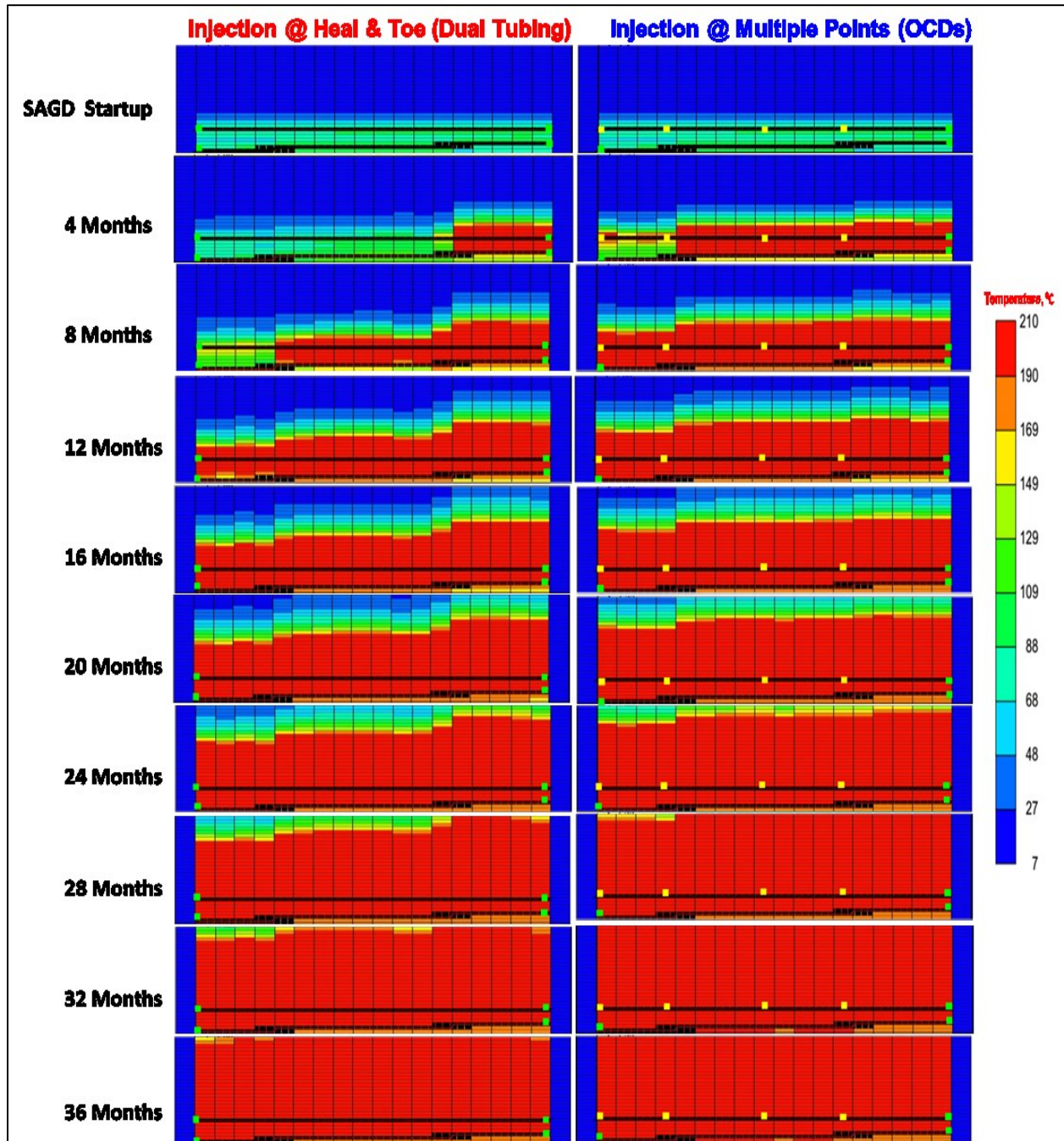


Figure 6-15: Steam Chamber Growth of the Optimized OCD and Dual-String Cases, Trajectory-1

Steam Distribution

Figure 6-16 shows steam injection profiles for three different cases of (1) toe injection only by long tubing, (2) heel and toe injection by short and long tubing, and (3) OCD installation at the end of SAGD first year. **Figure 6-16a** shows steam chamber and injection points. **Figure 6-16b** shows the distribution of the injected steam at sandface entry and **Figure 6-16c** depicts the percentage of the injected steam at each single steam injection point.

Case 1 has a single injection point where 100% of the steam is injected at the toe only, and the injected steam is concentrated at the toe section of the reservoir only. In this case, the middle and heel sections is left un-swept. To enhance steam chamber conformance in Case 2, dual point injection is implemented where 41% of the steam is injected at the heel through a short tubing string located by the injector horizontal landing point and 59% of the steam is injected at the toe through the long tubing injector. Compared to Case 1, better enhancement has been achieved, but the height of the developed steam chamber at the heel and middle sections still remain short compared to toe section. However, in Case 3, steam has been injected at multiple points through the OCD's installed on the long string, where 69%, 11%, 8%, 7% and 5% of the steam have been injected at the open ports starting from heel to toe, respectively. A more uniform steam distribution and chamber conformance has been achieved.

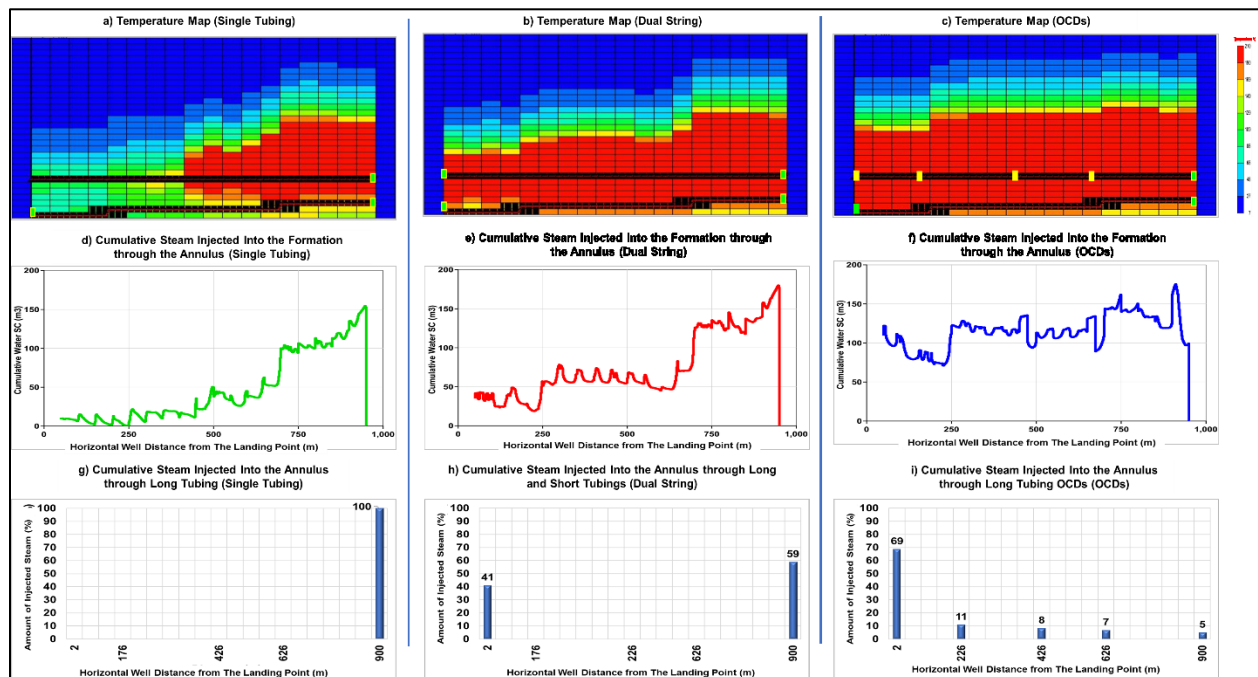


Figure 6-16: Distribution of Injected Steam at Different Points, Trajectory-1 at the End of Year 1

Production Data

Figure 6-17 and **Table 6-2** show cumulative bitumen production, cumulative steam injection, cSOR and NPV for the dual-string and optimized OCD cases. In both cases, the simulation run was terminated when the daily increment of the NPV became zero ($\frac{\Delta NPV}{\Delta t} = 0$). The dual-string case was terminated after 3,548 days (9.7 years) of SAGD operation, while the optimized OCD's case was terminated 305 days earlier, i.e., after 3,243 days (nearly 8.9 years). Comparing performance of the optimized OCD case and the conventional dual-string case demonstrates that the NPV of the optimized OCD case has a better performance (2% increment), equivalent to about \$607,500 positive cash flow.

Table 6-3 presents the SAGD performance data for both cases (dual-string and optimized OCD cases) when compared at the same project termination time (i.e., at optimized OCD termination time, 3,243 days). It can be observed that the enhancement in NPV becomes even better compared to the previous case (\$662,500 positive cash flow). The dashed red line in Figure 6-16 represents the extension of dual-string case performance until its daily increment of the NPV is zero.

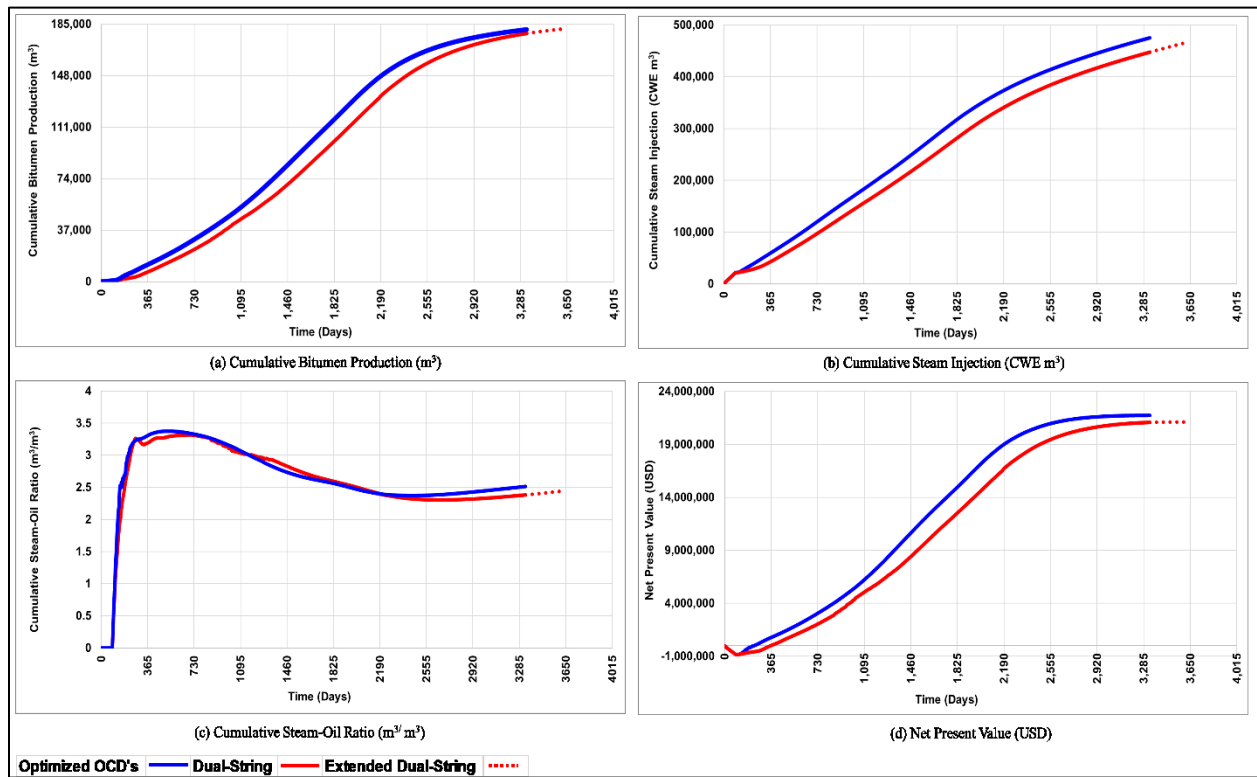


Figure 6-17: SAGD Performance Data of Optimized OCD and Dual-String Cases, Trajectory-1

Table 6-2: Summary of SAGD Performance Data at the End of SAGD Simulation, Trajectory-1

Case	Cumulative Oil Production (m³)	Cumulative Steam Injection (m³ CWE)	Cumulative Steam-Oil Ratio (m³/m³)	NPV (\$)	Project Life (Years)
Dual-String	181,775	467,070	2.46	21,128,653	9.7
Optimized OCD's	181,090	475,463	2.52	21,736,170	8.9
Difference (%)	0	2	2	3	-9

Table 6-3: Summary of SAGD Performance Data at the End of Optimized OCD's Case Simulation, Trajectory-1

Case	Cumulative Oil Production (m³)	Cumulative Steam Injection (m³ CWE)	Cumulative Steam-Oil Ratio (m³/m³)	NPV (\$)	Project Life (Years)
Dual-String	178,184	447,414	2.40	21,073,672	8.9
Optimized OCD's	181,090	475,463	2.52	21,736,170	8.9
Difference (%)	2	6	5	3	0

6.3 Study # 2: Trajectory-2 OCD's Optimization

6.3.1 Base Case Description

The base case of the study is based on Trajectory-2 model with a 2-m LGR described in **Figure 4-25**. As depicted in **Figure 6-18**, Trajectory-2 has parallel well pair with fixed TVD lateral separating distance of 5 m, but there are tortuosities along the overall trajectories paths, and this leads to having toe section of the well pair closer to reservoir ceiling compared to the middle and heel sections.

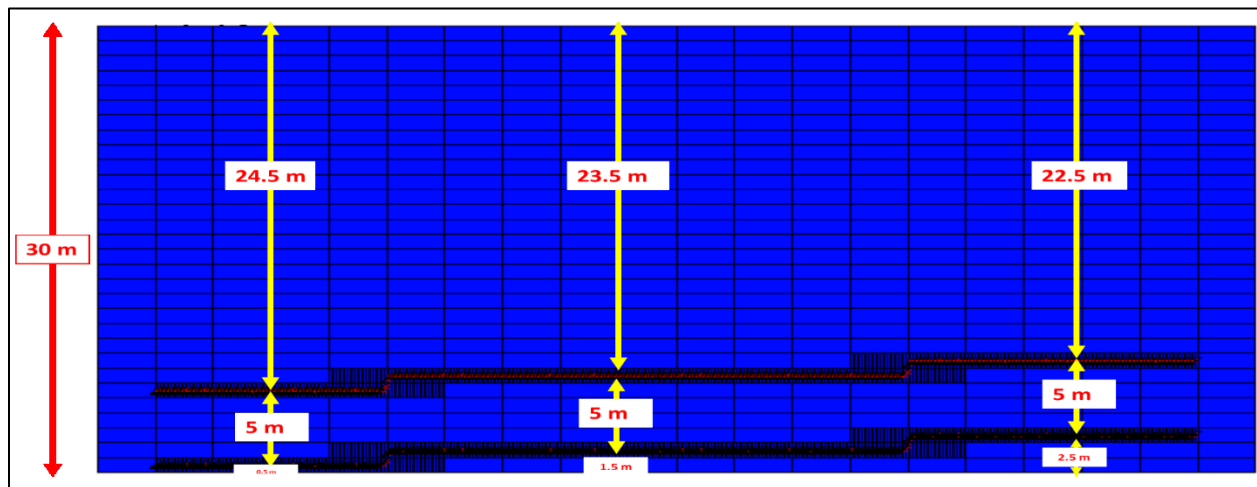


Figure 6-18: Trajectory-2 SAGD Well Pair Trajectories

Both injector and producer use the dual-string completion scheme as shown in **Figure 6-19**, i.e., 9 5/8" slotted liner and 4 1/2" short and long strings.

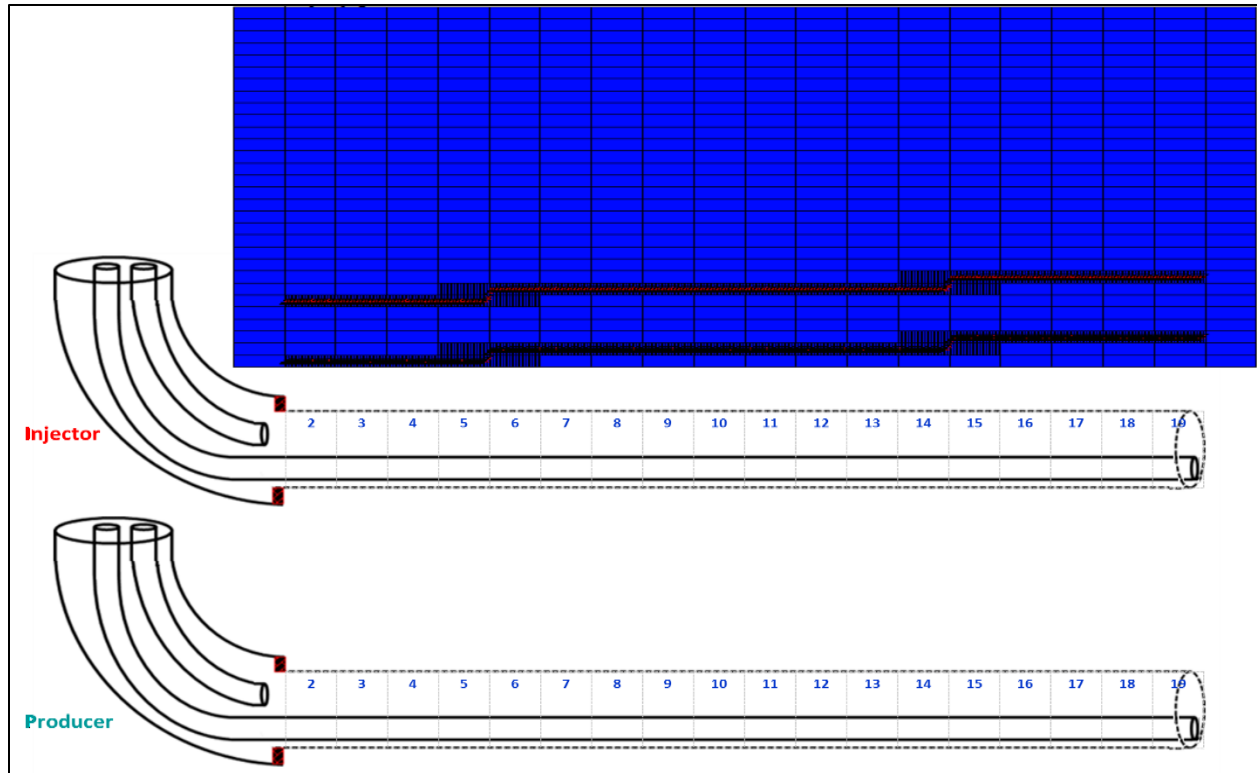


Figure 6-19: Trajectory-2 and Well Completion Scheme for the Base Case

6.3.2 Optimization Analysis with OCD Deployment

As shown in **Figure 6-20**, the injector completion (in the design of tubing-deployed OCD's optimization case) is modified where the short tubing string is removed and the long tubing is kept but equipped with four FCD's at 26 m, 226 m, 426 m and 776 m from landing point of the injector, and the toe is kept fully open to flow. The producer dual-string completion is kept without change. **Figure B-12** in **Appendix B** shows the assignment of orifice type OCD's at 13th child blocks of cells 2,6,10 and 17 of injector long tubing in CMG STARS input data file.

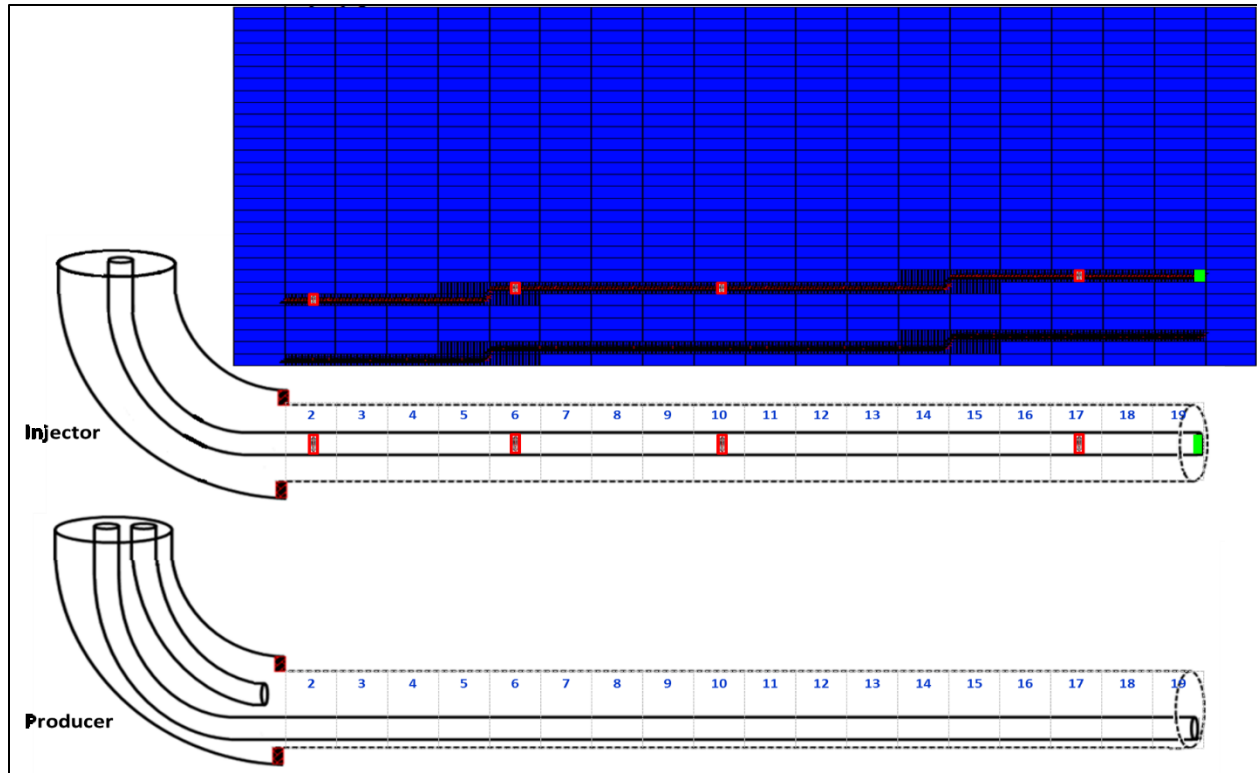


Figure 6-20: Trajectory-2 Tubing-Deployed OCD's Completion Diagram

OCD's # of Ports Parameterization

In total, four OCD's were assigned as parameters in CMG CMOST optimization tool. Also, number of ports were entered as sample values for each OCD with the range of (0-70) and constant increments of five.

Experiments and Samples

Initially, 25 experiments were generated using the full factorial sampling technique. **Figure B-13** in **Appendix B** show orthogonality value of 0.0135 (nearly orthogonal) indicating a good design quality (green zone).

Short-Term Optimization of Number of Ports

The short-term optimization run was done using the CMOST DECE optimizer. First, the 25 experiments were run. Next, 475 new cases were generated and run using DECE. **Figure 6-21** shows NPV's of short-term optimization results. The trend line has a positive slope indicating optimization convergence towards the optimum solution.

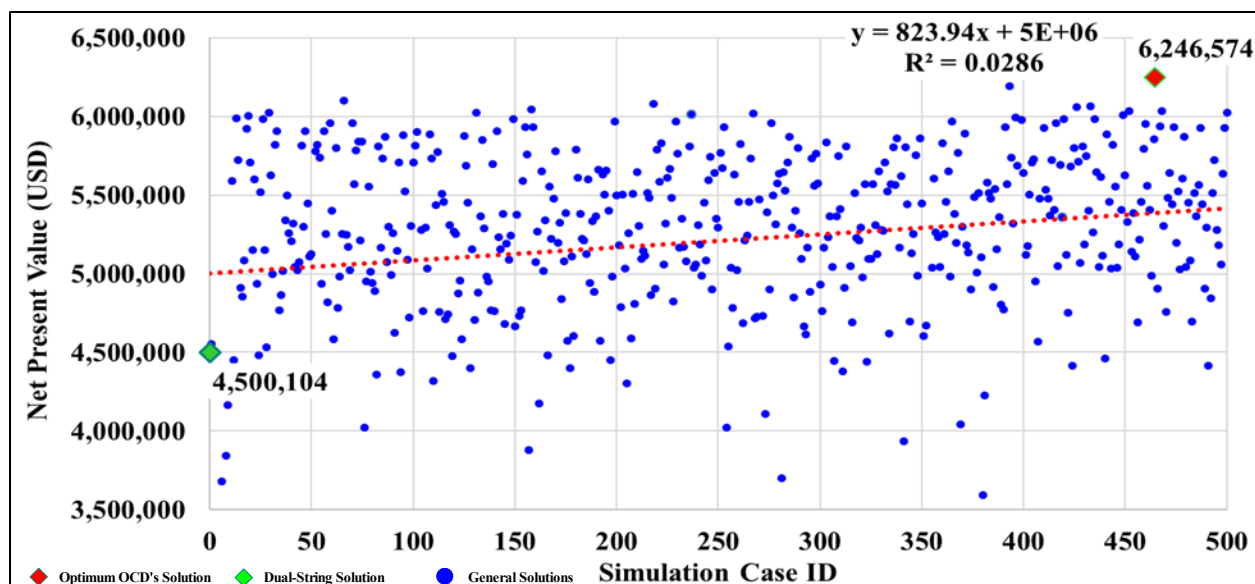


Figure 6-21: Trajectory-2 OCD's Optimization Results (Short-Term)

Long-Term Optimization of Number of Ports

After ranking short-term simulation cases according to the NPV, the top 50 simulation cases were allowed to run for an extended period until the end of SAGD project life. **Figure 6-22** shows the results of the long-term optimization runs. The optimum case was found to be the one with four OCD's having the following number of ports starting from the heel to toe: OCD#1: 65, OCD#2: 5, OCD#3: 40 and OCD#4: 60), and a NPV of \$21,126,515. Also, the conventional dual-string case was projected on the same chart for comparison purposes with the NPV of \$20,674,799.

Figure 6-23 depicts the completion diagram of Trajectory-2 with optimum OCD's locations and number of ports. Negative slope trend line indicates the NPV of the top 50 cases decrease according to the order of the case. This is expected as the short-term cases were ranked and labeled from Case #1 to 50 from the highest to lowest NPV.

The SAGD project life times (i.e., the time it takes for the NPV to peak) of the top 50 cases and their corresponding recovery factors are shown in **Figures C-3 and C-4** of **Appendix C**. The range of ultimate recovery factors for the top 50 cases is 69.3-70.5% and the optimized case has a recovery factor of 70%.

More cases (beyond top 50 cases) have been run for the full well life cycle to confirm the decreasing trend of the long-term NPV consistent with the NPV ranking. Results can be found in **Figures C-14 through C-16** of **Appendix C**.

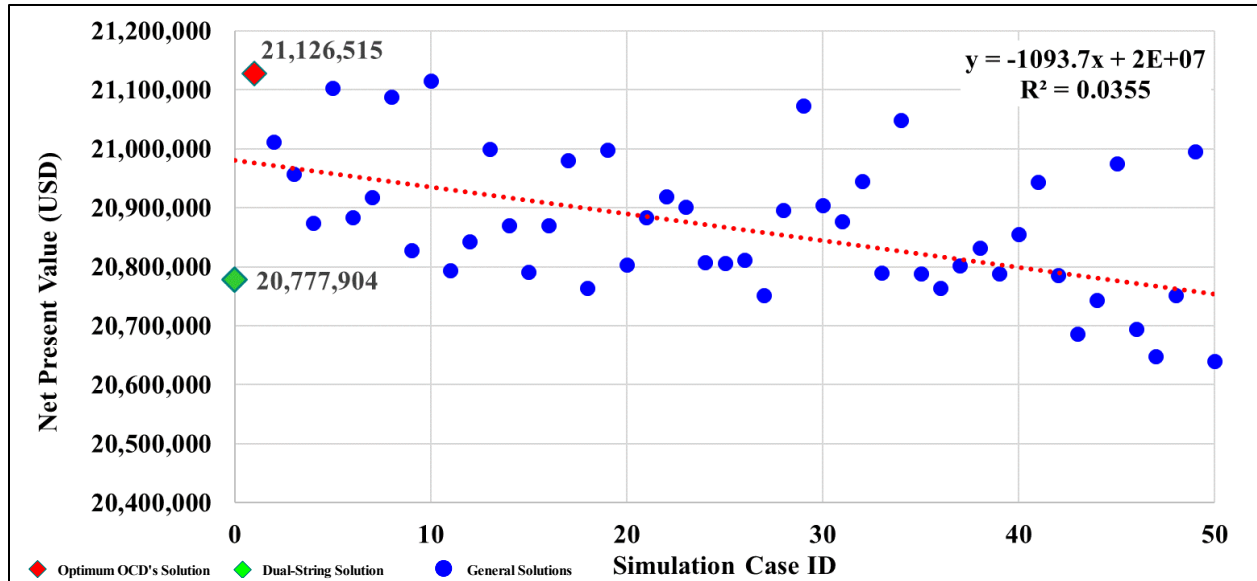


Figure 6-22: Trajectory-2 OCD's Optimization Results (Long-Term)

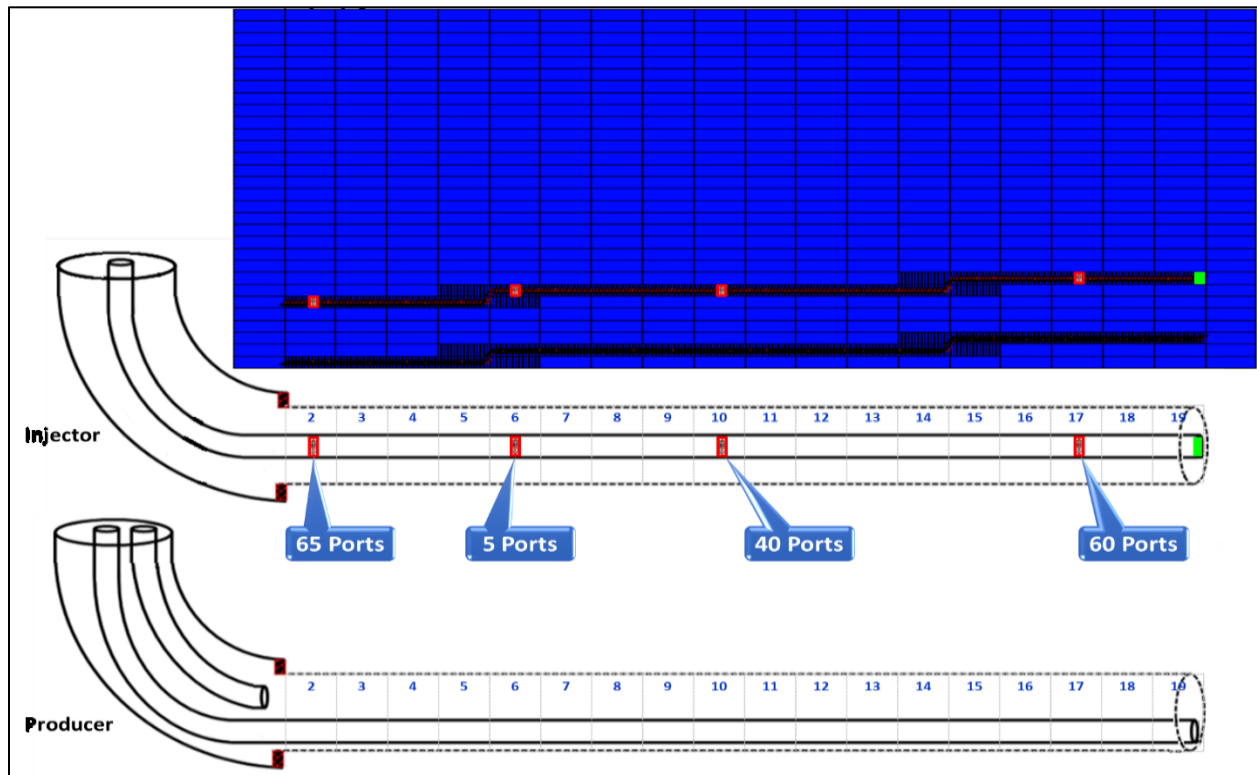


Figure 6-23: Optimum OCD Case for Trajectory-2

Optimum Range of Number of Ports

Figure 6-24 shows the number of ports for the top 5 optimized OCD's cases. It can be observed that the numbers are: 65-70 for OCD#1, 5-20 for OCD#2, 30-45 for OCD#3 and 50-65 for OCD#4. This finding suggests that conducting an additional optimization study by constraining the number

of ports within above ranges could result in even more optimum results. **Table 6-4** lists the number of ports and the NPV's for the top 5 cases.

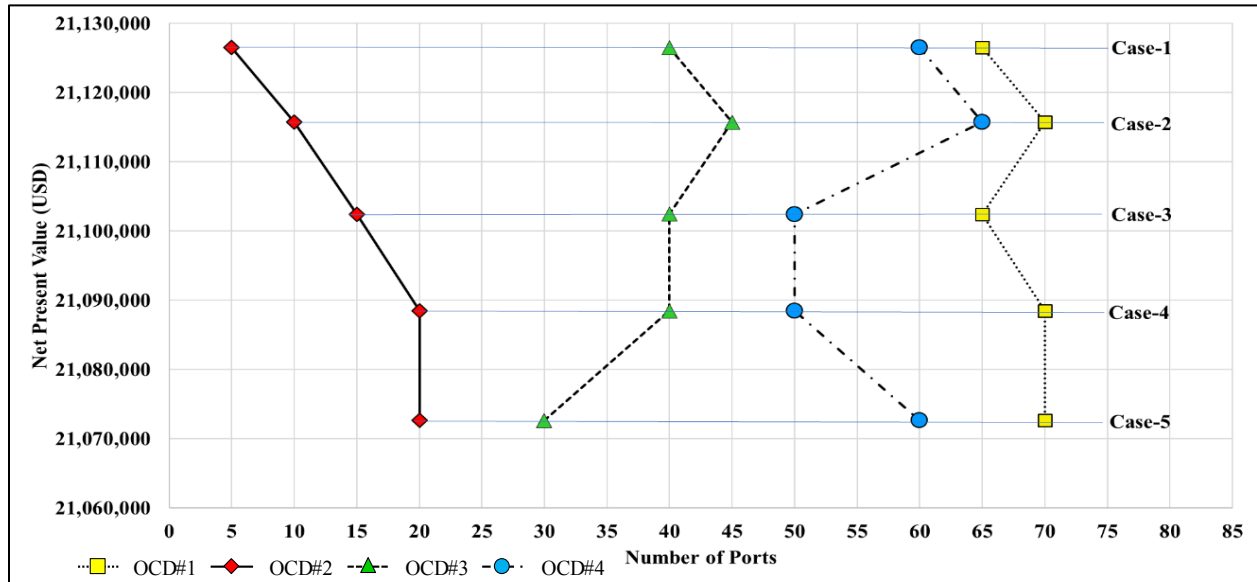


Figure 6-24: Optimum Number of Ports for Top 5 Designs, Trajectory-2

Table 6-4: Optimum Number of Ports for Top 5 Designs, Trajectory-2

ID	OCD's Distribution				NPV (USD)
	OCD#1	OCD#2	OCD#3	OCD#4	
1	65	5	40	60	21,126,515
2	70	10	45	65	21,115,722
3	65	15	40	50	21,102,431
4	70	20	40	50	21,088,450
5	70	20	30	60	21,072,651

6.3.3 Results Analysis

Steam Chamber for Optimized OCD's Case

Figure 6-25 shows steam chamber growth of the optimized OCD case in the sections parallel and perpendicular to the well pairs. A uniform steam chamber growth can be observed. At the end of the 3rd year, the steam chamber hits the reservoir ceiling, and then starts to expand laterally until it reaches the side boundaries of the reservoir at the end of the 6th year. The yellow marks on the injector well represents locations of the installed OCD's. The green marks at the toe depict fully open-to-flow toes. Consistent and uniform steam chamber growth can be seen throughout the SAGD project life.

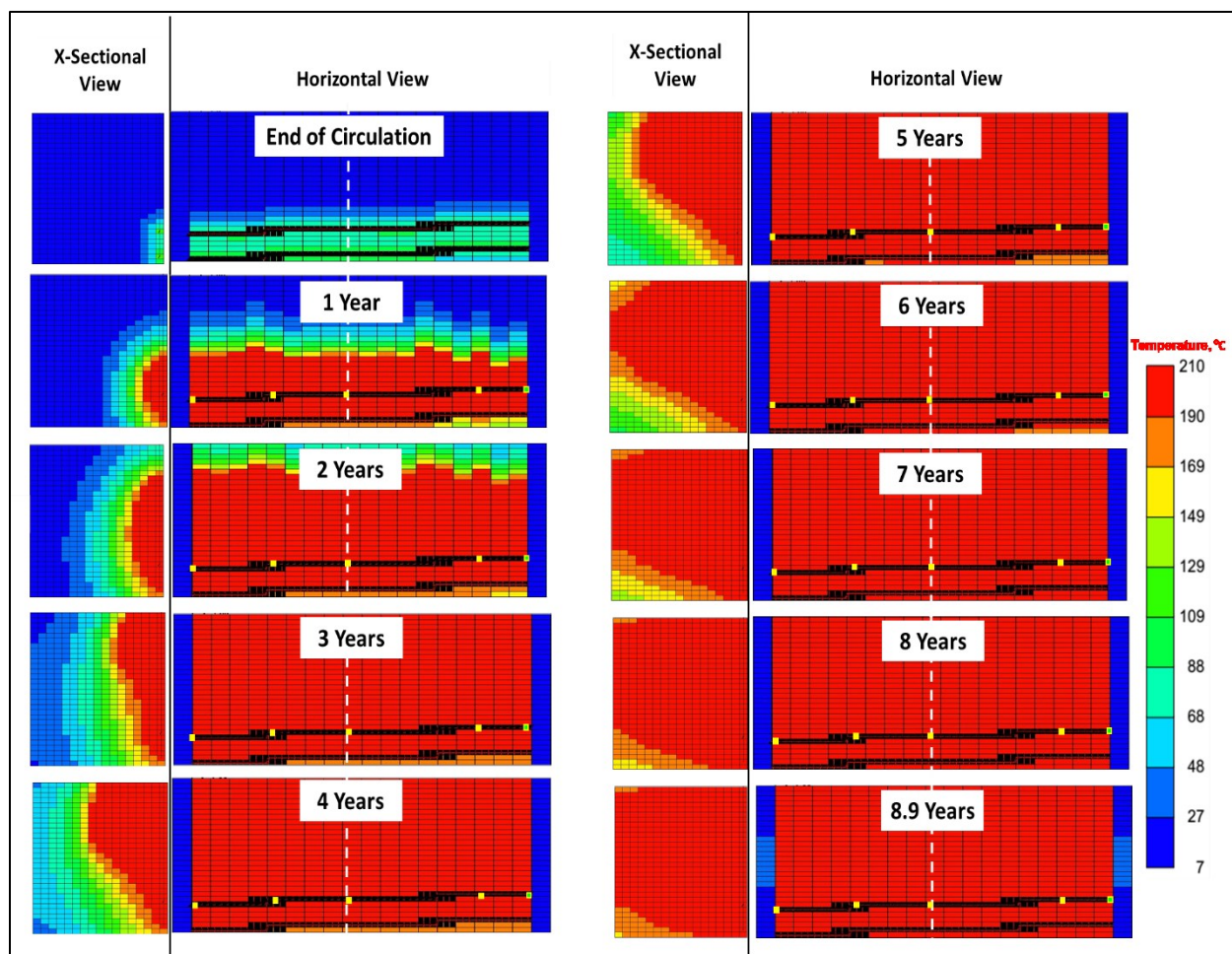


Figure 6-25 Trajectory-2 Temperature Maps of the Optimized OCD's Case SAGD Model at Different Stages

Steam Distribution via OCD's

Figure 6-26 shows the contribution of each single OCD and open toe to the total amount of steam injected by the end of the simulation run. Much of the steam (93%) is injected at the heel and the middle locations (heel: 75% and OCD#3: 18%). About 3% of the steam is injected at OCD#2 and only 2% at the open toe, and another 2% at the OCD next to the open toe (OCD#4).

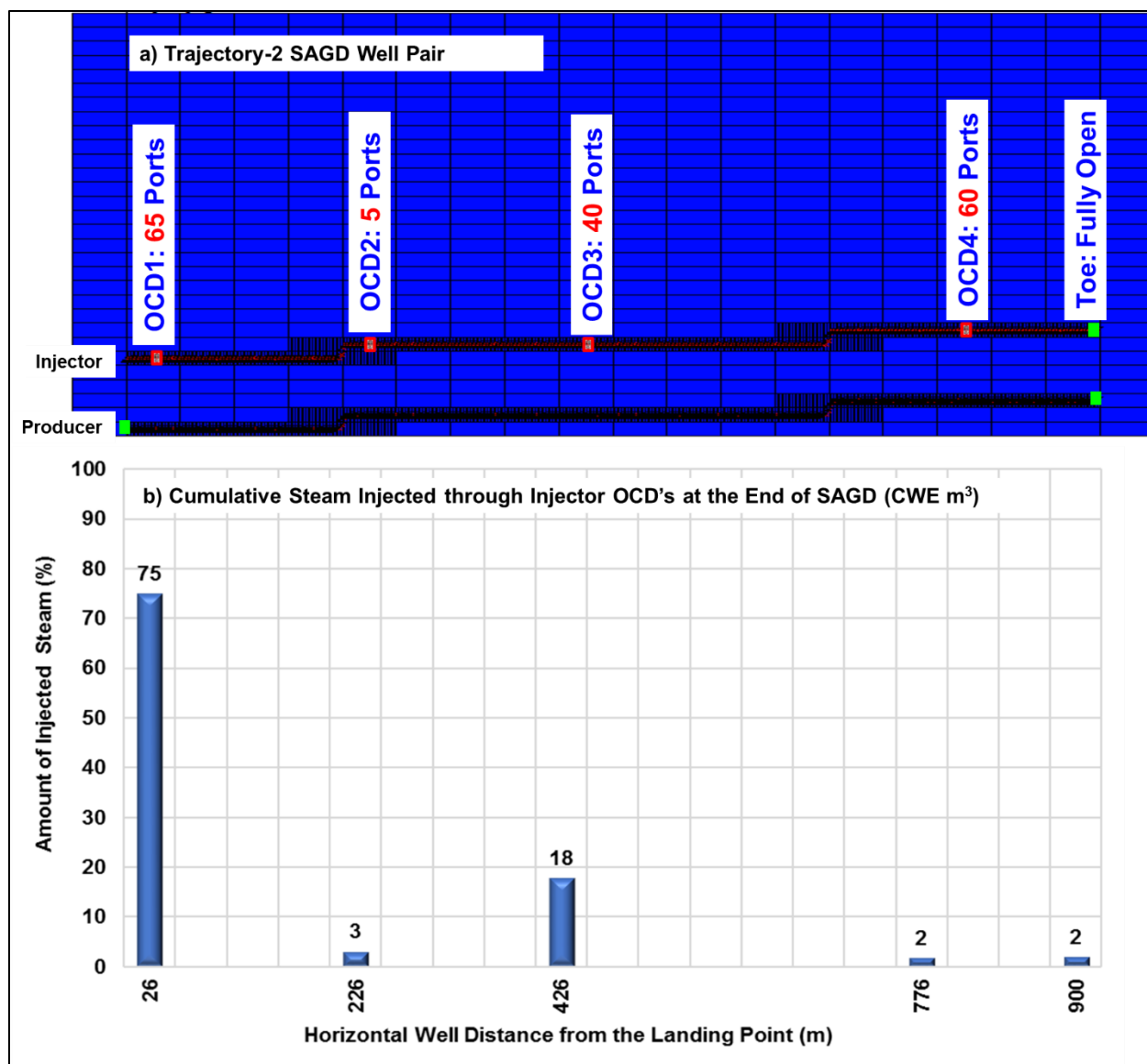


Figure 6-26: Distribution of Injected Steam Among Trajectory-2 OCD's at the End of SAGD Project Life

Injector Tubing/Annulus Pressure Profiles

Figure 6-27 presents the pressure profile for the tubing and tubing-liner annulus for the optimized OCD case. The profile indicates the large amount of the injected steam at the heel (75%) which seems to be caused by the large pressure drop across OCD#1. However, despite the high pressure drop across OCD#2, the cumulative injected steam through OCD#2 is only 3%. In fact, the optimized number of ports for OCD#2 is only five. Also, it's observed that contribution of OCD#2, OCD#3 and OCD#4 to cumulative injected steam are reduced with SAGD progress in time.

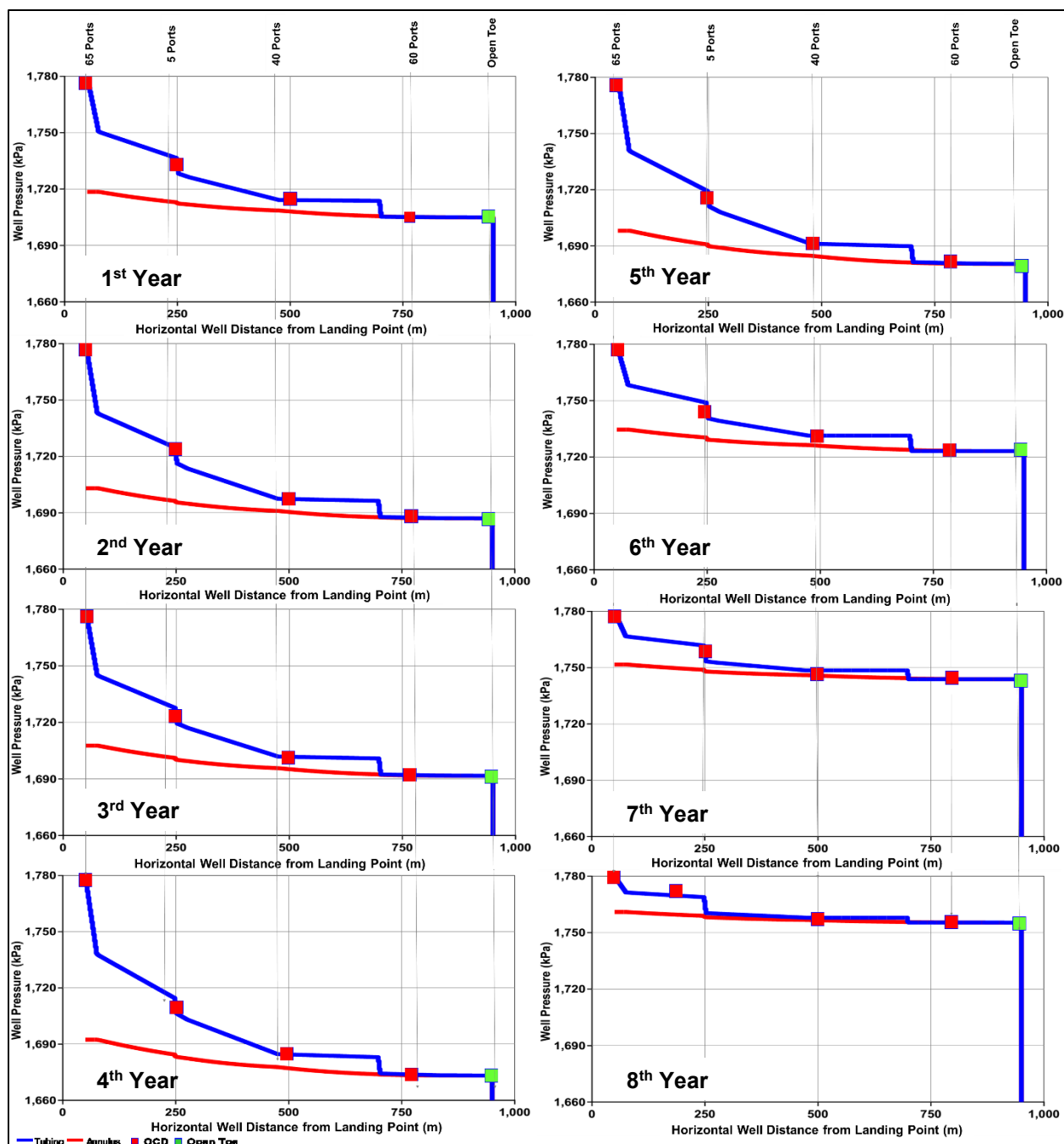


Figure 6-27: Trajectory-2 Optimum Case Injector Tubing/Annulus Pressure Profiles

Comparison with Dual-String Case

Pressure Profiles

Figure 6-28 compares the pressure profile inside the long injector tubing for the optimized OCD case with that of the dual-string case. In the optimized case, the pressure profile is seen to be less steep and the pressure gradients are observed to become smaller towards the tow. Frictional

pressure losses for the optimized case (90 kPa) are smaller by 52% compared to the same for the dual-string case (175 kPa). Also, it can be noticed the two excursion points of Trajectory-2 injector are reflected in the pressure profiles inside the long injector tubing for both optimized OCD and dual-string cases.

Figure 6-29 compares injector (Figure 6-31 a) and producer (Figure 6-31 b) annular pressure profiles of the optimized OCD cases and dual-string cases. The profiles show a higher average operating pressure of 1,680 kPa for the OCD model compared to 1,585 kPa for the dual string case.

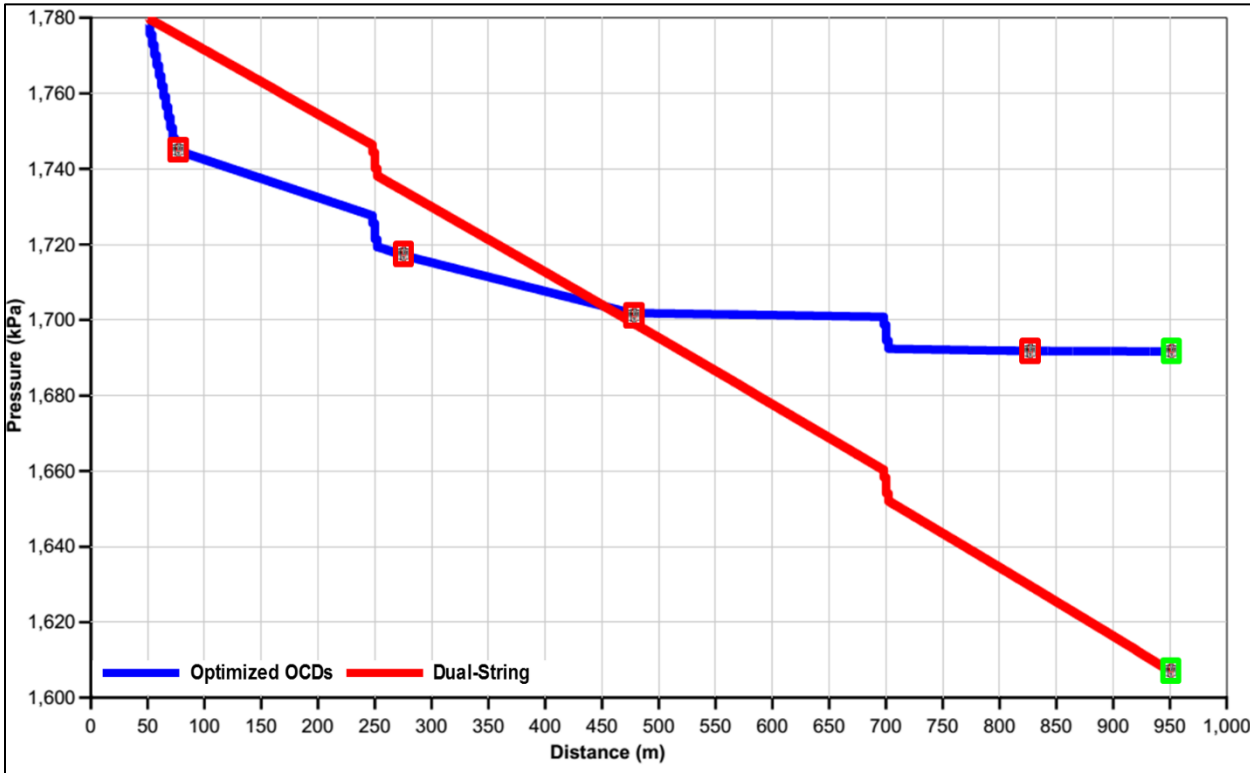


Figure 6-28: Pressure Profiles Inside Long Injector Tubing for Optimized OCD's and Dual-String Cases, Trajectory-2

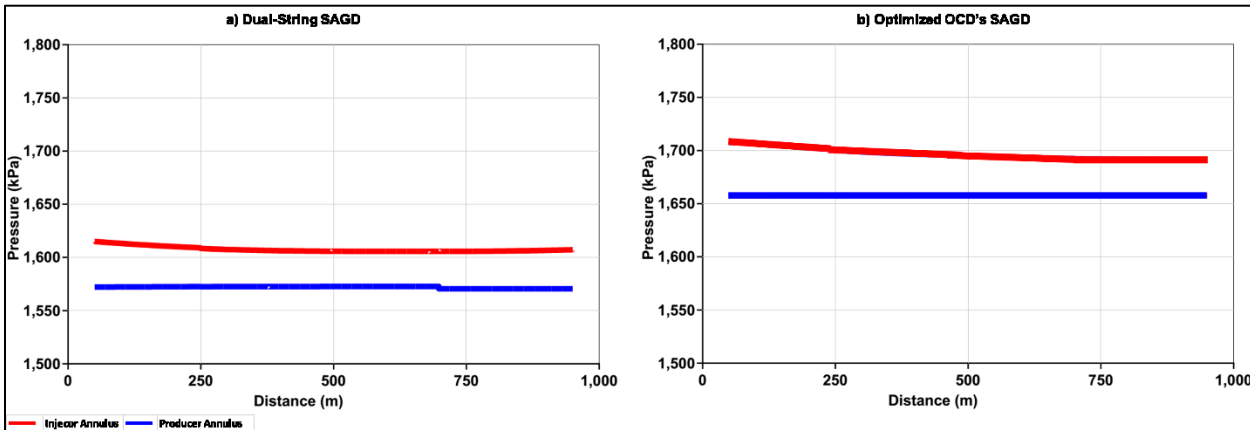


Figure 6-29: Annular Pressure Profiles, Optimized OCD and Dual-String Cases, Trajectory-2

Comparison of Steam Chamber Growth

Figure 6-30 depicts steam chamber growth, where almost no or poor steam chamber at the toe section in dual-string case, on the other hand uniform steam chamber growth can be noticed in case of optimized OCD's achieved by installing OCD#4.

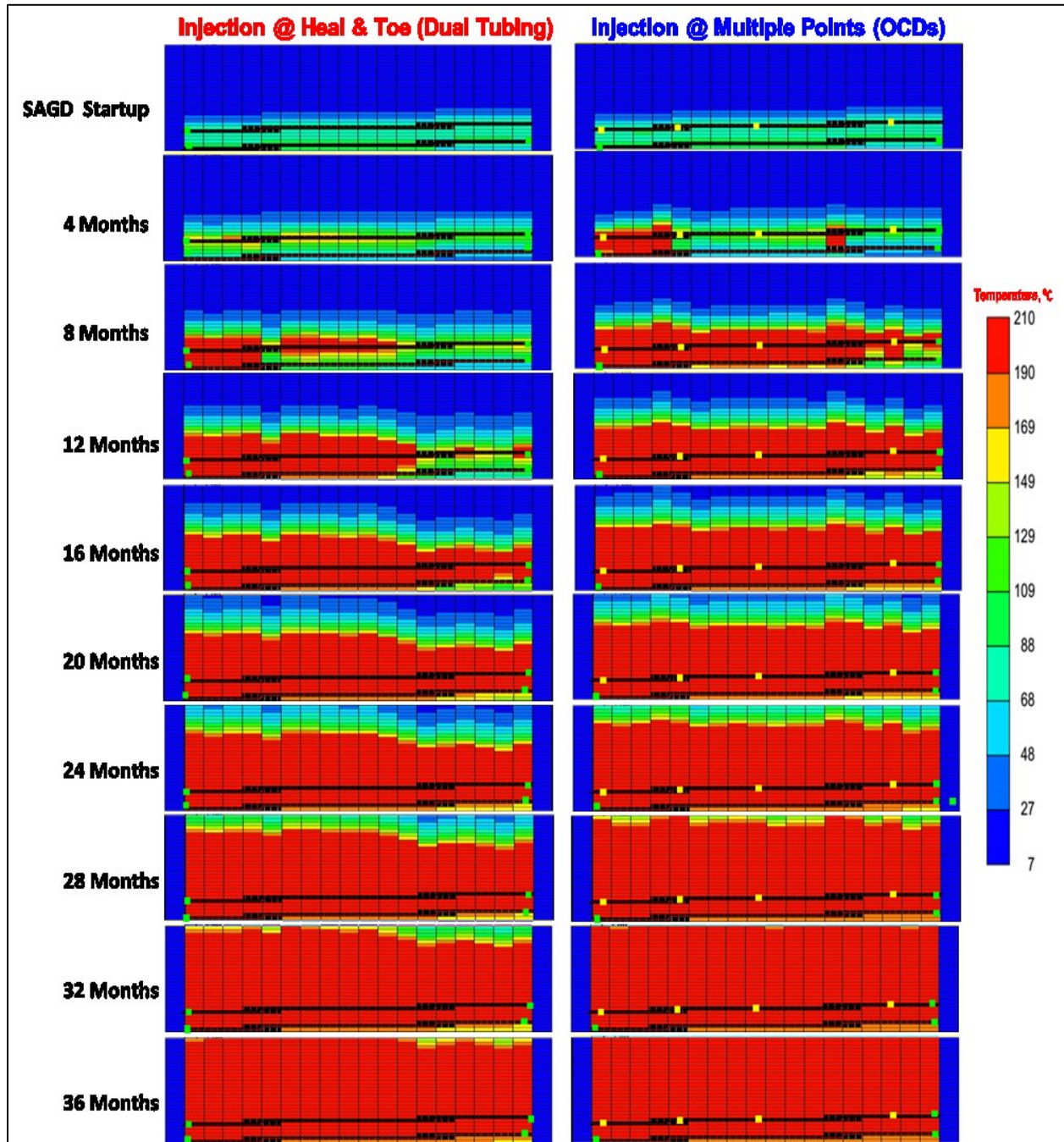


Figure 6-30: Steam Chamber Growth of the Optimized OCD and Dual-String Cases, Trajectory-2

Steam Distribution

Figure 6-31 shows steam injection profiles for cases of single-point injection (**Figure 6-31a**), dual-point injection (**Figure 6-31b**) and multi-point injection (**Figure 6-31c**) at the end of first year of SAGD. In single-point injection, although 100% of steam has been injected at the toe, the injected steam tends to escape and flow towards heel section of the injector under the effect of the gravity due to the dipping trajectory of the injector. Aiming to enhance steam conformance, dual points injection is implemented where 29% of the steam is injected at the heel through the short tubing string, and 71% of the steam is injected at the toe through the long tubing injector. Compared to single-point injection, better enhancement has been achieved in dual points case, but still the toe section is left unwept. However, in the third case (multi-points injection), steam is injected at multiple points via OCD's conveyed on the long string tubing, where 76% of the steam is injected at the heel, 18% at the middle OCD (OCD#3), 1% at the toe and the remaining steam through OCD#2 and OCD#4. Deployment of OCD's has resulted in developing a more uniform steam chamber.

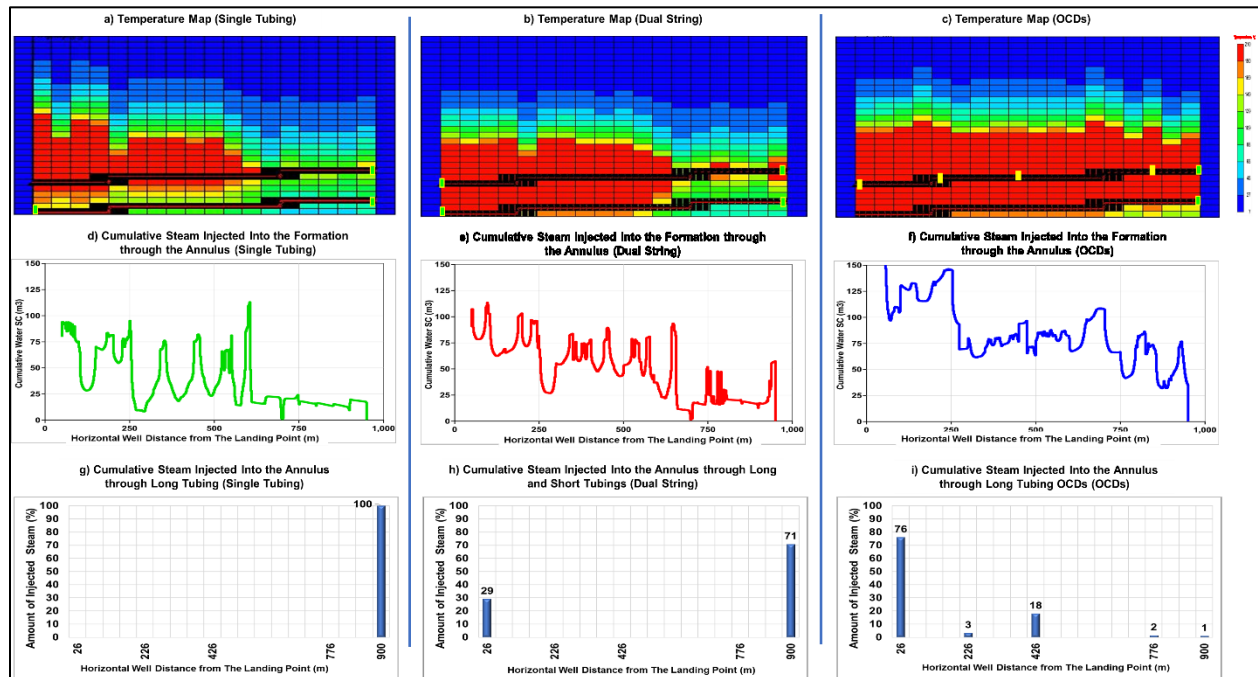


Figure 6-31: Distribution of Injected Steam at Different Points, Trajectory-2 at the End of Year 1

Production Data

Production and injection of conventional dual-string and optimized OCD cases are summarized in **Figure 6-32** and **Table 6-5**. Both cases were terminated after daily increment of the NPV became

zero ($\frac{\Delta NPV}{\Delta t} = 0$). First, the optimized OCD's case was terminated after 3,256 days (8.9 years). Then, the dual-string case was terminated after 3,618 days (9.9 years), i.e., almost one year after the optimized OCD's case. Comparing both cases shows that the NPV of the optimized OCD case has a better performance (2% higher), that is, \$348,611 more NPV. **Table 6-6** compares both cases at the same termination time (optimized OCD's case termination time), where \$451,716 increment can be noticed.

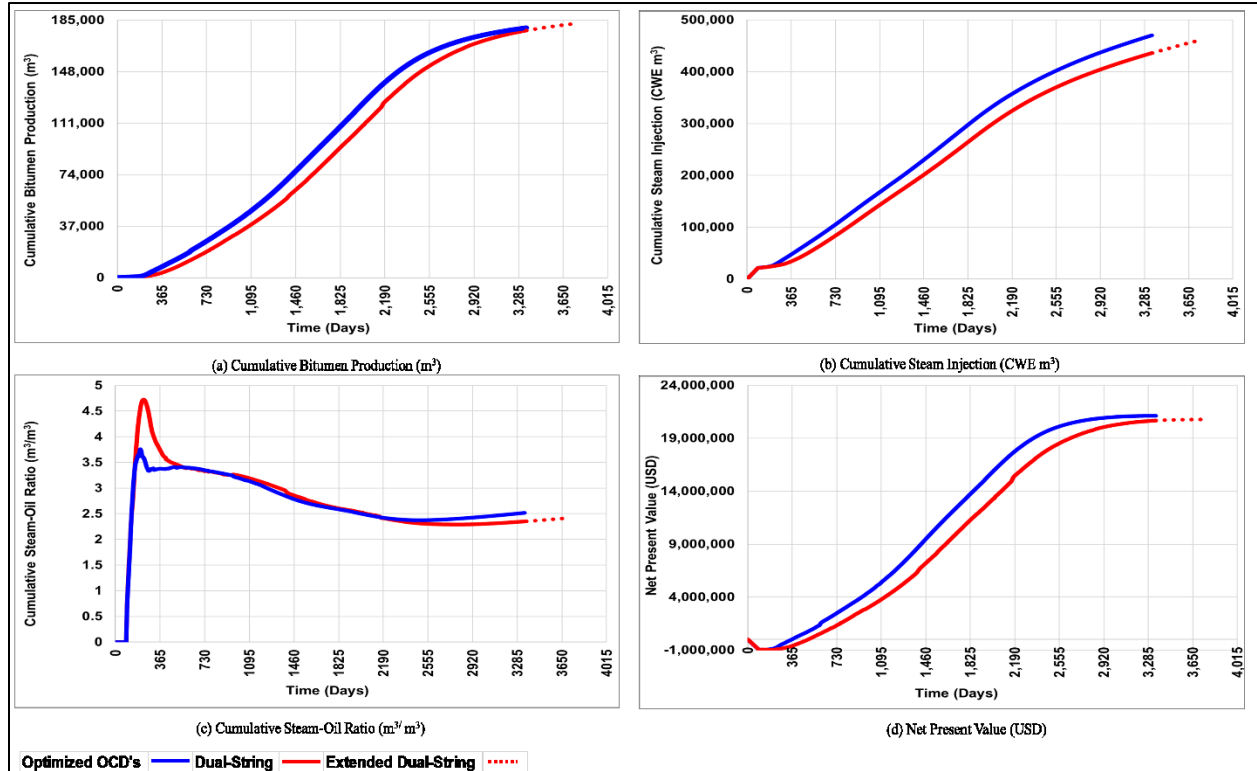


Figure 6-32: SAGD Performance Data of Optimized OCD's and Dual-String Cases, Trajectory-2

Table 6-5: Summary of SAGD Performance Data at the End of SAGD Simulation, Trajectory-2

Case	Cumulative Oil Production (m³)	Cumulative Steam Injection (m³ CWE)	Cumulative Steam-Oil Ratio (m³/m³)	NPV (\$)	Project Life (Years)
Dual-String	182,236	460,543	2.42	20,777,904	9.9
Optimized OCD's	179,554	470,416	2.51	21,126,515	8.9
Difference (%)	-1	2	4	2	-10

Table 6-6: Summary of SAGD Performance Data at the End of Optimized OCD's Case Simulation, Trajectory-2

Case	Cumulative Oil Production (m³)	Cumulative Steam Injection (m³ CWE)	Cumulative Steam-Oil Ratio (m³/m³)	NPV (\$)	Project Life (Years)
Dual-String	177,463	436,006	2.35	20,674,799	8.9
Optimized OCD's	179,554	470,416	2.51	21,126,515	8.9
Difference (%)	1	8	7	2	0

6.4 Study # 3: Trajectory-3 OCD's Optimization

6.4.1 Base Case Description

Figure 6-33 describes Trajectory-3 model. Both injector and producer have excursions at several locations. These excursions result in (3-7 m) variations in TVD lateral separating distance among different sections of the well pair.

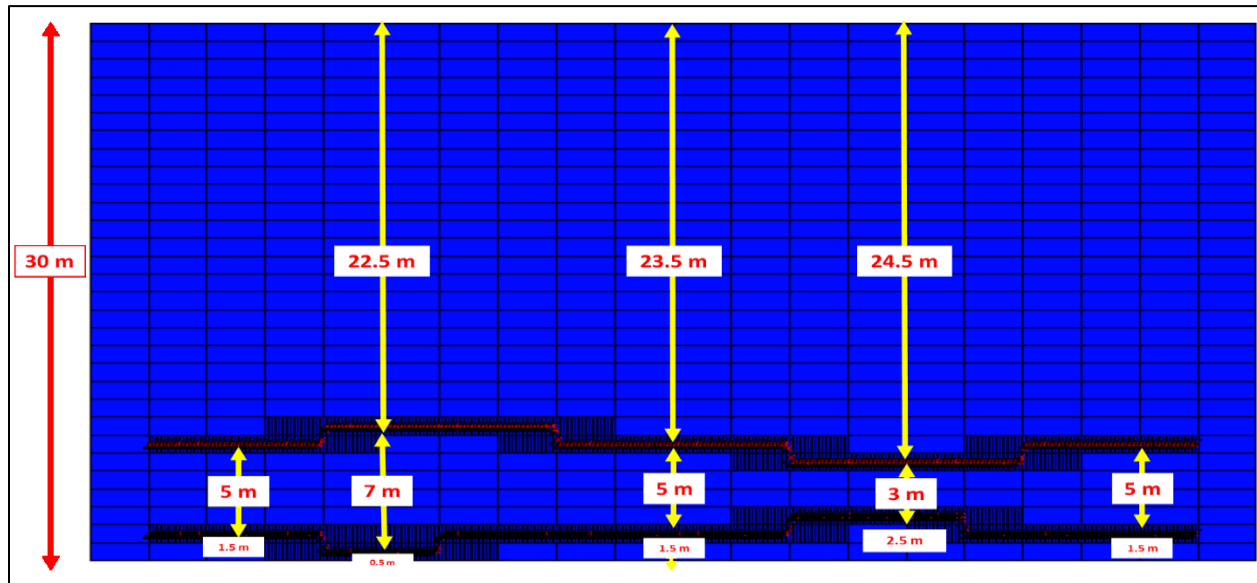


Figure 6-33: Trajectory-3 SAGD Well Pair Trajectories

As in previous cases, the dual-string completion scheme has been adapted as shown in **Figure 6-34**, i.e., 4 ½" short and long tubing strings are packed into 9 5/8" slotted liner.

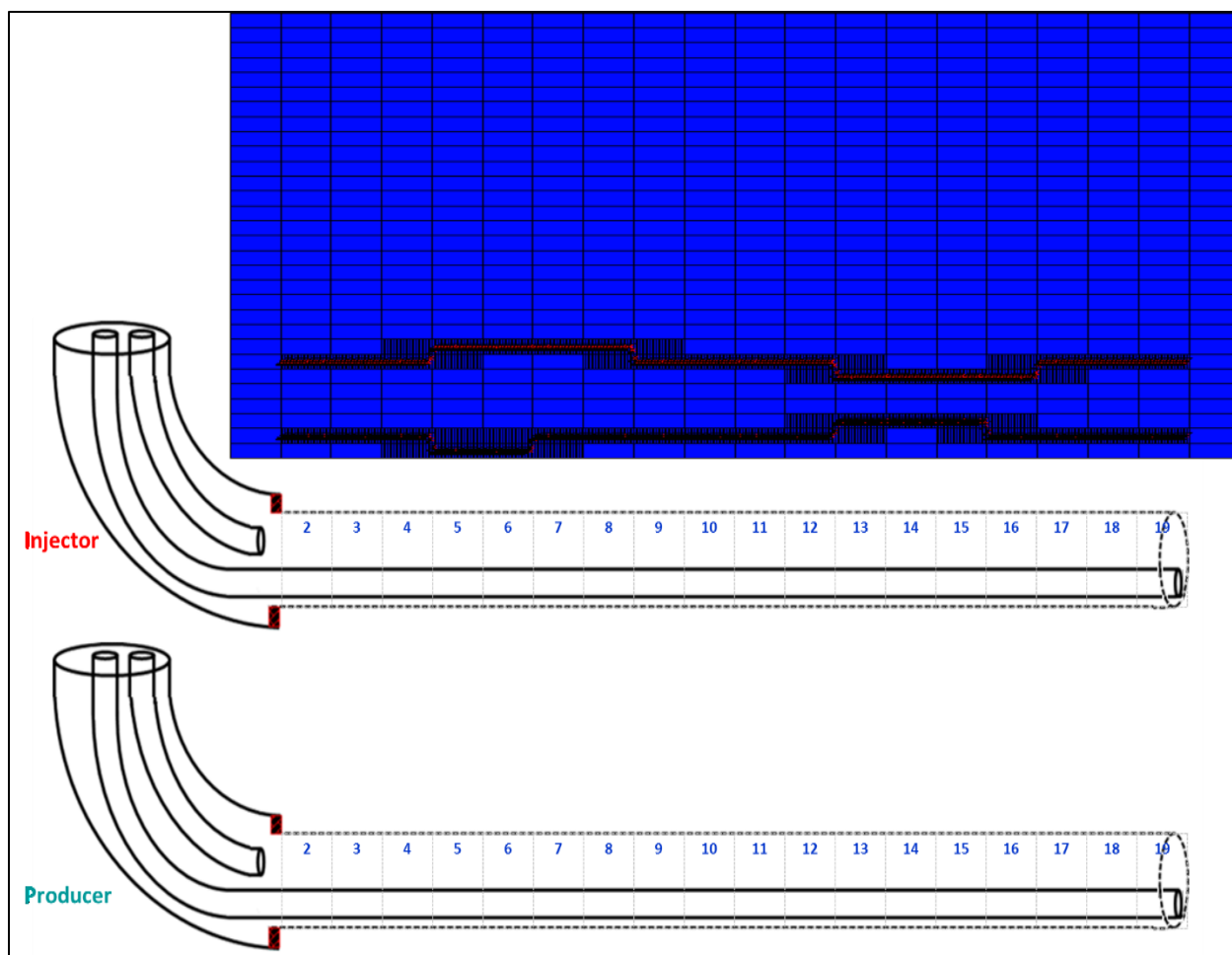


Figure 6-34: Trajectory-3 and Well Completion Scheme for the Base Case

6.4.2 Optimization Analysis with OCD Deployment

For Trajectory-3 optimization work, and as shown in **Figure 6-35**, four OCD's have been deployed among the long tubing of the injector at 26 m, 176 m, 326 m and 526 m away from the landing point, in addition to fully open-to-flow toe. The producer maintained its original dual-string completion scheme.

Figure B-14 in **Appendix B** shows assignment of orifice type OCD's at 13th child blocks of parent blocks 2,5,8 and 12 of injector long tubing in CMG STARS input data file.

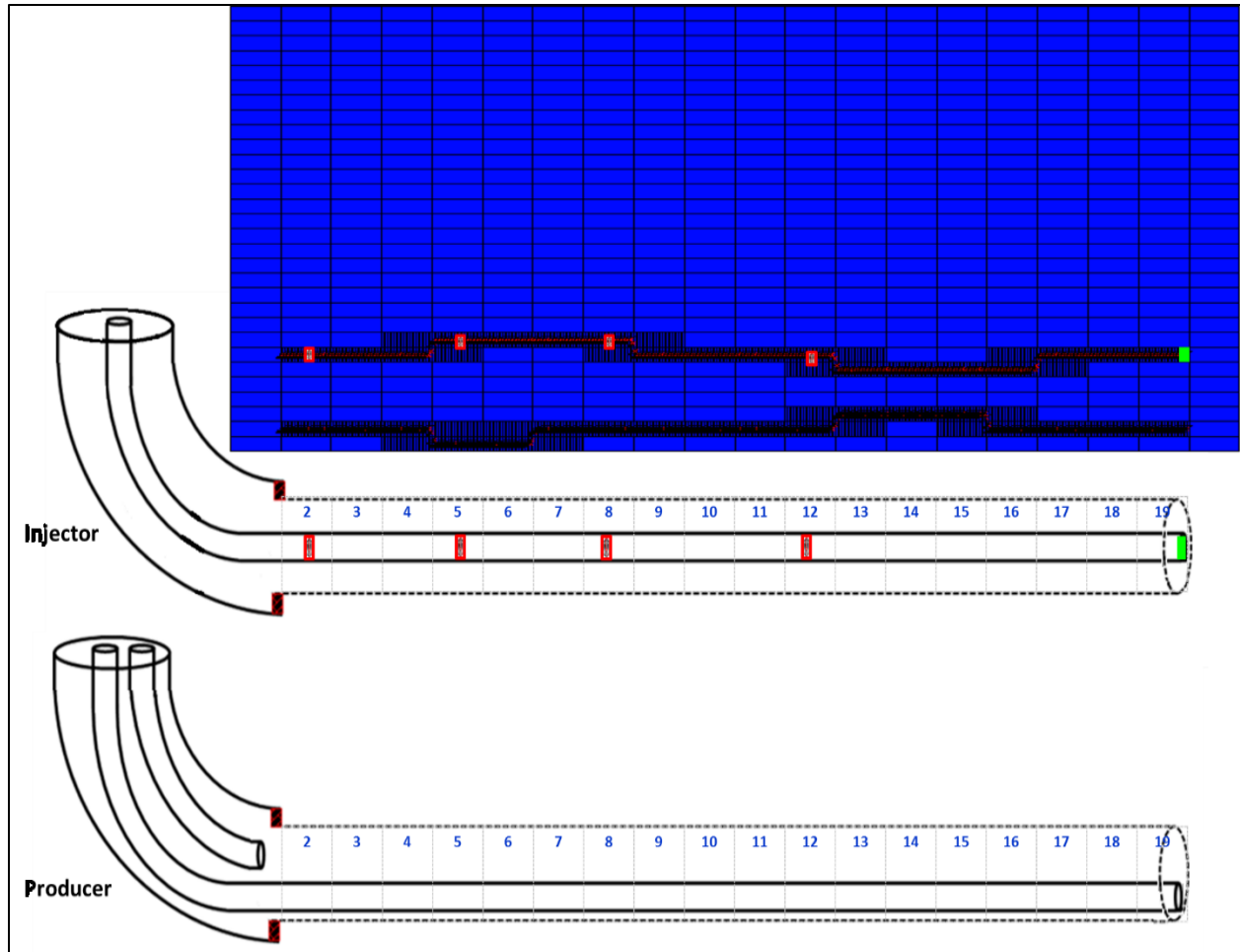


Figure 6-35: Trajectory-3 Tubing-Deployed OCD's Completion Diagram

OCD's # of Ports Parameterization

The four OCD's mentioned in the previous section have been assigned as optimization parameters in CMOST optimization tool. As in previous studies, number of ports (0-70 ports) have been entered as sample values for each OCD.

Experiments and Samples

A total 79 experiments were generated using Latin Hypercube Sampling Method. As shown in **Figure B-15** of **Appendix B**, orthogonality value of 0.0115 which is in the lower green zone indicates a reasonable design quality (nearly orthogonal).

Short-Term Optimization of Number of Ports

Short-term optimization results are shown in **Figure 6-36**. The conventional dual-string case has an NPV of 5,306,924, while the optimum case has \$6,985,949 NPV; that is, more than 31% increment in NPV. A positive general trend line can be observed as in two previous trajectories.

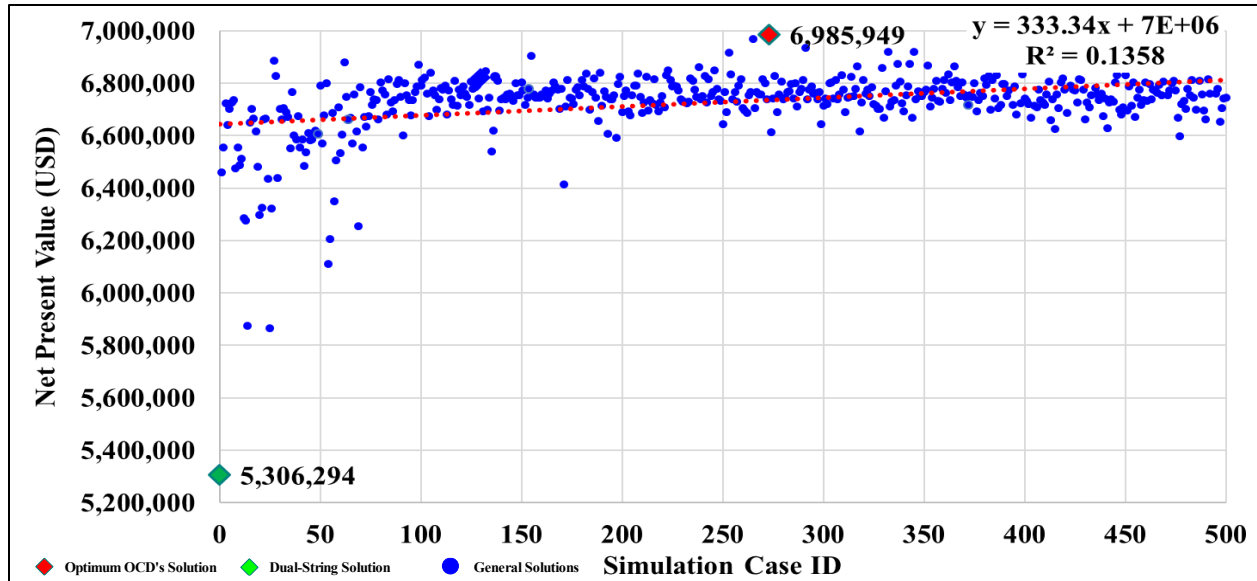


Figure 6-36: Trajectory-3 OCD's Optimization Results (Short-Term)

Long-Term Optimization of Number of Ports

The top 50 short-term cases were simulated for longer periods. Results reveal that the optimum case has a nil number of ports for OCD #4. Furthermore, the open toe does not contribute to flow and can be shut-in. The remaining OCD's have 60, 55 and 65 ports for OCD#1 OCD#2 and OCD#4, respectively. As shown in **Figure 6-37**, the NPV of the optimum case is 21,730,098 and that is about 5% higher than the same for the conventional dual-string scenario. **Figure 6-38** shows completion diagram of Trajectory-3 with the OCD locations and number of ports. As in previous trajectories, negative general solutions trend line can be noticed indicating that increment of NPV is proportional to the case order. **Figure C-5** in **Appendix C** shows the SAGD project life times for the top 50 cases of Trajectory-3. The ultimate recovery factors of the top 50 cases range from 70.0 to 71.1%, with the ultimate recovery ratio of the optimized OCD case being 71% (see **Figure C-6, Appendix C**).

As in Trajectory-1 and Trajectory-2, simulation cases have been run beyond the top 50 cases to confirm the decreasing trend of the long-term simulation according to the short-term NPV ranking. Results are shown in Figures **C-17** through **C-19** in **Appendix C**.

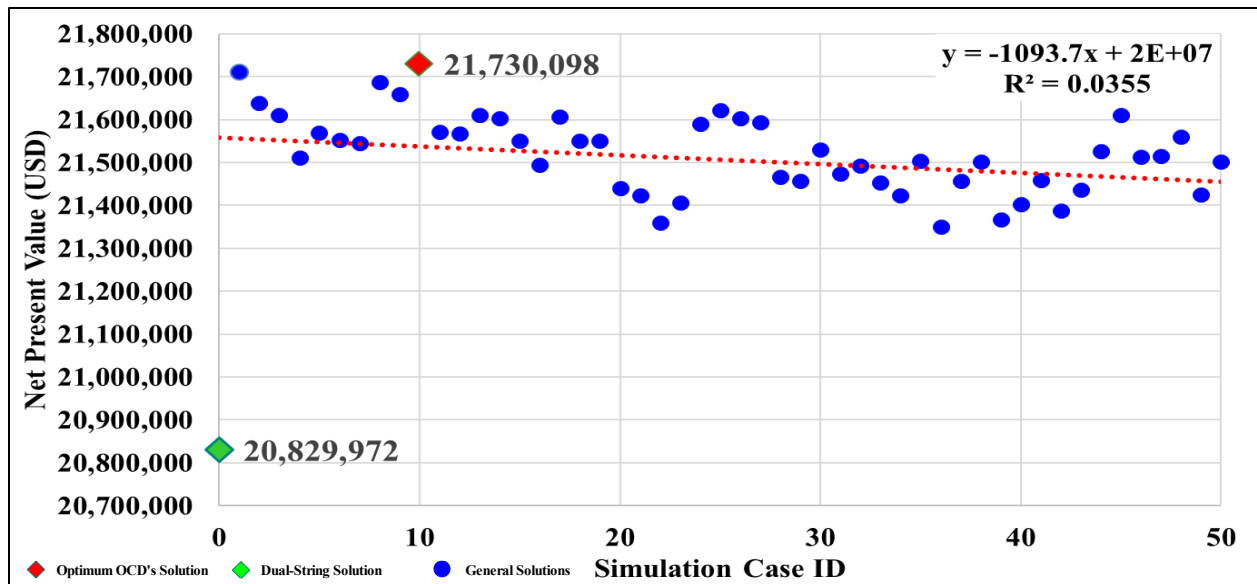


Figure 6-37: Trajectory-3 OCD's Optimization Results (Long-Term)

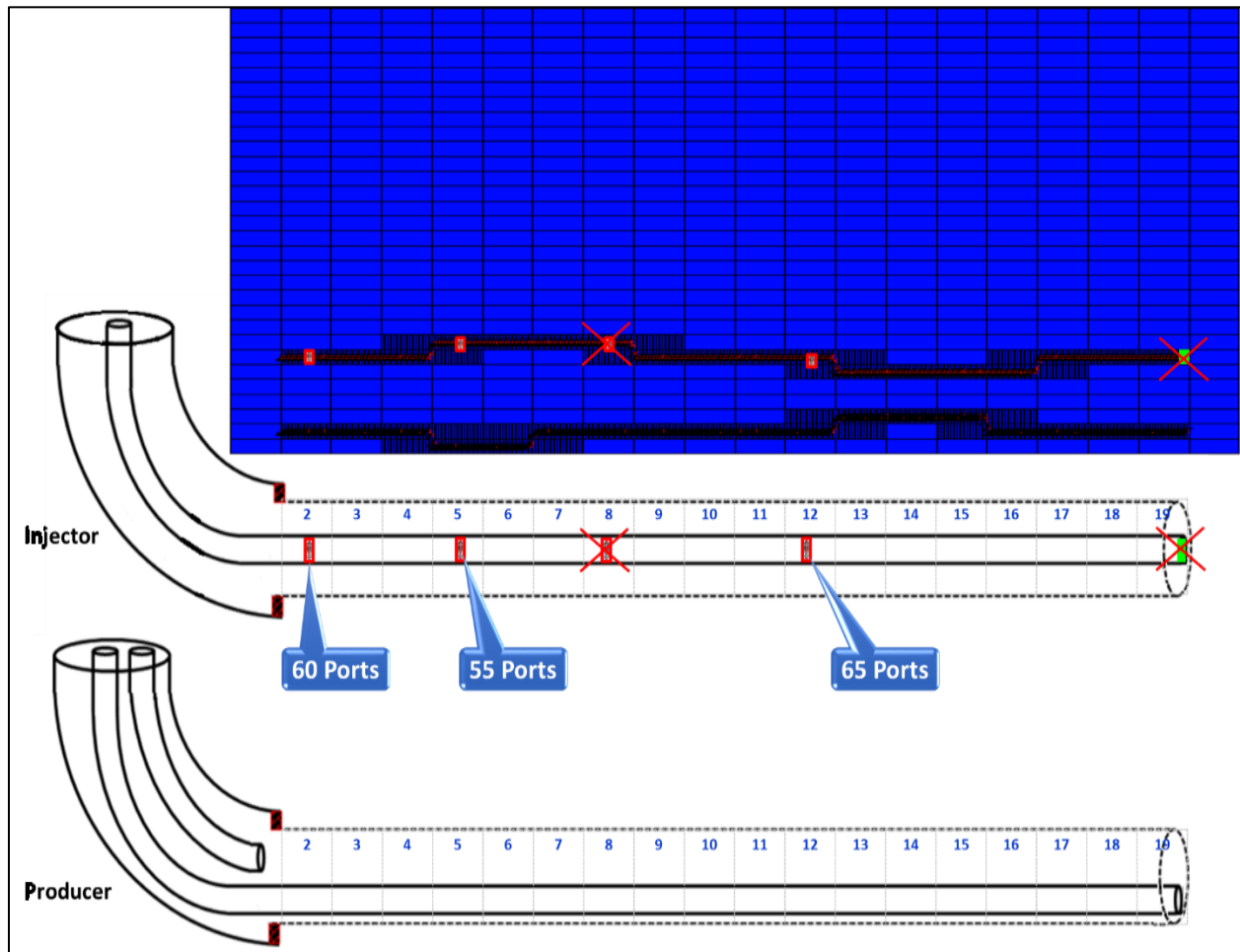


Figure 6-38: Optimum OCD Case for Trajectory-3

Optimum Range of Number of Ports

Figure 6-39 and Table 6-7 present the number of ports for the top five optimum case. Results indicate a relatively narrow range for the optimum number of ports for each OCD among the top five cases: 60-70 for OCD#1, 55-65 for OCD#2, 0-20 for OCD#3, and 50-56 for OCD#4.

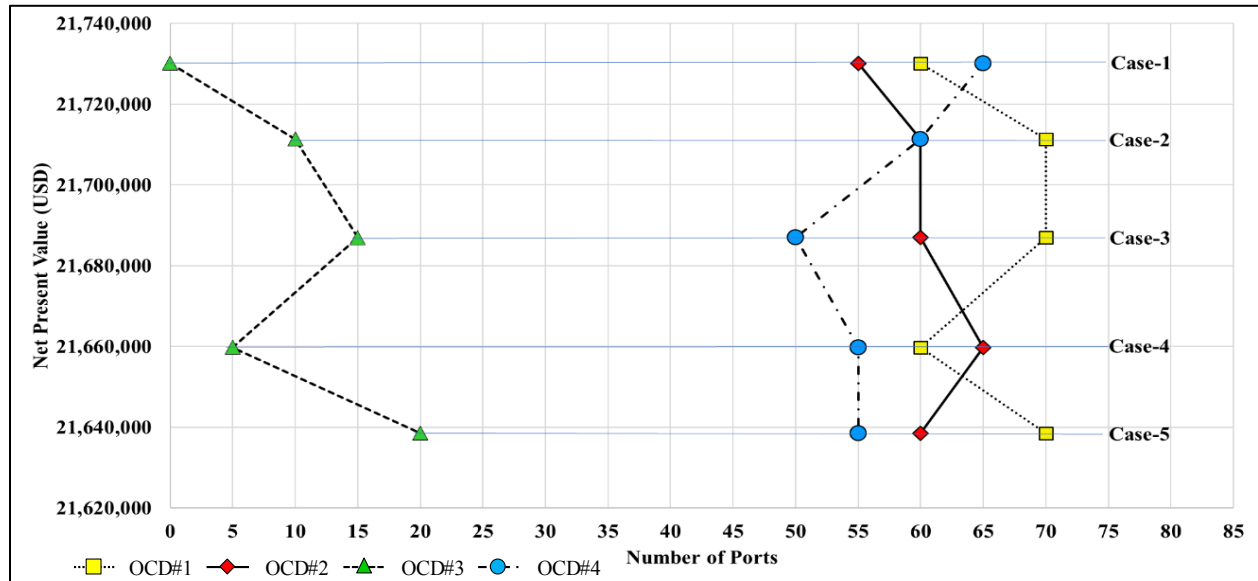


Figure 6-39: Optimum Number of Ports for Top 5 Designs, Trajectory-3

Table 6-7: Optimum Number of Ports for Top 5 Designs, Trajectory-3

No.	OCD's Distribution				NPV (USD)
	OCD#1	OCD#2	OCD#3	OCD#4	
1	60	55	0	65	21,730,098
2	70	60	10	60	21,711,367
3	70	60	15	50	21,686,968
4	60	65	5	55	21,659,786
5	70	60	20	55	21,638,559

6.4.3 Results Analysis

Steam Chamber for Optimized OCD's Case

Figure 6-40 shows axial and lateral views of steam chamber growth for the optimized OCD case for Trajectory-3 until the end of SAGD project life. Results indicate a good steam chamber conformance. As in previous cases, steam chamber reached the reservoir ceiling at the end of the 3rd year of SAGD and then expanded laterally.

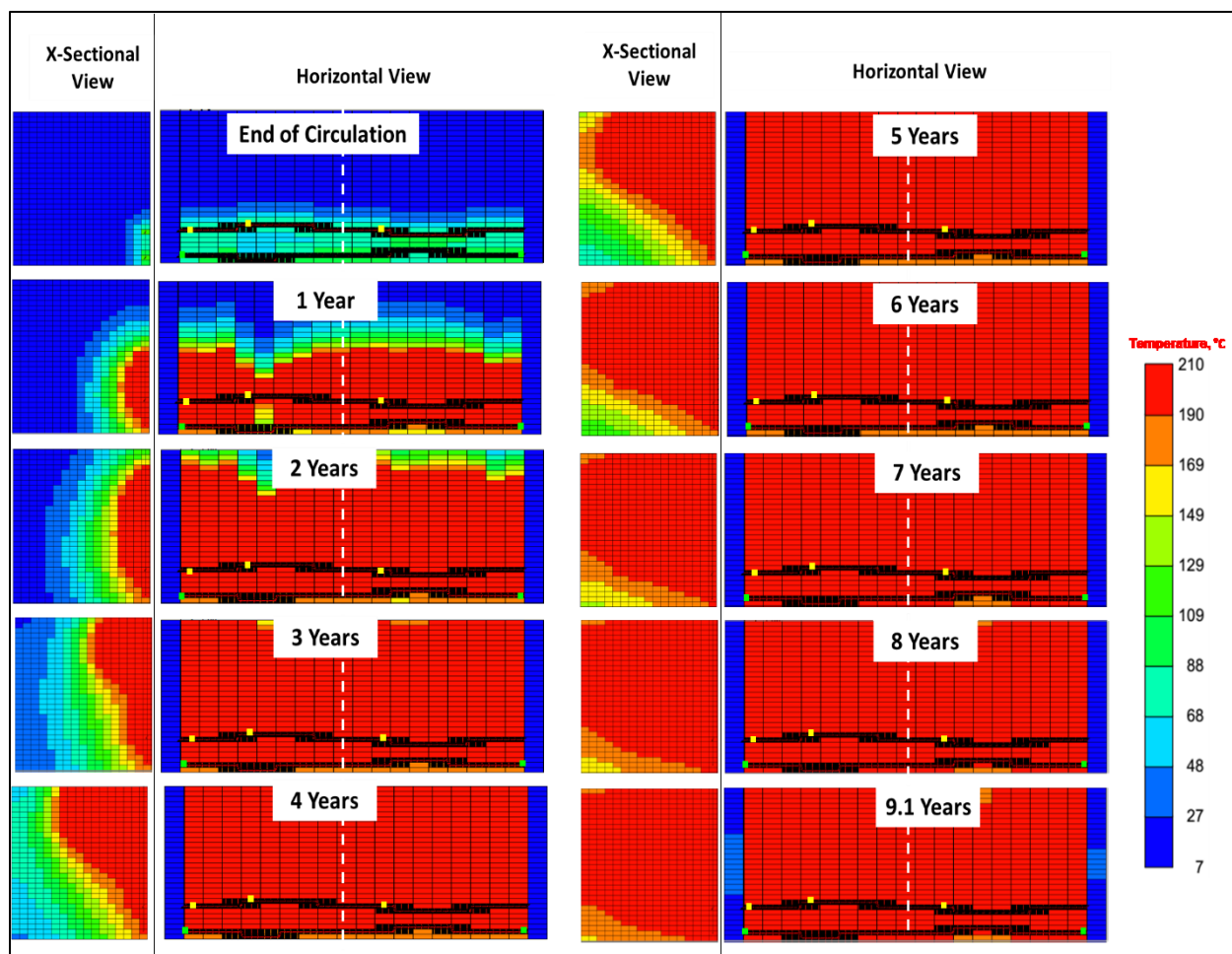


Figure 6-40: Trajectory-3 Temperature Maps of the Optimized OCD's Case SAGD Model at Different Stages

Steam Distribution via OCD's

Figure 6-41 shows contribution of each single OCD to the total amount of steam injected at the end of SAGD stage. 65% of the steam has been injected at the heel section of the well (via OCD#1), 19% via OCD#2, and 14% via OCD#4.

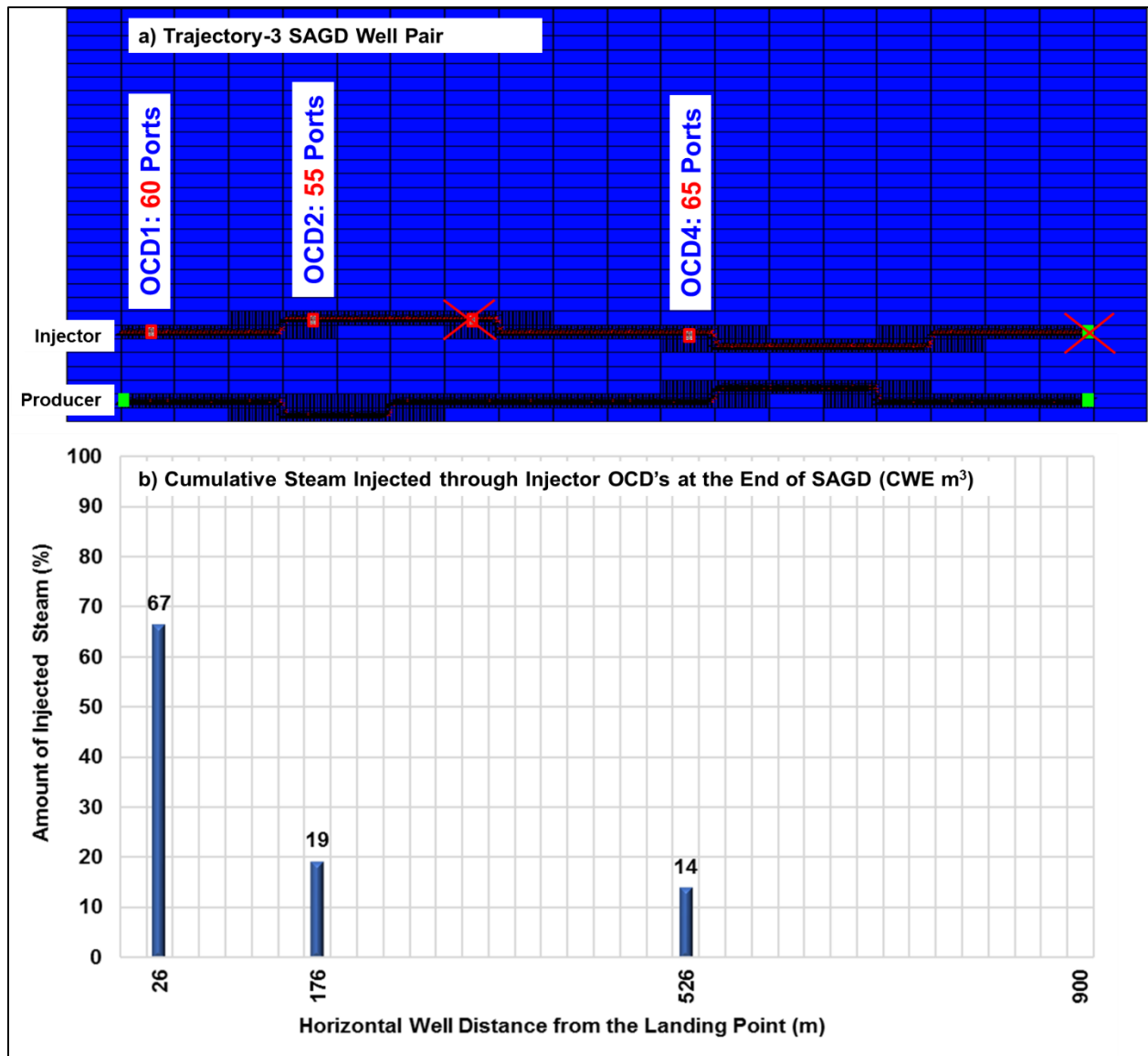


Figure 6-41: Distribution of Injected Steam Among Trajectory-3 OCD's at the End of SAGD Project Life

Injector Tubing/Annulus Pressure Profiles

Figure 6-42 shows tubing/annulus pressure profiles for the optimum OCD case for Trajectory-3. As in the previous trajectories, the largest amount of steam has been injected via OCD#1. The reduction in pressure drop at later SAGD stages reduced the contribution of OCD#2 and OCD#4 over time.

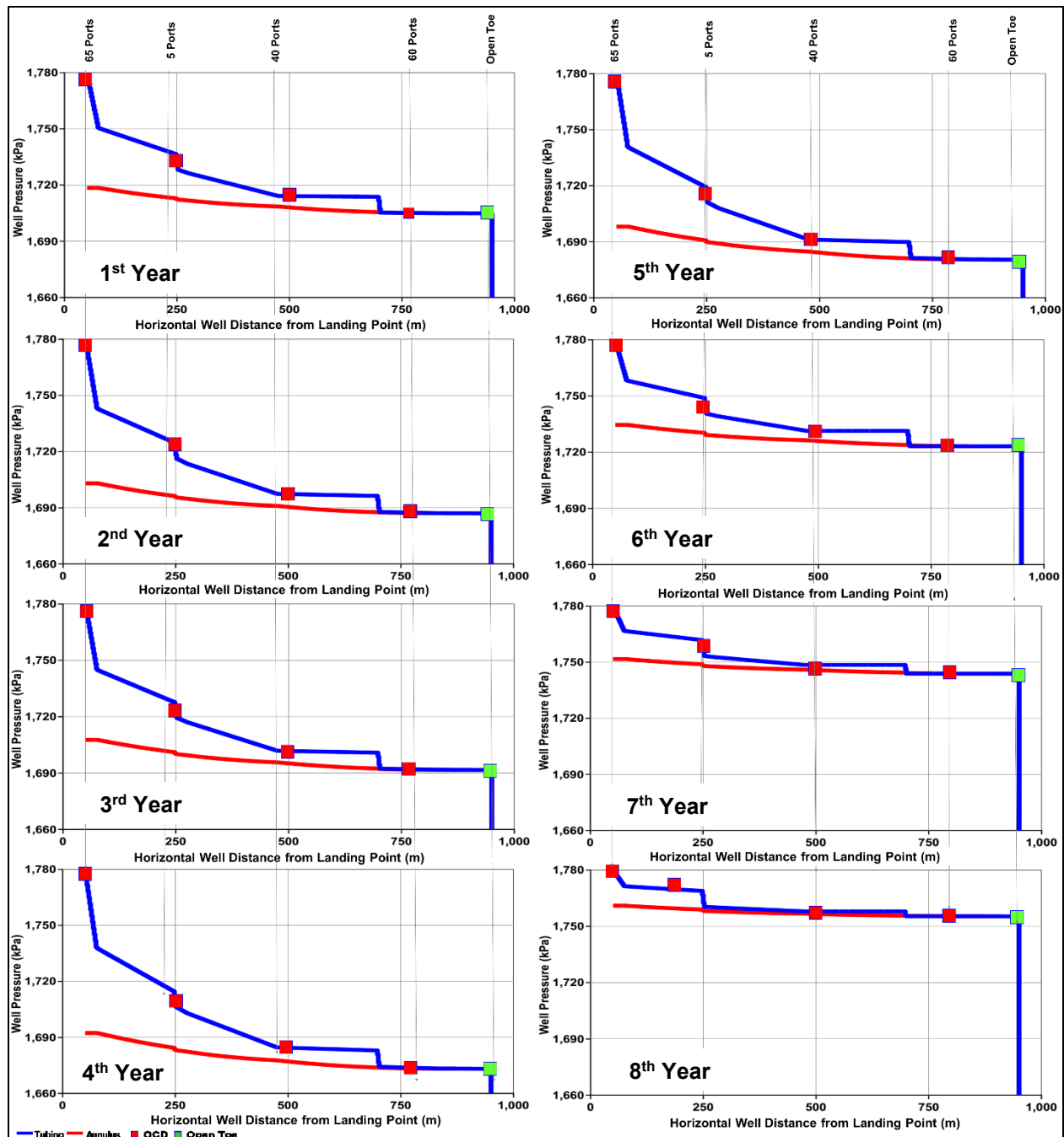


Figure 6-42: Trajectory-3 Optimum Case Injector Tubing/Annulus Pressure Profiles

Comparison with Dual-String Case

Pressure Profiles

Figure 6-43 shows pressure profiles of the optimized OCD and dual-string cases inside the injector long tubing at the end of 3rd year for Trajectory-3. Results indicate 175 kPa frictional pressure losses from heel to toe of the injector for the dual-string case, while it is only about 85 kPa for the

optimized OCD model. Also, as in Trajectory-2 case, pressure profiles inside the long injector for both cases are affected by the wellbore trajectory excursions. The outcome, as shown in **Figure 6-44**, is higher annular pressures for the optimized OCD case (**Figure 6-44b**) resulting in an enhancement in the overall SAGD operating conditions.

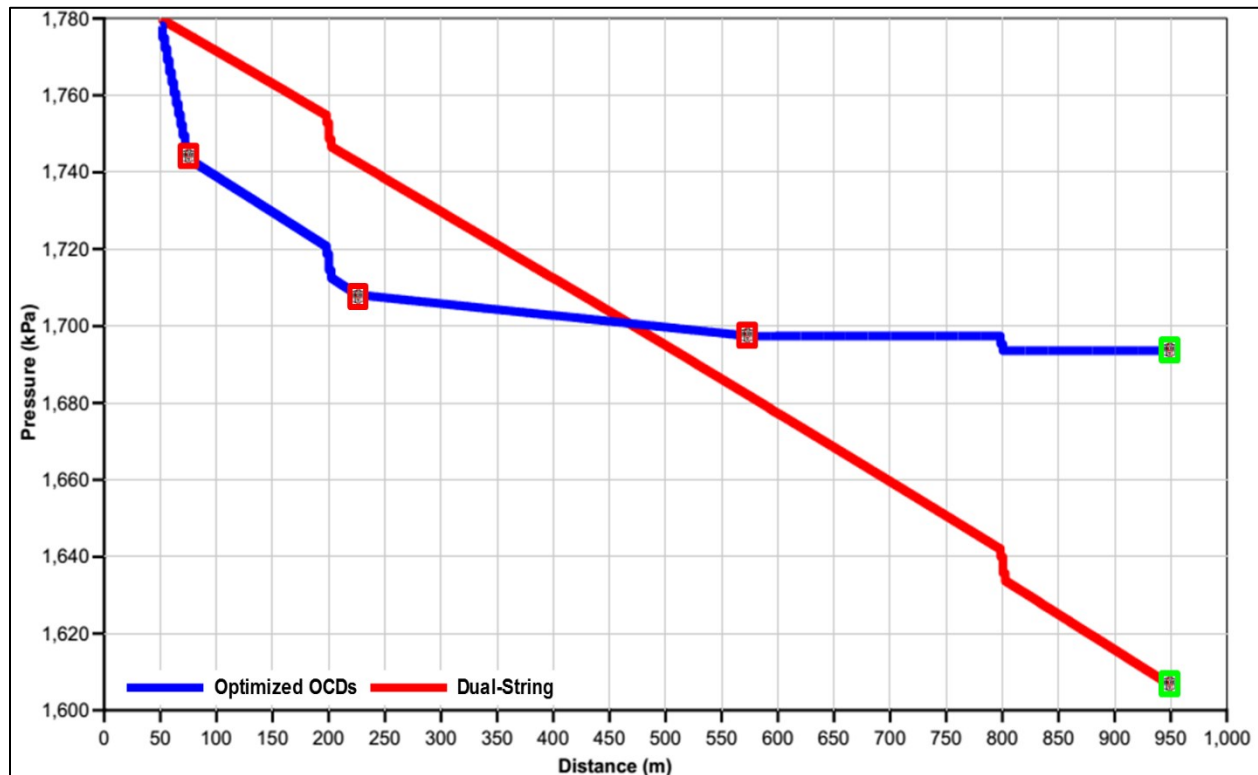


Figure 6-43: Pressure Profiles Inside Long Injector Tubing for Optimized OCD's and Dual-String Cases, Trajectory-3

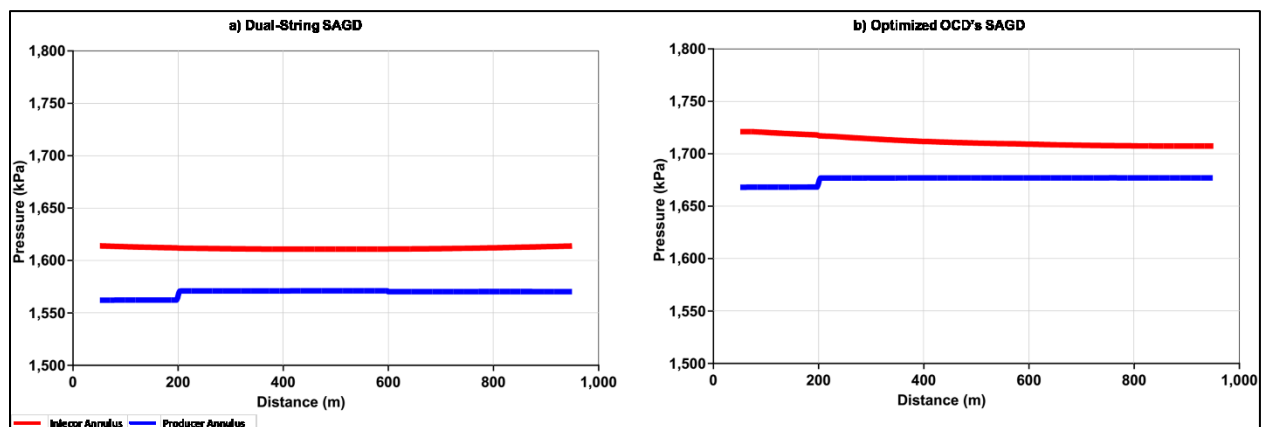


Figure 6-44: Annular Pressure Profiles, Optimized OCD and Dual-String Cases, Trajectory-2

Comparison of Steam Chamber Growth

Figure 6-45 depicts 3-years temperature maps for the optimized OCD and dual-string cases for Trajectory-3. A more uniform and consistent steam chamber growth can be noticed for the optimized OCD case. Also, it can be observed that the injected steam at the toe section of the dual-string case has no efficient heating effect during the first 1.5 years, and that is consistent with the optimized OCD's case where the toe section is closed and no need for it.

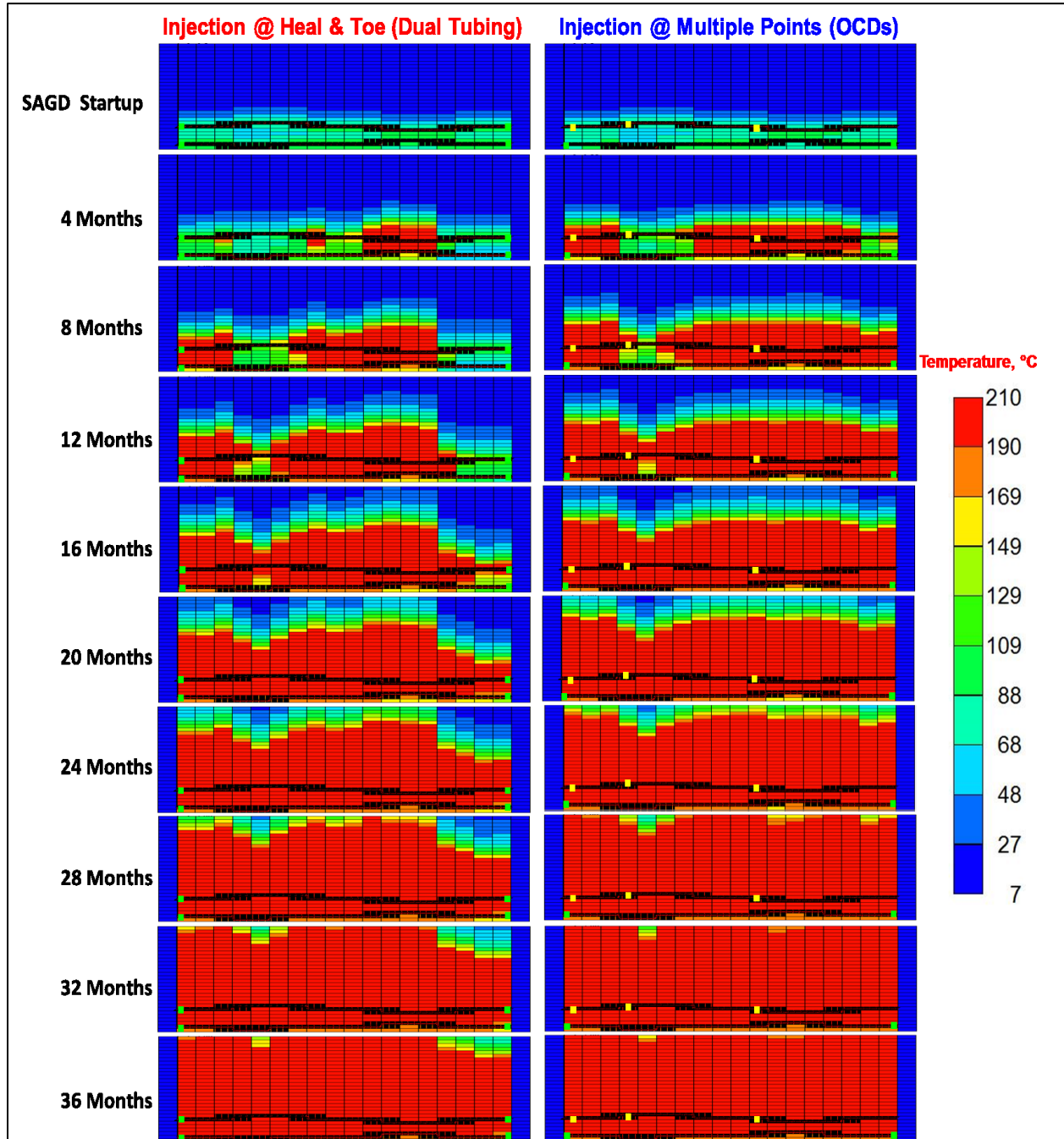


Figure 6-45: Steam Chamber Growth of the Optimized OCD and Dual-String Cases, Trajectory-3

Steam Distribution

Figure 6-46 shows steam injection distributions for three different cases at the end of first year of SAGD. In the first case (**Figure 6-46a**), 100% of the injected steam is delivered at the toe. Looking at the distribution of injected steam into the sandface and the temperature map in the reservoir indicates little steam penetration at the heel and toe segments; hence, a low SAGD performance. The second case is with dual-string completion scheme (**Figure 6-46b**), which shows a better steam distribution into the formation and a more enhanced steam chamber compared to the previous case. However, results still indicate little steam penetration at the toe segment. In the third case (**Figure 6-46c**), where OCD's have been deployed, results indicate 66% steam delivery through OCD#1 at the heel, 19% through OCD#2, and 12% through OCD#4. The outcome is a more even steam chamber growth and steam delivery into the formation. The segment with 7-m TVD lateral separation still demonstrates a poor performance compared to other segments. However, this segment will be swept by steam as SAGD continues beyond the first year.

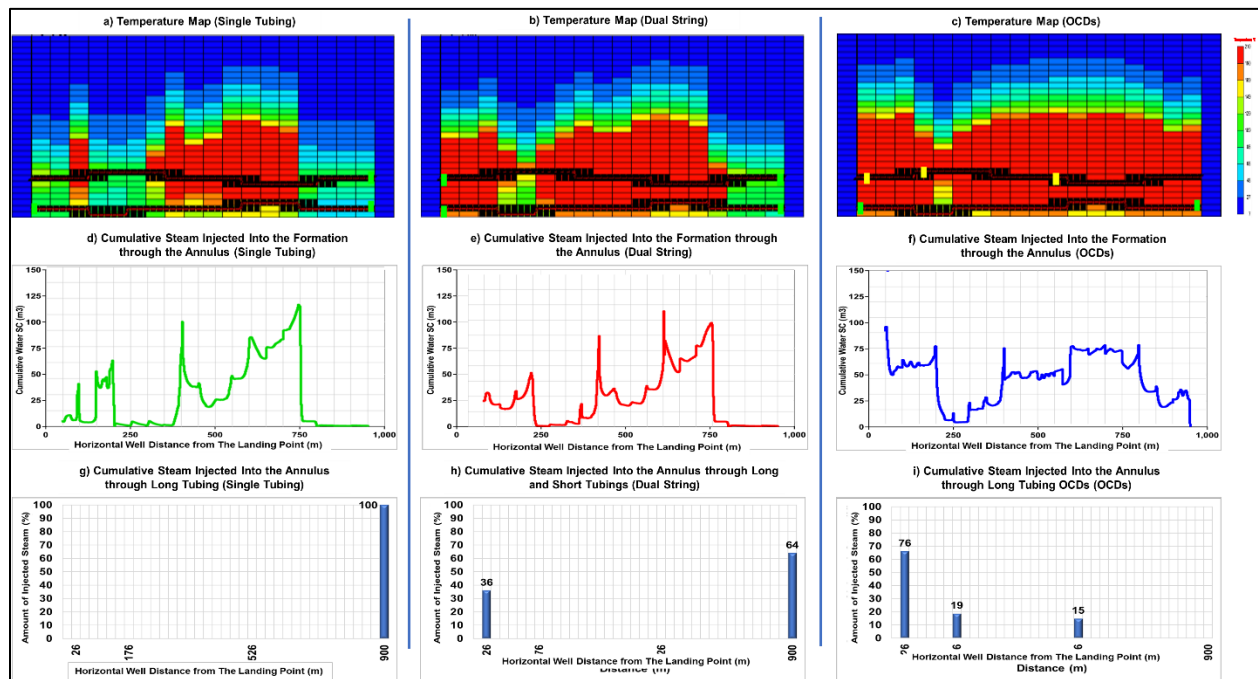


Figure 6-46: Distribution of Injected Steam at Different Points, Trajectory-3 at the End of Year 1

Production Data

Figure 6-47 and **Table 6-8** compare the performances of the models with the optimized OCD and dual tubing. For both cases, SAGD simulation runs have been terminated after the daily NPV increment becomes zero ($\frac{\Delta NPV}{\Delta t} = 0$). The dual-string case was terminated after 3,628 days (9.9

years) of SAGD operation, while the optimized OCD's case was terminated after 3,316 days (nearly 9.1 years). The optimized OCD case shows a 4% enhancement in NPV compared to the corresponding dual-string case, that is, equivalent to more than \$900,000 positive cash flow.

Table 6-9 compares SAGD Performance Data of both cases at the same termination time (9.1 years). Results indicate a better NPV enhancement for the optimized case by as much as 5%.

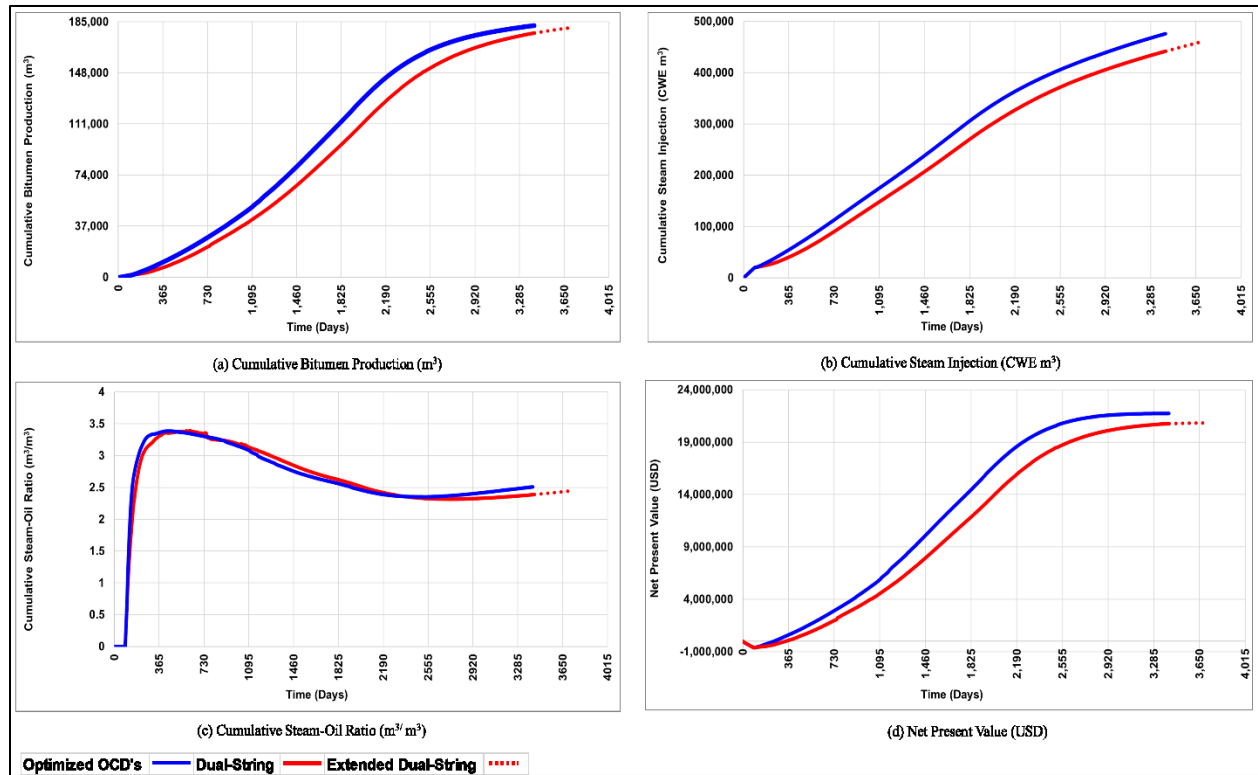


Figure 6-47: SAGD Performance Data of Optimized OCD's and Dual-String Cases, Trajectory-3

Table 6-8: Summary of SAGD Performance Data at the End of SAGD Simulation, Trajectory-3

Case	Cumulative Oil Production (m ³)	Cumulative Steam Injection (m ³ CWE)	Cumulative Steam-Oil Ratio (m ³ /m ³)	NPV (\$)	Project Life (Years)
Dual-String	180,802	461,559	2.45	20,829,972	9.9
Optimized OCD's	182,288	476,144	2.51	21,730,098	9.1
Difference (%)	1	3	2	4	-9

Table 6-9: Summary of SAGD Performance Data at the End of Optimized OCD's Case Simulation, Trajectory-3

Case	Cumulative Oil Production (m ³)	Cumulative Steam Injection (m ³ CWE)	Cumulative Steam-Oil Ratio (m ³ /m ³)	NPV (\$)	Project Life (Years)
Dual-String	176,908	441,652	2.39	20,745,020	9.1
Optimized OCD's	182,288	476,144	2.51	21,730,098	9.1
Difference (%)	3	8	5	5	0

6.5 Comparison of the Trajectories Results

6.5.1 Comparison of NPVs

Figure 6-48 compares optimization results of the three trajectories. For each trajectory, the NPV of optimized case (blue bars) and its corresponding dual-string case (red bars) are compared together. Comparing results of Trajectory-2 with results of Trajectory-1, it can be observed that the NPV of the optimized OCD case of Trajectory-2 has been brought up to almost the same level of Trajectory-1 dual-string case, and that is in reasonable match with fact that the only difference between the two trajectories is the excursions in Trajectory-2 injector compared to straight injector of Trajectory-1. That means a proper deployment of OCD's in Trajectory-2 injector has helped in neutralizing the effect of well pairs trajectories unwanted excursions.

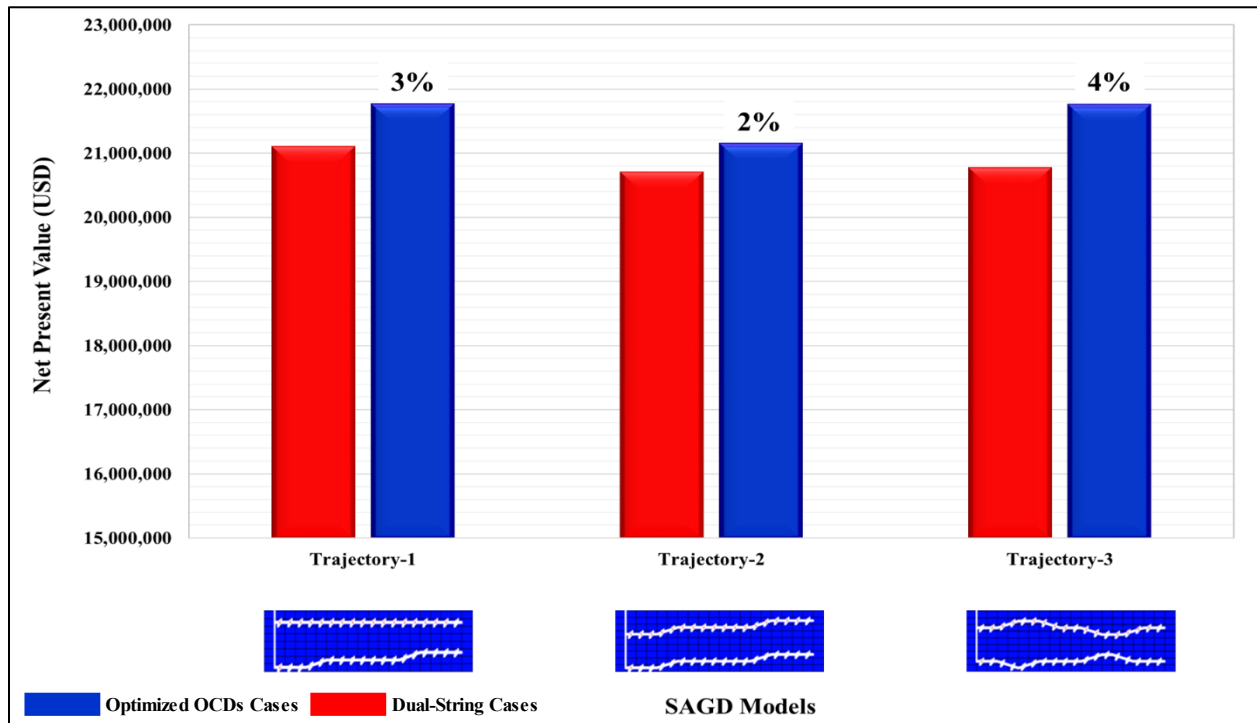
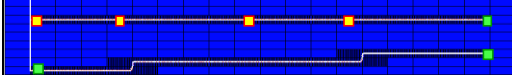
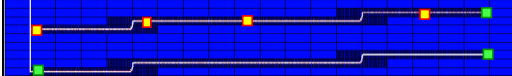
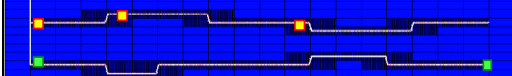


Figure 6-48: Comparison of NPV for Different Trajectories

Table 6-10 summarizes OCD's number of ports, well pair TVD lateral separating distance and cumulative injected steam via each OCD for all trajectories. For all trajectories, both heel and toe OCD's have high number of ports (60-70 ports)

Table 6-10: Summary of Different Trajectories OCD's Distributions

Trajectory	Item	OCD#1	OCD#2	OCD#3	OCD#4	Toe
Tr-1	OCDs Number of Ports	70	20	35	70	Open
	Well Pair TVD Lateral Separating Distance (m)	6	6	5	5	4
	Injector Elevation from the Bottom of the Reservoir (m)	6.5	6.5	6.5	6.5	6.5
	Cumulative Injected Steam at the End of SAGD (%)	69	11	9	7	4
	Injector/Producer Trajectories					
Tr-2	OCDs Number of Ports	65	5	40	60	Open
	Well Pair TVD Lateral Separating Distance (m)	5	5	5	5	5
	Injector Elevation from the Bottom of the Reservoir (m)	5.5	6.5	6.5	7.5	7.5
	Cumulative Injected Steam at the End of SAGD (%)	75	3	18	2	2
	Injector/Producer Trajectories					
Tr-3	OCDs Number of Ports	60	55	Closed	65	Closed
	Well Pair TVD Lateral Separating Distance (m)	7	5	Closed	5	Closed
	Injector Elevation from the Bottom of the Reservoir (m)	6.5	7.5	Closed	6.5	Closed
	Cumulative Injected Steam at the End of SAGD (%)	67	19	Closed	14	Closed
	Injector/Producer Trajectories					

6.5.2 Comparison of Fine Models Results

Table 6-11 through **6-13** are results of Trajectory-1, Trajectory-2 and Trajectory-3 models respectively after running the corresponding optimized OCD's and dual-string cases with super fine models (2-m models). Results show that SAGD production performance data of super fine models (2-m models) results are consistent with original models (50-m with 2-m LGR models).

Table 6-11: Summary of SAGD Performance of Optimized OCD's Case, Trajectory-1 Super Fine Model

Case	Cumulative Oil Production (m ³)	Cumulative Steam Injection (m ³ CWE)	Cumulative Steam-Oil Ratio (m ³ /m ³)	NPV (\$)	Project Life (Years)
Dual-String	181,711	466,823	2.46	21,123,132	9.7
Optimized OCD's	182,198	475,554	2.50	21,978,008	8.9
Difference (%)	0	2	2	4	-9

Table 6-12: Summary of SAGD Performance of Optimized OCD's Case, Trajecotry-2 Super Fine Model

Case	Cumulative Oil Production (m³)	Cumulative Steam Injection (m³ CWE)	Cumulative Steam-Oil Ratio (m³/m³)	NPV (\$)	Project Life (Years)
Dual-String	181,880	460,403	2.42	20,704,098	9.9
Optimized OCD's	181,512	474,677	2.51	21,408,579	8.9
Difference (%)	0	3	3	3	-10

Table 6-13: Summary of SAGD Performance of Optimized OCD's Case, Trajecotry-3 Super Fine Model

Case	Cumulative Oil Production (m³)	Cumulative Steam Injection (m³ CWE)	Cumulative Steam-Oil Ratio (m³/m³)	NPV (\$)	Project Life (Years)
Dual-String	179,256	461,541	2.47	20,488,726	9.9
Optimized OCD's	182,211	475,346	2.50	21,741,570	9.1
Difference (%)	2	3	1	6	-9

CHAPTER SEVEN: CONCLUSIONS AND FUTURE WORK

7.1 Summary

The work in this research aimed to minimize/neutralize the negative impacts of SAGD wellbore trajectory excursions in SAGD reservoirs using tubing-deployed outflow control devices. The results of the research work demonstrated an enhanced performance of the SAGD process due to a more uniform steam chamber growth, an enhanced bitumen production and a higher NPV compared to the conventional dual-string completion scheme.

The work in the thesis started by constructing a basic SAGD model representing a typical oil sands deposits in Western Canada (McMurray formation in Alberta oil sands deposits). Model dimensions, data and operating conditions were based on publicly available data of Suncor Mackay River SAGD project in Athabasca oil sands.

Starting from the basic SAGD model which has straight (ideal) well pair trajectories, three different scenarios were generated with each scenario having certain well pair trajectory excursions. The first scenario was Trajectory-1 where the injector was straight, while the producer had excursions at two different points, and these excursions caused variations in TVD lateral separating distance of 3-5 m. Trajectory-2 was based on Trajectory-1, where the only difference was that both injector and producer have excursions at the same points with a fixed TVD lateral separation of 5 m, but with variable distances from the base of the reservoir. Trajectory-3 had more complex and random paths for both injector and producer with TVD lateral separating distance of 3 m to 7 m at the narrowest and widest points, respectively.

7.2 Results of Grid Size Sensitivity Studies

To ensure that the optimization work is not affected by the numerical grid design, a sensitivity analysis was conducted prior to proceeding with the optimization work. The grid sensitivity study involved all four trajectory scenarios. Two types of grid sensitivity studies were carried out on each of the four scenarios. The first study involved the use of three different grid systems (fine-, medium, and coarse grid models with 12.5, 25 and 50-m grid blocks in the axial direction, respectively).

Results of the first grid size sensitivity study showed high variations in SAGD production performance data and steam chamber conformance among the three grid systems for each of the

four scenarios. The variations were found to be caused by four primary reasons: (1) poor modeling of heat transfer by conduction in the axial direction due to large axial lengths of grid blocks (12.5-m, 25-m and 50-m); (2) averaging well trajectory paths among large grid blocks, especially at excursions points, caused variations in calculated overall well injectivity/productivity indices; (3) averaging rapid changes in sensitive rock-fluid data in the vicinity of well pair; and (4) the coupling process of wellbore-reservoir models using CMG's FlexWell/STARS.

To solve the above-mentioned difficulties, another grid size sensitivity study was conducted using the Local Grid Refinement (LGR) technique. Six different grid systems were set up in the second grid sensitivity study (2-m, 10-m, 20-m, 30-m, 36-m and 50-m grid block lengths in axial direction). All models (except 2-m model) were refined by 2-m LGR in the grid blocks that contain well pair trajectory. Implementing LGR technique around well pair trajectories helped in accurate modeling of heat transfer by conduction in the axial direction, restoring the original well pair trajectories paths and more accurate modeling of changes in fluid thermal and flow properties near the wellbore.

Results of the second grid sensitivity study with LGR shows an excellent match in production data and steam chamber conformance among the six grid systems for each of the four trajectory scenarios. Also, simulation execution times in 50-m models with 2-m LGR models are significantly lower compared to the very fine grid models (2-m models), where average execution times has been brought from 114 hours down to two hours. Thus, the 50-m coarse-grid models with 2-m LGR were adopted as the default grid system for all trajectory scenarios for the optimization work.

7.3 Results of Optimization Work

7.3.1 Trajectory-1

The optimized OCD case of Trajectory-1 yielded 70 ports for OCD#1 (heel section), 20 ports at OCD#2, 35 ports at OCD#3 and 70 ports at OCD#4, in addition to the open toe section. The heel section of the dual-string completion case in Trajectory-1 has a higher liquid level caused by the lower producer elevation at the heel. This high liquid level at the heel suppresses steam chamber growth. However, installing OCD's helped in adjusting steam distribution and achieving a better steam chamber conformance at the heel section.

Distribution of cumulative amount of steam injected at the end of SAGD simulation period is decreasing starting from the heel towards the toe. Also, OCD#1 had the highest contribution to the total amount of steam injected, and this was due to the relatively large annular cross-sectional area compared to the same for the tubing. Although OCD#4 (closer to the toe section) has 70 ports, it has the least contribution to the total amount of steam injected at the end of SAGD simulation period, because the available pressure differential is too small.

The optimized OCD's case of Trajectory-1 using 9 5/8" slotted liner has been run again using smaller slotted liner (7") and results have more significant contribution of OCD's among other sections further away from the heel to the cumulative steam injection.

7.3.2 Trajectory-2

Both wells in Trajectory-2 had excursions, but they were parallel, where the TVD lateral separating distance was fixed at 5 m. However, these excursions caused the toe section of the well pair to be closer to the reservoir ceiling compared to the heel section.

For the dual-string completion scheme, it was shown that steam injected at toe section tends to travel back towards the heel section under the effect of gravity due to dipping trajectory of the injector. Since the injected steam doesn't stay at the toe section, the toe section remains undrained with high subcool and shorter steam chamber height in the vertical direction.

The optimized OCD case has 65 ports at OCD#1, 5 ports at OCD#2, 40 ports at OCD#3 and 60 ports at OCD#4, in addition to the fully open toe. Looking at the cumulative amount of steam injected has shown that OCD#1 (65 ports) and OCD#3 (40 ports) were the most important ones, where their contribution to the cumulative injected steam is 93%. Only 7% of all injected steam is provided by the open toe section and OCD#2 and 4.

7.3.3 Trajectory-3

Trajectory-3 had more complex well pair trajectory excursions compared to Trajectory-1 and Trajectory-2. Temperature maps in dual-string completion case have shown a poorer steam chamber growth and a higher liquid level at the toe and 7-m TVD lateral separation sections. In this case, steam also does not stay at high TVD lateral separating distance and toe sections due to gravity. Hence, the injected steam tends to travel down towards sections that have a lower TVD. Optimization results show 60 ports for OCD#1, 55 ports for OCD#2, zero ports for OCD#3 and 65 ports for OCD#4, in addition to a nil contribution from the open toe. 67% of the total amount

of steam is injected at the heel section (OCD#1) and the remaining 33% is distributed at different sections among the well pair via OCD#2 and OCD#4 only.

7.4 Conclusions

Several findings and conclusions can be drawn from the work in this research. It is known that conduction is an essential heat transfer mechanism in both lateral (I-Direction) and vertical (K-Direction) directions in SAGD process. However, grid size sensitivity analysis demonstrated that conduction mechanism plays a key role in heat transfer in the axial well pair path directions in SAGD (J-Direction). Thus, it is important to adopt a finer gridding scheme (e.g. LGR) near the well pair.

The optimization work for different trajectories revealed that the heel OCD, i.e., OCD#1, is the main contributor to steam injection into the SAGD system for the cases attempted in this work. A vast majority of steam injected via tubing (67%- 75% among the three trajectories) enters the injector annulus via OCD#1 and then travels to other sections of the injector through the large annular space. The remaining amount of steam (25%-33%) is injected at different sections of the injector via other OCD's (OCD#2, OCD#3 and OCD#4) and toe depending on excursions of well pair trajectories.

Also, it has been noticed that some OCD's or toe sections in some trajectories have nil or very little contributions to the total amounts of injected steam (e.g. OCD#4 and toe in Trajectory-1).

Comparing temperature maps of SAGD early-stages of dual-string and optimized OCD's cases (for different trajectories) have shown that the early-stages (first three years of SAGD until steam chamber reaches reservoir ceiling) are critical to uniform development of SAGD steam chamber and to the success of the overall SAGD process.

Improvements of SAGD performance in the optimized OCD cases are mainly achieved by increasing overall amounts of injected steam, delivering steam to areas that have poor sweep efficiencies and elevated SAGD operating conditions (producer and injector annulus pressure) due to minimized pressure losses to friction. For these reasons, all optimized OCD's cases have slightly higher cumulative injected steam and terminal cSOR (compared to their corresponding dual-string injection cases). However, they are still considered as optimum cases because they have higher cumulative oil production and NPV.

Optimum number of ports in each OCD for each optimized case mainly depends on the available pressure drop across OCD between the injector tubing and annuls, in addition to the TVD lateral separation and other factors.

The efficiency of OCD's use in a SAGD injector mainly depends on the cross-sectional area of the annular space between the slotted liner and the tubing, i.e., smaller annular cross-sectional area, more chances for the injected steam to travel through the tubing and pass into the formation through the OCD's orifices, hence more efficient SAGD process compared to using high diameter slotted liners.

For large diameter slotted liners (9 5/8") and regardless of well pair trajectory, the heel OCD (OCD#1) should have a high number of ports (60-70 ports in the attempted cases). Also, the last OCD next the toe (OCD#4) should have a high number of ports (60-70 ports in the attempted cases). The high number of ports in the latter case doesn't secure high injection rate at OCD#4, but it is necessary to pass a part of the remaining steam using a small available pressure drop across the OCD orifices. The effect of OCD's is complementary. The distribution of the middle OCD's and their corresponding number of ports depend on TVD lateral separating distance well pair, elevation of well pair from the bottom of the reservoir and the available pressure drop across the OCD'S orifices.

The work done in this research is different from what have been done by other researchers from several perspectives, for instance: 1) none of the published research work addressed the effect of well pair trajectory excursions on SAGD performance, 2) none of the studies examined the effect of different mesh size configuration scenarios on the quality of the results, but the work in this research performed detailed mesh size sensitivity analysis prior to proceeding with optimization work in order make sure that optimization results will not be affected by numerical mesh design, 3) another important feature that have been utilized in this research is the Local Grid Refinement techniques, where a detailed workflow has been proposed to implement Local Grid Refinement to reduce simulation run time without compromising quality of the model, 4) Also, the optimization work of the research proposed an optimization workflow to implement short-term and long-term concept on large scales (higher number of cases and longer simulation periods), where short-term simulation was done for 500 cases for 3 years and long-term simulation was done for longer periods.

7.5 Future Work

The scope of work in this research was limited to the improvement of SAGD process performance by optimization of design and placement of OCD's along the injector. However, involvement of ICD's on the producers simultaneously with OCD's may yield more improvement in SAGD operations.

Performance of other SAGD reservoirs with different geological settings can also be enhanced by properly-optimized placement of OCD's/ICD's. Some of the different reservoir types that have not been covered in this research include SAGD reservoirs with bottom water, gas cap, low reservoir ceiling, mud channels, heterogeneous geological properties or a combination of all or some of these different settings.

Coding a customized optimization algorithm to optimize flow control devices use for each type of SAGD reservoir can be an effective tool for quick and reliable optimization solutions.

REFERENCES

- Al Marzouqi, A. A. R., Helmy, H., Keshka, A. A.-S., Elasmr, M., & Shafia, S. (2010, January 1). Wellbore segmentation using Inflow Control Devices: Design & Optimization Process. Society of Petroleum Engineers. doi:10.2118/137992-MS.
- Alberta Energy Regulator. (2013, December 14). Talk About SAGD Report. Government of Alberta.
- Anderson, M. T., & David, K. (2012, January 1). SAGD Startup: Leaving the Heat in the Reservoir. Society of Petroleum Engineers. doi:10.2118/157918-MS.
- Banerjee, S., & Hascakir, B. (2017, April 23). Flow Control Devices in SAGD Completion Design: Enhanced Heavy Oil/Bitumen Recovery Through Improved Thermal Efficiencies. Society of Petroleum Engineers. doi:10.2118/185703-MS.
- Banerjee, S., Jobling, R., Abdelfattah, T. A., & Nguyen, H. T. (2013, September 30). The Role of Autonomous Flow Control in SAGD Well Design. Society of Petroleum Engineers. doi:10.2118/166266-MS.
- Becerra, O., Kearl, B., & Sanwoolu, A. (2014, June 10). A Systematic Approach for Inflow Control Devices Testing in Mackay River SAGD Wells. Society of Petroleum Engineers. doi:10.2118/170055-MS.
- Boone, T. J., Youck, D. G., & Sam, S. (1998, January 1). Targeted Steam Injection Using Horizontal Wells with Limited Entry Perforations. Society of Petroleum Engineers. doi:10.2118/50429-MS.
- Butler, R. M. (1994, February 1). Steam-Assisted Gravity Drainage: Concept, Development, Performance And Future. Petroleum Society of Canada. doi:10.2118/94-02-05.
- Butler, R. M., & Stephens, D. J. (1981, April 1). The Gravity Drainage of Steam-heated Heavy Oil to Parallel Horizontal Wells. Petroleum Society of Canada. doi:10.2118/81-02-07.
- Butler, R. M., McNab, G. S., & Lo, H. Y. (1981). Theoretical studies on the gravity drainage of heavy oil during in-situ steam heating. *The Canadian Journal of Chemical Engineering*, 59(4), 455–460. <https://doi.org/10.1002/cjce.5450590407>.

Bybee, K. (2008, March 1). Production Operations: Inflow-Control Devices. Society of Petroleum Engineers. doi:10.2118/0308-0081-JPT.

Cenovus Energy. (2011, December 20). Cenovus TL ULC. Telephone Lake Project. Volume 1 Project Description.

Cenovus Energy. (2012, June 20). Cenovus Christina Lake In-situ Oil Scheme. 2011 - 2012 Update. The Energy Resources Conservation Board (ERCB).

Chang, J., Ivory, J., & Tunney, C. (2012, December 1). Numerical Simulation of Steam-Assisted Gravity Drainage With Vertical Slimholes. Society of Petroleum Engineers. doi:10.2118/148803-PA.

Chen, Z. (2013). A Genetic Algorithm Optimizer with Applications to the SAGD Process. M.Sc. Thesis, University of Calgary, Calgary.

Chien, S.-F. (1990, March 1). Critical Flow of Wet Steam Through Chokes. Society of Petroleum Engineers. doi:10.2118/17575-PA.

Coates, R., Pierce, G., & Fung, H. (2005, Dec 13). Impact of Methane Loss on Bitumen Viscosity. Joint Industry Project for Alberta Energy Research Institute. Alberta Research Council Inc., Edmonton.

Collins, P. M. (2005, January 1). Geomechanical Effects on the SAGD Process. Society of Petroleum Engineers. doi:10.2118/97905-MS.

Collyer, D. (2011, April 15). EA and the Oil Sands – A Producer Perspective. Canadian Association of Petroleum Producers.

Computer Modeling Group (CMG). (2015). CMOST User Guide Enhance & Accelerate Sensitivity Analysis, History Matching, Optimization & Uncertainty Analysis. Version 2015

Computer Modeling Group (CMG). (2015). Flexible Wellbore Data Entry User Guide. Version 2015.

Computer Modeling Group (CMG). (2015, January 20). STARS User Guide, Advanced Processes & Thermal Reservoir Simulator. Version 2015.

- Coronado, M. P., Garcia, L., Russell, R., Garcia, G. A., & Peterson, E. R. (2009, January 1). New Inflow Control Device Reduces Fluid Viscosity Sensitivity and Maintains Erosion Resistance. Offshore Technology Conference. doi:10.4043/19811-MS.
- Dehdari, V., and Deutsch, C.V. (2012, January 1). Ranking Reservoir Realizations Using SAGD Proxy and Gradual Deformation Method.CCG Annual Report No. 14. Paper 204.
- Fedutenko, E., Yang, C., Card, C., & Nghiem, L. X. (2012, January 1). Forecasting SAGD Process Under Geological Uncertainties Using Data-Driven Proxy Model. Society of Petroleum Engineers. doi:10.2118/157942-MS.
- Fermaniuk., B. (2013). Sand Control in Steam Assisted Gravity Drainage (SAGD) Wellbores and Process of Slotted Liner Design and Manufacture. MEng Thesis, University of Calgary, Calgary.
- Garcia, G. A., Coronado, M. P., & Gavioli, P. (2009, January 1). Identifying Well Completion Applications for Passive Inflow-Control Devices. Society of Petroleum Engineers. doi:10.2118/124349-MS.
- Ghesmat, K., & Zhao, L. (2015, December 1). SAGD Well-Pair Completion Optimization Using Scab Liner and Steam Splitters. Society of Petroleum Engineers. doi:10.2118/170076-PA.
- Good, W. K, Rezk, C., & Felty, B. D. (1997, March 1). Possible effects of gas caps on SAGD performance. Calgary: Alberta Energy.
- Ito, Y., & Suzuki, S. (1996, January 1). Numerical Simulation of the SAGD Process In the Hangingstone Oil Sands Reservoir. Petroleum Society of Canada. doi:10.2118/96-57.
- Jones, C., Morgan, Q. P., Beare, S. P., Awid, A. E., & Parry, K. (2009, January 1). Design, testing, qualification and application of orifice based inflow control devices. International Petroleum Technology Conference. doi:10.2523/IPTC-13292-MS.
- Kaiser, T. M. V., Wilson, S., & Venning, L. A. (2002, December 1). Inflow Analysis and Optimization of Slotted Liners. Society of Petroleum Engineers. doi:10.2118/80145-PA.
- Khan, R. A., & Awotunde, A. A. (2016, November 13). Optimal parameters selection for SAGD

and VAPEX processes. *Journal of Petroleum Exploration and Production Technology*. doi:10.1007/s13202-016-0302-2.

Kumar, A., Oballa, V., & Card, C. (2010, January 1). Fully-Coupled Wellbore Design and Optimization for Thermal Operations. Society of Petroleum Engineers. doi:10.2118/137427-MS.

Kyanpour, M., & Chen, Z. (2014, September 24). Design and Optimization of Orifice based Flow Control Devices in Steam Assisted Gravity Drainage: A Case Study. Society of Petroleum Engineers. doi:10.2118/171109-MS.

Letourneau, D. (2015, June 1). Flow Control Devices: An Emerging SAGD Technology. *Journal of the Canadian Heavy Oil Association*.

Li, P., Chalaturnyk, R. J., & Tan, T. B. (2006, January 1). Coupled Reservoir Geomechanical Simulations For the SAGD Process. *Petroleum Society of Canada*. doi:10.2118/06-01-02.

Wang, J., Liu, F. (Changyi), & Morris, P. (2013, June 11). A Practical Approach to History-matching Large, Multi-well SAGD Simulation Models: A MacKay River Case Study. Society of Petroleum Engineers. doi:10.2118/165555-MS

Livescu, S., Brown, W. P., Jain, R., Grubert, M., Ghai, S. S., Lee, L.-B. W., & Long, T. (2010, January 1). Application of a Coupled Wellbore/Reservoir Simulator to Well-Performance Optimization. Society of Petroleum Engineers. doi:10.2118/135035-MS.

Al Marzouqi, A. A. R., Helmy, H., Keshka, A. A.-S., Elasmr, M., & Shafia, S. (2010, January 1). Wellbore segmentation using Inflow Control Devices: Design & Optimization Process. Society of Petroleum Engineers. doi:10.2118/137992-MS

Noroozi, M., Melo, M., Montoya, J., & Neil, B. (2015, November 23). Optimizing Flow Control Devices in SAGD Operations: How Different Methodologies are Functional. Society of Petroleum Engineers. doi:10.2118/178468-MS.

Noroozi, M., Melo, M., Singbeil, R. P. Pete., & Neil, B. (2014, September 24). Investigation of Orifice Type Flow-Control Device Properties on the SAGD Process Using Coupled Wellbore Reservoir Modeling. Society of Petroleum Engineers. doi:10.2118/171131-MS.

Oballa, V., Buchanan, L. (2009, Mar 08). Flexible Wellbore Model Coupled to Thermal Reservoir Simulator. *World Heavy Oil Congress*. Paper No. 2009-308. Puerto la Cruz, Venezuela.

Oballa, V., Coombe, D. A., & Buchanan, L. (1997, April 1). Aspects of Discretized Wellbore Modelling Coupled to Compositional/Thermal Simulation. Petroleum Society of Canada. doi:10.2118/97-04-04.

Parmar, G., Zhao, L., & Graham, J. (2009, January 1). Start-up of SAGD Wells: History Match, Wellbore Design and Operation. Petroleum Society of Canada. doi:10.2118/09-01-42.

Perkins, T. K. (1993, December 1). Critical and Subcritical Flow of Multiphase Mixtures Through Chokes. Society of Petroleum Engineers. doi:10.2118/20633-PA.

Riel, A., Burton, R. C., Wheeler, T. J., Vachon, G. P., & Heidari, M. R. (2014, June 10). An Innovative Modeling Approach to Unveil Flow Control Devices Potential in SAGD Application. Society of Petroleum Engineers. doi:10.2118/170045-MS.

Shu, W. R. (1984, June 1). A Viscosity Correlation for Mixtures of Heavy Oil, Bitumen, and Petroleum Fractions. Society of Petroleum Engineers. doi:10.2118/11280-PA.

Stalder, J. (2013, March 1). Test of SAGD Flow-Distribution-Control Liner System in the Surmont Field, Alberta, Canada. Society of Petroleum Engineers. doi:10.2118/153706-PA.

Stone, T. W., Law, D. H.-S., & Bailey, W. J. (2013, June 11). Control of Reservoir Heterogeneity in SAGD Bitumen Processes. Society of Petroleum Engineers. doi:10.2118/165388-MS.

Suncor Energy. (2015, December 17). Suncor MacKay River Project 2014 AER Performance Presentation: Subsurface Commercial Scheme Approval No . 8668 The Suncor Strategy, (8668).

Suncor Energy. (2017, December 13). Aalberta's Energy Supply/Demand Outlook Executive Summary. Report No. ST 98.

Vincent, K. D., MacKinnon, C. J., & Palmgren, C. T. S. (2004, January 1). Developing SAGD Operating Strategy using a Coupled Wellbore Thermal Reservoir Simulator. Society of Petroleum Engineers. doi:10.2118/86970-MS

Yang, C., Card, C., & Nghiem, L. (2009, September 1). Economic Optimization and Uncertainty Assessment of Commercial SAGD Operations. Petroleum Society of Canada.

doi:10.2118/09-09-33.

Yuan, J. Y., Huang, H., Mintz, R., Wang, X., Jossy, C., & Tunney, C. (2004, January 1). Wet Electric Heating for Starting Up SAGD/VAPEX. Petroleum Society of Canada. doi:10.2118/2004-130.

APPENDIX A: GRID SIZE SENSITIVITY ANALYSIS WITH CONVENTIONAL GRIDS

To conduct grid size sensitivity studies, three different grid systems have been constructed for each trajectory (fine, medium and coarse-grid models). Details are addressed the next few sections.

A.1 Fine-Grid Model

As shown in **Figure A-1**, the fine-grid model has dimensions of ($I \times J \times K = 17 \times 74 \times 30$) and 37,740 blocks in total, with each single grid block (other than 50-m side blocks) having dimensions of ($I \times J \times K = 2\text{m} \times 12.5\text{m} \times 1\text{m}$).

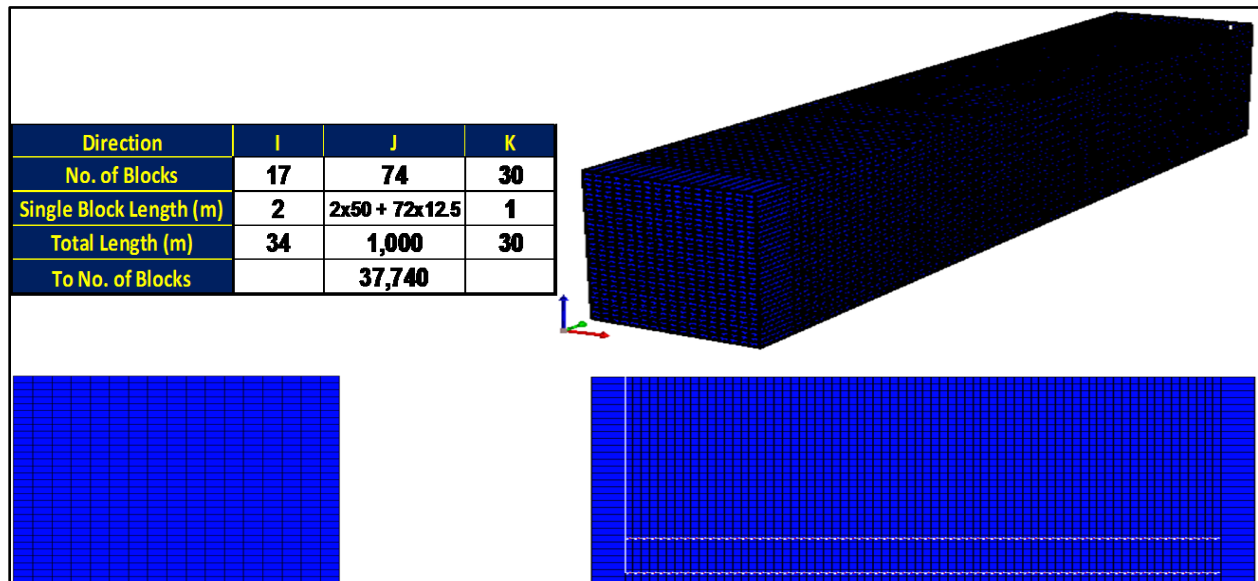


Figure A-1: Fine Grid System (12.5-m in Axial Direction)

A.2 Medium-Grid Model

As shown in **Figure A-2**, the medium-grid model has dimensions of ($I \times J \times K = 17 \times 38 \times 30$) and 19,380 blocks in total, with each single grid block (other than 50m side blocks) having dimensions of ($I \times J \times K = 2\text{m} \times 25\text{m} \times 1\text{m}$), i.e., J-direction length is 25-m, and that is two times bigger than fine-grid model J-Direction length (12.5-m).

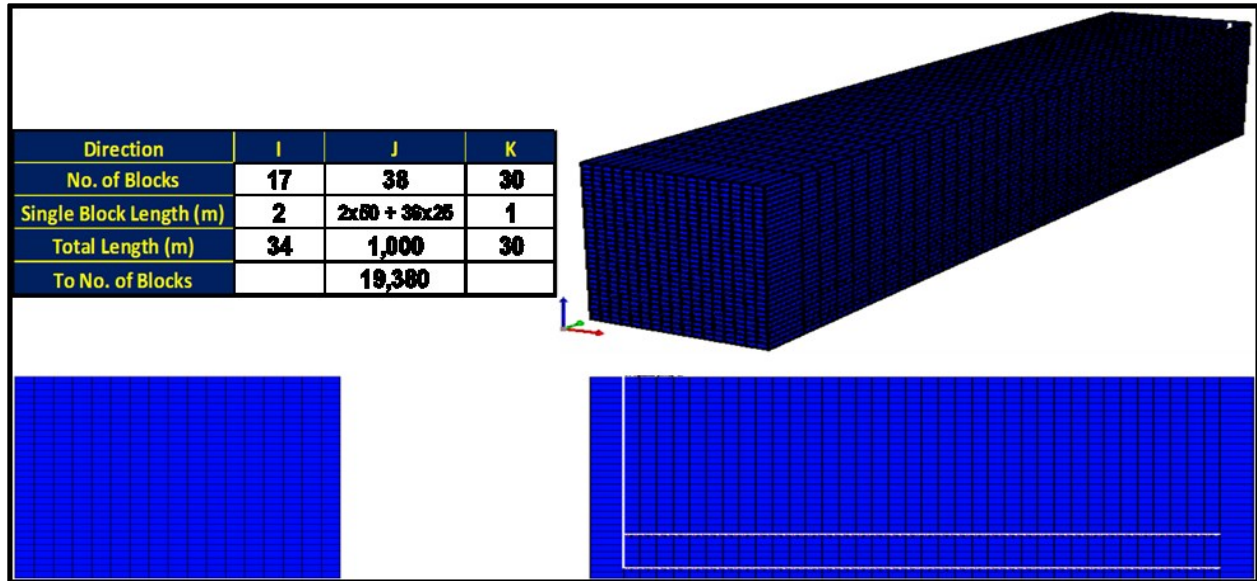


Figure A-2: Medium Grid System (25-m in Axial Direction)

A.3 Coarse-Grid model

Figure A-3 describes the Coarse model that has 10,200 blocks with dimensions of ($I \times J \times K = 17 \times 20 \times 30$), each single grid block has dimensions of ($I \times J \times K = 2 \text{m} \times 50 \text{m} \times 1 \text{m}$), i.e., J-direction length is 50-m, and that is four times bigger than fine-grid model J-Direction length (12.5-m).

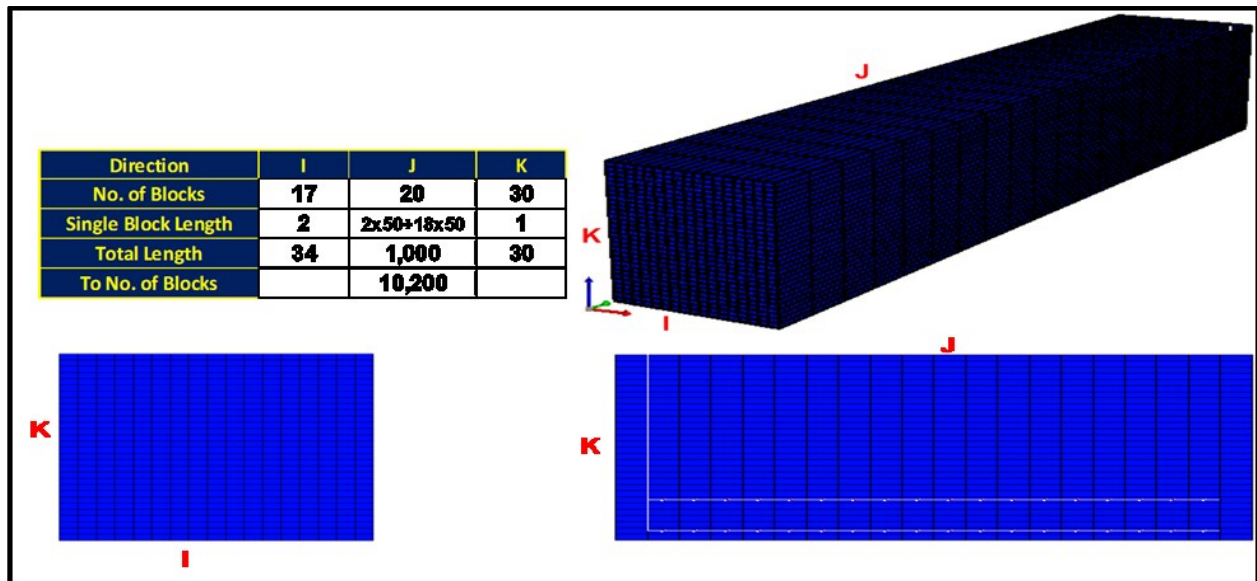


Figure A-3: Coarse Grid System (50-m in Axial Direction)

A.4 Ideal Trajectory

Three different cases of Ideal Trajectory have been built based on the coarse, medium and fine grid systems defined in the previous section.

A.4.1 Production Data

Figure A-4 depicts cumulative oil production, cumulative steam injection, cSOR and NPV of the three grid systems together. Plots in red color always indicate fine-grid model, plots in green are for medium-grid model and plots in blue are for coarse-grid model. As summarized in **Table A-1**, results are in good match where the maximum and terminal deviations (at the end of 10-years simulation run) for all production data are less than 1%.

Table A-1: Deviations of Ideal Trajectory Models SAGD Performance Data from Fine-Grid Model

Model	Differences							
	Cumulative Oil		Cumulative Steam Injection		Cumulative SOR		NPV	
	Max. (%)	Terminal (%)	Max. (%)	Terminal (%)	Max. (%)	Terminal (%)	Max. (%)	Terminal (%)
Fine	--	--	--	--	--	--	--	--
Medium	0.6	0.3	0.7	0.5	0.0	-0.1	0.2	0.0
Coarse	0.2	0.2	0.5	0.0	0.2	0.2	0.0	0.0

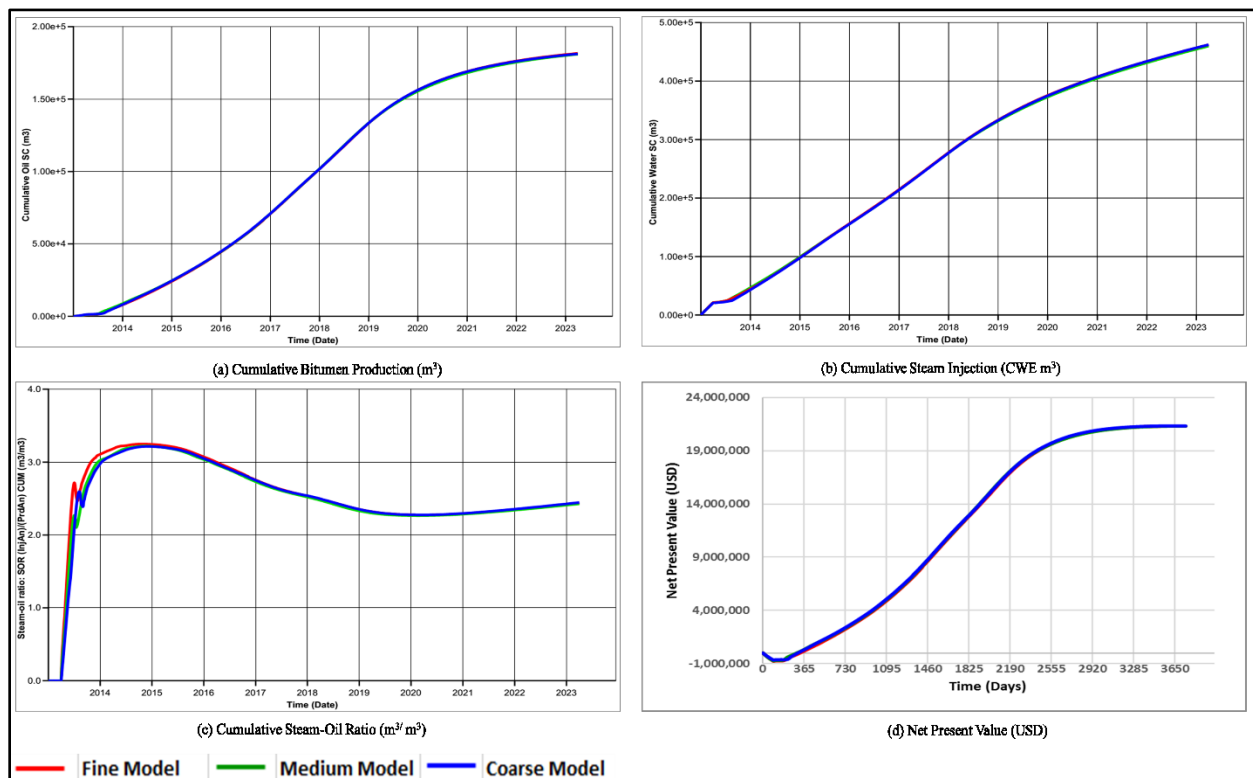


Figure A-4: SAGD Performance Data of Ideal Trajectory Models of Different Grid Systems

A.4.2 Steam Chamber

Figure A-5 is temperature map (steam chamber) of Ideal Trajectory coarse, medium and fine-grid models for the first 3 years of SAGD. Few discrepancies close to the heel section in medium-grid model temperature map compared to fine and coarse-grid models can be seen.

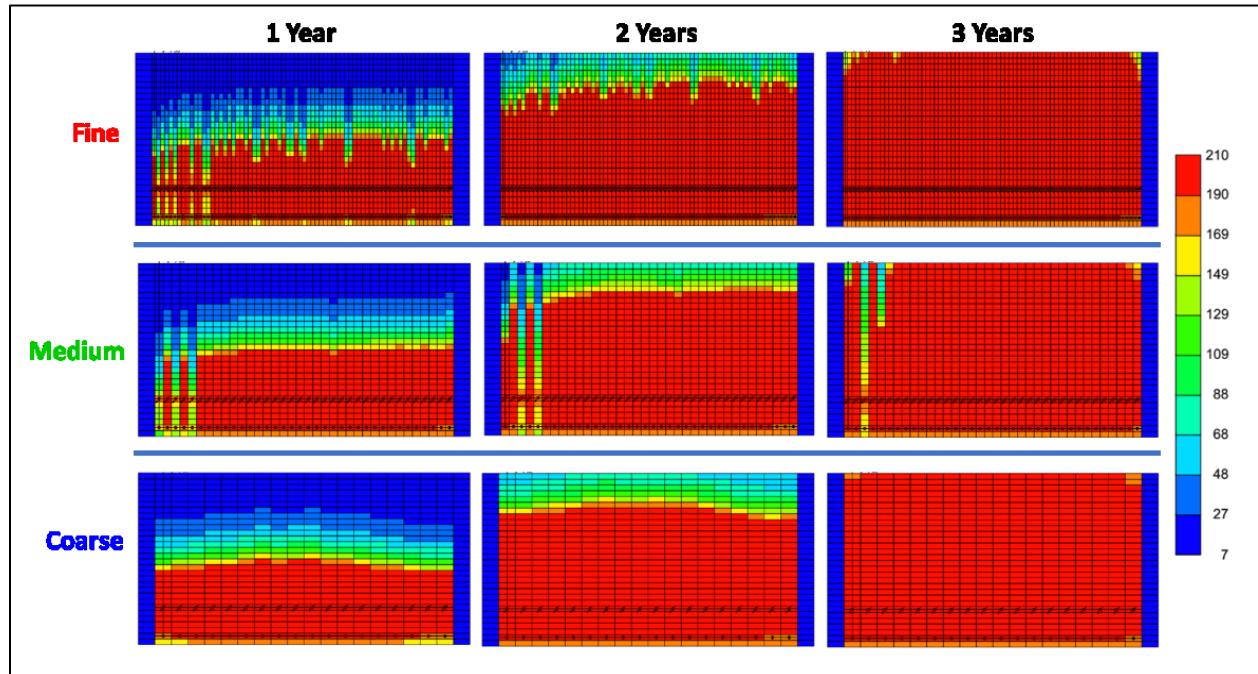


Figure A-5: Temperature Maps of Ideal Trajectory Models of Different Grid Systems

A.5 Trajectory-1

Three different cases of Trajectory-1 have been built based on the same fine, medium and coarse-grid model dimensions described previously in this chapter. The only difference is that the producer trajectory has been changed as shown in **Figure A-6**.

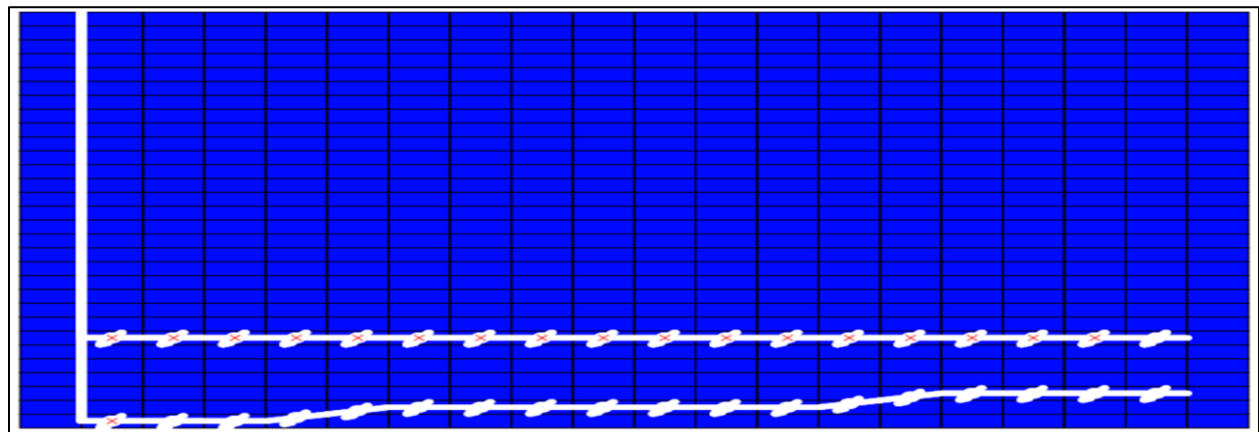


Figure A-6: Trajectory-1 Model Well Pair Trajectory

A.5.1 Production Data

Figure A-7 shows cumulative oil production, cumulative steam injection, cSOR and NPV's of the three models together. Variations in production data are more obvious compared to the previous Ideal Trajectory. Also, the summary in **Table A-2** indicate larger differences in the maximum and terminal deviations of production data compared to fine-grid model (6% and 2% for the medium and coarse-grid models respectively).

Table A-2: Deviations of Trajectory-1 Models SAGD Performance Data from Fine-Grid Model

Model	Differences							
	Cumulative Oil		Cumulative Steam Injection		Cumulative SOR		NPV	
	Max. (%)	Terminal (%)	Max. (%)	Terminal (%)	Max. (%)	Terminal (%)	Max. (%)	Terminal (%)
Fine	--	--	--	--	--	--	--	--
Medium	4.0	0.4	1.7	0.4	2.4	0.0	5.6	1.4
Coarse	1.5	0.5	0.7	0.1	1.0	0.4	0.8	0.8

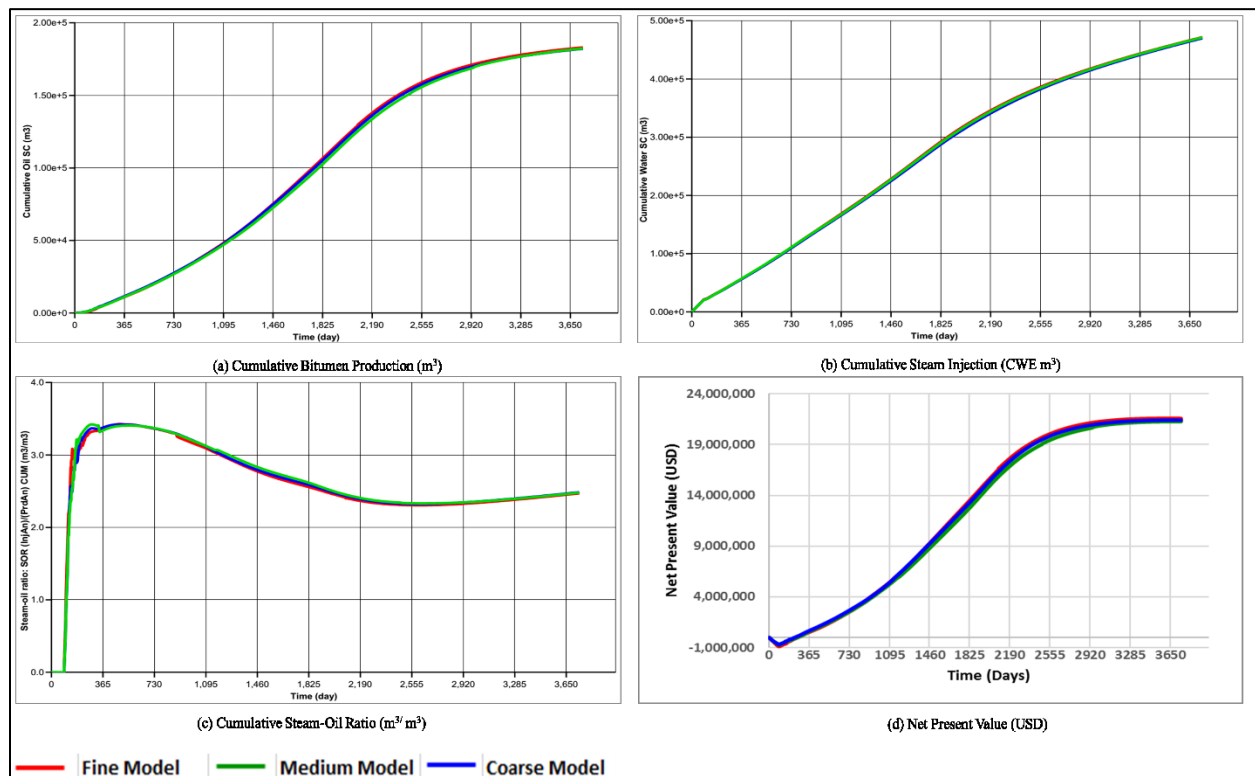


Figure A-7: SAGD Performance Data of Trajectory-1 Models of Different Grid Systems

A.5.2 Steam Chamber

Figure A-8 shows temperature maps (steam chamber) of Trajectory-1 coarse, medium and fine-grid models for the first 3 years of SAGD. Discrepancies are more noticeable, especially at producer trajectory excursion points.

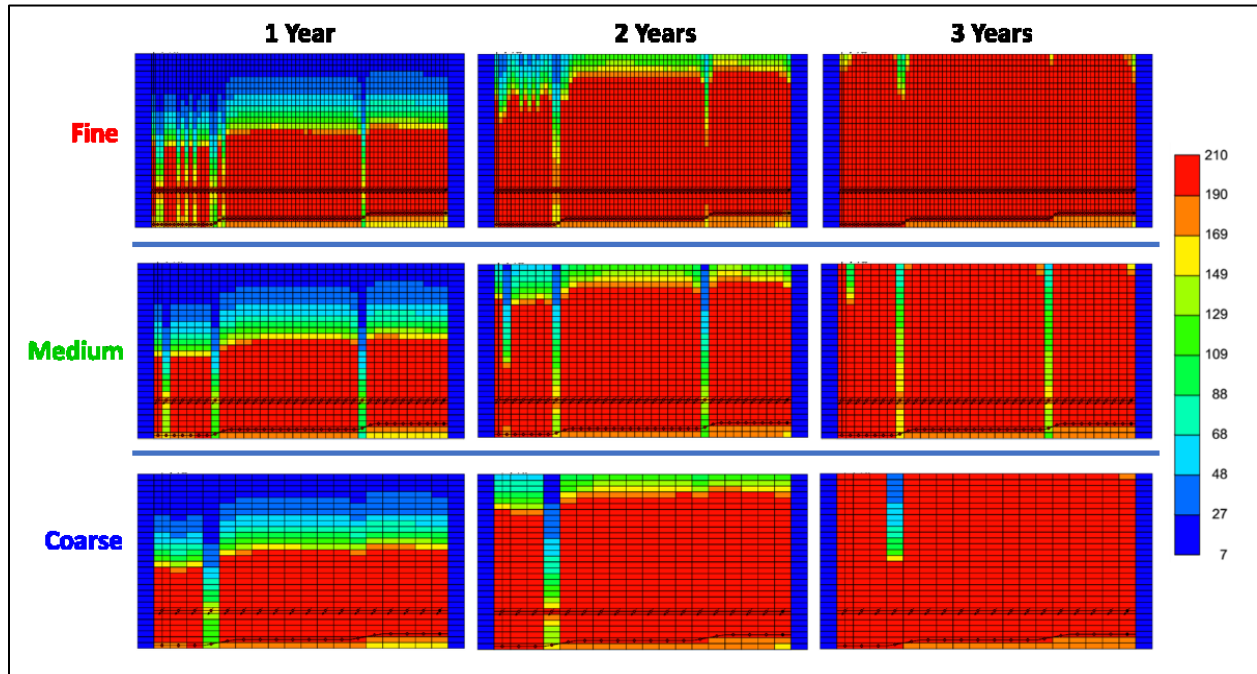


Figure A-8: Temperature Maps of Trajectory-1 Models of Different Grid Systems

A.6 Trajectory-2

Another set of three different cases have been built for a new trajectory system (Trajectory-2) with the same previous dimensions, but with both injector and producer trajectories having excursions as shown in **Figure A-9**:

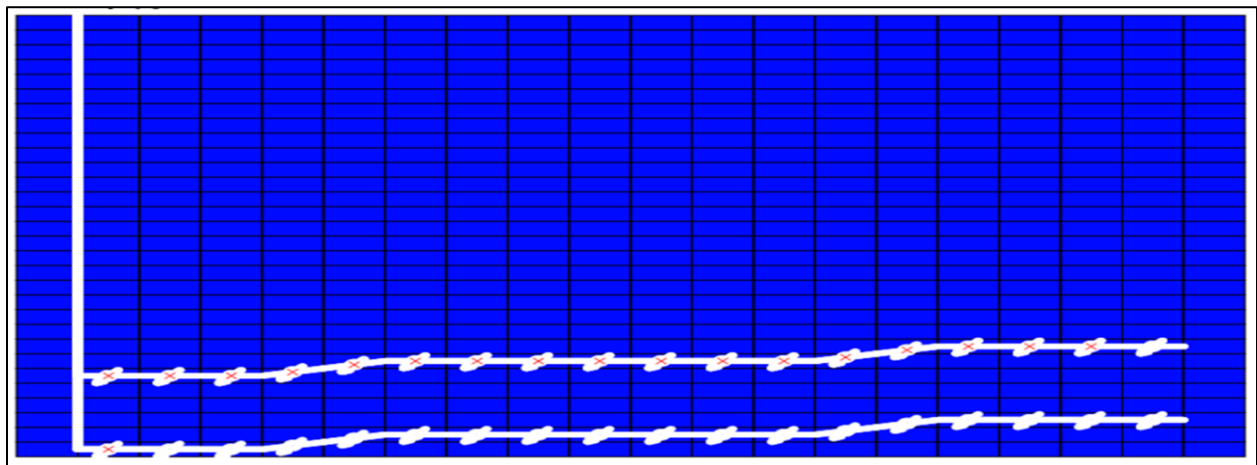


Figure A-9: Trajectory-2 Model Well Pair Trajectory

A.6.1 Production Data

As seen in **Figure A-10** and **Table A-3**, variations in cumulative oil production, cumulative steam injection, cSOR and NPV between the three models are getting bigger compared to the previous case (Trajectory-1). Maximum and terminal deviations are more than 8.5% and 9.2% for the medium and coarse-grid model respectively compared to the corresponding fine-grid model.

Table A-3: Deviations of Trajectory-2 Models SAGD Performance Data from Fine-Grid Model

Model	Differences							
	Cumulative Oil		Cumulative Steam Injection		Cumulative SOR		NPV	
	Max. (%)	Terminal (%)	Max. (%)	Terminal (%)	Max. (%)	Terminal (%)	Max. (%)	Terminal (%)
Fine	--	--	--	--	--	--	--	--
Medium	8.5	-0.1	5.4	0.8	3.7	-0.9	12.9	1.6
Coarse	9.2	1.6	6.0	1.8	4.1	-0.1	13.0	4.1

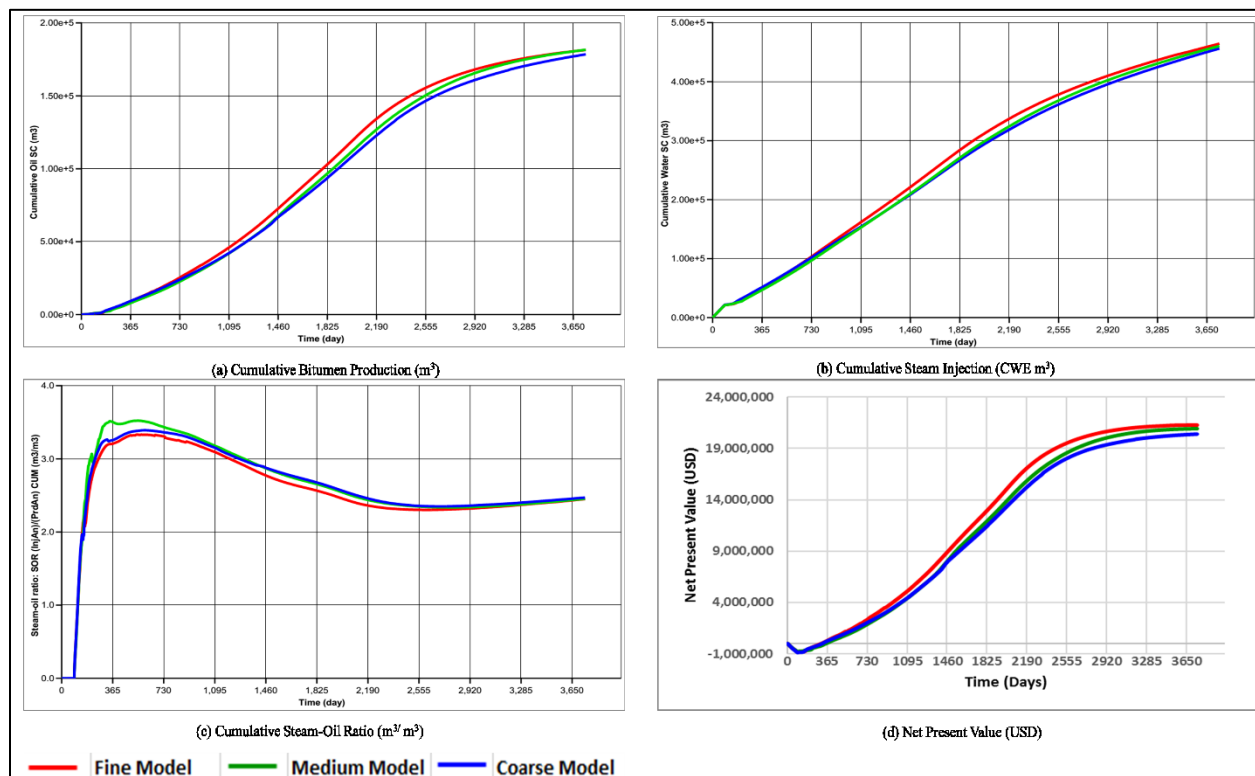


Figure A-10: SAGD Performance Data of Trajectory-2 Models of Different Grid Systems

A.6.2 Steam Chamber

Figure A-11 shows temperature maps of Trajectory-2 coarse, medium and fine-grid model for the first 3 years of SAGD. Differences between the three models are obvious, in addition to more steam chamber discrepancies at trajectory excursion points.

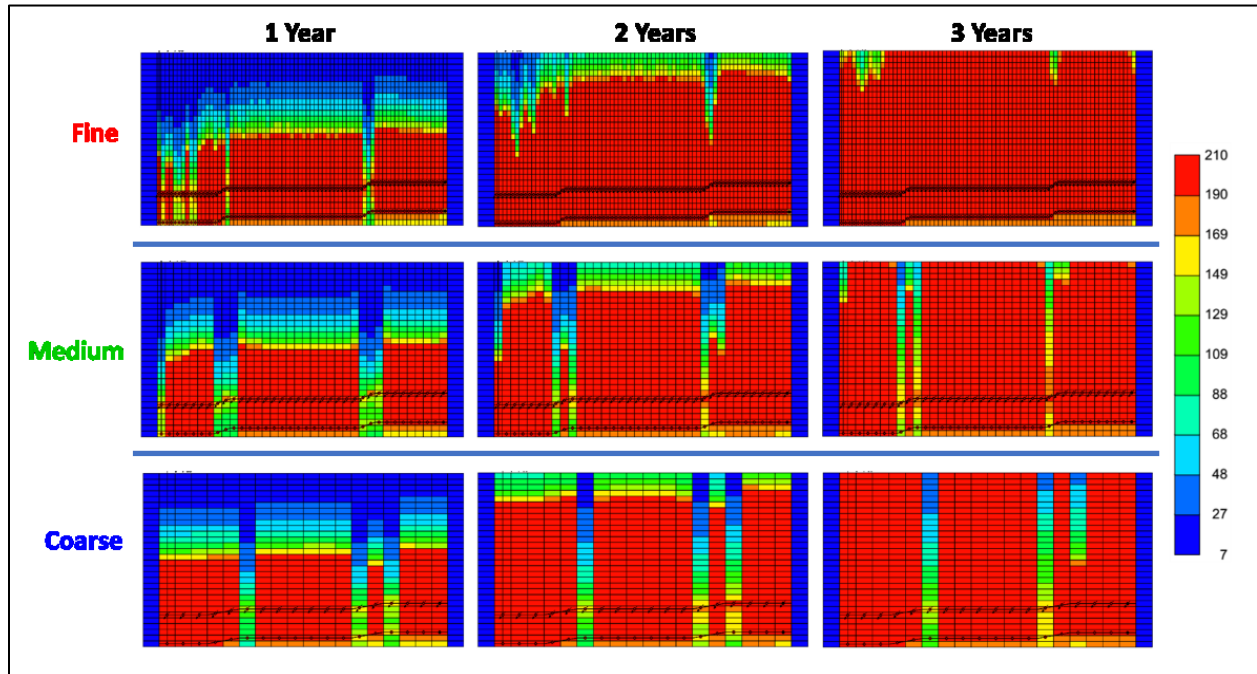


Figure A-11: Temperature Maps of Trajectory-2 Models of Different Grid Systems

A.7 Trajectory-3

Both injector and producer in Trajectory-3 have more severe and irregular excursions as shown in **Figure A-12**:

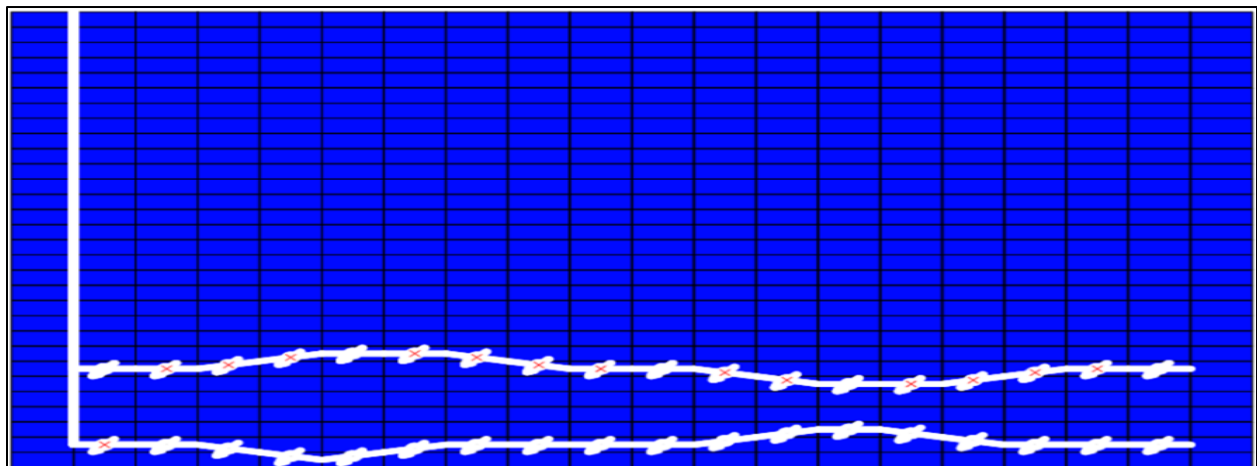


Figure A-12: Trajectory-3 Model Well Pair Trajectory

A.7.1 Production Data

Significant variations in production data and their corresponding terminal deviations can be seen in case of Trajectory-3 as shown in **Figure A-13** and summarized in **Table A-4**, where maximum and terminal deviations in some cases exceed 44% and 29 % for the medium-grid and coarse-grid models respectively.

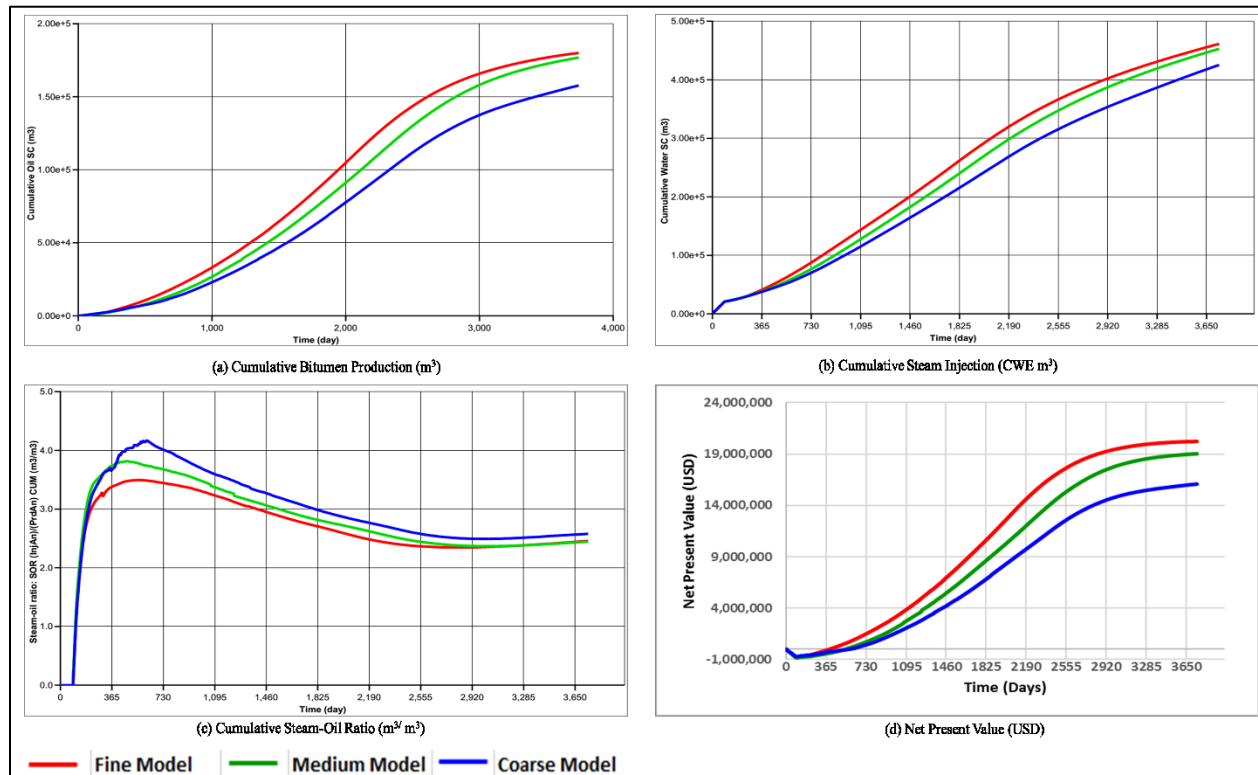


Figure A-13: SAGD Performance Data of Trajectory-3 Models of Different Grid Systems

Table A-4: Deviations of Trajectory-3 Models SAGD Performance Data from Fine-Grid Model

Model	Differences							
	Cumulative Oil		Cumulative Steam Injection		Cumulative SOR		NPV	
	Max. (%)	Terminal (%)	Max. (%)	Terminal (%)	Max. (%)	Terminal (%)	Max. (%)	Terminal (%)
Fine	--	--	--	--	--	--	--	--
Medium	16.5	1.8	10.5	1.8	7.4	-0.1	26.6	5.9
Coarse	29.1	12.4	19.3	7.7	13.9	5.2	44.2	20.5

A.7.2 Steam Chamber

More severe inconsistency in steam temperature maps can be noticed as shown in **Figure A-14**:

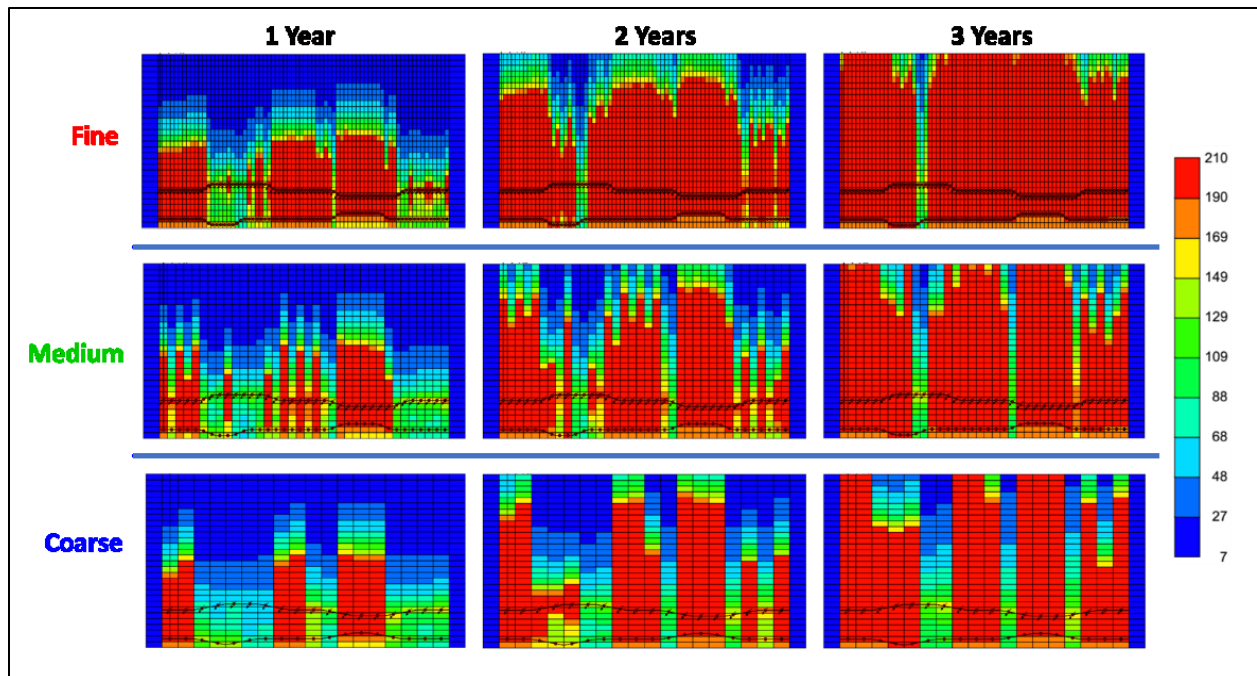


Figure A-14: Temperature Maps of Trajectory-3 Models of Different Grid Systems

A.8 Optimized Cases Side Elements/Fine Grids Analysis

SAGD well pairs are drilled within the designated drainage pad, i.e., within a certain distance from the lease boundaries (typically 50-m) and that creates side elements or SAGD shoulders in the model. All SAGD models constructed in this research use a fixed side element of 50-m width. Since those 50-m side elements have not been refined in the SAGD models in this research work, all the OCD optimized cases addressed in Sections 6.2, 6.3 and 6.4 have been run once again with the side elements refined with 2-m LGR. Furthermore, the optimized cases were also run with super fine grids that use 2-m grid block sizes in the axial and lateral directions (J-Direction and I-Direction respectively).

Figure A-15 shows a comparison of Trajectory-1 temperature maps for the optimized OCD case with 50-m side element, 2-m LGR side element and super fine grid blocks (i.e., 2-m in the axial and lateral directions). During the first five years of SAGD, temperature maps are consistent among the three models. More accurate modeling of heat transfer by conduction from the model to side elements can be seen for the 2-m LGR and super fine-grid models.

Production data of the three models (**Figure A-16**) are in excellent match with almost no differences. This is because heat losses from the SAGD model boundaries to side elements is the same for all models regardless of the side element gridding system and the only difference is how this lost heat is being distributed among the side elements in each model. **Figure A-17** through **A-20** depict the same temperature maps and production for Trajectory-2 and Trajectory-3.

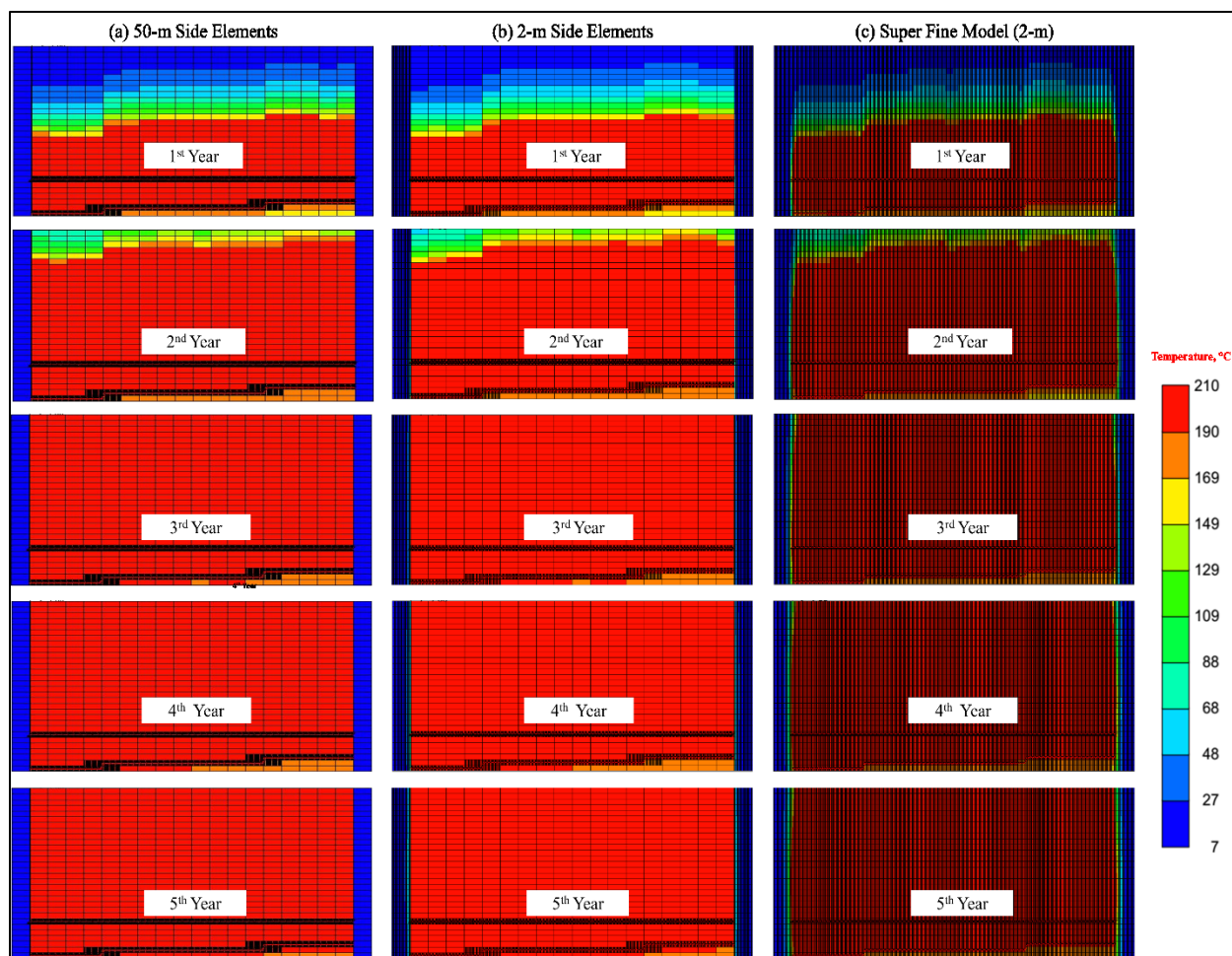


Figure A-15: Temperature Maps with Different Side Elements Grid Sizes, Trajectory-1

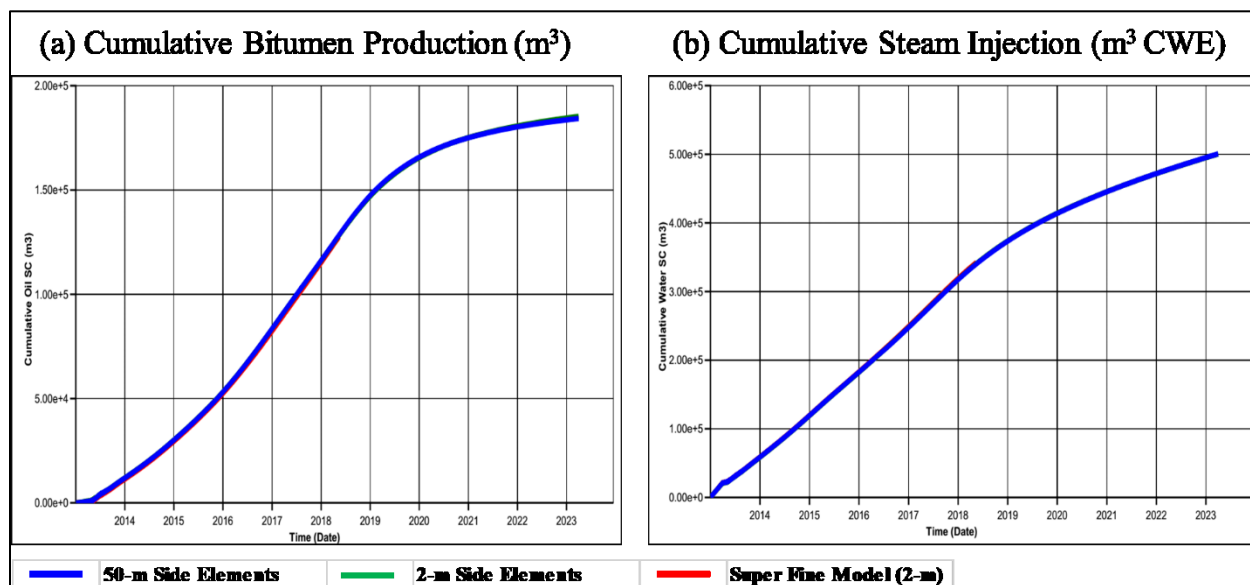


Figure A-16: SAGD Performance Data of Trajectory-1 Model with Different Side Elements Grid Sizes

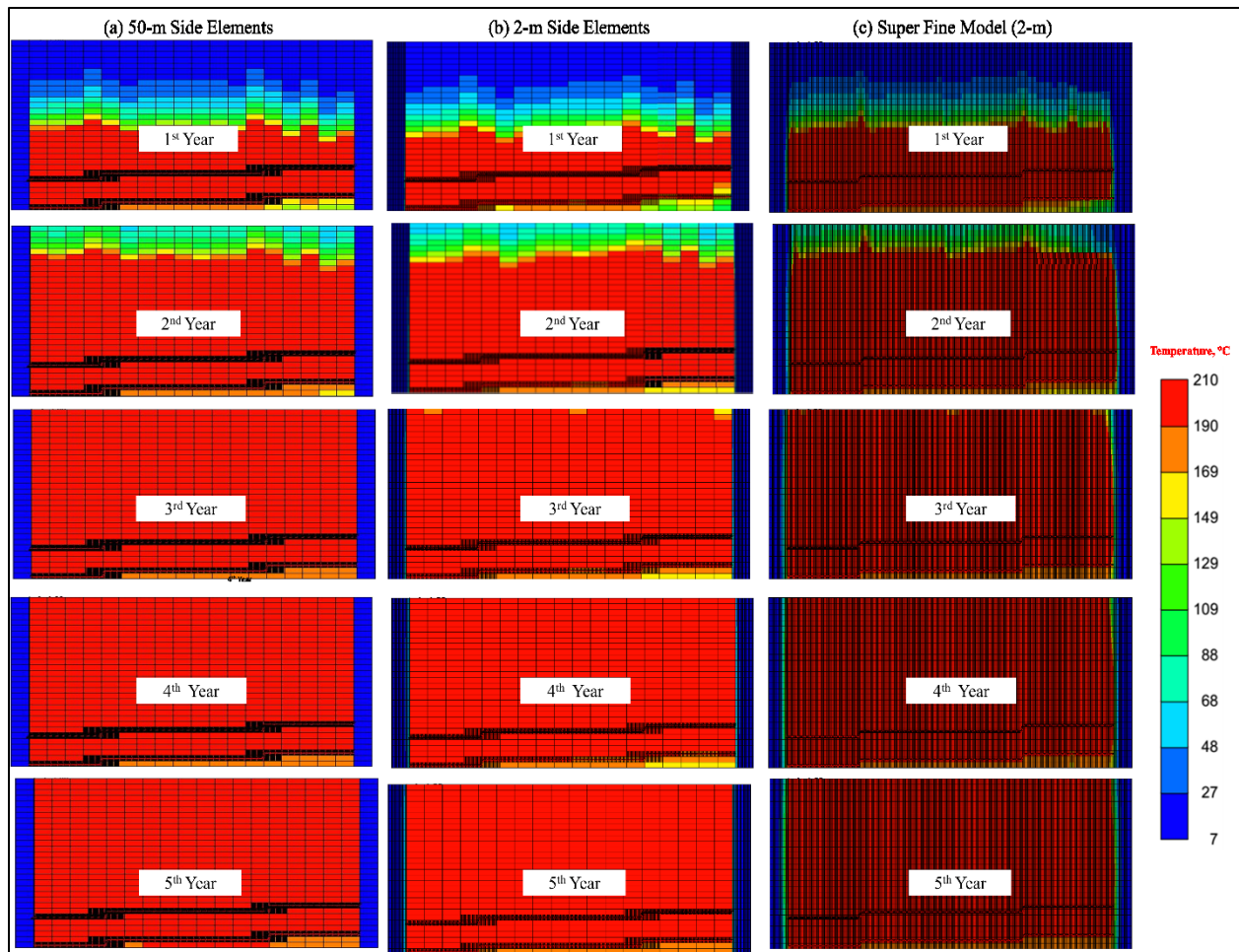


Figure A-17: Temperature Maps with Different Side Elements Grid Sizes, Trajectory-2

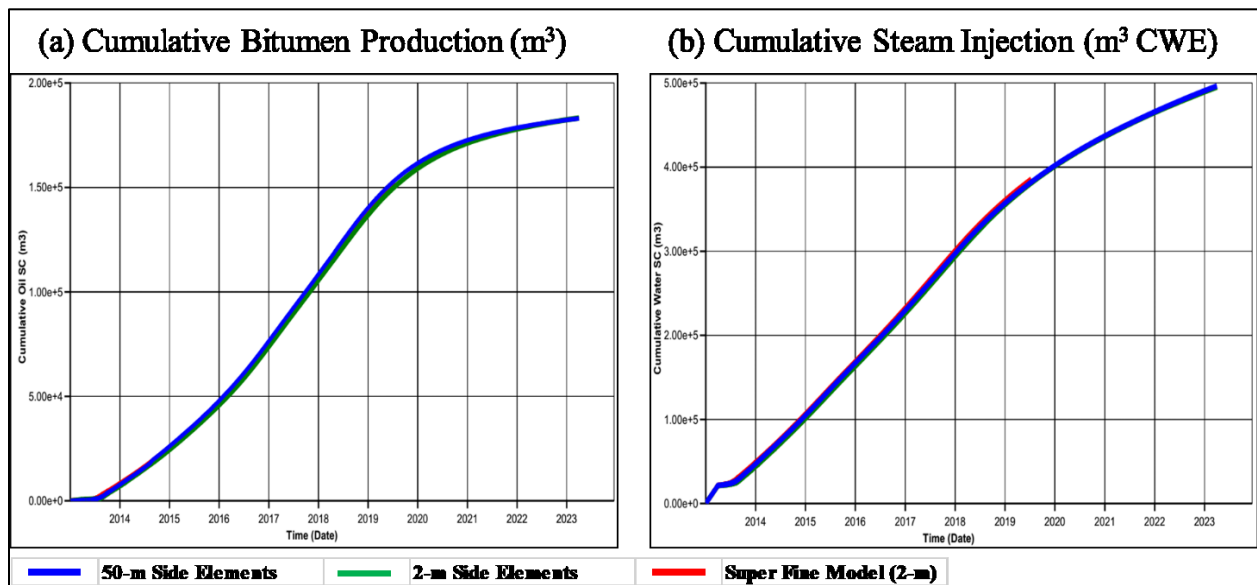


Figure A-18: SAGD Performance Data of Trajectory-2 Model with Different Side Elements Grid Sizes

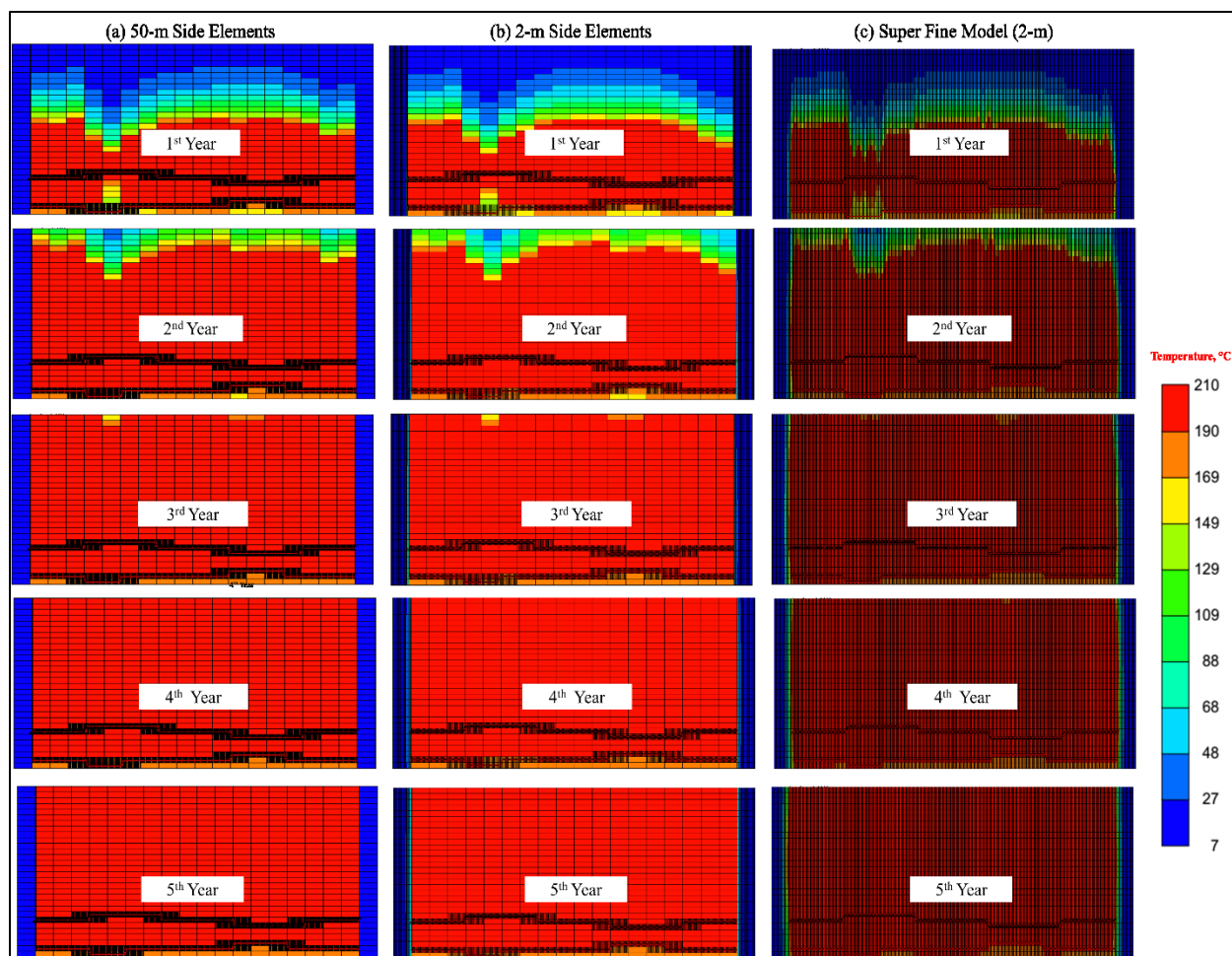


Figure A-19: Temperature Maps with Different Side Elements Grid Sizes, Trajectory-3

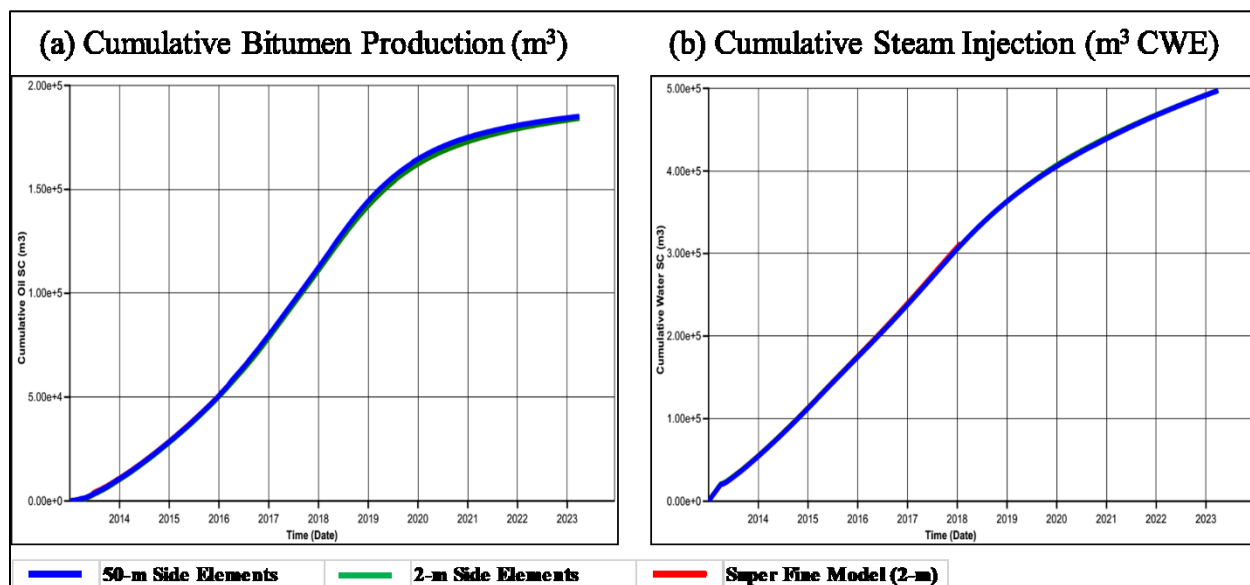


Figure A-20: SAGD Performance Data of Trajectory-3 Model with Different Side Elements Grid Sizes

A.9 Analysis of Variations in Production Data/Steam Chamber

In section 4.3 of Chapter 4, LGR technique was implemented on all models prior to conducting grid size sensitivity analysis. However, any grid size sensitivity analysis without LGR in the vicinity of well pairs (as described in Sections A.2, A.3 and A.4) causes high variations in results of production data and steam chamber growth during the early-stages of SAGD. Degree of variations increases with the increase of well pair trajectory complexity.

Four major reasons have been identified as the primary causes of those variations in results among grid sensitivity analysis without LGR. These four reasons are discussed:

A.9.1 Averaging of Well Trajectories Excursion Points

Inaccurate modeling of well trajectories changing points in coarser models causes variations in the values of well indices used in the simulator, and these variations directly affect well productivity and injectivity. **Figure A-21** depicts values of well index for the same well but modeled with different block size systems. In the coarse-grid model (50-m model), the well trajectory changing point has been modeled with two points only, and that yielded well index of $(4.698 \times 10^6 \text{ md} \times \text{m})$, and with four points in medium-grid model (25-m model) and gave well index of $(4.72 \times 10^6 \text{ md} \times \text{m})$, while the fine-grid model (12.5-m model) used eight points to model the same trajectory and resulted in a well index of $(4.73 \times 10^6 \text{ md} \times \text{m})$.

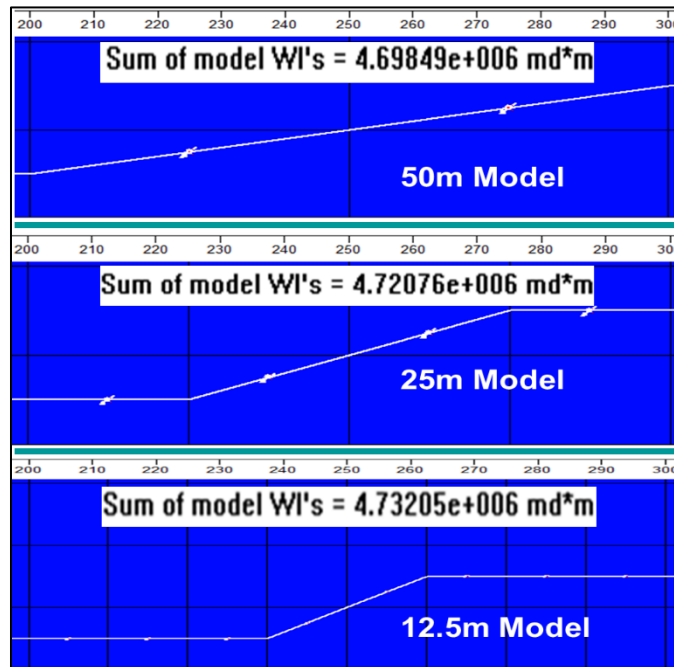


Figure A-21: Effect of Block Size on Modeling Trajectory Excursion Points

A.9.2 Rough Estimation of Conduction Heating Effect

Poor modeling of heat transfer by conduction mechanism in 12.5-m block size in J-Direction doesn't really reflect the actual heat transfer by conduction in axial direction. Furthermore, the situation gets even worse when longer blocks such as 25-m or 50-m are used. This is why cold vertical bars (unswept zones) appear in temperature maps of different trajectories shown in **Figures A-5, A-8, A-11, and A-14**. Also, it can be noticed that width of those vertical cold bars increase as axial block length increases from 12.5-m to 50-m.

To investigate the effect of heat transfer by conduction mechanism, two simple models with 150m well pair length were built. The first case was modeled using fine grids (2-m in axial direction), and the second model was built using coarse blocks (50-m in axial direction). Each of the two models had only a single perforation in the middle. **Figure A-22** shows temperature maps of the two models during the first two years. It can be observed that the fine-grid model has higher resolution and more accurate temperature map growth. In the fine-grid models, although the steam enters formation through only one 2-m length block, we can still notice that the blocks adjacent the perforated blocks have acquired high temperatures by conduction mechanism, and the effect of conduction diminishes as grid blocks get further far away from the perforated one. In case of coarse-grid model, temperature map has been roughly averaged among axial length of 50-m.

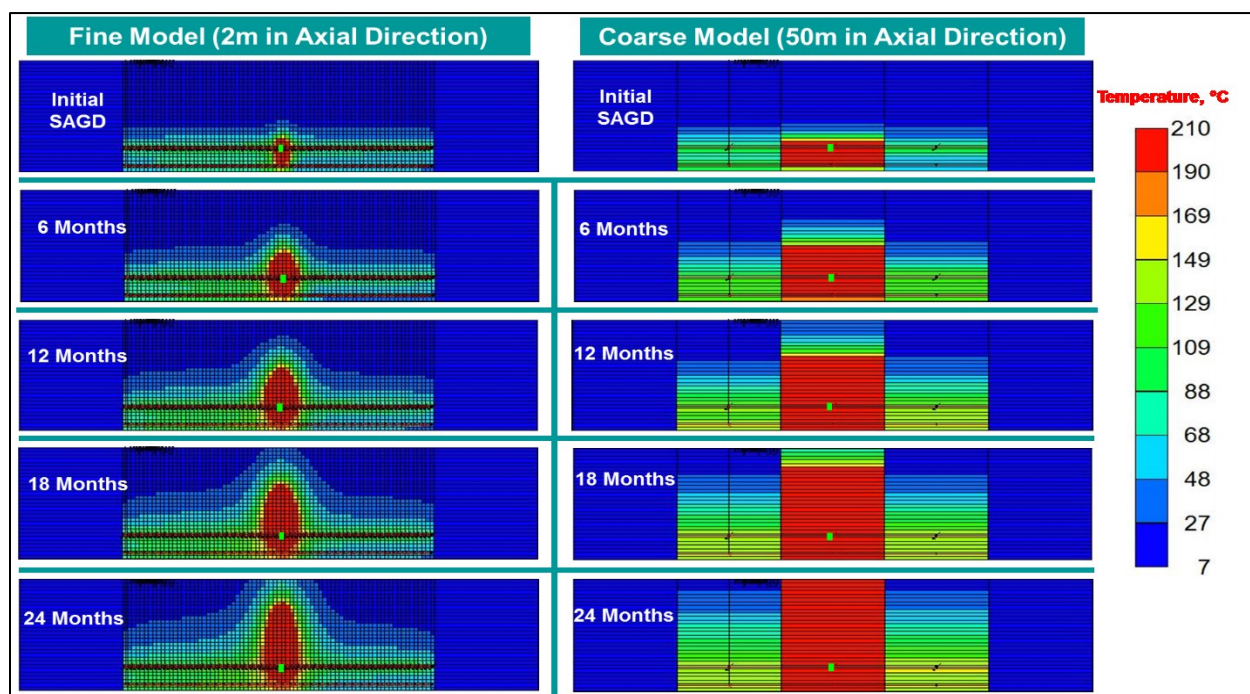


Figure A-22: Modeling of Heat Transfer by Conduction with Fine and Coarse Grid Blocks

Averaging the effect of heat transfer by conduction with the effect coupling wellbore/reservoir model (will be addressed in the next section) causes development of cold vertical bars at certain locations among the horizontal section of well pair. This can be referred to the fact that CMG FlexWell and coupling process have some deficiencies, that is, sometimes CMG FlexWell fails to deliver accurate discretized wellbore solution, and subsequently some reservoir blocks open-to-flow at sand face develop zero injection rate blocks, and if those zero injection rate blocks are very large, they will be unable to model heat transfer by conduction, subsequently, those blocks and corresponding vertical blocks will have no steam and will lead to forming cold vertical bars as shown in **Figure A-23**:

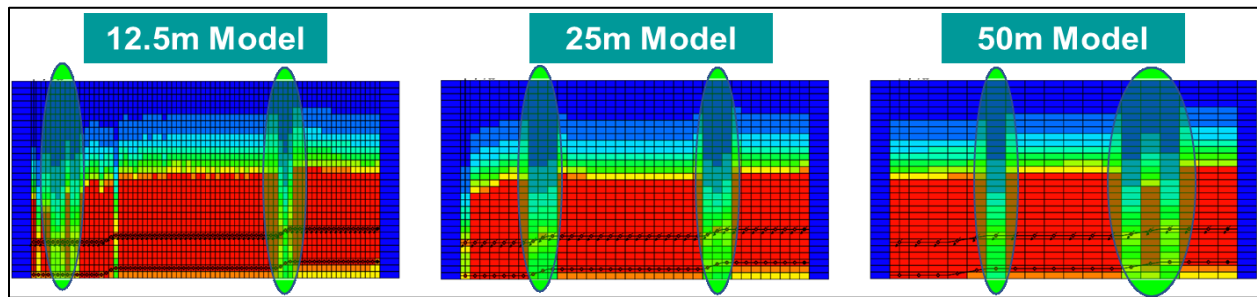


Figure A-23: Unswept Zones Due to FlexWell/STARS Coupling

A.9.3 Effect of Wellbore/Reservoir Coupling Process

Accurate modeling of complex wellbore configurations such as slotted liners and nested tubings as shown in **Figure A-24**, require use of FlexWell, where frictional pressure losses, changes in flow regimes and fluid compositional changes along horizontal sections of these nested pipes and adjacent reservoir sand face have significant impacts on SAGD performance, especially during early-stages of SAGD. CMG FlexWell is coupled with CMG STARS as discussed in Section 3.4 of Chapter 2, but this coupling process causes numerical problems.

To confirm the coupling effect and numerical convergence problems resulted from linking these two different software packages (CMG FlexWell and CMG STARS), the Ideal Trajectory model has been rebuilt using classical sink/source approach instead of CMG FlexWell.

As shown in **Figure 4-25**, in sink/source well models, the fluids flow from/into tubings, or even in the horizontal section of the annulus is not modeled. The only parts that can be modeled in sink/source model are flow terms from/into reservoir.

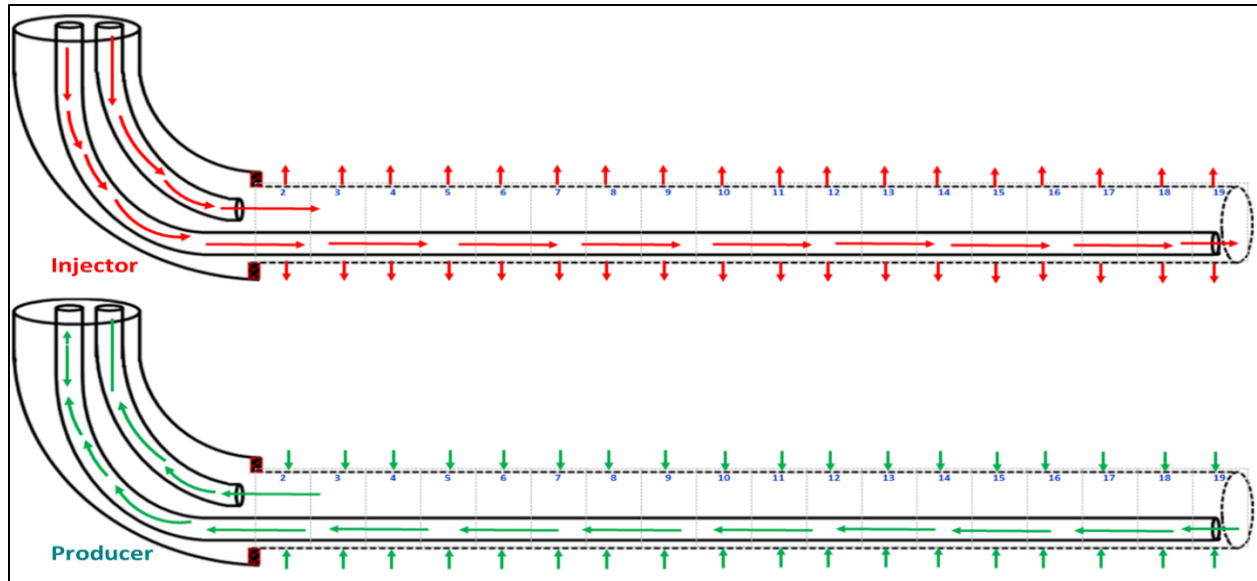


Figure A-24: Wellbore Configuration Modeling in SAGD Using FlexWell

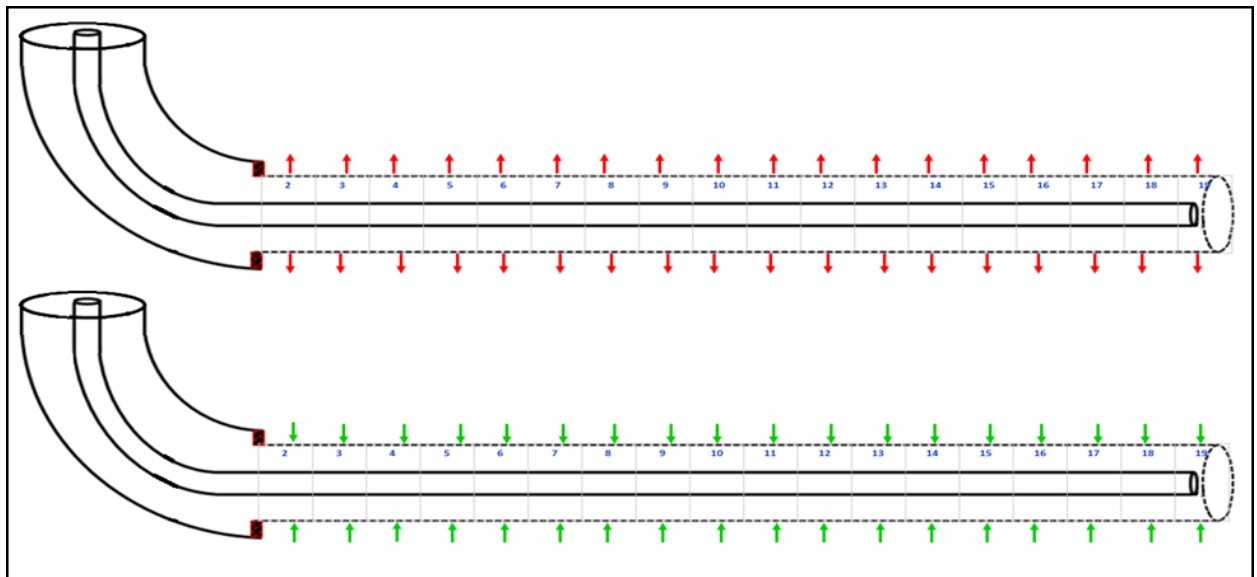


Figure A-25: Wellbore Configuration Modeling in SAGD Using Simple Sink/Source Models

Simulation results of Ideal Trajectory using the above-described sink/source model resulted in smooth, flat-front and consistent steam chamber growth and production data among fine-grid, medium-grid and coarse-grid models as shown in **Figure A-26**. Furthermore, comparing production data of the original Ideal Trajectory fine-grid model (with FlexWell) with the three new models of sink/source model have shown excellent match as shown in **Figure 4-27**.

A constant difference (22,000 m³ CWE) in the cumulative injected steam of the original Ideal Trajectory can be observed. This is because the pre-SAGD heating in the sink/source models

cannot be modeled using circulation technique because it requires nested tubings, thus it has been modeled using a different technique (Heaters).

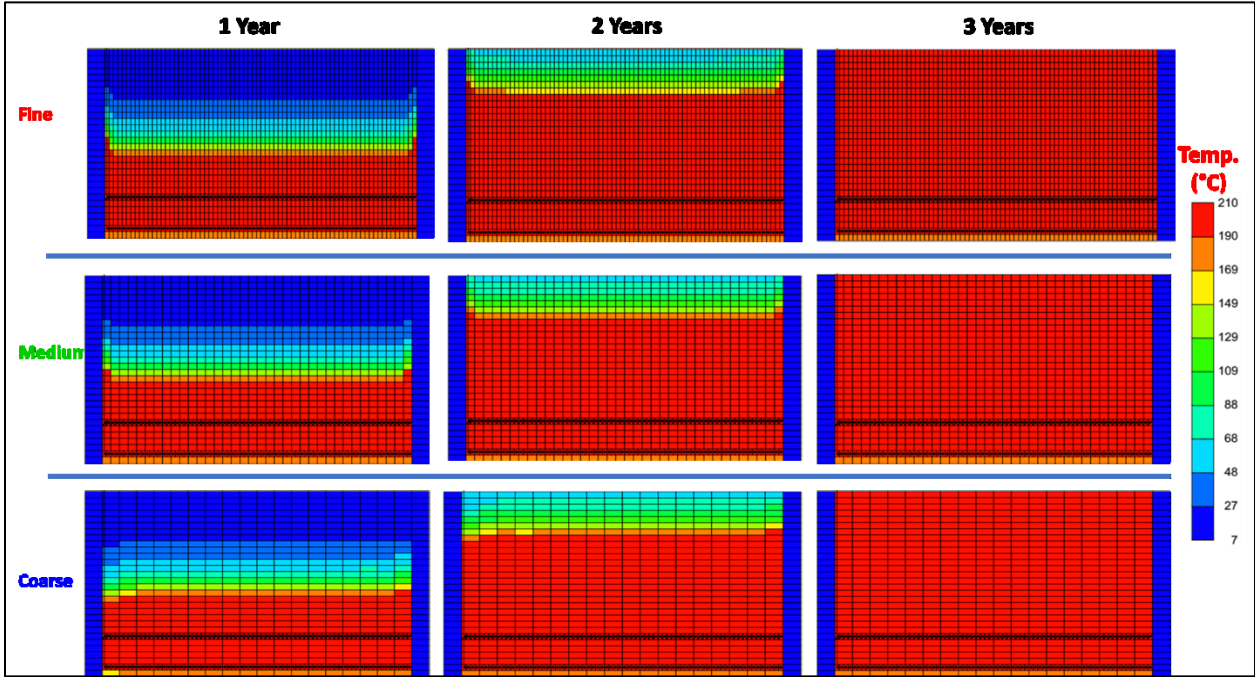


Figure A-26: Temperature Maps of Ideal Trajectory SAGD Models with Sink/Source Well Models

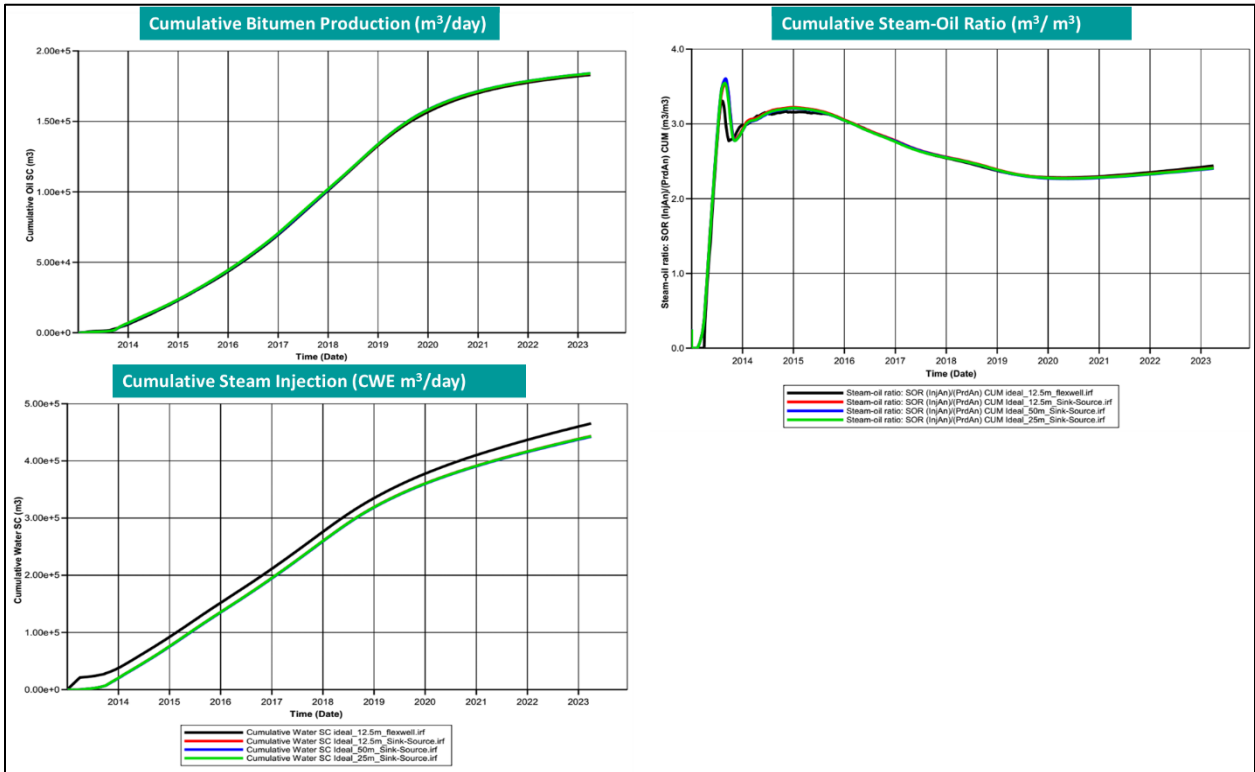


Figure A-27: Production Data of Ideal Trajectory SAGD Model with Sink/Source Well Models

A.9.4 Effect of Averaging of Rock/Fluid Data

The third reason for variations in production data and steam chamber growth is averaging of sensitive rock-fluid and temperature-viscosity data among large grid blocks in the vicinity of SAGD well pair where changes in temperature and other flow properties are rapid and large, especially during early-stages of SAGD. **Figure A-28** depicts the effect of averaging properties in a coarse-grid model (50-m) and fine-grid model (12.5-m) grid systems.

Another important feature that can be affected by the temperature and flow properties changes in large grid blocks is the presence of live steam (steam trap). **Figure A-29** describes this effect where two blocks having the same dimensions and same steam trap criteria (steam trap for both blocks is 4 m^3 CWE), in case#1 the amount of steam that exists inside is block is 3 m^3 CWE which is less than the defined steam trap criteria (4 m^3 CWE), thus larger amount of fluid was produced (20 m^3 , composed of 17 m^3 of fluid in addition to the entire amount of steam that exists inside the block, 3 m^3 CWE). In case#2, only small portion of fluid (15 m^3) could be produced because the production was choked by the set steam trap criteria, i.e., in order to satisfy the steam trap criteria, only 4 m^3 CWE of steam out of already existing 7 m^3 of CWE steam and 11 m^3 of liquid was allowed to be produced. Accordingly, production bottom hole pressure was increased to enforce the steam trap criteria.

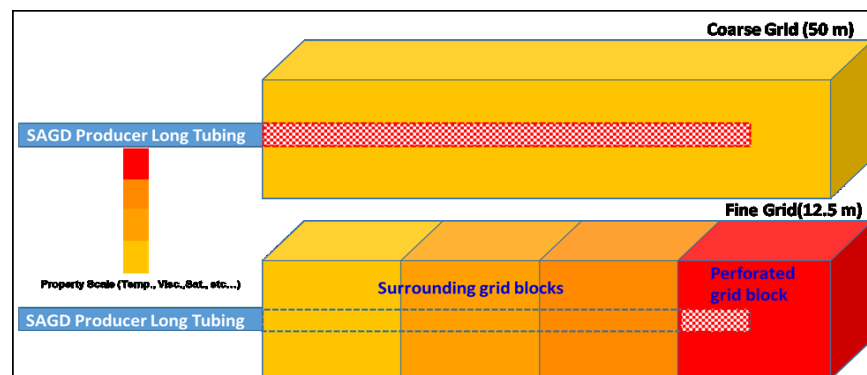


Figure A-28: Effect of Properties Averaging Among Coarse/ Fine Grid Systems in SAGD Models

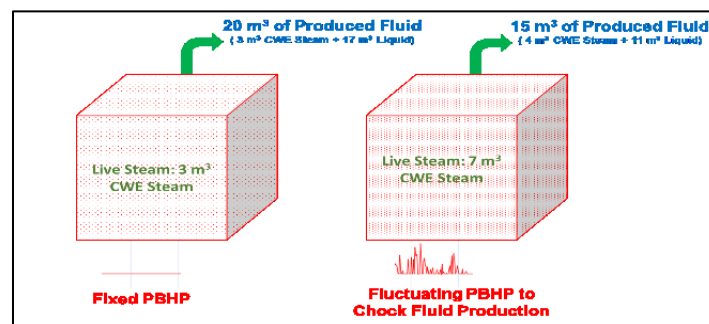


Figure A-29: Effect of Properties Changes on Steam Trap

APPENDIX B: CMG SOFTWARE INTERFACE

The figures in this appendix are snapshots taken from different CMG software modules interface (i.e., STARS, BUILDER, CMOST, etc....) to illustrate modeling and optimization stages.

Figure B-1 shows the list of Engines available in CMG CMOST module. These engines are used for different purposes such history matching and optimization.

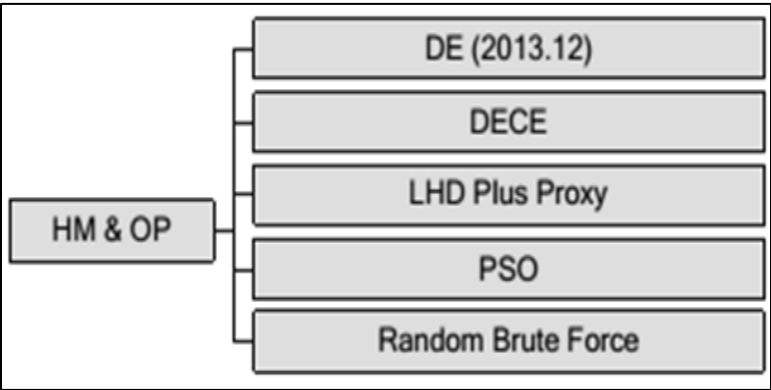


Figure B-1: CMG CMOST Engines

Figure B-2 is the interface of optimization parameters and parameters properties assignment in CMG CMOST. In our case optimization parameters are OCD#1, OCD#2, OCD#3, OCD#4, and OCD#5. Each of these parameters has a ranges of property values which is the number of ports in our case.

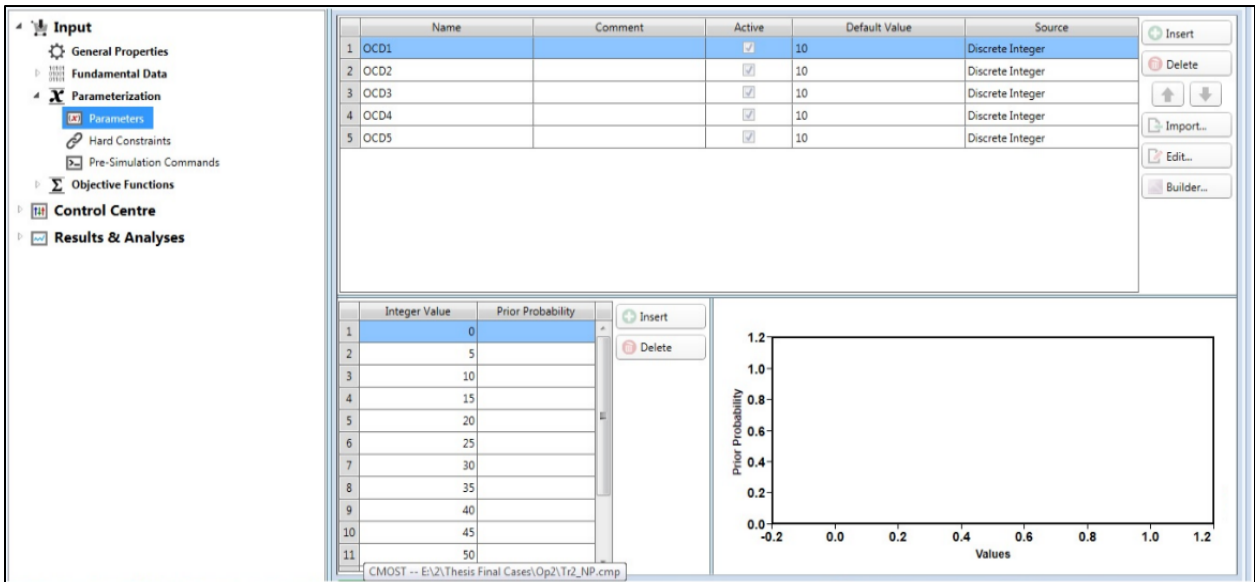


Figure B-2: Optimization Parameters Assignment in CMG CMOST

Figure B-3 depicts assignment of optimization objection function. The spreadsheet which contains the NPV OBJECTIVE function has been mount to the CMOST optimizer through this interface.

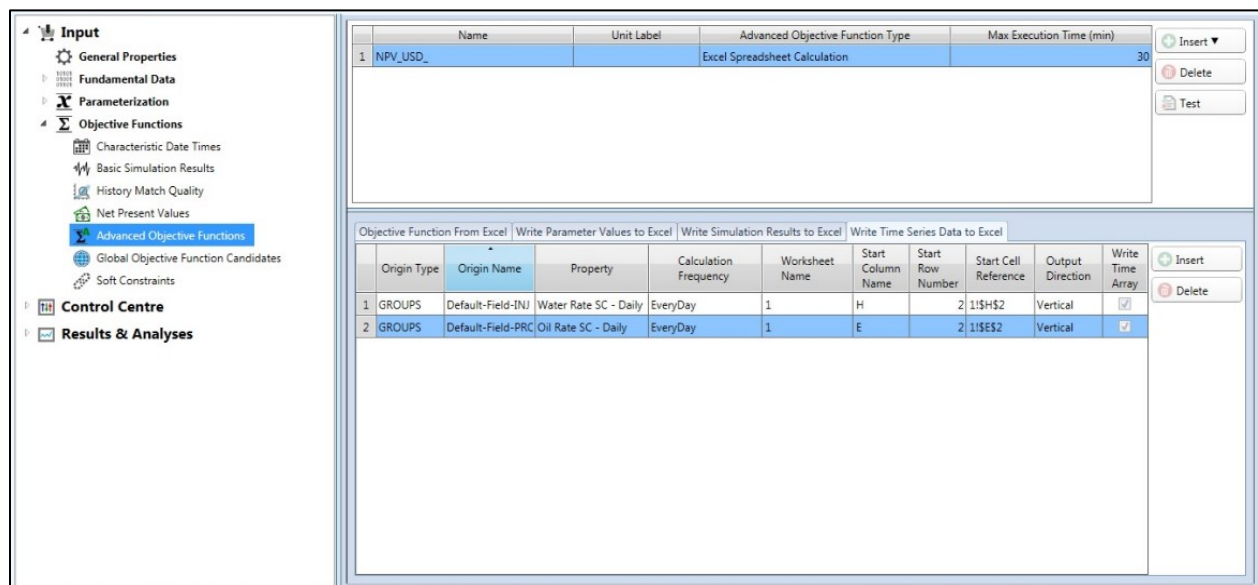


Figure B-3: Optimization Parameters Objective Function CMG CMOST

Figure B-4 is a snapshot of CMG CMOST internal optimizer used to enhance quality of selected sampling parameters. **Figure B-5** depicts quality check indicator of the selected sampling parameters.

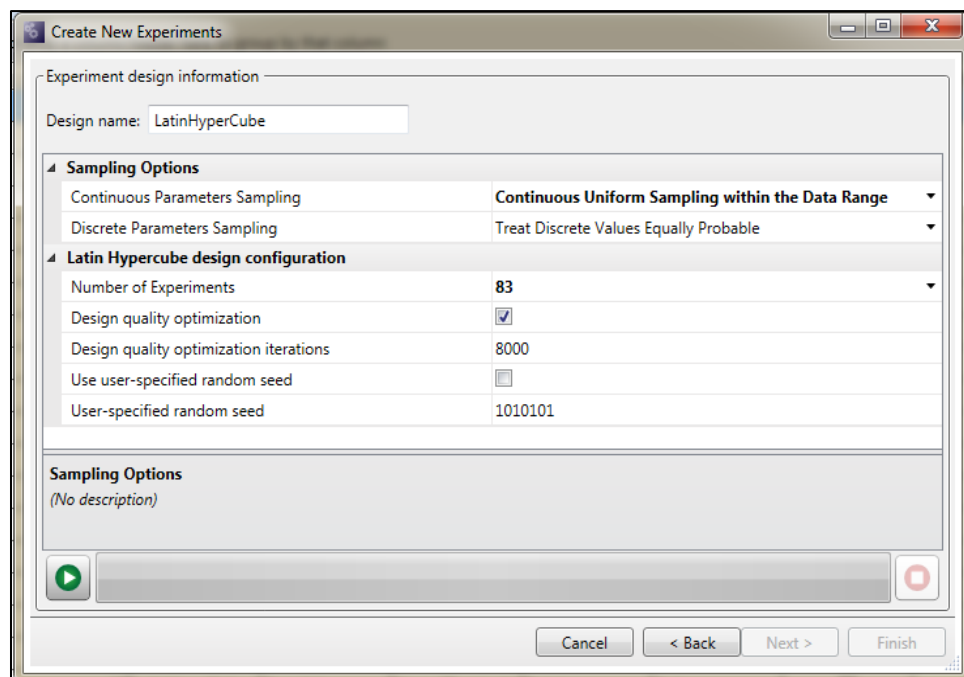


Figure B-4: Design of Experiments in CMG CMOST

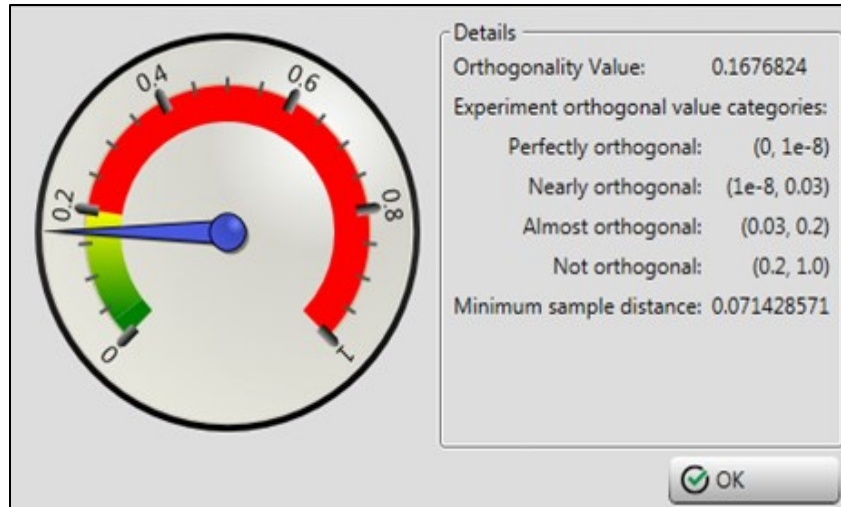


Figure B-5: Experiment Design QC in CMG CMOST

Figure B-6 if CMG CMOST Designed Exploration and Controlled Evolution (DECE) optimization algorithm flowchart.

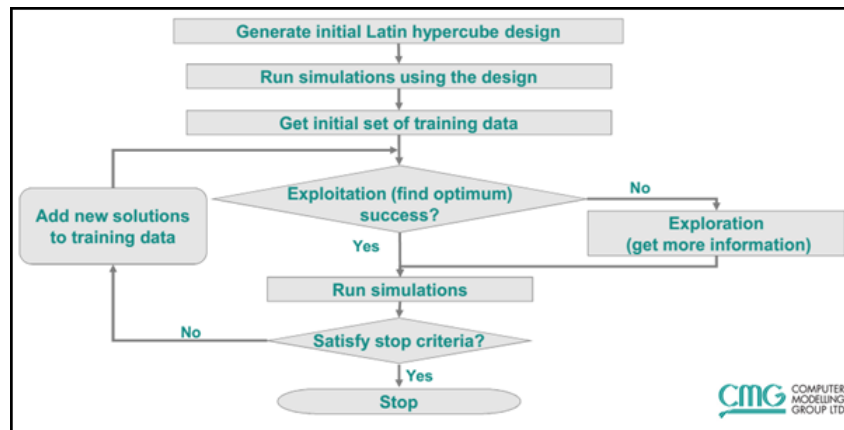


Figure B-6: CMG CMOST DECE Optimizer Algorithm

Figures B-7 and B-8 are plots of the optimization objective function parameters (daily bitumen production rate and daily steam injection rate respectively). The overlapped in green color represent general solutions, while the black and red colors are the plots of base case and optimum case respectively. **Figure B-9** shows simulation cases IDs plotted against their corresponding objective function (NPV).

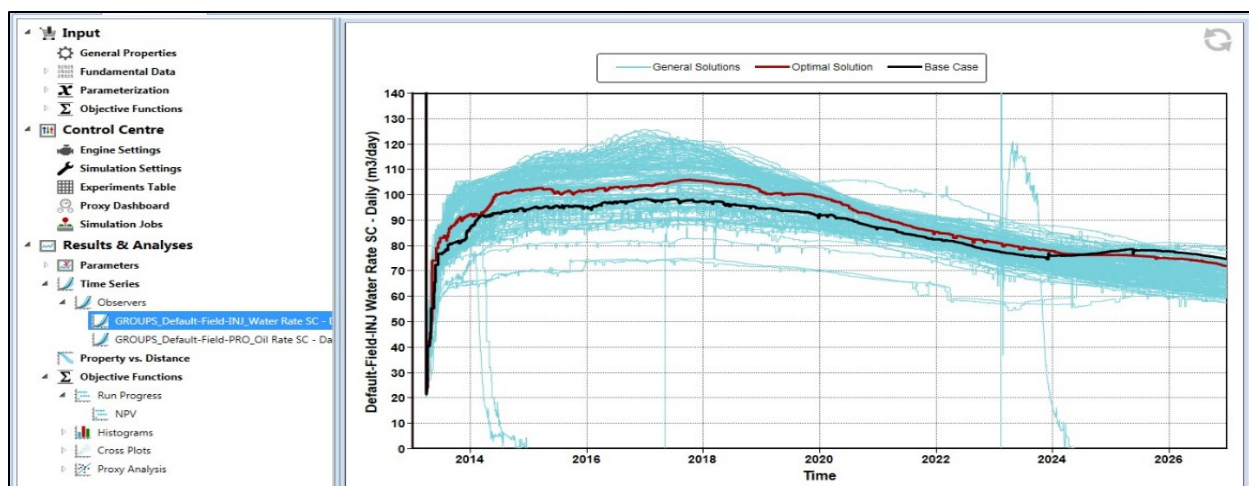


Figure B-7: Optimization Cases Steam Injection Rates in CMG CMOST

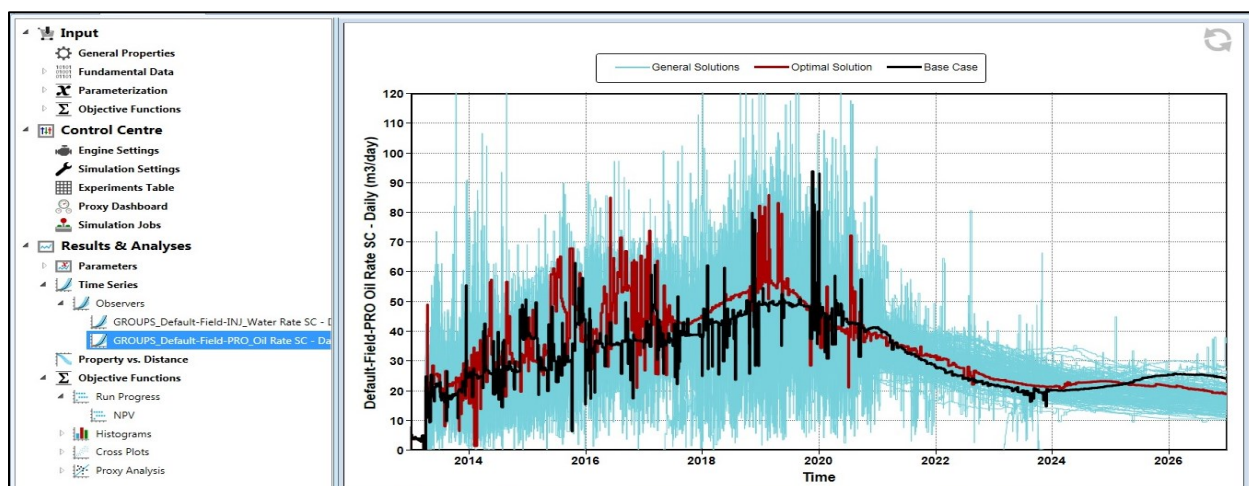


Figure B-8: Optimization Cases Oil Production Rates in CMG CMOST

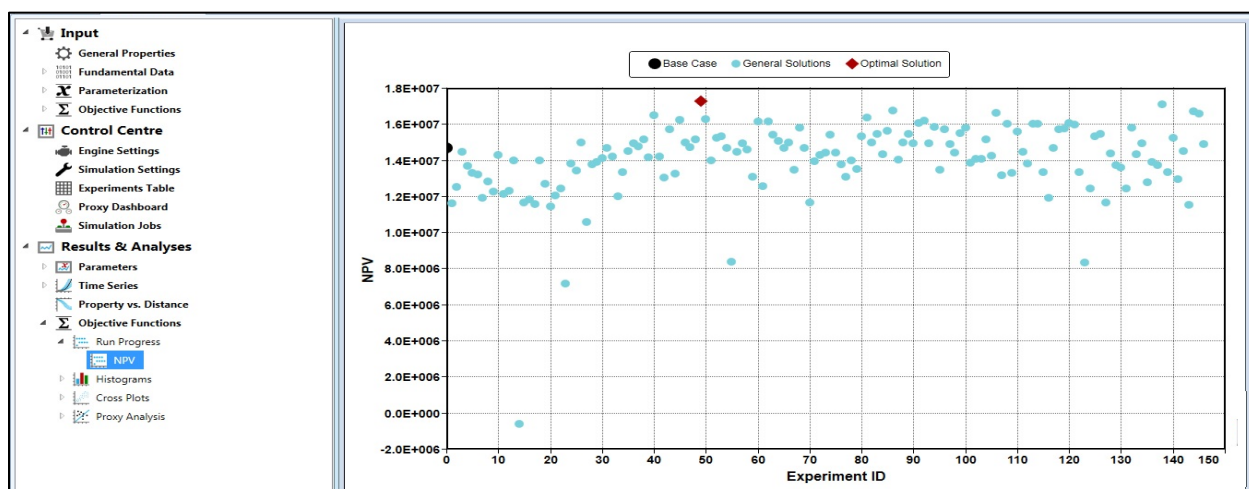


Figure B-9: NPV Objective Function in CMG CMOST

Figures B-10, B-12 and B-14 are snapshots of OCD modeling sections in CMG simulation data file for Trajectory-1, Trajectory-2 and Trajectory-3 respectively.

Figures B-11, B-13 and B-15 represent quality check indicators of the selected sampling parameters of Trajectory-1, Trajectory-2 and Trajectory-3 cases respectively.

Tr-1_OCDs_Base.dat									
6061									
6062	*FCDL-PARAM 'InjLong'								
6063									
6064	17	2	24	/	1	1	1	ORIF	0.01 0.65 10
6065									
6066	17	5	24	/	1	13	1	ORIF	0.01 0.65 10
6067									
6068	17	10	24	/	1	13	1	ORIF	0.01 0.65 10
6069									
6070	17	14	24	/	1	13	1	ORIF	0.01 0.65 10

Figure B-10: Trajectory-1 OCD's Modeling in CMG

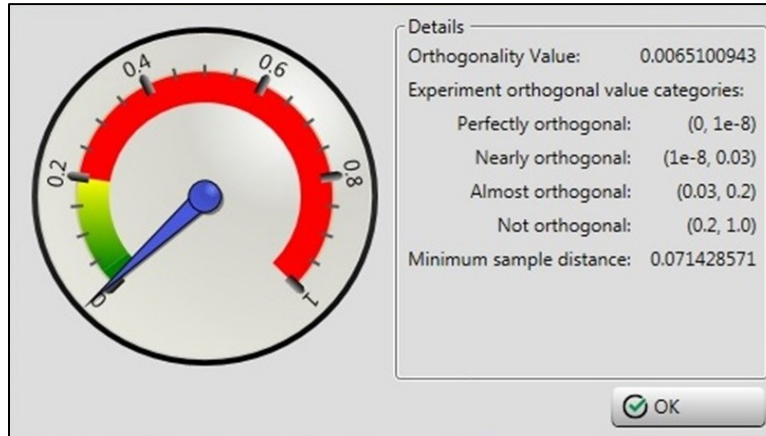


Figure B-11: Trajectory-1 OCD's Optimization Experiment Design Quality Check

Tr-2_OCD_Short_Base.dat									
6022	*FCDL-PARAM 'InjLong'								
6023									
6024	17	2	25	/	1	13	1	ORIF	0.01 0.65 10
6025									
6026	17	6	24	/	1	13	1	ORIF	0.01 0.65 10
6027									
6028	17	10	24	/	1	13	1	ORIF	0.01 0.65 10
6029									
6030	17	17	23	/	1	13	1	ORIF	0.01 0.65 10

Figure B-12: Trajectory-2 OCD's Modeling in CMG

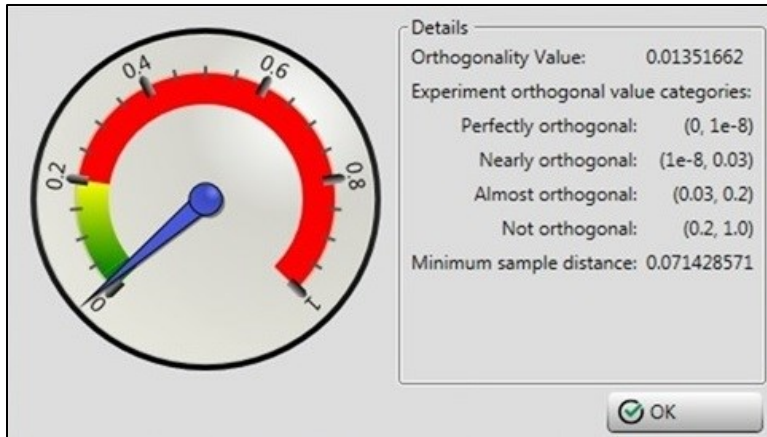


Figure B-13 Trajectory-2 OCD's Optimization Experiment Design Quality Check

ComplexTr_Short_Base.dat									
6017	*FCDL-PARAM 'InjLong'								
6018									
6019									
6020	17	2	24	/	1	13	1	ORIF	0.01 0.65 10
6021									
6022	17	5	23	/	1	13	1	ORIF	0.01 0.65 10
6023									
6024	17	8	23	/	1	13	1	ORIF	0.01 0.65 10
6025									
6026	17	12	24	/	1	13	1	ORIF	0.01 0.65 10
6027									
6028									

Figure B-14: Trajectory-3 OCD's Modeling in CMG

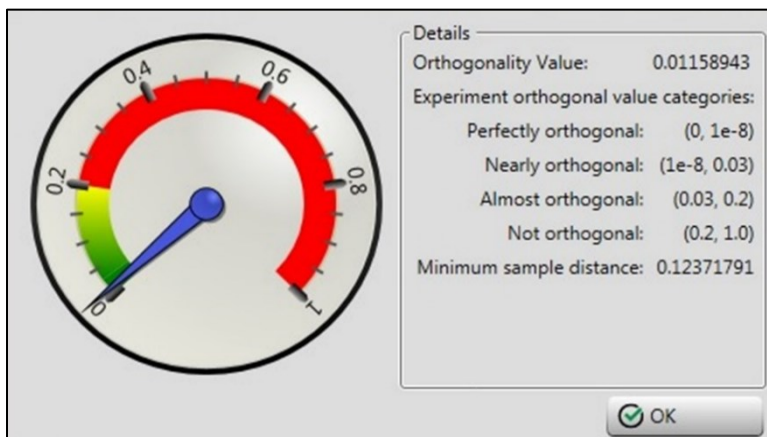


Figure B-15: Trajectory-3 OCD's Optimization Experiment Design Quality Check

APPENDIX C: MISCELLANEOUS TOPICS

C.1 Long-Term Optimization Work SAGD Simulation Run Times

Figures C-1, C-3 and C-5 represent SAGD project lives (simulation termination times) of long-term (top 50) cases of Trajectory-1, Trajectory-2 and Trajectory-3 respectively. All cases have simulation terminations times between 8.7 years and 9.4 years, but each individual case has its own simulation termination time. **Figures C-2, C-4 and C-6** are recovery factor of top 50 cases of Trajectory-1, Trajectory-2 and Trajectory-3 respectively.

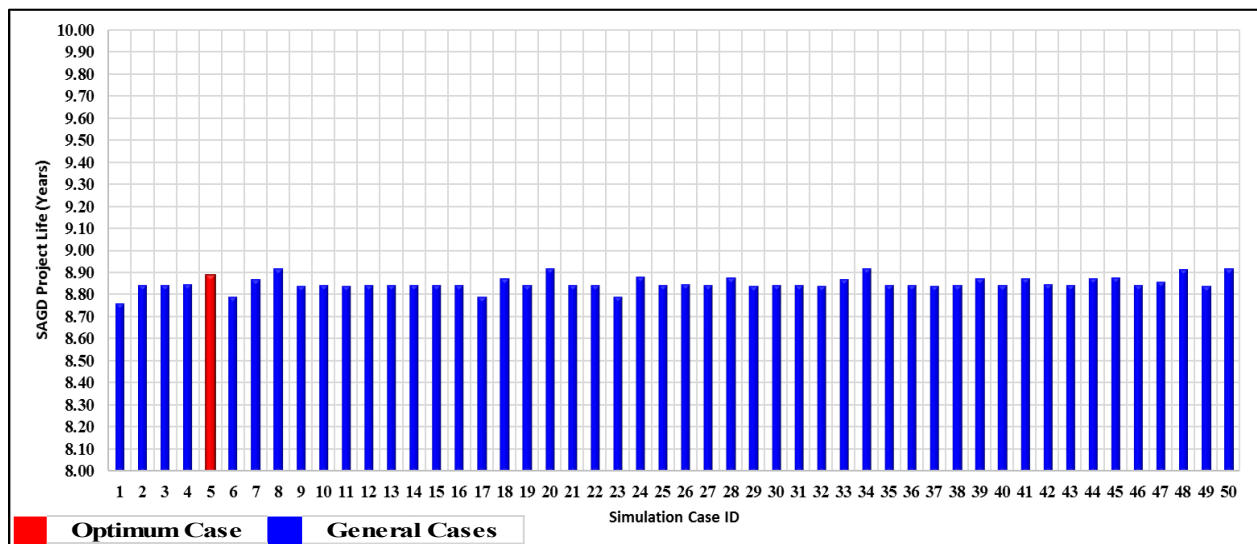


Fig C-1: Trajectory-1 Optimization Top 50 Cases Simulation Run Times

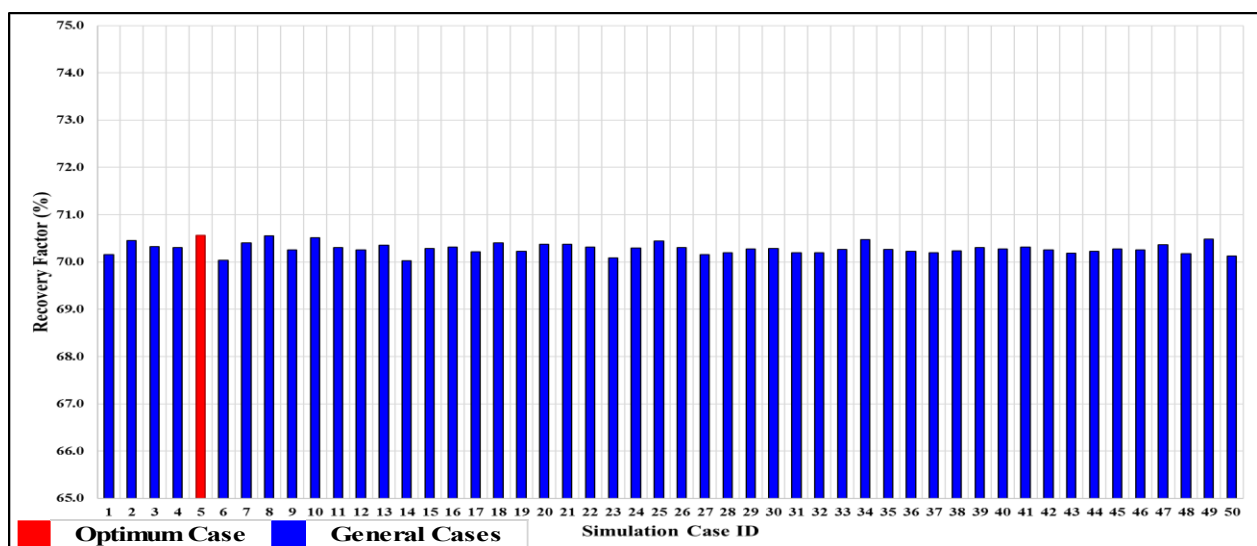


Fig C-2: Trajectory-1 Optimization Top 50 Cases Recovery Factors

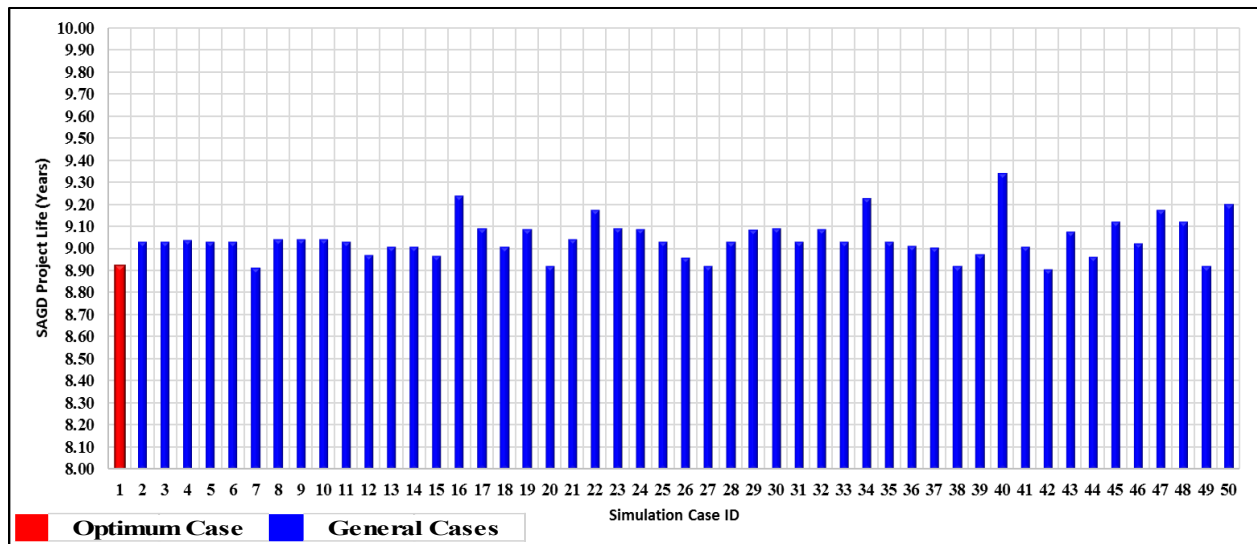


Fig C-3: Trajectory-2 Optimization Top 50 Cases Simulation Run Times

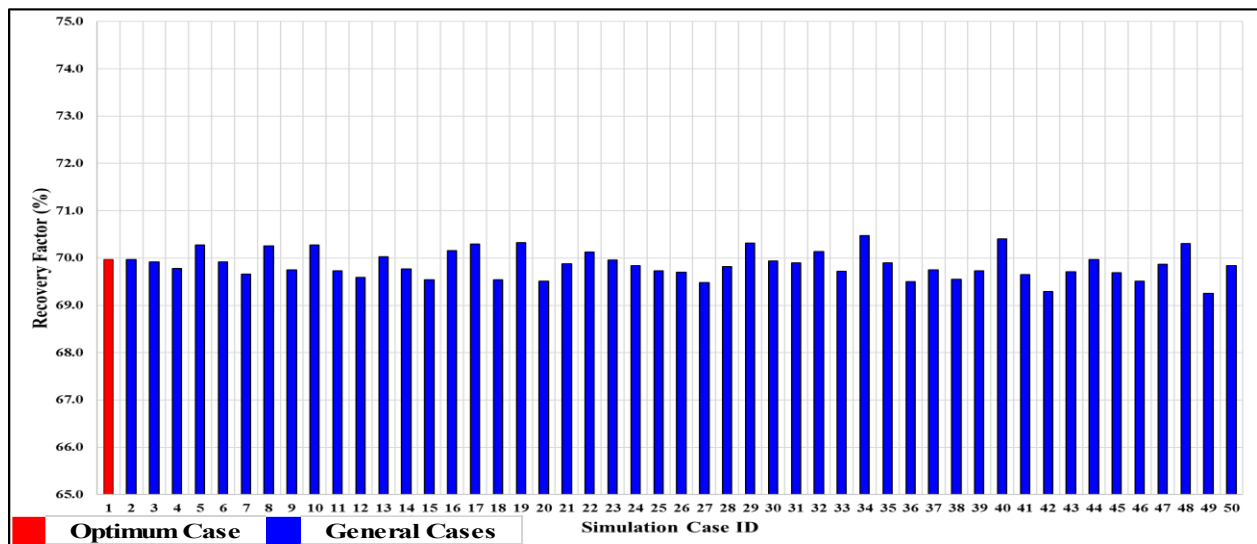


Fig C-4: Trajectory-2 Optimization Top 50 Cases Recovery Factors

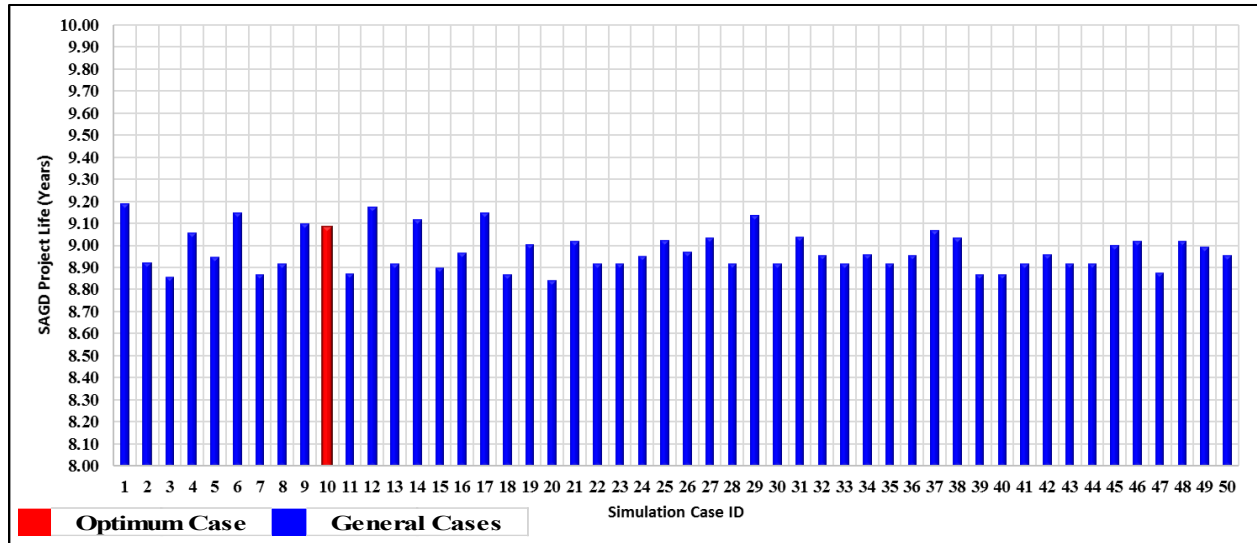


Fig C-5: Trajectory-3 Optimization Top 50 Cases Simulation Run Times

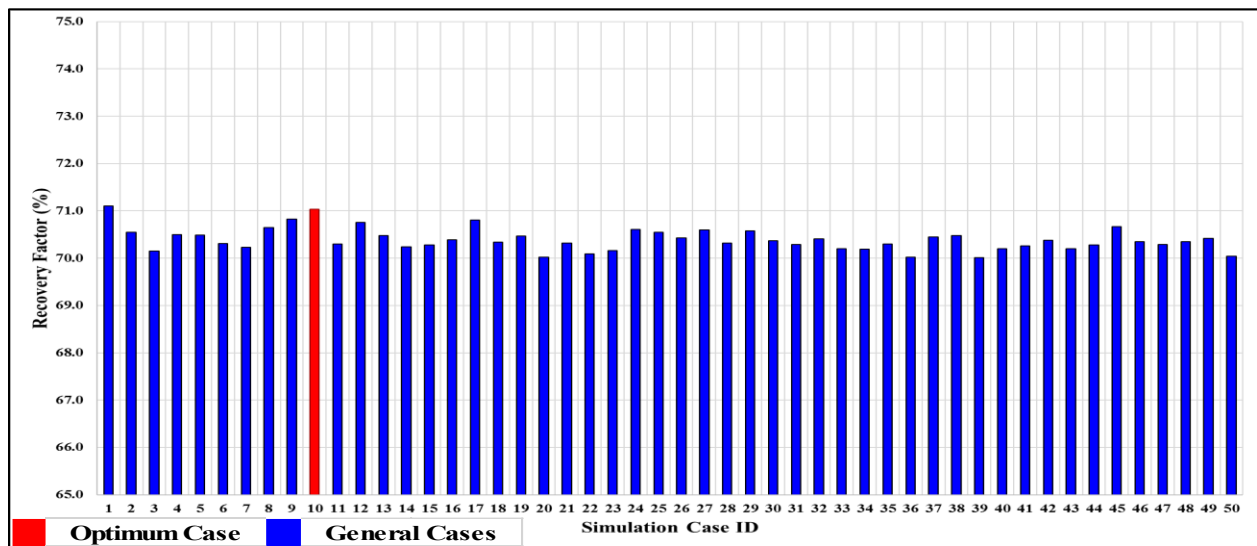


Fig C-6: Trajectory-3 Optimization Top 50 Cases Recovery Factors

C.2 Design of Short-Term Optimization Work

The optimization work carried out in Chapter 6 of this research involved short-term optimization (3 years) followed by long-term optimization technique. The following sections discuss the basis of choosing this technique and the choice of 3-Year period for short-term optimization.

C.2.1 Previous Work by Others

Noroozi et al. (2014) adopted a similar approach in optimizing number of ports in both OCD's and ICD's. For OCD's, CMG DECE has been used to run short-term optimization for 21 cases for 16 months (**Figure C-7**), then the best three cases were selected as candidates for further analysis through long-term optimization for six years. **Table C-1** shows results of the optimum solution

selected from the top 3 cases of the long-term optimization compared to the base case. The authors have also used the same methodology for the optimization of ICD's number of ports where the short-term run was performed for two years (**Figure C-8**), then long-term run was performed for six years to determine the optimum solution as shown in (**Table C-2**).

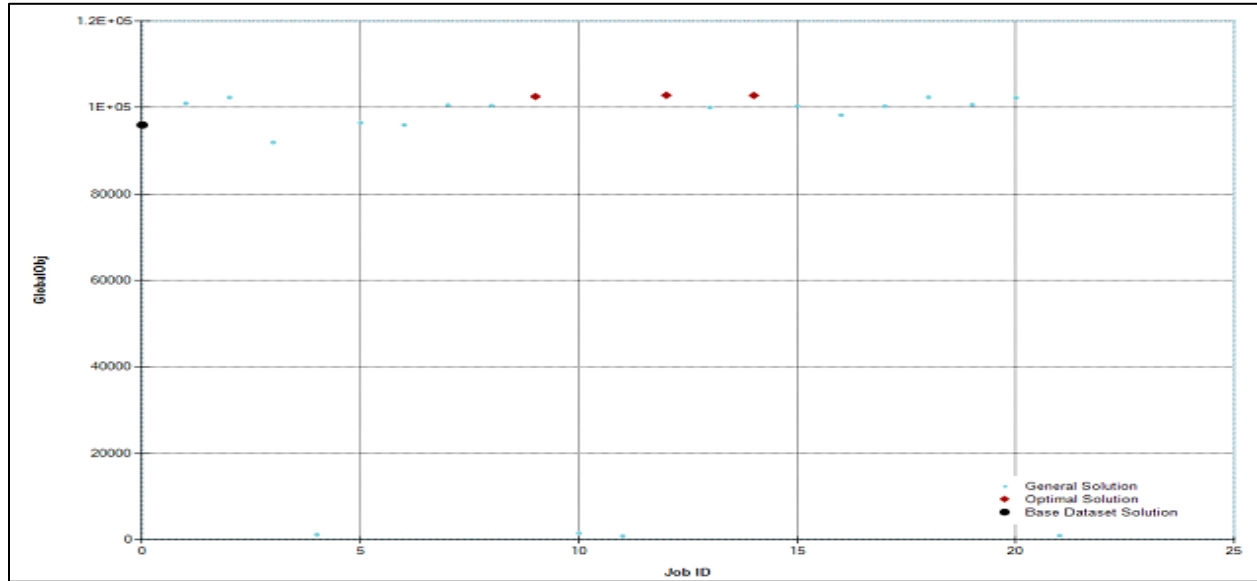


Figure C-7: Optimization of Number of Ports for Injection FCD's (16-Month Forecast), Noroozi et al. (2014)

Table C-1: Ultimate Optimum Solution for Injection FCD's (6-Year Forecast), Noroozi et al. (2014)

Year	NPV for Base Case (Optimal case from step-1) (MS)	NPV for Optimal Case (MS)	Increase in NPV (MS)
1	5.1	5.9	0.85
2	21.9	22.4	0.52
3	34.2	35.2	0.96
4	47.1	49.4	2.34
5	61.9	63.6	1.71
6	69.7	69.8	0.03

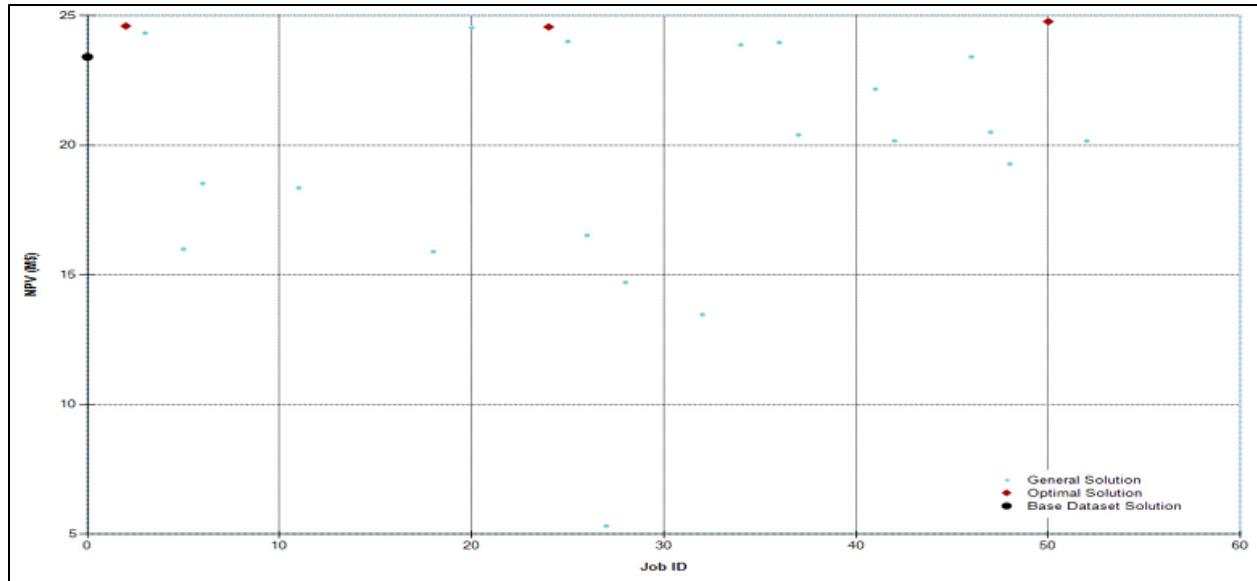


Figure C-8: Optimization of Number of Ports for Production FCD's (2-Year Forecast), Noroozi et al. (2014)

Table C-2: Ultimate Optimum Solution for Production FCD's (6-Year Forecast), Noroozi et al. (2014)

Year	NPV for Base case (No FCDs) (M\$)	NPV for optimal case by optimizing injection FCDs (Steps 1 & 2) (M\$)	NPV for ultimate Optimal case (Step 3 & 4) (M\$)
1	0.4	6.7	7.7
2	10.2	23.4	24.8
3	18.7	36.2	37.9
4	25.5	50.6	53.7
5	29.5	67.2	69.1
6	30.9	75.4	75.9

C.2.2 SAGD Early-Stages

Since SAGD start-up is a crucial step for the success of the SAGD process (Parmar et al. 2009), The more uniform steam chamber propagation and growth at early-stages of SAGD process, the better overall performance of SAGD process for the whole SAGD project life. To investigate this phenomenon, two cases were selected from Trajectory-1 optimization work for comparison and analysis. The first case (Case A) has high NPV for both short-term and long-term runs, it also has uniform steam chamber growth. The second case (Case B), has low performance, where short-term and long-term simulation runs have lower NPV, in addition to poorer steam chamber growth compared to Case A.

As shown in **Figure C-9-b**, NPV of Case A is always higher than NPV of Case B. **Figure C-9-a** depicts the difference in NPV between both cases. The difference NPV between the two cases reached \$1,646,469, and reached a maximum of \$2,435,841 after five years, after that it started to decline until down to \$1,335,132 at the end of Case A SAGD simulation time. It can be observed

that more than 67% of maximum difference between the cases has been developed within the first 3 years, and that shows the importance of early-stage SAGD process.

Figure C-10 depicts temperature maps of cases A and B. More uniform steam chamber growth can be observed in Case A both laterally and horizontally. Also, full vertical steam chamber growth in Case A has been achieved earlier than Case B.

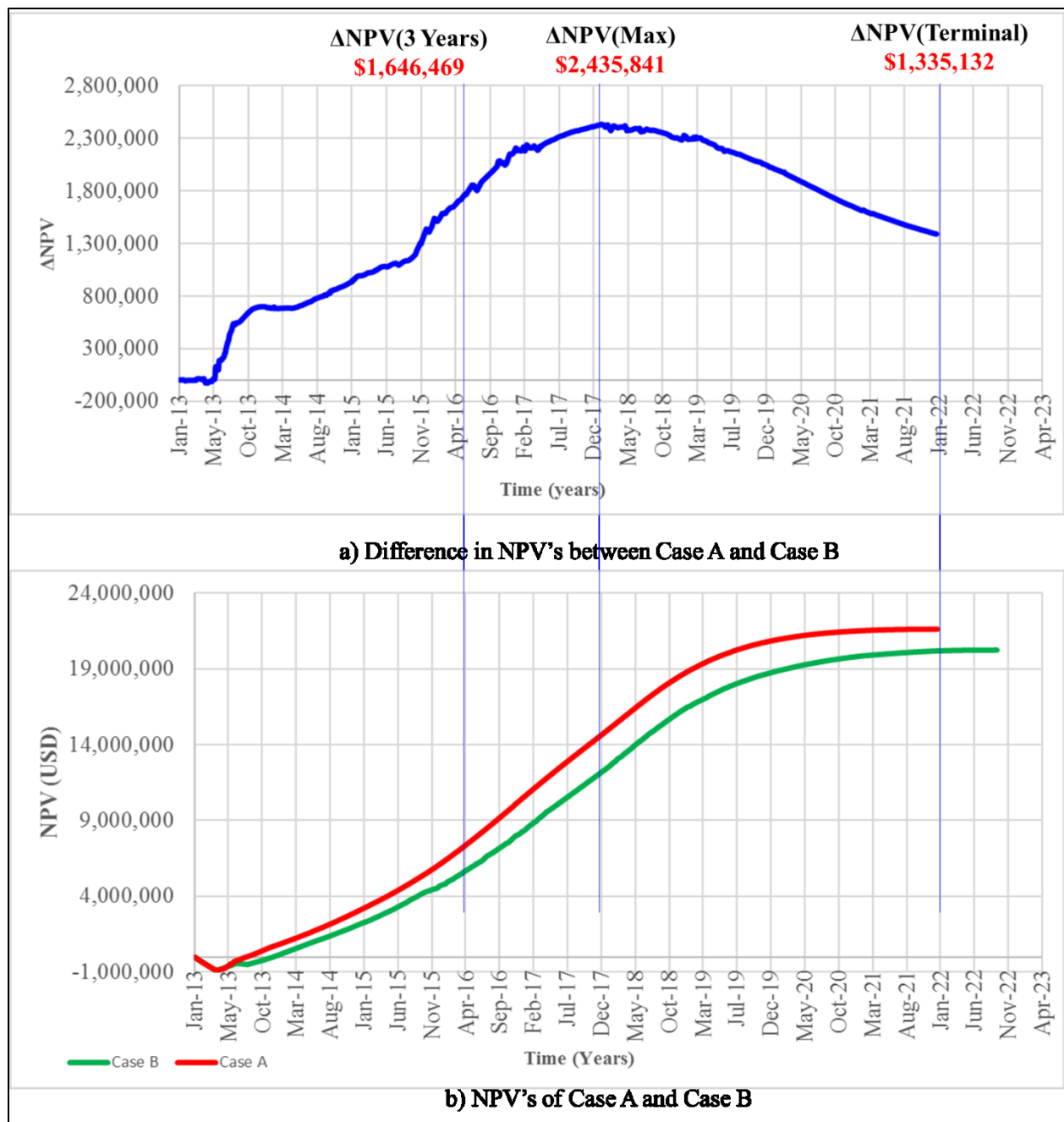


Figure C-9: Comparison of NPV's of Case A and Case B

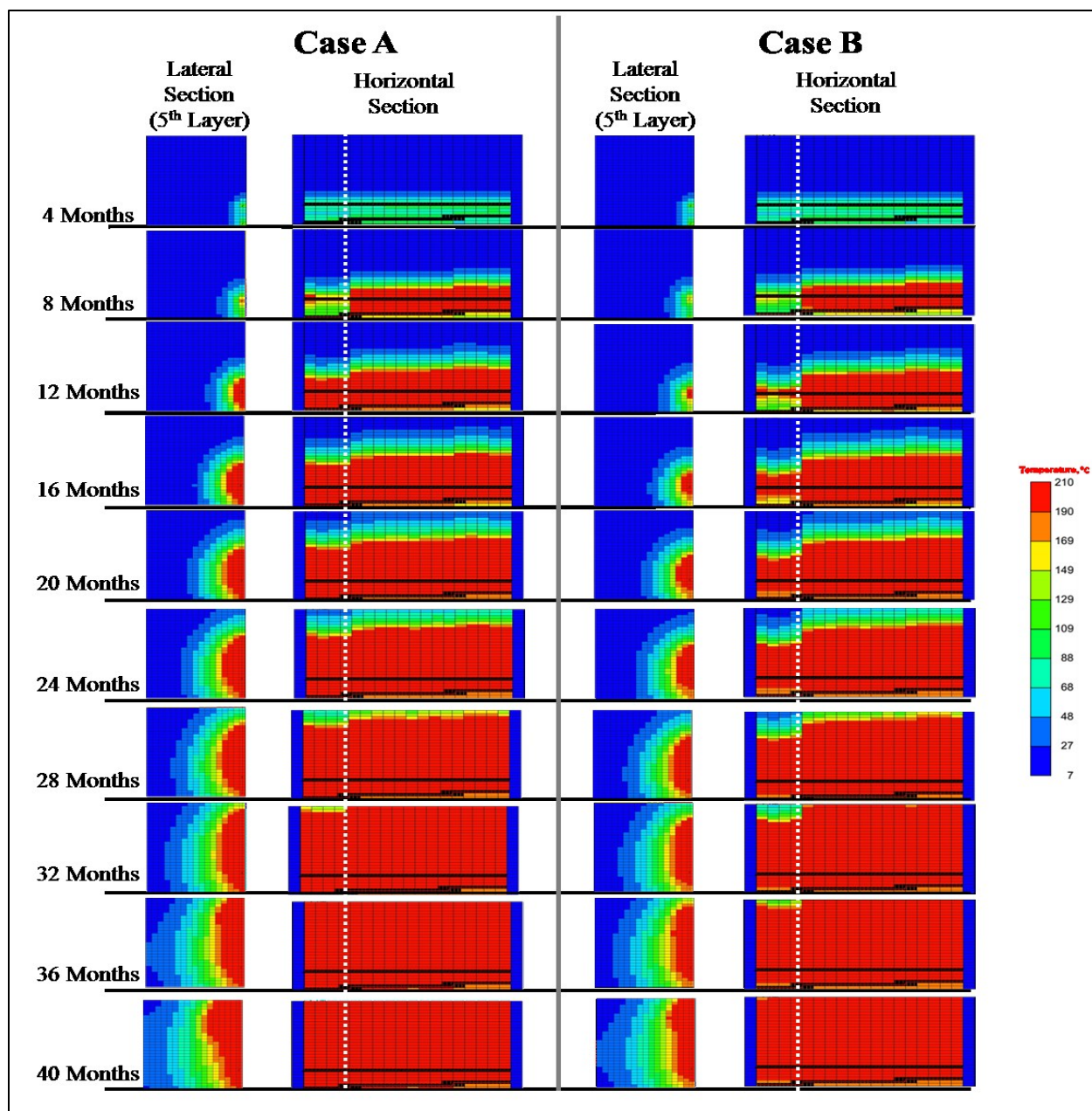


Figure C-10: Temperature Maps of Case A and Case B

Table C-3 summarizes differences in NPV's between the two cases at different stages. Case A SAGD project life has been terminated after 3,197 days with terminal NPV of \$21,599,013. Case B has been terminated 261 days later, i.e., after 3,458 days with terminal NPV of 20,263,881.

Table C-3: NPV's of Case A and Case B at Different Stages

Time	Case A NPV	Case B NPV	Δ NPV
3 Years	\$7,222,167	\$5,575,698	\$1,646,469
4.8 (Max.)	\$15,005,757	\$12,569,916	\$2,435,841
End of SAGD	\$21,599,013	\$20,263,881	\$1,335,132

C.2.3 Decreasing Trend of Ranked Long-Term Optimization Cases

As shown in Chapter 6, top 50 (long-term) optimization cases of all trajectories have shown decreasing trends. However, to illustrate that the decreasing trend will continue even for cases beyond top 50 cases, all short-term cases of Trajectory-1 depicted in **Figure 6-4** of **Chapter 6** have been ranked (form high to low) as shown in **Figure C-11**, and then 18 more cases (with constant intervals) were chosen for further confirmatory long-term run analysis as shown in **Figure C-12**. Upon running the additional 18 candidate cases until the end of SAGD project life, continuous decreasing trend has been noticed as shown in **Figure C-13**.

The approach has been applied on the other trajectories. **Figure C-14** through **C-16** show results of Trajectory-2 and **Figure C-17** through **C-19** show results of Trajectory-3.

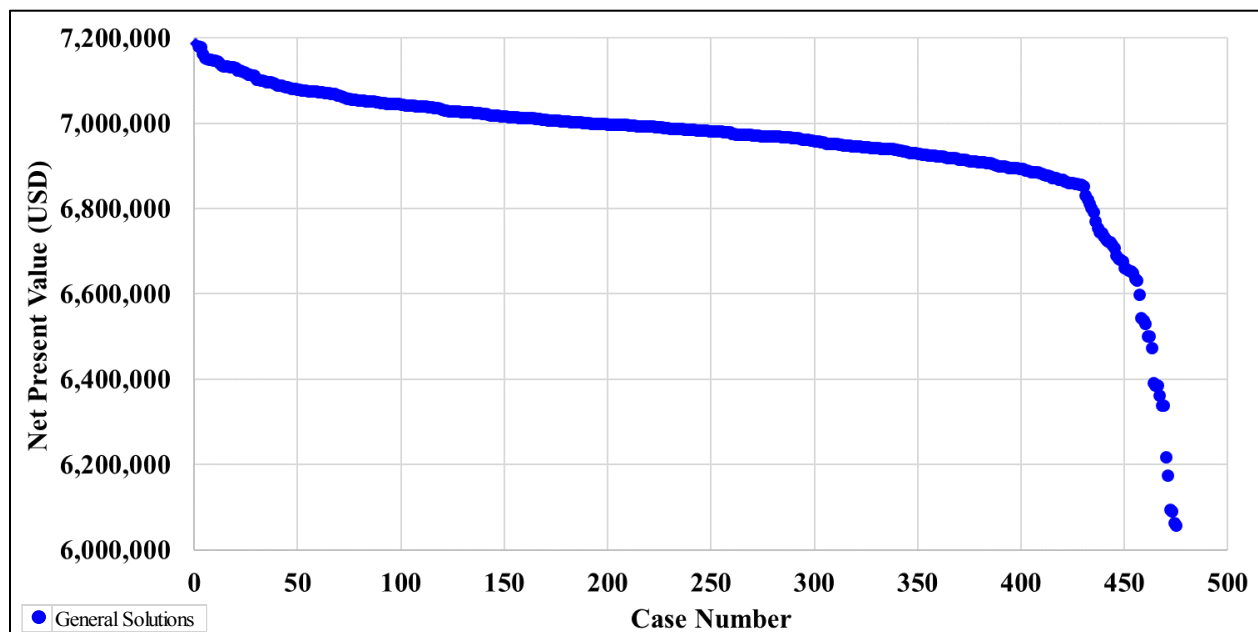


Figure C-11: Short-Term Cases Ranking Based on NPV, Trajectory-1

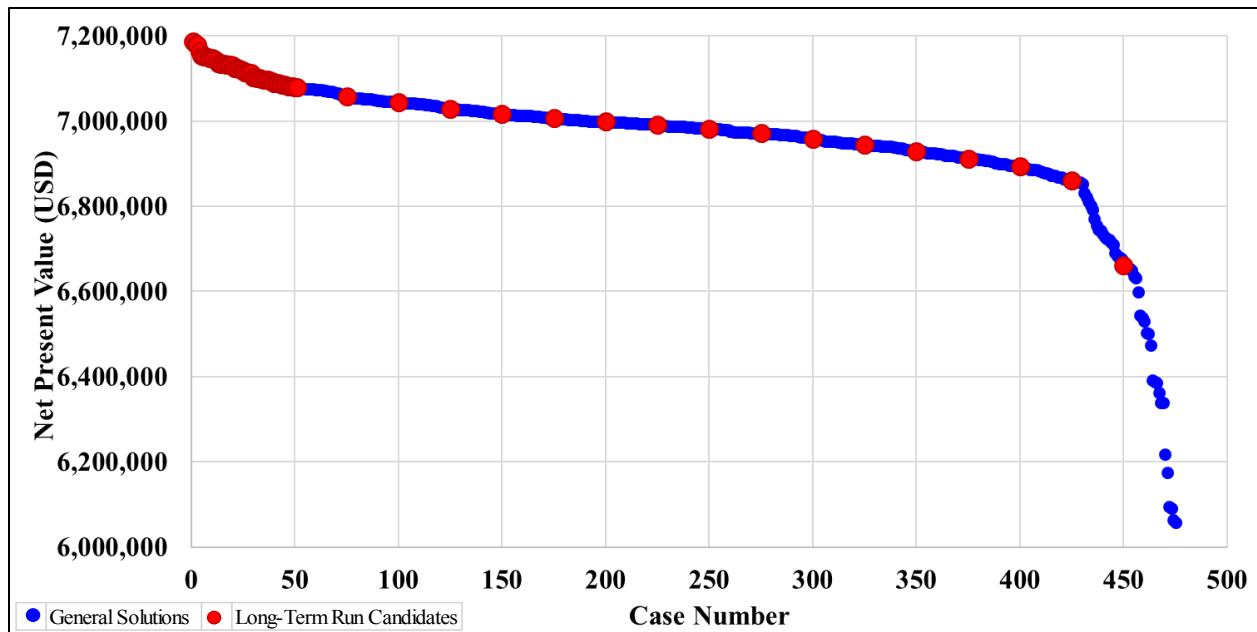


Figure C-12: Short-Term Ranked Cases and Long-Term Run Candidates, Trajectory-1

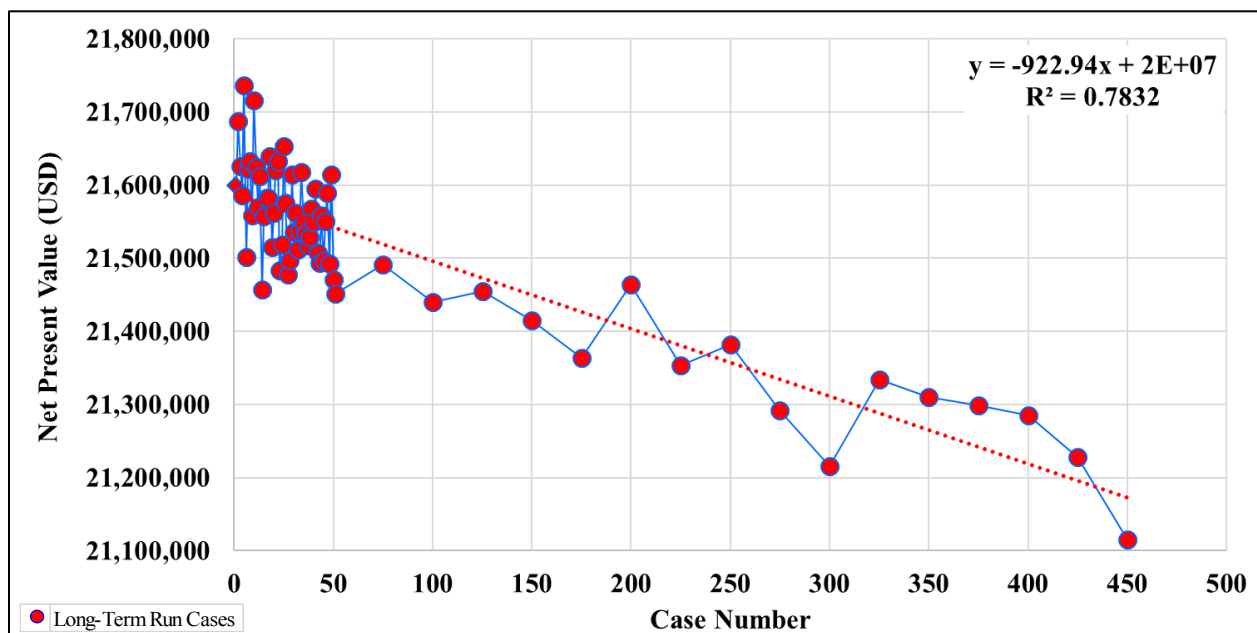


Figure C-13: Long-Term Run Cases NPV's, Trajectory-1

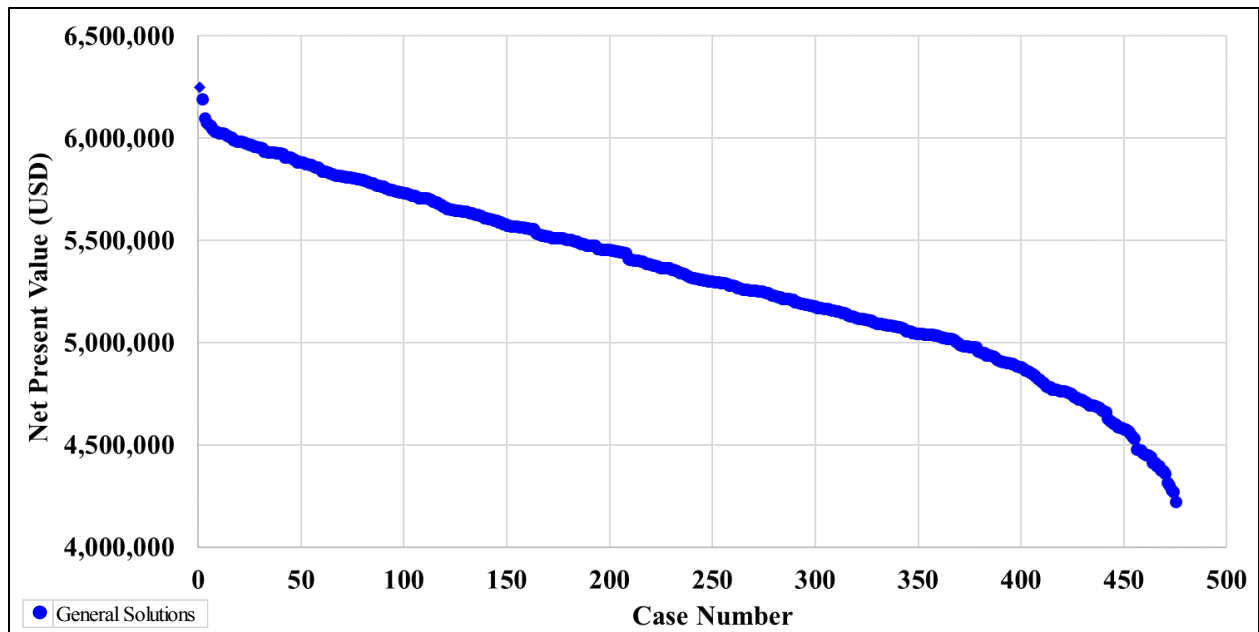


Figure C-14: Short-Term Cases Ranking Based on NPV, Trajectory-2

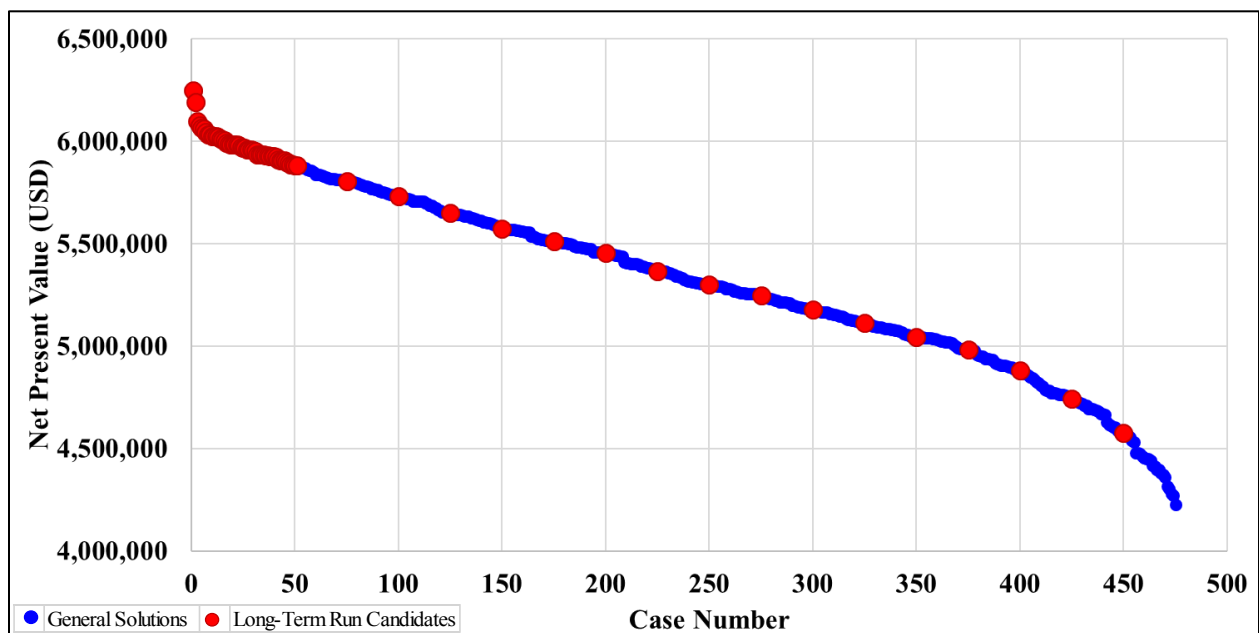


Figure C-15: Short-Term Ranked Cases and Long-Term Run Candidates, Trajectory-2

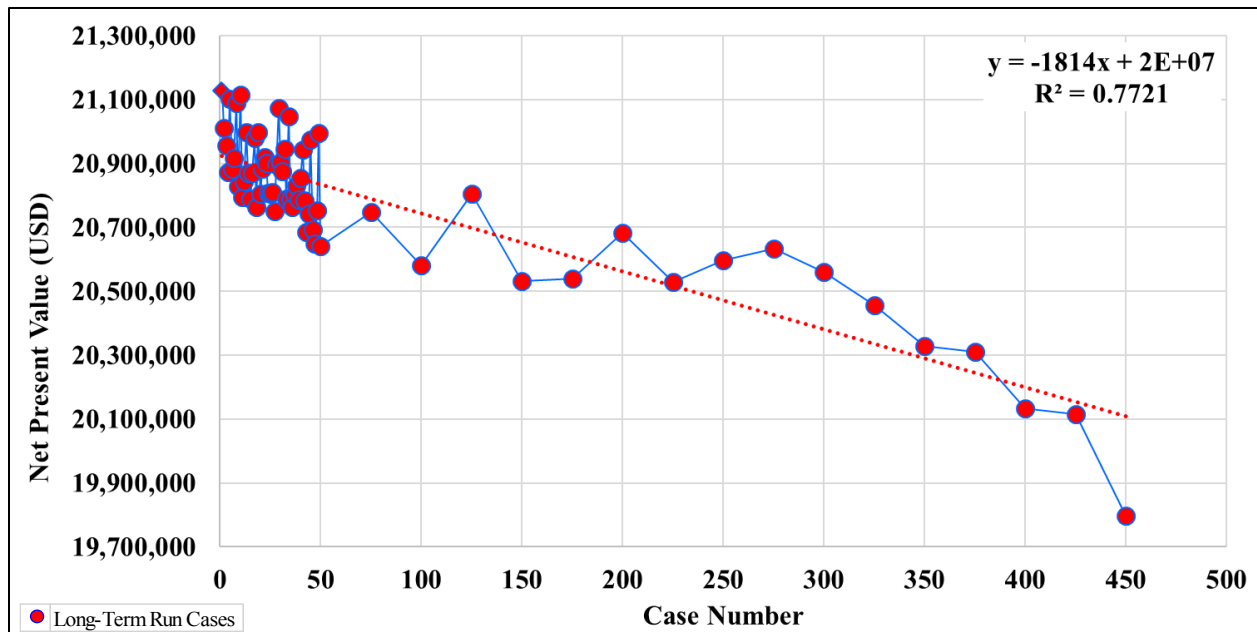


Figure C-16: Long-Term Run Cases NPV's, Trajectory-2

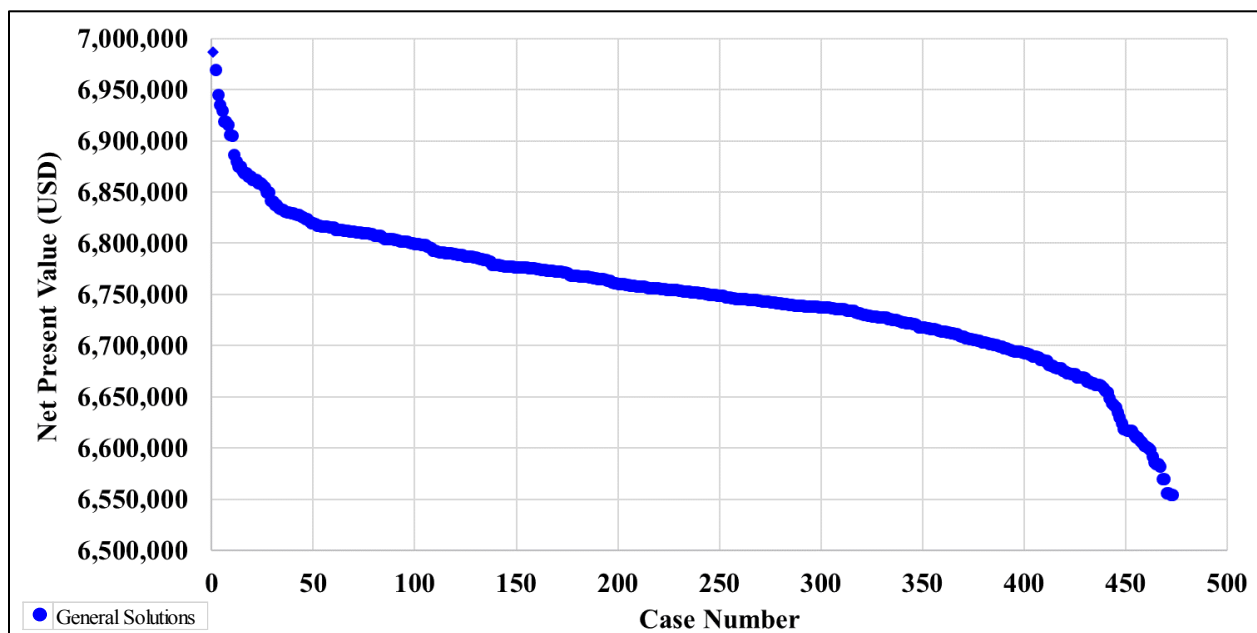
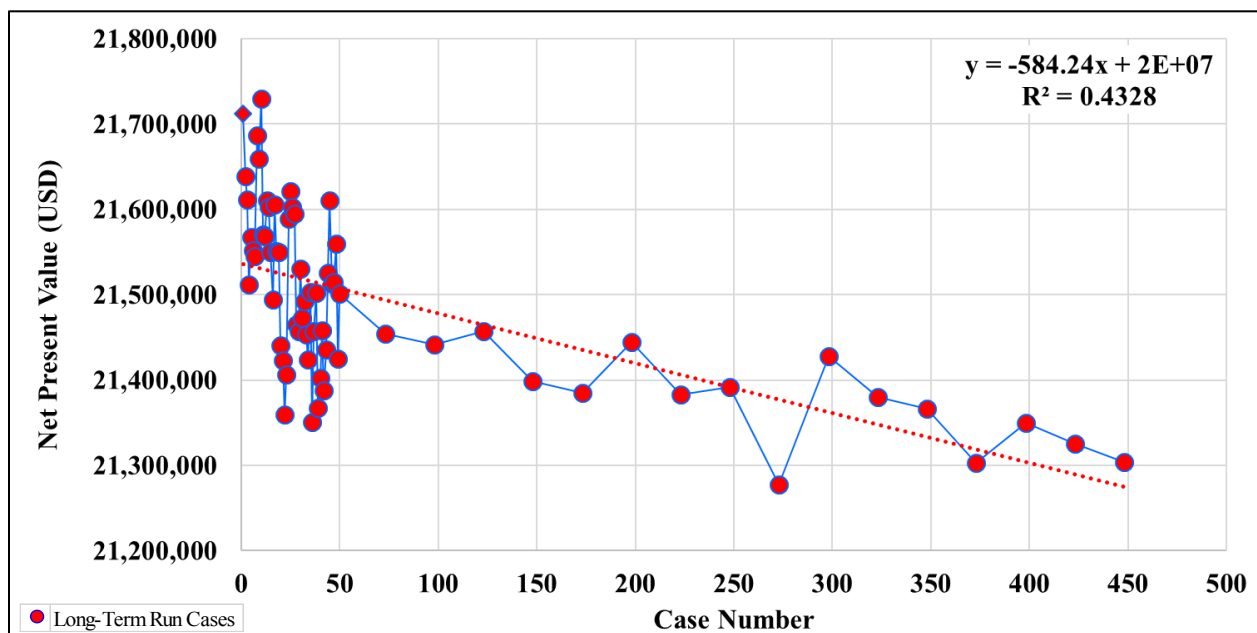
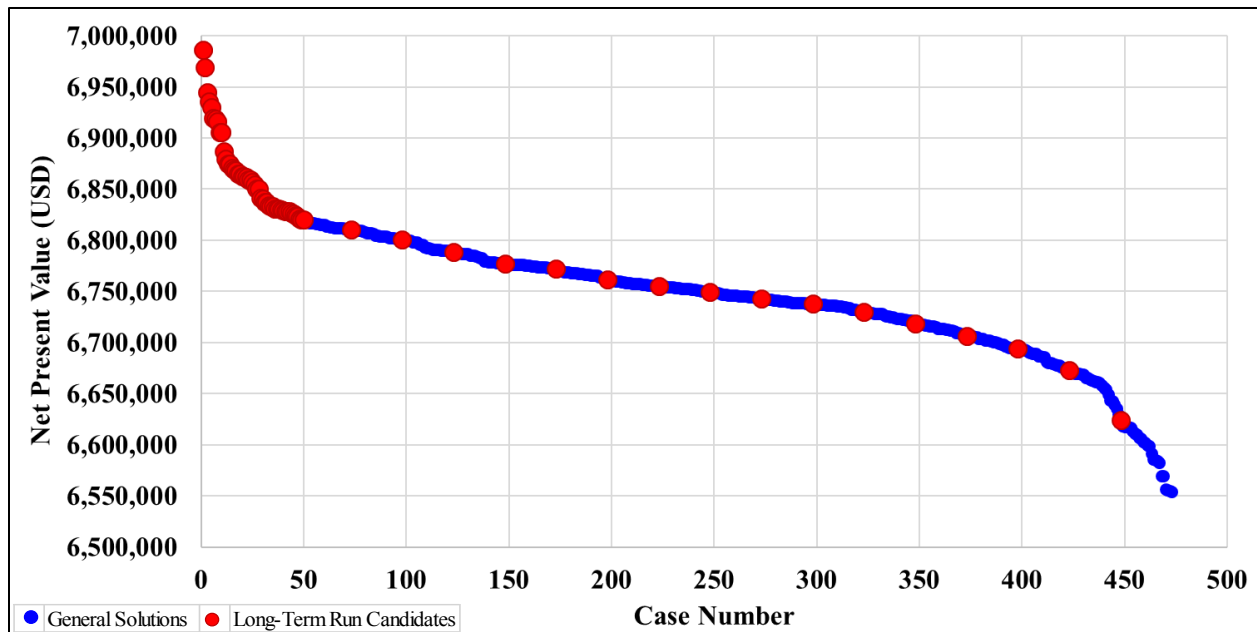


Figure C-17: Short-Term Cases Ranking Based on NPV, Trajectory-3



C.3 Downhole Installation of OCD's

Number of ports per single OCD and length of the OCD tool itself greatly vary depending on the manufacturer and the desired downhole completion configuration. For instance, Variflux™ is a steam splitter developed by Variperm has length of 42” and 64 nozzles. **Figure C-20** shows specifications of Variflux steam splitter. Also, Haliburton manufactured OCD's (Equiflow® OptiSteam™) with various number of ports (24-36 ports) as depicted in **Figure C-21**. Also, Kyanpour and Chen (2014) utilized various number of ports (8-20 ports) ranges in their models.

Tubing Sizes		Material	Weight	Min I.D.	Max O.D.	Tool Length	Shifting Profile
3.5 in	L-80 Pup Joint	9.2lb/ft	275.6	2.7 in	5.0 in	42 in	Otis B - 42B0178
4.5 in	L-80 Pup Joint	11.6lb/ft	315.0	3.7 in	5.7 in	42 in	Otis B - 42B0238
88.9mm	L-80 Pup Joint	13.7 kg/m	315.0	68.6 mm	127 mm	1066.8 mm	Otis B - 42B0178
114.3mm	L-80 Pup Joint	173 kg/m	590.6	90.7 mm	144.8mm	1066.8 mm	Otis B - 42B0238




Figure C-20: Variflux™ Steam Splitter, (Variperm Canada Limited 2017)

EquiFlow® OptiSteam™ FCD Technology				
FCD OD	4.30-in. (109.2 mm)	4.80-in. (121.9 mm)	5.80-in. (147.3 mm)	6.80-in. (172.7 mm)
Minimum Bore ID	1.87-in. (47.5 mm)	2.313-in. (58.8 mm)	2.813-in. (71.5 mm)	3.81-in. (96.8 mm)
Quantity of Nozzles (10 mm ID)	24	28	32	36
Standard Metallurgy	NACE 4140	NACE 4140	NACE 4140	NACE 4140
Standard Temperature Rating	520°F (271°C)	520°F (271°C)	520°F (271°C)	520°F (271°C)




Figure C-21: OptiSteam™ Steam Splitter, (Haliburton 2017)

Depending on the desired downhole configuration, number of ports per single joint can be either concentrated in a single area using one OCD device or distributed among a limited length of the horizontal section using multiple OCD's conveyed in one joint. The work in this research has maximum number of 70 ports and they can be accommodated by max of two OCD devices

conveyed in a 2-m length pipe as modeled previously in **Figures B-10, B-12 and B-14** of **Appendix B** and shown in **Figure C-22**:

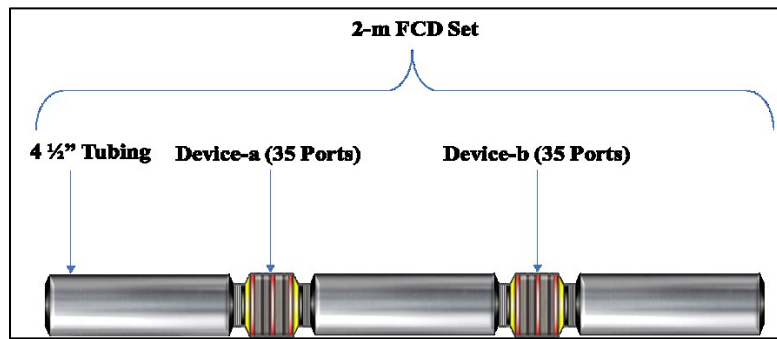


Figure C-22: Single OCD Set Composed of Two Pieces of OCD Devices